MODEL STUDIES OF ADSORBATE ORDERING, ADSORPTION AND REACTION USING MONTE-CARLO SIMULATIONS

Thesis by

Hway-Chuan Kang

In Partial Fulfillment of the Requirements
for the Degree of
Doctor of Philosophy

California Institute of Technology
Pasadena, California

1990

(Submitted September 11, 1989)

This thesis is dedicated to my mother.

Acknowledgements

I would like to express my greatest appreciation for the inestimable intellectual support that my research advisor and mentor, Henry Weinberg, has given me. These past few years of working with him has been a great pleasure. It has also been a profitable experience for me to have interacted with the other members of the Weinberg group. I express my appreciation to those who have helped show me the way: Greg, Mike, Jim, John V., John P., Wilman, Yong-Kui, Dale, Chun-Yu, You-Qi, Buddie, Brian and Eric. I would also like to thank Mike, Randy, Tom and Bill for their collaboration.

For the invaluable computer resource which he helped to provide, I wish to thank Vaxman Dave Malerba. I also thank Kathy Lewis for her indispensable help in various departmental matters.

In my years at Caltech I have benefitted from knowing a number of friends who have helped make my graduate student days enjoyable. It has been a great pleasure to know Greg, Ricky, Alex, Atta, Chris, Judy, Chak, Thu, In-Seok, Chi-Fai, Chi Fong, Boon-Khim and Sing-Ung. And, to O. much is owed.

Abstract

The application of Monte-Carlo simulations to study thermally excited time-dependent phenomena is examined. The diffusion coefficient and the exponent for domain growth for a square lattice gas experiencing equal and repulsive nearest-neighbor and next-nearest-neighbor interactions are calculated for three different dynamics: Kawasaki; Metropolis and energy-barrier. All three dynamics satisfy detailed balance, but the diffusion coefficient is found to show a different temperature dependence for each. The growth exponents for Kawasaki and energy-barrier dynamics are in close agreement, and larger than that for Metropolis dynamics. This difference arises because the domain sizes reached were not sufficiently large.

In further Monte-Carlo simulations of the same lattice gas model using dynamics which allow precursor-mediated migration, the growth exponent of fourfold degenerate ordered (2x1) domains on a square lattice is found to be $1/2$. If the growth law is written as $l \sim At^{1/2}$, A is found to be proportional to $D^{1/2}$, where D is the diffusion coefficient of the adsorbed particle. Kawasaki dynamics simulations at zero temperature are performed for the growth of $(\sqrt{3}\mathrm{x}\sqrt{3})R30°$ domains on a triangular lattice. The results show that the low temperature behavior is markedly dependent upon the details of the lateral interactions and the range of the particle hops. This latter result demonstrates the strong influence of a precursor state on growth kinetics.

Monte-Carlo analysis of molecular beam reflectivity measurements of the probability of molecular adsorption of ethane on the Ir(110)-(1x2) surface shows that a precursor state can also be rather important in adsorption. We show that the experimental data can be explained by adsorption occurring in two channels: direct and precursor-mediated. In this case the precursor is an ethane molecule trapped in a second layer on top of the first layer of molecularly adsorbed ethane. From the simulations we were also able to calculate the energy barriers for diffusion

and desorption of an ethane molecule in the precursor state.

Monte-Carlo simulations of a Langmuir-Hinshelwood reaction between two interacting species were also performed. The parametrization of the reaction rate coefficient that is implicit in an Arrhenius plot is examined. It is shown that the effective energy barrier and preexponential factor obtained from an Arrhenius plot show strong compensation when the overlayer configuration is strongly temperature dependent. This can explain the anomalously high reaction or desorption preexponential factors observed for some adsorbed systems.

It is also shown that a Langmuir-Hinshelwood reaction occurring between two species, even when they are non-interacting, can lead to configurational effects. Compact 'islands' consisting solely of either species A or species B are observed in simulations. An order parameter which allows an analogy between the reacting system and magnetic systems to be drawn is defined. The reactivity of the catalyst surface is inversely proportional to the 'island' size.

Table of Contents

INTRODUCTION

A surface can be considered to be a defect in a crystalline solid because the three dimensional periodicity which exists within the bulk is lost in the surface region. However, crystal surfaces still possess two-dimensional periodicity and their structure can always be described in terms of one of the five two-dimensional Bravais lattices along with a basis of atoms for each lattice point. Consequently, the atoms at the surface of the crystal presents a two-dimensionally periodic array of sites at which molecules can be adsorbed. In some cases, such as the adsorption of rare gases, the binding energy between the adsorbed molecules and the substrate is so weak that the structure of the adsorbed layer is independent of the substrate structure. However, for adsorption of small molecules on transition metal surfaces the two-dimensional periodicity of the array of adsorption sites means that adsorption can be modeled by a lattice gas. The basic elements of such a description are the lattice type at which sites the particles are adsorbed, the lateral interactions between the adsorbed particles and the chemical potential of the adsorbed species. Having specified these, a Hamiltonian can be written as follows:

$$H = \sum_{(i \neq j)} J_{ij} c_i c_j,$$

where c_i, the site occupation variable, is unity if site i is occupied and zero if it is vacant and J_{ij} is the interaction energy between two particles, one at site i and the other at site j. Knowing the Hamiltonian, the grand canonical partition function for the adsorbed system can be written as

$$Z = \sum_{\mathbf{c}} z^{N_{\mathbf{c}}} \exp(-\beta \sum_{(i \neq j)} J_{ij} c_i c_j),$$

where the first sum is over all the configurations $\mathbf{c}$ of the lattice gas, $z \equiv \exp(\beta\mu)$ is the fugacity and μ is the chemical potential of the adsorbed species. The total

number of adsorbed particles for configuration **c** is equal to $N_{\mathbf{c}}$. Although a lattice-gas system (and its equivalent Ising spin system) can be formulated rather easily, the calculation of the partition function and, hence, the thermodynamic or mechanical properties of the system is by no means an easy task **(1)**. Many approximate analytical methods have been developed to deal with this problem. The most widely used are mean-field approximations. Various formulations of the renormalization group method have also been used quite successfully to study lattice-gas (Ising) systems, in particular, to provide the theoretical understanding of the universality of critical properties **(2)**.

For most adsorbed systems, however, it is most convenient and simple to use Monte-Carlo sampling **(3,4)** to obtain exact values, at least in principle, for the thermodynamic and mechanical properties. Mean-field approximations, although quite useful qualitatively, generally give incorrect phase-diagrams, for instance. Renormalization methods which are rigorously valid only in the vicinity of the critical point have also been used to calculate the entire phase diagrams of adsorbed systems. However, they are inconvenient because generally, at each renormalization, many new effective interactions are introduced and approximations have to be used to avoid this. Monte-Carlo methods have been used with immense success in many cases in which the lattice-gas system cannot otherwise be studied accurately. It must be noted that we have been discussing equilibrium properties of adsorbed systems. Although Monte-Carlo methods have also been widely used to investigate the time evolution of an adsorbed system which is not in equilibrium, such use has not been carefully examined. In contrast to molecular dynamics, which basically performs numerical integrations of the equations of motion for each particle in the system, the use of Monte-Carlo methods in studying systems which evolve in time is based upon the numerical solution of a master-equation in which the transition probabilities have to be specified. In Chapter 1 various ways of specifying these transition probabilities are briefly, but carefully, examined.

Although we begin with a study of the use of Monte-Carlo methods for time evolving systems, this thesis is concerned mainly with the application of Monte-Carlo simulations to understand some of the properties of adsorbed systems, insofar as they are modeled by lattice gases. Since there are lateral interactions between the particles of a lattice gas, the free energy of the system depends upon the configuration of the particles on the lattice. A random distribution has the largest entropy, but particular ordered distributions may have the lowest energy. The equilibrium configuration of a lattice gas at any temperature is, therefore, arrived at by a balance between these two opposing forces. Hence, when a lattice gas is cooled below a particular temperature, it is possible for a transition to occur from a disordered state to an ordered state. Such order-disorder transitions are widely observed in adsorbed systems and the purpose of studying them is twofold. Firstly, it is possible to obtain the strengths of the lateral interactions between the adsorbed molecules by matching the experimental phase diagrams to the calculated ones. Secondly, adsorbed systems provide the testing ground for the present understanding of phase transitions since much of the analytical or numerical work in this area is done for two-dimensional systems, these being the simplest non-trivial systems. Regardless of whether a phase transition occurs, the distribution of the lattice-gas particles is frequently influenced strongly by the temperature and the fractional surface coverage of the particles. This means that the local configuration around a lattice-gas particle is quite dependent upon temperature and fractional surface coverage. Since the particles interact laterally, different local configurations will lead to different diffusion, adsorption, desorption or reaction rates. Understanding this is important since these processes are the basic building blocks of catalytic phenomena. We investigate the kinetics of domain growth and the influence of the configuration of the adsorbed layer on reaction rate coefficients.

Using a lattice gas to model an adsorbed layer of molecules may be considered to be a mesoscopic description of the system. It is not macroscopic because the

position of each particle is followed. However, it is not microscopic because the lattice gas particle that is used to simulation the adsorbate particle can, at best, be considered to be the time-averaged position of the molecule adsorbed at a site. The vibrations of the adsorbed molecule are not simulated, and the elementary processes of adsorption, desorption, diffusion and reactions are not considered in terms of the quantum mechanics of the electron wavefunctions that provide the interactions between the adsorbed molecules and the substrate and between the adsorbed molecules themselves. The process of diffusion, for instance, is simulated by hops from one lattice site to the next, with the hops occuring at some specified rate which, in principle, can be obtained from a more microscopic description. It should be clear that the main role of an investigation at this mesoscopic level is an elucidation of the importance of configurational effects. However, lattice gas models can incorporate certain features of some dynamical processes. The adsorption of a molecule onto a crystal surface does not necessarily occur in one direct step **(5)**. The impinging molecule may be trapped temporarily in a weakly bound precursor well in which the binding is due to van der Waals forces before it reaches the adsorption well in which a chemical bond is formed. Precursor-mediated adsorption or diffusion, for instance, can be modeled by lattice gases. Indeed, one theme which runs through our work is the simulation of processes in which a precursor channel plays an important role.

We have seen that ordering of lattice-gas particles can occur because of the lateral interactions that exist between them. When there are attractive lateral interactions between the particles, it is possible to form 'islands' when the surface is cooled below a transition temperature. However, it is also possible to obtain similar 'islands' even in the absence of lateral interactions. These latter 'islands' are specific examples of the 'dissipative' structures that have been widely studied in non-equilibrium transitions **(6,7)**. Since a major purpose of our work is to study the influence of the configuration of an adsorbed layer on processes important to

catalysis, we also conduct an investigation of a Langmuir-Hinshelwood reaction model in which the interplay between diffusion, adsorption and reaction results in fractional surface coverage inhomogeneities. In our work we attempt to provide a 'thermodynamic' interpretation of the underlying kinetic forces that produce the 'dissipative' structure in the model.

References

1. H.E. Stanley, **Introduction to Phase Transitions and Critical Phenomena**, Oxford University Press, Oxford 1971.
2. **Phase Transitions and Critical Phenomena**, Vol 6, Eds. C. Domb and M.S. Green, Academic Press, New York, 1976.
3. **Monte-Carlo Methods in Statistical Physics**, Ed., K. Binder, Topics in Current Physics, Vol. 7, Springer-Verlag, Heidelberg, 1979.
4. **Applications of the Monte-Carlo Methods in Statistical Physics**, Ed., K. Binder, Topics in Current Physics, Vol. 36, Springer-Verlag, Heidelberg, 1983.
5. W.H. Weinberg, in **Kinetics of Interface Reactions**, Eds., H.J. Kreuzer and M. Grunze, Springer-Verlag, Heidelberg, 1987, p. 94.
6. G. Nicolis and I. Prigogine, **Self-Organization in Nonequilibrium Systems**, Wiley Interscience, New York, 1977.
7. H. Haken, **Synergetics**, Springer-Verlag, New York, 1983.

Chapter 1.

Dynamic Monte-Carlo with a Proper Energy Barrier: Surface Diffusion and Two-Dimensional Domain Ordering

This chapter was published as a paper by H.C. Kang and W.H. Weinberg, in *The Journal of Chemical Physics*, **90**, 2824 (1989).

ABSTRACT

A new model is presented and discussed that allows Monte-Carlo simulations to be carried out *with a proper energy barrier crossing.* Results are presented for the surface diffusion coefficient and the growth exponent of domain ordering of a half-monolayer of adatoms experiencing nearest and next-nearest neighbor repulsive lateral interactions (equal in magnitude), both on a square lattice. The results are compared with those derived using both Kawasaki dynamics and a Metropolis walk. The reasons why neither of the latter methods can be expected, in general, to describe thermally excited, time-dependent phenomena are explained and discussed.

I. Introduction

Monte-Carlo simulations are widely used **(1-3)** to study both the dynamic and the static behavior of systems with many interacting particles. In the investigation of static behavior, the simulations can be used to generate the statistically most important configurations. One commonly used algorithm is the Metropolis walk **(4)**, which samples the configurations as follows. From an initial configuration, a new configuration can be generated, for instance, by a single spin flip in an Ising model. The new configuration is accepted with probability unity if its energy is less than that of the original configuration. Otherwise, it is accepted with probability $e^{-(E_f - E_i)/k_B T}$, where E_f and E_i are the energies of the new and the old configurations, respectively. Such algorithms search for the configurations of lowest free energy. For studying static behavior, the sequence of configurations that are generated need not correspond to the real evolution of the system towards the state of lowest free energy. The problem of conversion from simulated time t_s to real time t_r does not arise.

In studying dynamic behavior, however, the sequence of configurations generated by the Monte-Carlo procedures is meant to simulate the time-evolution of the system, and, hence, it is important to know how to convert t_s to t_r in this case. (Most Monte-Carlo studies have reported their results in terms of t_s.) At the very least, it is necessary to know that t_s scales linearly with t_r. Investigating the dynamic behavior of a system by Monte-Carlo techniques is equivalent to approximating the actual behavior of the system by a stochastic process **(1,2)**. Consider the motion of adsorbed molecules on a crystal surface. This is often simulated by a lattice gas, the particles of which migrate by hopping from one site on the lattice to another. Frequently, the lattice-gas particles are only allowed to hop from their original sites to vacant, nearest-neighbor sites. The lattice-coordination number z is dictated by the symmetry of the crystal surface, and the lattice-gas particles are allowed to interact with each other. A lattice-gas particle is picked randomly

from an initial configuration. Then one of the z nearest-neighbor sites is picked randomly. If the chosen nearest-neighbor site is occupied, the procedure is begun again. If the chosen nearest-neighbor site is vacant, the probability $w(c_i, c_f)$ of a successful hop from the original site to the chosen site is computed and compared to a random number r $(0 \leq r \leq 1)$. The particle then hops if $w(c_i, c_f) \geq r$; otherwise, it remains at its original site. The configuration is changed from c_i to c_f because of the hop. Each time a particle is picked, the time is increased by one Monte-Carlo step (MCS). If we take $1/\tau$ to be the attempt frequency, then the real time corresponding to one MCS is τ/N, where N is the total number of particles, assuming that each particle is excited once by the heat-bath, provided by the crystal, in each time interval τ. This Monte-Carlo technique then is a method of 'solving' the master equation

$$\frac{dP(c_f,t)}{dt} = \sum_{c_i} \frac{w(c_i,c_f)P(c_i,t)}{\tau} - \sum_{c_i} \frac{w(c_f,c_i)P(c_f,t)}{\tau}, \tag{1}$$

where $P(c,t)$ is the probability distribution of configurations at time t. For the Monte-Carlo dynamics to be consistent with detailed balance at thermal equilibrium, it is necessary that

$$w(c_i,c_f)P_{eq}(c_i) = w(c_f,c_i)P_{eq}(c_f), \tag{2}$$

and

$$P_{eq}(c) = Z^{-1}exp(-H[c]/k_BT), \tag{3}$$

where H is the Hamiltonian and Z is the partition function of the system, and P_{eq} is the probability distribution of configurations at equilibrium. Detailed balance, of course, does not completely specify $w(c_i, c_f)$.

One choice of $w(c_i, c_f)$, which satisfies detailed balance, is the Metropolis walk **(4)**, for which

$$\begin{aligned} w_m(c_i,c_f) &= exp(-\delta E/k_BT) \quad \text{for} \quad \delta E > 0, \\ &= 1 \quad \text{for} \quad \delta E \leq 0, \end{aligned} \tag{4}$$

where $\delta E = H[c_f] - H[c_i]$. Another common choice for $w(c_i, c_f)$ for lattice-gas systems with conservation of total number of particles is Kawasaki dynamics **(5-7)**, for which

$$w_k(c_i, c_f) = \frac{exp(-\delta E/2k_BT)}{exp(-\delta E/2k_BT) + exp(\delta E/2k_BT)}, \tag{5}$$

and Kawasaki dynamics also satisfy detailed balance. However, the dynamics of thermally excited processes are *properly* described by

$$w_e(c_i, c_f) = exp[-E_b(c_i, c_f)/k_BT], \tag{6}$$

where $E_b(c_i, c_f)$ is the energy barrier for a particle to hop, which changes the configuration from c_i to c_f. This has been used in some previous Monte-Carlo simulations of adsorbed gases **(8-13)**. When using Kawasaki dynamics, τ can be considered to be a temperature-dependent quantity, $e^{Q/k_BT}/\nu$, where Q is an average energy barrier that the particles have to surmount when hopping from site to site, and ν is the frequency of the frustrated translational motion parallel to the surface **(1,2)**. The quantity Q is temperature dependent because the configuration of the lattice-gas particles is temperature dependent. However, with Kawasaki dynamics τ is normally taken to be the unit of time, and the temperature dependence of Q is lost from the simulation. From this point of view, we can consider Kawasaki dynamics to be a procedure for sampling which merely satisfies the detailed balance condition for the equilibrium configuration distribution. On the other hand, w_e *is a physical quantity:* the probability of success for thermally excited barrier crossing. When using w_e in a simulation, τ would simply be $1/\nu$.

II. Results and Discussion

The probability w_k can be regarded as resulting from a rescaling of w_e. Consider a particle hopping from site i to site j over an energy barrier, as shown in Fig. 1. The relationship between w_k and w_e is

$$w_k(i,j) = Aw_e(i,j), \tag{7}$$

where

$$A = [exp(\frac{\delta E}{2k_BT} + \frac{|\epsilon|}{k_BT})]/[exp(\frac{\delta E}{2k_BT}) + exp(-\frac{\delta E}{2k_BT})], \tag{8}$$

and ϵ is defined in Fig. 1. In an interacting lattice-gas system, the difference in energy for each pair of sites will depend on the local configuration around the pair. Thus there will be a specific value of A for each type of neighborhood in which a pair of sites finds itself. In the case where there is no lateral interaction between the particles of the lattice gas, there is only one value of A. In this case, even if the microscopic events actually occur with probabilities w_e, a simulation can be done using Kawasaki dynamics. The real time is then $t_r = \tau S/AN$; whereas if the simulation had been done with probabilities w_e, then the real time would be $t_r = \tau S/N$, where S is the number of Monte-Carlo steps. In order to obtain the real time, the time obtained using Kawasaki dynamics just needs to be multiplied by the factor A, if the underlying dynamics are actually described by the probabilities w_e. *This, however, is not possible if there are lateral interactions and, hence, more than one value of A.*

Let us now compare the processes of hopping between sites i and j and sites j and k. Generally, the three sites have different energies, and the values of A defined by Eq.(8) for the pairs of sites (i,j) and (j,k) are not equal. If we normalize $w_e(i,j)$ with respect to $w_e(i,j) + w_e(j,i)$, we find that

$$\frac{w_e(i,j)}{w_e(i,j) + w_e(j,i)} = w_k(i,j). \tag{9}$$

Hence, Kawasaki dynamics rescale the probabilities of barrier crossing so that for the barrier between any two sites (i,j), $w_k(i,j) + w_k(j,i) = 1$, cf. Eq.(5). For barriers where $w_e(i,j) + w_e(j,i) > 1$, the sum of the rates of hopping is decreased; whereas for barriers where $w_e(i,j) + w_e(j,i) < 1$, this sum is increased. As a result of this rescaling, Kawasaki dynamics require shorter computational times for simulating processes where the values of w_e are very small. When the values of w_e are very small, a 'hop' has to be attempted many times before it is successful. Hence, computer time can become prohibitive.

In such cases, which occur when the temperature of the lattice gas is relatively low, Monte-Carlo simulations should not be done by addressing particles at random. Rather, all the possible hops should be grouped according to their values of w_e. Then a particular hop (a particular particle and a particular lattice direction) is picked according to the *relative probability* $P_q = n_q w_{e,q} / \sum_q n_q w_{e,q}$ where n_q is the number of possible hops in the qth group which has a probability of success equal to $w_{e,q}$. This is done by generating a random number r such that $0 < r \leq 1$. The first value of s for which $\sum_{q=1}^{s} P_q \geq r$ is the group of hops that is selected. One hop out of all the possible hops in the sth group is selected at random. The configuration is changed each time a particular hop is picked. This algorithm for Monte-Carlo simulations, where the probability of success of a hop is determined before the hop is picked, rather than after, is called the 'n-fold' way **(14)**. It makes it feasible to do simulations, both dynamic and static, when the probability of a change in the configuration is much smaller than unity. In the calculation of static quantities, the configurational changes do not have to correspond to physical events. It is only important that the transition probabilities which are used produce the correct equilibrium solution of the the master equation, cf. Eq. (1). However, for calculating dynamic quantities, the configurational changes correspond to real events, such as the hopping of an adatom from one adsorption site to another. Hence, for simulations of dynamic processes the choice of the time increment for

each sampling step is crucial. The hop attempt frequency is $1/\tau$, and the average number of attempts that occurs before a hop in the qth group is successful is $1/w_{e,q}$. Thus the time is increased by $\tau/Nw_{e,q}$ for each hop in the qth group, where N is the total number of particles. The factor of $1/N$ occurs because each particle provides a clock, but all the N clocks are running in parallel. We have used this procedure to simulate the dynamics of domain ordering on a square lattice gas with equal and repulsive nearest and next-nearest neighbor interactions. At a fractional coverage of 0.5, the lattice gas forms fourfold degenerate (2x1) ordered domains below a critical temperature given by $k_BT_c/\phi \sim 0.525$ **(15)**, where ϕ is the strength of the lateral interactions. The values of the barriers $E_b(c_i, c_f)$ are obtained from the model (harmonic) potentials shown in Fig. 2, in which

$$E_i = k\zeta^2/2 + \alpha_i, \tag{10}$$

and

$$E_f = k(\zeta - \lambda)^2/2 + \alpha_f, \tag{11}$$

where k is the force constant of the harmonic wells, α_i and α_f are the heights of the bottoms of the initial and final adsorption wells, ζ is the coordinate for hopping, and λ is the lattice constant. In this case,

$$\alpha_i = \phi N_i, \tag{12}$$

where N_i is the total number of occupied nearest and next-nearest neighbor sites, i.e., the energy zero is the energy of an ' isolated' adatom. The quantity $E_b(c_i, c_f)$ is the difference in energy between the point of intersection of E_i and E_f and the bottom of the well described by E_i. In our simulations, we have set $k\lambda^2 = 20\phi$ **(16)**, and we have studied diffusion of the lattice gas and the kinetics of domain growth with Monte-Carlo techniques using w_k and w_e. If $\lambda \sim 3$ Å , $\phi \sim 2$ kcal/mol and $\mu \sim 10$ AMU, then $k\lambda^2 = 20\phi$ implies an adatom frustrated translational frequency parallel to the surface of $\nu_{\|} \sim 72$ cm^{-1}. We have also performed simulations with

the Metropolis walk algorithm for the temperature regime where domain growth occurs.

The initial configurations are generated by randomly placing 5000 particles on a 100x100 lattice, so that the effective initial temperature for all runs is infinity and the fractional coverage is one-half. We performed 30 runs for each temperature and obtained the mean-square displacement of the particles from the simulations for $0.6\phi/k_B \leq T \leq 5\phi/k_B$. After an initial period of time to allow the system to "forget" its initial configuration, the mean-square displacement varies linearly with time, with a slope proportional to the diffusion coefficient. The temperatures are sufficiently high that the effect of the order-disorder transition **(17)** on the diffusion behavior is not observed. We plot in Fig. 3 the logarithm of the slope as a function of the reciprocal of the corresponding temperature in order to obtain the effective energy barrier to diffusion. The asterisks are results from simulations using w_k, and the circles are results from simulations using w_e. Since we used only temperatures above the critical temperature, we did not observe a significant variation in the energy barrier for diffusion. The average diffusion barrier obtained using the probabilities w_e varies from $\sim 2.6\phi$ at the higher temperatures to $\sim 3.0\phi$ at the lower temperatures. As the temperature is lowered, the probability of finding local configurations which are energetically more favorable, and thus have a higher diffusion barrier, becomes higher. Thus, the average diffusion barrier is expected to increase slightly with decreasing temperature, even when the lattice gas is still above the critical temperature for ordering. At an infinite temperature, where the correlation length is zero, the average neighborhoods of a particle before and after a hop are the same, and α_i and α_f are equal. With our model, this gives a diffusion barrier of 2.5ϕ.

By the same argument, at an infinite temperature, Kawasaki dynamics would show a zero energy barrier to hopping. Our results for simulations using Kawasaki dynamics, indicated by the asterisks in Fig. 3, show that the average barrier tends

to zero at high temperatures. However, the values obtained from simulations using w_k at finite temperatures cannot be easily interpreted since, as described earlier, we can consider each w_k to result from a rescaling of a corresponding w_e. Using the procedure described earlier for small w_e, t_r is increased by $\tau/Nw_{e,q}$ for each hop. If a simulation is carried out with this procedure but using the probabilities w_k, the time increment for each hop is $\tau/Nw_{k,q}$. If, however, for each hop in the simulations using w_k, we increase t_r by $\tau A_q/Nw_{k,q}$, we obtain the results shown by the crosses in Fig. 3. The results are also shown in Table 1. The additional factor of A_q for each hop, the value of A_q depending on the type of hop, means that *the correct time increment is used for each hop.* As discussed earlier the probabilities w_k are obtained by rescaling the values of $w_e(i,j)$ and $w_e(j,i)$ by $w_e(i,j)+w_e(j,i)$. For temperatures which are relatively low, each value of w_e is very small, and this rescaling increases the probability of hopping so that the diffusion coefficient is higher when using Kawasaki dynamics. However, for temperatures which are sufficiently high so that $w_e(i,j) + w_e(j,i) > 1$, this rescaling would actually lower the probability of hopping and, hence, lower the diffusion coefficient. This may be seen by comparing the asterisks and the crosses in Fig. 3. The rescaled Kawasaki results are in good agreement with those using the proper energy barrier at temperatures which are high compared to ϕ/k_B, with progressively greater disagreement at progressively lower temperatures. This may be seen by comparing the circles and the crosses in Fig. 3, and it is shown more clearly in Fig. 4 where we plot the temperature dependence of D_r/D_e, the ratio of the diffusion coefficient obtained from using w_k (and rescaling the time for each hop by A_q) to the diffusion barrier obtained from using w_e. This behavior is observed because at high temperatures the relative probabilities P_q calculated from w_e and from w_k for each type of hop are approximately the same. However, the lower the temperature, the greater the difference between the value of P_q calculated from w_e and that calculated from w_k. This affects the time evolution since the moves are picked according to their relative

probabilitites. Hence, as discussed earlier, in lattice-gas systems with lateral interactions, *simulations using Kawasaki dynamics are not equivalent to simulations using* w_e. Only when there are no lateral interactions can rescaling the time give equivalent results. At sufficiently high temperatures, using Kawasaki dynamics is approximately equivalent to using w_e because $A_q \sim 1/2$, a constant regardless of the local configuration. Simulations using the Metropolis walk would be expected to also show similar deviations from simulations using w_e.

Lattice-gas diffusion has been investigated rather extensively by Monte-Carlo methods. In some of these studies, the transition probabilities were computed by considering the *energy difference* between the final and the initial configurations. Both Kawasaki dynamics **(17-19)** and the Metropolis walk **(20,21)** have been used. In other studies **(8-13)** the transition probabilities were computed by considering the *energy barrier* between the final and the initial configurations. We have shown here that the particular choice of transition probabilities influences the temperature dependence of the diffusion coefficient. As was noted previously in studies where Metropolis walk simulations were used to obtain the temperature dependence of the diffusion coefficient, these time-dependent Monte-Carlo simulations used a clock the timescale of which is not known **(21)**. If another set of transition probabilities such as w_e or w_k were used, then the ratio of the calculated diffusion coefficients at a specific temperature would depend on the ratio of the respective timescales. This would not be an obstacle if the ratio were independent of the temperature. However, we have shown that this is not the case, and that the experimentally accessible temperature dependence of the diffusion coefficient for thermally excited motion of adsorbed particles can be incorrectly computed if inappropriate transition probabilities are used.

Kawasaki dynamics **(5-7)** have been widely used to study the kinetics of domain growth **(22-34)**. One of the major issues is the value of the growth exponent x defined by $l \sim t^x$, where l is an average length scale of the ordered domains and t

is the time. *Since such simulations are for temperatures that are low compared to* ϕ/k_B, *it is very important to compare the results from simulations using* w_k *and* w_e. The results from simulations of lattice gas diffusion above have shown that the ratio of the timescales for simulations using w_e and w_k is temperature dependent, i.e., we have shown that there is a temperature-dependent multiplicative factor relating the timescales in simulations using w_e and simulations using w_k. This multiplicative difference between the timescales would not affect the isothermal value of the growth exponent. *However, it is not clear whether a linear relationship holds between the timescales of Monte-Carlo simulations which use different values of* $w(c_i, c_f)$. Under conditions where the simulations have reached equilibrium, this is not an important consideration. In this case, the average value of the factor A, cf., Eq.(8), is constant since the distribution of types of hops that are taken is stationary. Hence, a linear relationship holds between the timescales of simulations using w_e and those using w_k or w_m. This is the reason for observing, in the diffusion simulations discussed above, the same linear scaling of mean-square displacement with time whether w_e or w_k was used. However, for simulations where the system is far from equilibrium, the distribution of types of hops that are taken changes as the simulations proceed. This is the case for simulations of domain growth. Since x is the exponent of the time, the value of x obtained from simulations can be accurate only if x is obtained in a regime of domain growth where the distribution of types of hops that are taken in the simulations changes in concert with that in a real system. We cannot compare simulations directly with a real system, but we can compare the time evolution in simulations which use different transition probabilities. This would determine whether or not the choice of the transition probabilities is important for simulations of systems evolving towards equilibrium.

We have performed simulations at a temperature $T = 0.3325\phi/k_B$ using w_k, w_m and w_e. For the simulations for w_e and w_m, we used a $LxL = 100x100$ lattice and performed 40 runs. For the simulations for w_k, we performed only 15 runs

since reliable data are already available for this case **(31)**. All simulations were allowed to run sufficiently long that the final domain sizes are approximately $L/3$. For the simulations using w_e and w_m, we also performed five runs each on 200x200 lattices to ensure that "finite-size effects" do not influence the results. Time is measured in Monte-Carlo steps, as usual, for the simulations using both Kawasaki dynamics and the Metropolis walk. For the simulations using w_e, real time is calculated explicitly, as discussed earlier. The results are shown in Figs. 5-8. Simulations using Kawasaki dynamics for this system at the same temperature have been performed previously, and our results for Kawasaki dynamics, which are shown in Fig. 5, agree with those simulations **(31)**. The growth exponent we obtained using Kawasaki dynamics is $x_k \sim 0.34 \pm 0.01$, where the uncertainty here (and below) refers to one standard deviation in a linear least-squares fit to the calculated data. This growth exponent is obtained from the data points between the arrows indicated in Fig. 5. In Fig. 6 we show the results from simulations using the Metropolis walk, where the data points between the arrows give a growth exponent of $x_m \sim 0.277 \pm 0.007$. (If all data points are included, the best fit gives $x_m \sim 0.300 \pm 0.008$). Figure 7 shows the results from a single run using w_e, and Fig. 8 shows the average of 45 runs using w_e. The data points between the arrows in Fig. 8 give $x_e \sim 0.329 \pm 0.004$. Just as we can regard $w_k(c_i, c_f)$ to be the result of rescaling $w_e(c_i, c_f)$ with respect to $w_e(c_i, c_f) + w_e(c_f, c_i)$, we can consider $w_m(c_i, c_f)$ to be the result of rescaling $w_e(c_i, c_f)$ with respect to $max[w_e(c_i, c_f), w_e(c_f, c_i)]$. Our results show that t_s in the simulations using the Metropolis algorithm does not scale linearly with t_s in the simulations using Kawasaki dynamics. The values of x_k and x_e, however, are in rather close agreement. This means the value of x can be affected by the type of transition probabilities that is used even though the total particle number is conserved in all cases. This, as we suggested above, can arise because the distribution of hops that are taken is changing in these simulations, and they do not change in concert for simulations using different forms for $w(c_i, c_f)$.

We conclude that all interpretations of dynamic Monte-Carlo simulations must be made with some care. For instance, the value of $x = 1/3$ has been suggested for the system that we have studied on the basis of simulations using Kawasaki dynamics **(34)**. It was argued that this value results from the long-range diffusion of lattice-gas particles from domain walls with excess local density to domain walls with deficit local density. Clearly, the same long-range diffusion of lattice-gas particles must also occur when a Metropolis walk is used. However, our results indicate a significantly different growth exponent for the Metropolis walk. We can conclude that with other constraints the same (such as the conservation law for the total particle number and the degeneracy of the ground state), the choice of the transition probabilitites can influence the value of x that is calculated. This can be interpreted to mean that if the microscopic processes, in two otherwise similar systems, have different forms for $w(c_i, c_f)$, then the values of x could be different. This serves to underscore in a dramatic fashion the importance of correctly converting simulation time to real time, and this occurs naturally for thermally excited processes when employing the proper energy-barrier model that we have developed.

III. Conclusions

In conclusion, we have demonstrated the importance of the choice of the transition probabilities in Monte-Carlo simulations. We find that the ratio of time scales using different choices for $w(c_i, c_f)$ is dependent on temperature and affects calculations of diffusion coefficients, particularly at low temperatures. We also find that under non-equilibrium conditions the timescales using different choices for $w(c_i, c_f)$ do not necessarily scale linearly. This affects the calculation of dynamic quantities such as the growth exponent of ordered domains using Monte-Carlo simulations. In general, the correct growth exponent can be obtained only if the transition probabilities that are used correctly describe the microscopic dynamics, which for thermally excited processes have the form $e^{-E_b(c_i,c_f)/k_BT}$. Specifically, we find that for the

ordering of fourfold degenerate (2x1) domains on a square lattice, the growth exponent obtained using the Metropolis walk is $x_m \sim 0.277$, and is significantly different from the value $x_e \sim 0.329$ obtained from simulations using w_e within the context of an energy-barrier crossing model we have developed. The value of x_e is quite close to that of x_k (using Kawasaki dynamics) so that the non-linearity between the timescales using w_e and w_k is not large, at least in the regime where the domain growth exponents were obtained. However, as we have argued above, x_e not x_k should be the correct growth exponent for the thermally excited process of domain growth of adsorbed particles.

Acknowledgment: This research was supported by the National Science Foundation under Grant No. DMR-8500789.

References

1. **Monte-Carlo Methods in Statistical Physics** K. Binder, Ed., Topics in Current Physics, Vol. 7, Springer-Verlag, Heidelberg, 1979.
2. **Applications of the Monte-Carlo Methods in Statistical Physics**, K. Binder, Ed., Topics in Current Physics, Vol. 36, Springer-Verlag, Heidelberg, 1983.
3. O.G. Mouritsen, **Computer Studies of Phase Transitions and Critical Phenomena**, Springer-Verlag, Heidelberg, 1984.
4. M. Metropolis, A.W. Rosenbluth, M.N. Rosenbluth, A.N. Teller and E. Teller, J. Chem. Phys. **21**, 1087 (1953).
5. K. Kawasaki, Phys. Rev. **145**, 224 (1966).
6. K. Kawasaki, Phys. Rev. **148**, 375 (1966).
7. K. Kawasaki, Phys. Rev. **150**, 285 (1966).
8. M. Bowker and D.A. King, Surface Sci. **71**, 583 (1978).
9. D.A. Reed and G. Ehrlich, Surface Sci. **102**, 588 (1981).
10. D.A. Reed and G. Ehrlich, Surface Sci. **105**, 603 (1981).
11. E.S. Hood, B.H. Toby and W.H. Weinberg, Phys. Rev. Letters **55**, 2437 (1985).
12. C.H. Mak, H.C. Andersen and S.M. George, J. Chem. Phys. **88**, 4052 (1988).
13. H.C. Kang and W.H. Weinberg, to be published.
14. A.B. Bortz, M.H. Kalos and J.L. Lebowitz, J. Comp. Phys. **17**, 10 (1975).
15. K. Binder and D.P. Landau, Phys. Rev. B **21**, 1941 (1980).
16. Additional runs with $k\lambda^2 = 800\phi$ show that the growth-exponent is not influenced to within statistical error by a change in the value of $k\lambda^2/\phi$.
17. A. Sadiq and K. Binder, Surface Sci. **128**, 350 (1983).

18. R. Kutner, K. Binder and K. Kehr, Phys. Rev. B **26**, 2967 (1982).

19. R. Kutner, K. Binder and K. Kehr, Phys. Rev. B **28**, 1846 (1983).

20. N. Tringides and R. Gomer, Surface Sci. **145**, 121 (1984).

21. X.P. Jiang and H. Metiu, J. Chem. Phys. **88**, 1891 (1984).

22. K. Binder and D. Stauffer, Phys. Rev. Letters **33**, 1006 (1974).

23. K. Binder, C. Billotet and P. Mirold, Z. Phys. B **30**, 183 (1978).

24. K. Binder, Phys. Rev. B **15**, 4425 (1977).

25. J. Marro, J.L. Lebowitz and M.H. Kalos, Phys. Rev. Letters **30**, 289 (1982).

26. P.S. Sahni, J.D. Gunton, S.L. Katz and R.H. Timpe, Phys. Rev. B **25**, 289 (1982).

27. P.S. Sahni and J.D. Gunton, Phys. Rev. Letters **45**, 369 (1980).

28. S.A. Safran, Phys. Rev. Letters **46**, 1581 (1981).

29. P.S. Sahni and J.D. Gunton, Phys. Rev. Letters **47**, 1754 (1981).

30. P.S. Sahni, G. Dee, J.D. Gunton, M.K. Phani, J.L. Lebowitz and M.H. Kalos, Phys. Rev. B **24**, 410 (1981).

31. S. Sadiq and K. Binder, J. Stat. Phys. **35**, 517 (1984).

32. P.S. Sahni, G.S. Grest and S.A. Safran, Phys. Rev. Letters **50**, 60 (1983).

33. S.A. Safran, P.S. Sahni and G.S. Grest, Phys. Rev. B **28**, 2693 (1983).

34. J. Vinals and J.D. Gunton, Surface Sci. **157**, 473 (1985).

$k_B T / \varphi$	D_e	D_r	D_k
0.60	0.00675± 0.00007	0.00751± 0.00009	0.159±0.017
0.75	0.0178±0.0002	0.0196±0.0003	0.213±0.003
1.00	0.0486±0.0006	0.00512±0.0005	0.273±0.003
2.00	0.219±0.003	0.218±0.002	0.367±0.004
3.00	0.343±0.004	0.347±0.004	0.395±0.006
5.00	0.479±0.004	0.484±0.005	0.403±0.003

Table 1.

The diffusion coefficients are in units of $\lambda^2 \tau^{-1}$.

The subscripts e, r and k denote energy-barrier, rescaled Kawasaki and Kawasaki, respectively.

The standard deviations are shown for each datum point.

Figure Captions

Figure 1. Quantities used in Eq. (8) to rescale w_e to w_k, when hopping from site i to site j.

Figure 2. Model for diffusion barrier described by Eqs. (10) and (11). The bottoms of the potential wells at the adsorption sites i and f are α_i and α_f, respectively. The bottom of the potential well for an adsorption site with no nearest or next-nearest neighbor adatom is the zero of energy.

Figure 3. Plot of lnD vs. ϕ/k_BT, where D, in units of λ^2/τ, is the slope of the mean-square displacement of an adatom vs. time, i.e., the diffusion coefficient. The quantity ϕ is the lateral interaction strength, λ is the lattice constant, and τ is the inverse of the attempt frequency. The circles are data for simulations using w_e, the asterisks are data for simulations using w_k, and the crosses are data for simulations using w_k but with time rescaled as explained in the text.

Figure 4. Plot of D_r/D_e vs. k_BT/ϕ. The quantity D_r is the diffusion coefficient obtained for simulations using w_k and rescaled time. The quantity D_e is the diffusion coefficient obtained for simulations using w_e.

Figure 5. Average of 15 Kawasaki dynamics runs for ordering of fourfold degenerate (2x1) domains on a square lattice at a fractional coverage of one-half and a temperature of $0.3325\phi/k_B$. The quantity ϕ is the lateral interaction strength. The lattice size used is 100x100. The best fit for the growth exponent using the data points between the arrows is $x_k = 0.34 \pm 0.01$. This agrees well with the extensive work of Sadiq and Binder who obtained a value of $x_k \sim 0.35$ **(30)**.

Figure 6. Average of 45 Metropolis runs for the same system as in Fig. 5. Forty runs were done on a lattice of 100x100, and five runs were done on a lattice of

200x200. For the domain sizes that were reached, no finite size effects were observed. The best fit for the growth exponent using the data points between the arrows is $x_m = 0.277 \pm 0.007$. If all the data points are used, a best fit of $x_m = 0.300 \pm 0.008$ is obtained.

Figure 7. A typical single run using the energy-barrier model. The fractional coverage is one-half and the temperature is $0.3325\phi/k_B$, i.e., the same as in Figs. 5 and 6. The additional parameter necessary in these simulations is the force constant of the model harmonic potential wells illustrated in Fig. 2. For our simulations, we have set the force constant to be $k = 20\phi/\lambda^2$, where ϕ is the lateral interaction strength and λ is the lattice constant.

Figure 8. Average of 45 runs using the energy-barrier model, of which a typical single run is shown in Fig. 7. (The simulation parameters are summarized there.) Forty runs were done on a lattice of 100x100, and five runs were done on a lattice of 200x200. For the domain sizes reached here, no finite size effects were observed. The best fit for the growth exponent using the data points between the arrows is $x_e = 0.329 \pm 0.004$.

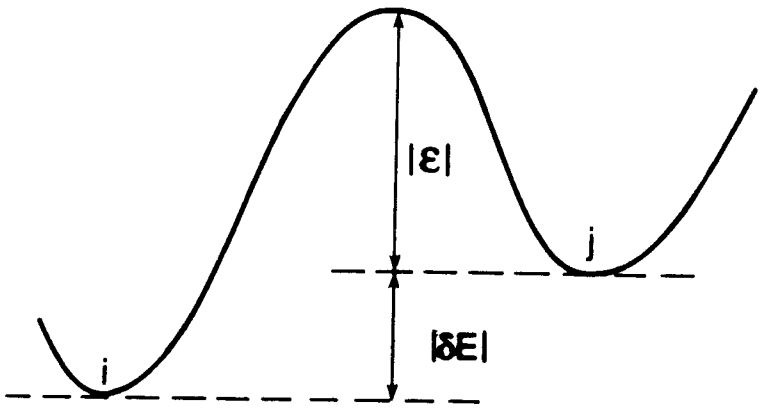

Figure 1

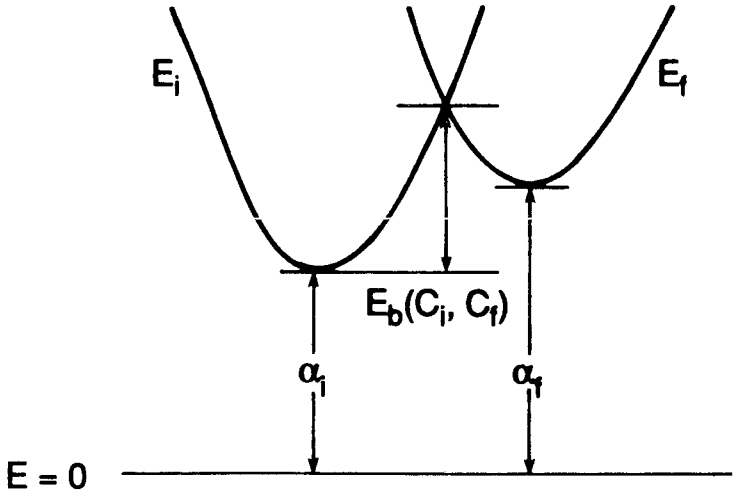

Figure 2

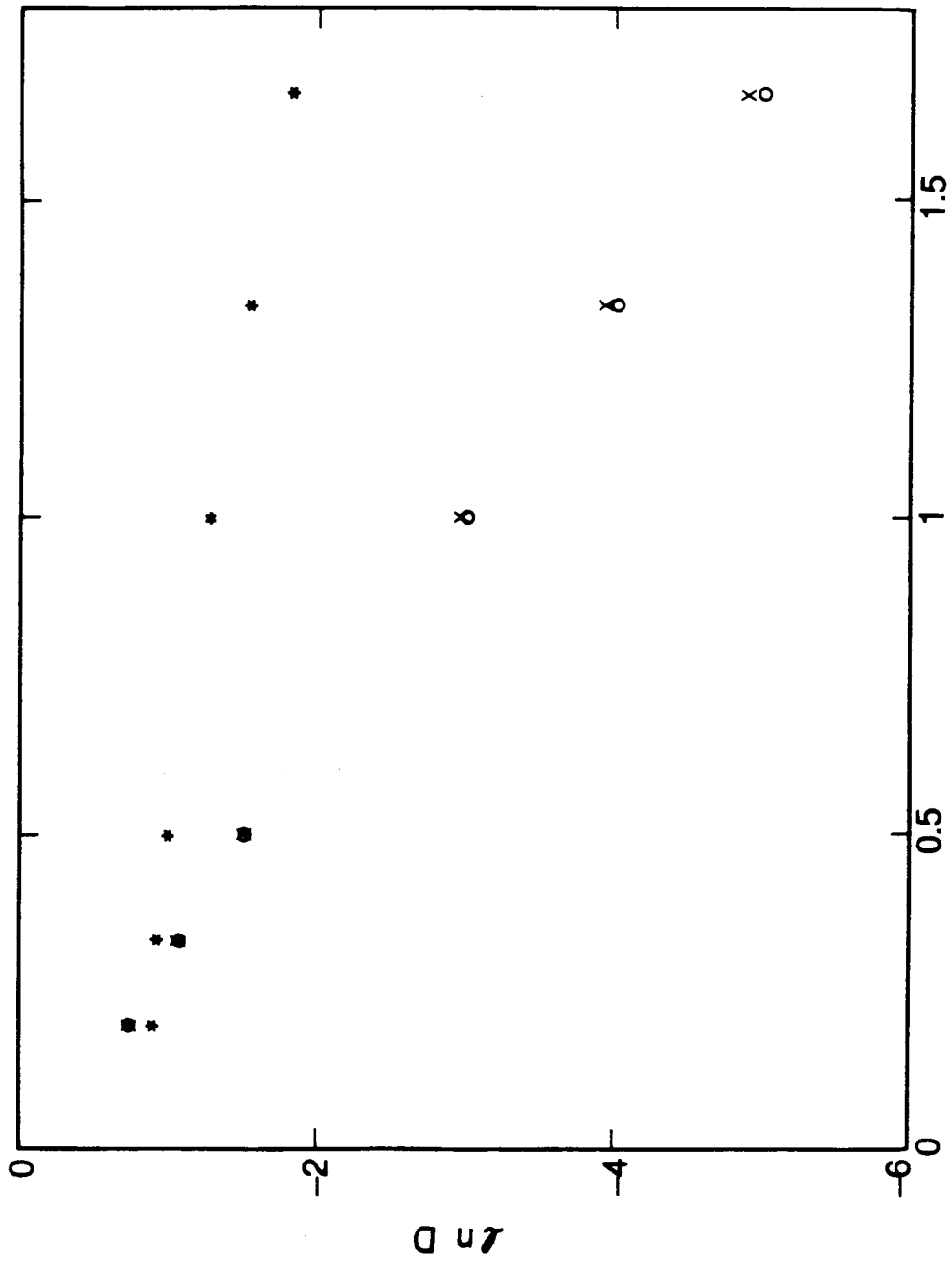

Figure 3

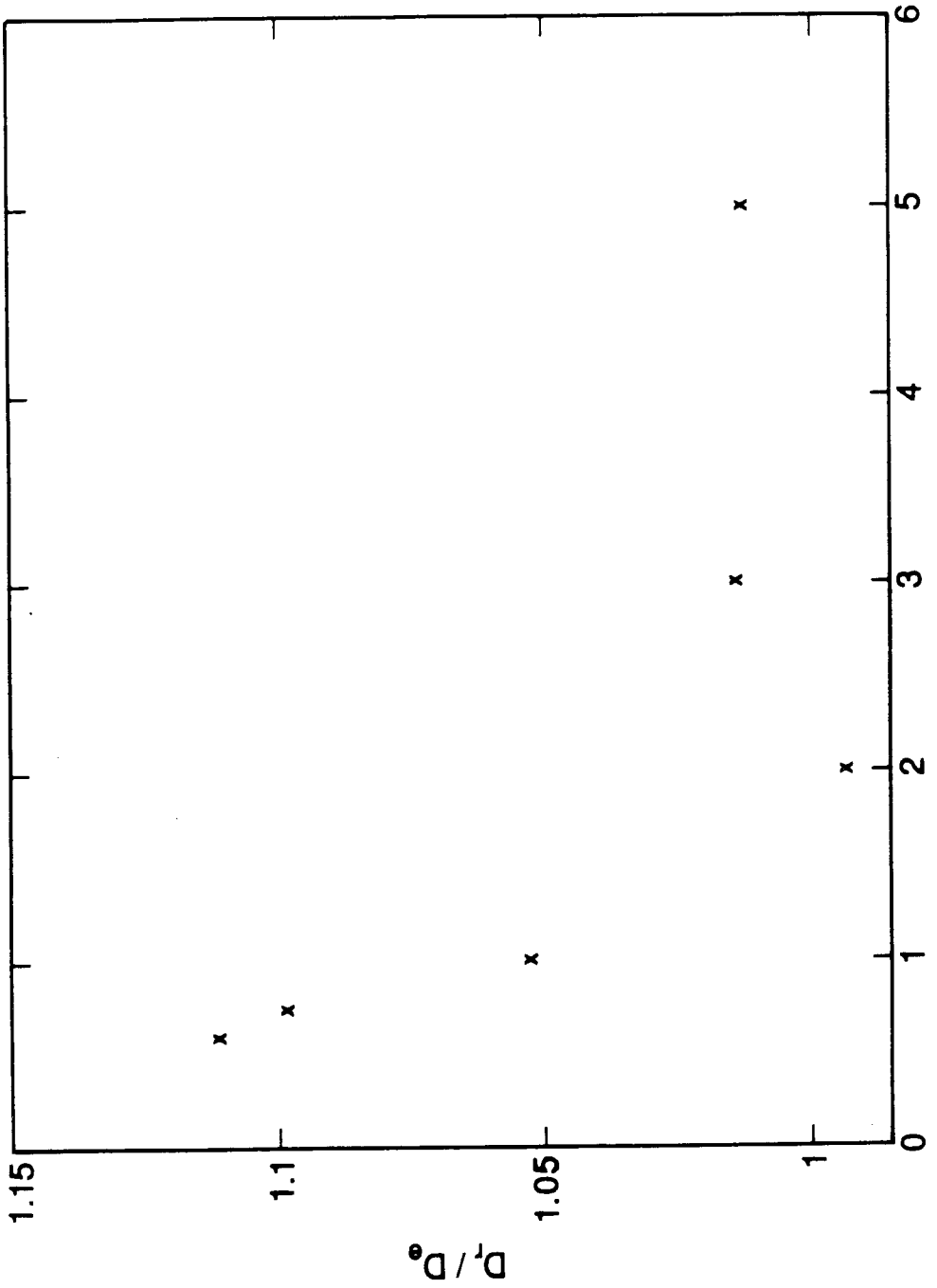

Figure 4

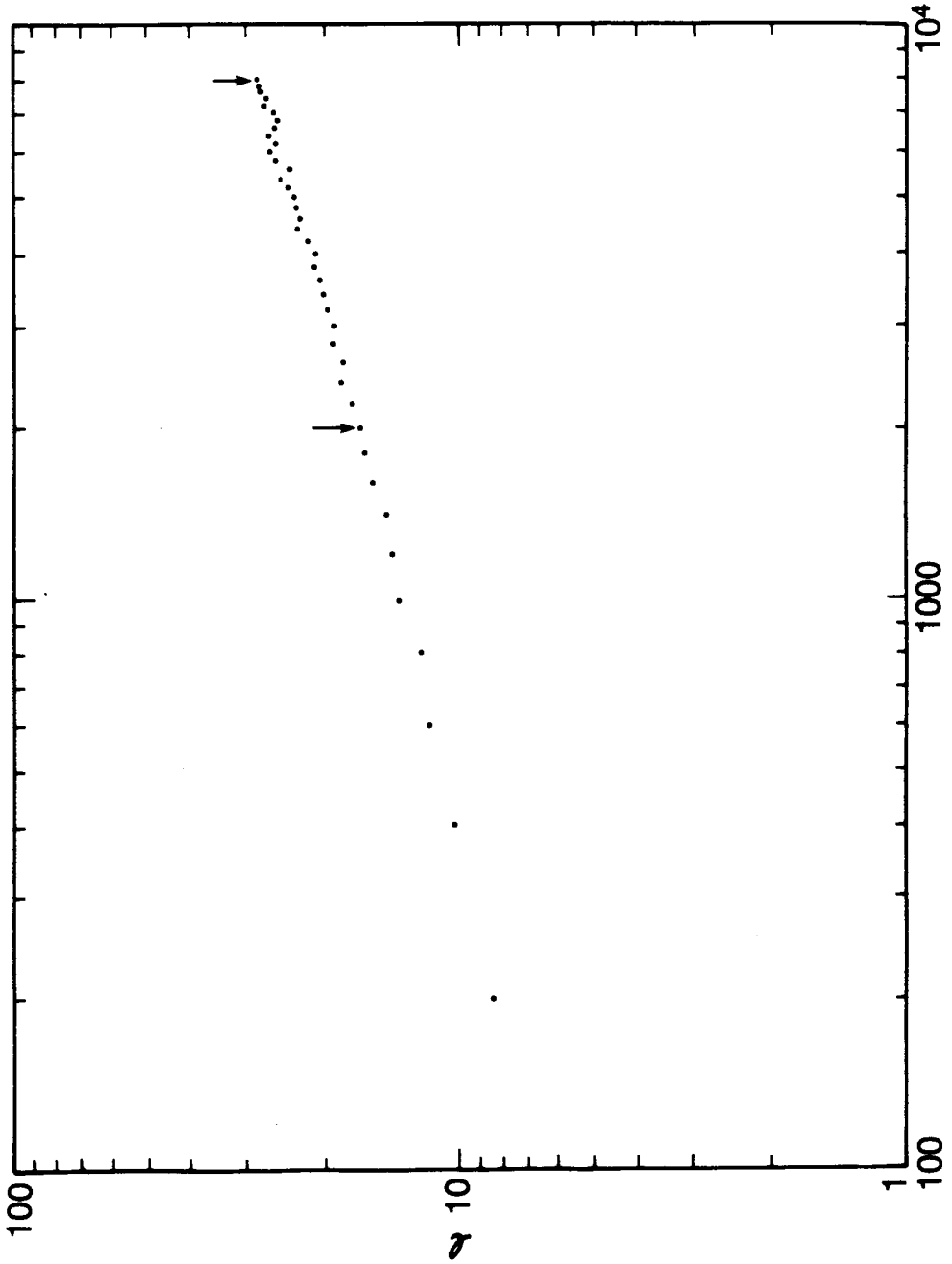

Figure 5

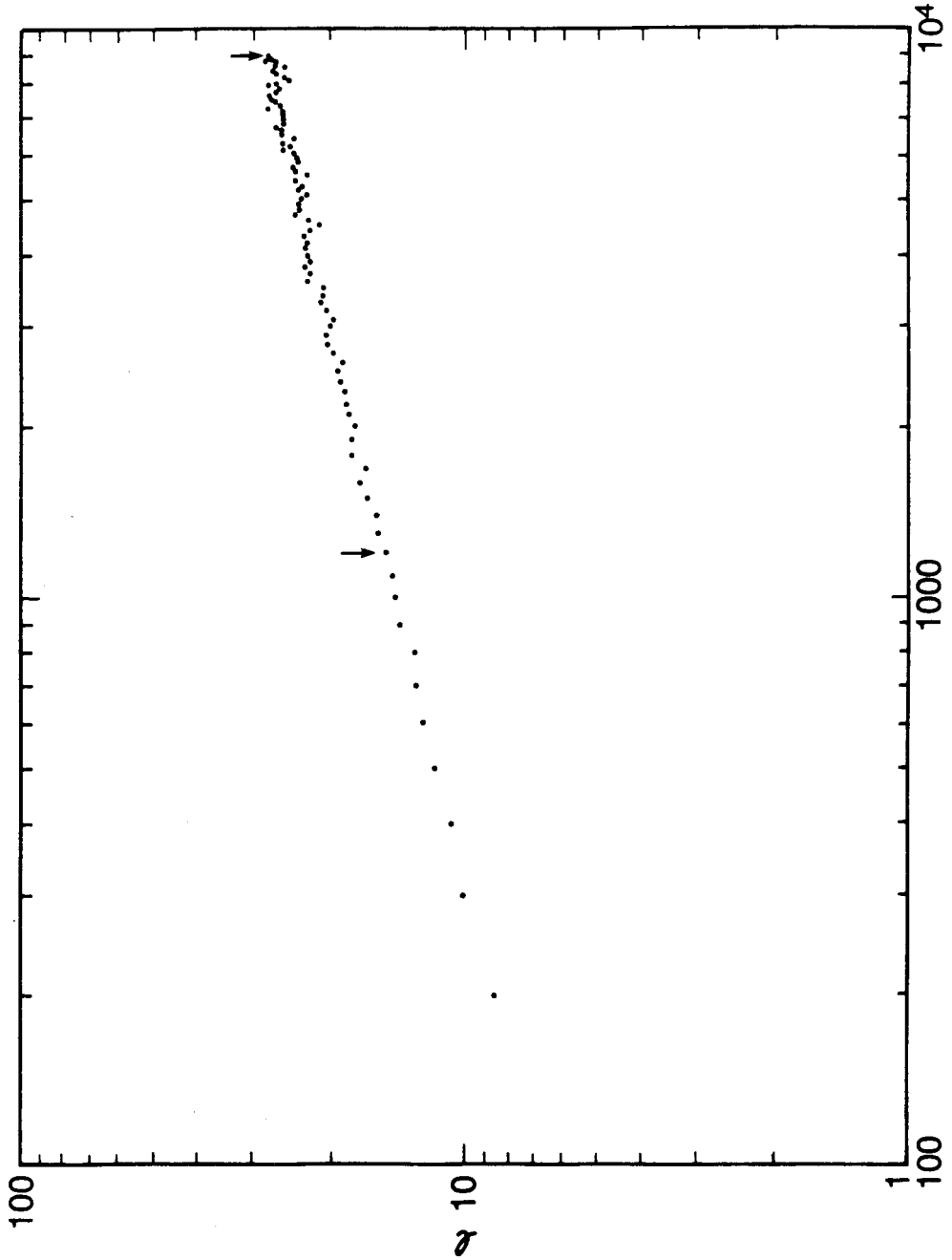

Figure 6

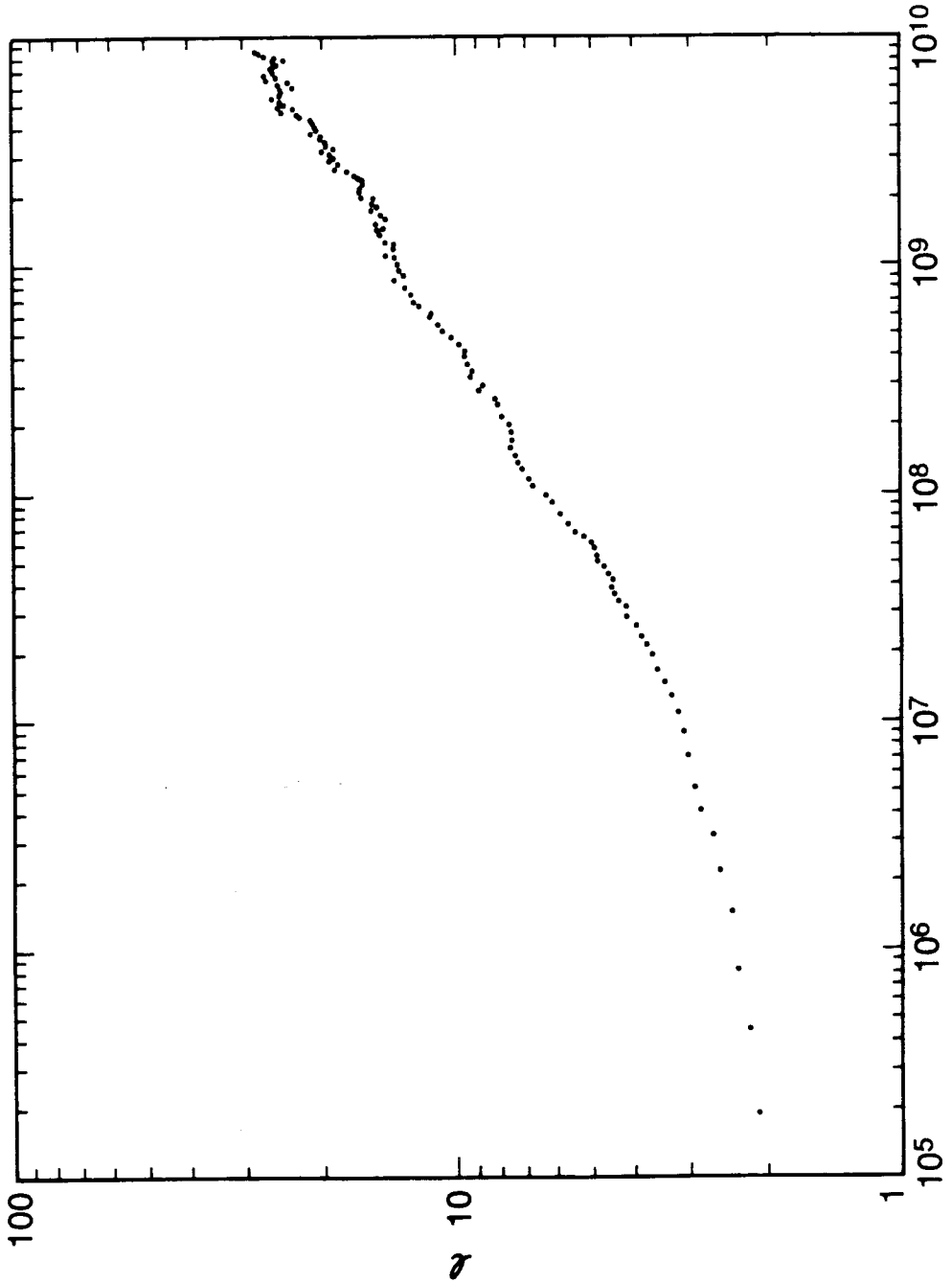

Figure 7

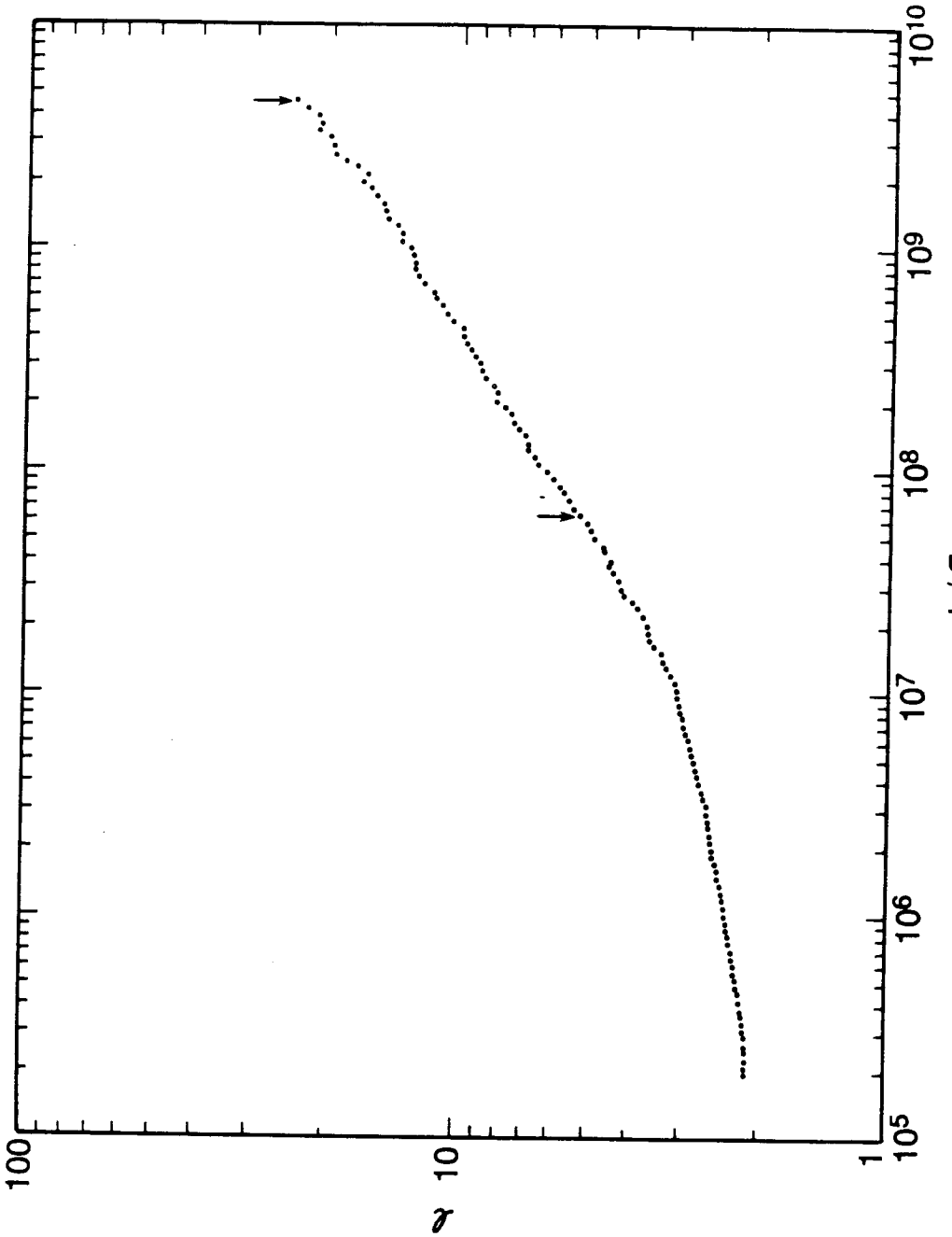

Figure 8

Chapter 2.

Kinetics of Precursor-Mediated Ordering of Two-Dimensional Domains

This chapter was published as a paper by H.C. Kang and W.H. Weinberg, in *The Physical Review B*, **38**, 11543 (1988).

ABSTRACT

Monte-Carlo simulations have been carried out to study the kinetics of precursor-mediated ordering of a lattice gas with nearest and next-nearest neighbor repulsive interactions. We find that the growth exponent x is affected strongly by the rate at which a precursor is deexcited into a chemisorbed state. If this rate is high, x is close to the value obtained for conservation of density. If this rate is low, x is close to the value for non-conserved density even though the total number of particles is actually conserved. We conclude that the length of precursor 'hops' influences the growth exponent.

PACS numbers: 68.35.F, 68.35.J, 68.35.R, 81.60, 82.65.M

When an adsorbed system is quenched below an order-disorder transition temperature, ordered *domains* begin to form. If the ground state is degenerate, the local configurations at the boundaries between domains are not those with the lowest free energy. To reduce the total free energy of the system, the lengths of these boundaries are reduced, and the domain sizes become larger. In Monte-Carlo studies of the kinetics of domain growth with lattice gas models, two types of dynamics have been used widely: Kawasaki dynamics and Glauber dynamics **(1-3)**. In Kawasaki dynamics, which simulate closed systems, particles migrate from one lattice site to a vacant nearest-neighbor lattice site. Glauber dynamics, which simulate open systems, allow exchange of particles with an external reservoir.

By analogy to static critical phenomena, it has been proposed **(4,5)** and observed **(6-9)** that at late stages of growth, when the domain sizes are much larger than all microscopic lengths, the growth law has a power law form $l \sim t^x$, where l is the length scale of the domains. The physics of domain growth is governed by only one length scale: the size of the domains. One of the main goals in the study of kinetics of domain growth is to determine the value of the growth exponent x and to establish the factors that affect its magnitude.

For a square lattice gas that orders into a c(2x2) structure, the degeneracy is $p = 2$, and the growth exponent is $x = 1/2$, independent of whether Kawasaki or Glauber dynamics are used **(10-20)**.The situation, however, is not so clear for $p > 2$. This occurs, for example, in the case of a lattice gas with equal repulsive nearest and next-nearest neighbor interactions on a square lattice. In this case a (2x1) structure with $p = 4$ occurs when the lattice gas is quenched below the transition temperature. For a fractional coverage of 0.5, this transition temperature is $1/\beta_t\phi = 0.525$ **(21)**, where ϕ is the lateral interaction strength. Sadiq and Binder **(22)** have studied this system in detail, showing that $x \sim 0.35$ for Kawasaki dynamics and $x \sim 1/2$ for Glauber dynamics. In the case of Kawasaki dynamics, they argued that domain growth is governed by the diffusion of an excess (or deficit) fractional coverage at

the domain walls. It was suggested that diffusion of the adsorbed particles from regions of excess to regions of deficit fractional coverage is necessary for domain growth, and that such a mechanism gives rise to $x \sim 1/3$ (**23**). An investigation by Vinals and Gunton (**24**) of a lattice gas model for hydrogen chemisorbed on Fe(110) was not able, however, to verify this conjecture (**22**). This system has both a (2x1) and a (3x1) phase. The (2x1) phase has degeneracy $p = 2$, and the (3x1) phase has degeneracy $p = 3$. Although domain walls with excess fractional coverage exist for both phases, it was found that $x = 1/2$ for the (2x1) phase, whereas the value of x ranged from ~ 0.14 to ~ 0.25 for the (3x1) phase. Hence, for $p > 2$ domain growth is not well understood. Indeed, a recent Monte-Carlo study even suggested that the Sadiq-Binder result of $x \sim 0.35$ is due to crossover from zero to the true asymptotic value which is 1/2 **(25)**.

These dynamical models have not heretofore considered the possibility of a precursor state. In many real systems, however, precursor states are important intermediates for surface diffusion **(26)**, adsorption and surface reactions **(27,28)**. The preexponential factor for diffusion D_0 of hydrogen adatoms on the Pt(111) surface has been found experimentally **(26)** to be 1.0 cm^2-s^{-1} (at a fractional coverage of 0.24). If we take the lattice constant λ to be 3.0 Å and the vibrational frequency parallel to the surface ν to be 10^{13} s^{-1}, then the value of the preexponential for a random-walk between sites is $D_0 = \lambda^2\nu/4 = 2.25 \times 10^{-3} cm^2$-$s^{-1}$. The high experimental value is strong evidence for the existence of a stable precursor particle that executes many 'hops' before it is deexcited into a chemisorption state. Therefore, we have investigated a lattice gas model with both a strongly bound chemisorption state and a weakly bound, mobile precursor state. We consider a square lattice gas with identical and repulsive nearest and next-nearest neighbor interactions in order to compare with previous results that did not include a precursor state **(22)**. Here two possible adsorption states exist at each site on the lattice, a strongly bound chemisorption state and a weakly bound precursor state. A particle in the

chemisorbed state can only be excited into the precursor state at the same site. On the other hand, a particle in the precursor state can experience one of the four following fates: (1) It can be deexcited into the chemisorbed state at the same site (if there is not another particle chemisorbed there already); (2) It can desorb from the lattice (if the system is open); (3) It can migrate into the precursor state of a nearest neighbor site; or (4) It can remain in the precursor state at the same site. We allow adsorption from the gas phase into the precursor state at any site when an open system is being modeled.

There are five microscopic processes the rates of which we have to consider: excitation, deexcitation, migration, desorption and adsorption. The excitation-deexcitation potential is modeled by two intersecting parabolae, as illustrated in Fig. 1, where $E_1 = k_1\zeta^2/2 + \alpha_1$ and $E_2 = k_2(\zeta - \zeta_0)^2/2 + \alpha_2$, and the variable ζ is the excitation coordinate with origin at the equilibrium position of the chemisorbed particle. The model parameters are k_1, k_2, α_1, α_2 and ζ_0. The zero of energy is the bottom of the chemisorption well of an isolated particle. The bottom of the precursor well is α_2, and the bottom of the chemisorption well is given by $\alpha_1 = \phi_{nn}N_{nn} + \phi_{nnn}N_{nnn}$, where the subscripts indicate nearest and next-nearest neighbor sites, N is the number of occupied sites, and ϕ is the strength of the lateral interaction. The top of the barrier is the point of intersection of the two parabolae. The barrier heights for excitation E_{exc} and deexcitation E_{dex} are therefore functions of the local configuration of chemisorbed particles. We investigate only cases where the precursor density is vanishingly small and hence need not consider the interaction between precursor particles. We assume there is no interaction between a chemisorbed particle and a precursor particle **(28)**. Thus, α_2 is independent of the local configuration of adsorbed particles. The migration and desorption barriers of the precursor, E_{mig} and E_{des}, are also assumed to be constants, independent of the local configuration **(28)**. If we take the 'attempt frequency' to be τ^{-1} for each of the microscopic processes, the probabilities of success in each attempt is

the appropriate Boltzmann factor. The probability of adsorption p_{ads} is assumed to be constant and is chosen according to the value of the probability of desorption and the constraint of constant average fractional coverage.

The method we use differs from those used by previous investigators in two ways. First, the probability of success of a microscopic event is calculated using the *proper energy barrier* which has to be surmounted to go from the initial state to the final state. This is in contrast to Kawasaki and Glauber dynamics where the probability of success of an event is calculated using the *difference in energy of the initial and final states.* It can be shown that the Kawasaki probability is in general not equivalent to the probability calculated using the proper energy barrier, and hence *Kawasaki dynamics do not correctly describe the kinetics of barrier crossing* **(29)**.

Second, the probabilities of success of the various microscopic processes vary over many orders of magnitude. To carry out the simulation, we divide the microscopic processes into a 'fast' group and a 'slow' group. The 'fast' group consists of processes that a precursor particle undergoes, i.e., deexcitation into a chemisorption state, migration to a nearest neighbor precursor state, and, in the case of open systems, desorption into the external reservoir. The choice of which event in the slow group to pick during the simulation is made similarly to the 'n-fold' way **(30)**. We group the slow excitation and adsorption events into classes i, each corresponding to a probability p_i of a successful attempt, and m_i is the number of potential events in each class i. For instance, if there were a total of n_i chemisorbed particles with a particular environment such that the probability of successful excitation were p_i, then $m_i = n_i$. An event in class i is chosen with relative probability $R_i = m_i p_i / \sum_i m_i p_i$. Having chosen an event in class i, the time is increased by $6\tau/p_i$. The factor of six is due to the assumption of equipartition of energy, i.e., the heat bath excites a chemisorbed particle with equal probability in six directions, and only one of these can produce a precursor particle. Once a precursor particle is

produced, it can either migrate, deexcite, desorb or remain where it is. Again the attempt frequency in each of the six directions is the same, and the time increment for each attempt is τ. The time is incremented by τ even if the precursor remains in its original location. The unitarity condition is $(p_{dex} + p_{des} + 4p_{mig} + p_0)/6 = 1$, where p_{dex} is the conditional probability for successful deexcitation given that the precursor is excited towards the surface and p_{des} is the conditional probability for successful desorption given that the precursor is excited away from the surface. Similarly, p_{mig} is the conditional probability for successful migration in one of the four possible directions for migration, given that the precursor is excited in that direction. p_0 is the sum of the six conditional probabilities of failure. When the precursor either deexcites or desorbs, we go to the slow events again and either excite or adsorb another particle into the precursor state.

The values of the parameters used are summarized in the caption for figure 2. Table 1 shows the probabilities of successful excitation of the chemisorbed particle and deexcitation of the precursor particle for the extreme cases of zero and eight repulsive interactions. We used the same temperature as Sadiq and Binder **(22)**, $1/\beta\phi = 0.3325$; and we constrained α_2/ϕ to be equal to ten. If we assume a value of 1.5 kcal/mole for the lateral repulsion, then the system has a temperature of 251 K, and the excitation energy of an isolated chemisorbed particle is 15.0 kcal/mole. The probability of successful desorption is set equal to 0.3 for simulations in set A and 0.06 for simulations in set B. The value of p_{ads} is 4.32×10^{-9} for set A and 8.64×10^{-10} for set B. Sets C, D and E are closed systems. Each of the sets of parameters shown in Table 1 utilized 20 runs each with a lattice size of 100×100 and 5 runs each with a lattice size of 120×120. We did not detect any finite-size effects although this could be due to the similarity in size of the lattices. The domain sizes were calculated by evaluating the area of each individual domain and taking the average. The length scale as a function of time $l(t)$ was then obtained by taking the square root of the average area, and we did not let $l(t)$ exceed

$\sim L/3$. Since our lattice sizes are only 100x100 and 120x120, there is a possibility of our not having reached the asymptotic regime. However, our domain sizes are comparable to those attained in **(22)** which we take as a benchmark. Initial random configurations with a fractional coverage of 0.5, and periodic boundary conditions were used. The growth exponents are shown in figure 1. These were obtained by least-squares fitting of all the data points between the arrows. If $1/\tau \sim 10^{13}$ s^{-1}, this corresponds to domain growth at $0.5 < t < 200$ s.

In Kawasaki dynamics, a particle that hops successfully then occupies one of the nearest neighbor sites to the original site. In Glauber dynamics, a particle that desorbs from the lattice has a uniform probability of *attempting* to readsorb on each site of the lattice, thus allowing a more efficient search for domain configurations of lowest free energy. In the precursor-mediated ordering described here, a chemisorbed particle is first excited into the precursor state, after which it may either deexcite into its original site, migrate to a neighboring site, or (in the case of an open system) desorb. In the limit of *strong coupling* of the precursor to the lattice, the distribution of sites into which it attempts to deexcite will be peaked sharply at its original site. In this case, the search for the lowest free energy configurations is even less efficient than with Kawasaki dynamics (where the distribution of sites is composed of delta-functions at the nearest neighbor sites). In the opposite limit of *weak coupling* of the precursor to the lattice where the probability of deexcitation is low, the distribution of sites into which the precursor attempts to deexcite will be more uniform over the lattice. When $p_{mig} >> p_{dex}$, the precursor particle can be excited or deexcited into a site on the lattice at any distance from its original chemisorption site. There is no constraint for deexcitation(readsorption) into the nearest-neighbor site. Thus, the range for particle 'hops' becomes like what it is when using Glauber dynamics, although the total density is still conserved.

This discussion can be quantified by considering the results for sets C, D and E of Table 1 which are closed systems. The growth exponent obtained for this system

by Sadiq and Binder **(22)** using Kawasaki dynamics is ~ 0.35. In set E, p_{dex} is high (cf., Table 1), and *x is less than the value obtained using Kawasaki dynamics.* This is the case in the experimentally obtained growth exponent of 0.28 ± 0.05 for O on W(110) which orders into (2x1) domains and may have a degeneracy of $p = 4$ **(31)**. More stable precursors in sets C and D (cf., Table 1) increase the growth exponent to *values higher than expected for a closed system described by Kawasaki dynamics.* Sets A and B of Table 1 simulate open systems in which all parameters except for the probabilities of adsorption and desorption are the same (and also equal to those of the closed system of set C, cf., Table 1). The contribution of particle exchange via adsorption and desorption is greater in set A and $x \sim 0.5$. With a lower rate of desorption and adsorption, set B has a growth exponent that is smaller than that expected for open systems (cf., set A) but greater than that of an otherwise identical closed system (cf., set C).

To summarize, we have presented a description of precursor-mediated ordering at surfaces, a situation that is expected to obtain in 'real' systems **(26-29)**. Hence, experimental values of the growth exponent can be used as a qualitative assessment of the stability of the precursor state. For systems in which both surface migration and particle exchange via desorption and adsorption occur, the experimental growth exponent can be used to gauge the relative rates of these processes. Simulations of a simpler model which still preserves the feature of precursor-mediated migration are discussed in Chapter 2 of this thesis

Acknowledgment: This work was supported by the National Science Foundation under Grant No. DMR-8500789.

References

1. **Monte-Carlo Methods in Statistical Physics** K. Binder, Ed., Topics in Current Physics, Vol. 7, Springer-Verlag, Heidelberg, 1979.
2. **Applications of the Monte-Carlo Methods in Statistical Physics,** K. Binder, Ed., Topics in Current Physics, Vol. 36, Springer-Verlag, Heidelberg, 1983.
3. O.G. Mouritsen, **Computer Studies of Phase Transitions and Critical Phenomena**, Springer-Verlag, Heidelberg, 1984.
4. K. Binder and D. Stauffer Phys. Rev. Letters **33**, 1006 (1974).
5. K. Binder, C. Billotet and P. Mirold, Z. Phys B **30**, 183 (1978).
6. K. Binder, Phys. Rev. B **15**, 4425 (1977).
7. J. Marro, J.L. Lebowitz and M.H. Kalos, Phys. Rev. Letters **30**, 289 (1982).
8. P.S. Sahni, J.D. Gunton, S.L. Katz and R.H. Timpe, Phys. Rev. B **25**, 289 (1982).
9. C.M. Knobler and N.C. Wong, J. Chem. Phys. **85**, 1972 (1981).
10. I.M. Lifshitz, Sov. Phys. JETP **15**, 939 (1962).
11. I.M. Lifshitz and V. Slyozov, J. Phys. Chem. Solids **19**, 35 (1961).
12. M. Hilbert, Acta. Met. **13**, 227 (1965).
13. P.S. Sahni and J.D. Gunton, Phys. Rev. Letters **45**, 369 (1980).
14. S.A. Safran, Phys. Rev. Letters **46**, 1581 (1981).
15. P.S. Sahni and J.D. Gunton, Phys. Rev. Letters **47**, 1754 (1981).
16. P.S. Sahni, G. Dee, J.D. Gunton, M.K. Phani, J.L. Lebowitz and M.H. Kalos, Phys. Rev. B **24**, 410 (1981).
17. H. Furukawa, Phys. Rev. A **23**, 1535 (1981).
18. H. Furukawa, Phys. Rev. A **28**, 1717 (1983).

19. P.S. Sahni, G.S. Grest and S.A. Safran, Phys. Rev. Letters **50**, 60 (1983).

20. S.A. Safran, P.S. Sahni and G.S. Grest, Phys. Rev. B, **28**, 2693 (1983).

21. K. Binder and D.P.Landau, Phys. Rev. B **21**, 1941 (1980).

22. S. Sadiq and K. Binder, J. Stat. Phys **35**, 517 (1984).

23. It has been shown theoretically that diffusion in the ordering of binary alloys gives x=1/3 **(11)**.

24. J. Vinals and J.D. Gunton, Surface Sci. **157**, 473 (1985).

25. H.C. Fogedby, O.G. Mouritsen, Phys. Rev. B **37**, 5962, 1988.

26. E.G. Seebauer and L.D. Schmidt, Chem. Phys. Letters **123**, 129 (1986).

27. W.H. Weinberg, in **Kinetics of Interface Reactions**, M. Grunze and H.J. Kreuzer, Eds., Springer-Verlag, Heidelberg, 1987, p.94; and references therein.

28. E.S. Hood, B.H. Toby and W.H. Weinberg, Phys. Rev. Letters **55**, 2437 (1985).

29. H.C. Kang and W.H. Weinberg, in preparation.

30. A.B. Bortz, M.H. Kalos, J.L. Lebowitz, J. Comp. Phys. **17**, 10, 1975.

31. M.C. Tringides, P.K. Wu, M.G. Lagally, Phys. Rev. Lett. **59**, 315, 1987.

Set	α_1/ϕ	p_{exc}	p_{dex}
A, B, C	0	$8.6798448 \times 10^{-14}$	1.0000000
	8	1.1494297×10^{-4}	0.0470738
D	0	$2.6870601 \times 10^{-14}$	0.3095745
	8	1.7452212×10^{-5}	0.0071473
E	0	$8.6798448 \times 10^{-14}$	1.0000000
	8	1.5827465×10^{-3}	0.6481999

Table 1. Probabilities of success for excitation and deexcitation of an isolated particle and one with eight nearest and next-nearest neighbor repulsive interactions.

Figure Captions

Figure 1. Model for excitation-deexcitation potential.

Figure 2. $l(t)$ for each set has been multiplied by an offset factor, f for clarity. f is 1,2,8,4,16 for sets A,B,C,D,E respectively. For sets A,B, and C $k_1\zeta_0^2/\phi = 20$ and $k_2\zeta_0^2/\phi = 10$. For set D $k_1\zeta_0^2/\phi = 40$ and $k_2\zeta_0^2/\phi = 10$. For set E $k_1\zeta_0^2/\phi = 20$ and $k_2\zeta_0^2/\phi = 1$.

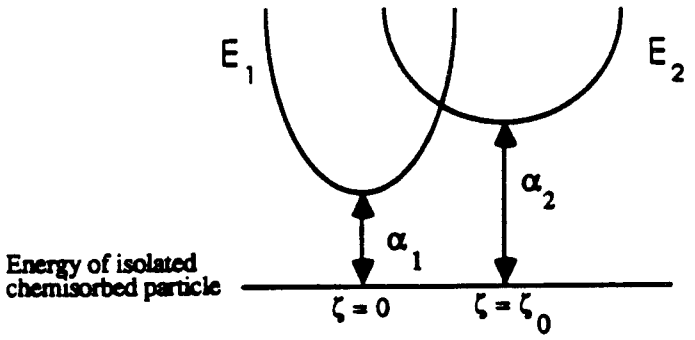

Figure 1.

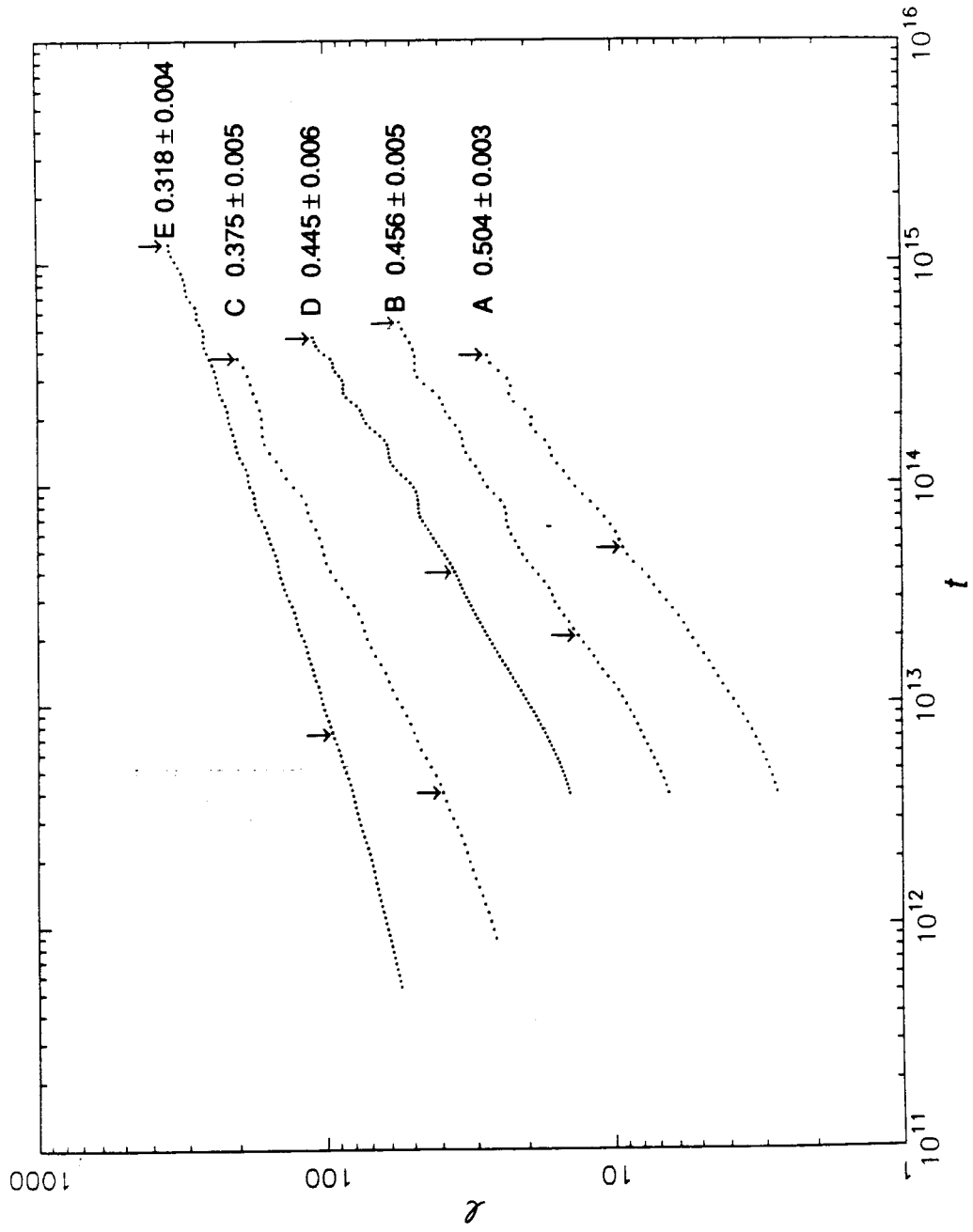
E 0.318 ± 0.004
C 0.375 ± 0.005
D 0.445 ± 0.006
B 0.456 ± 0.005
A 0.504 ± 0.003
1000
100
10
1
γ
10^11
10^12
10^13
10^14
10^15
10^16
t

Figure 2

Chapter 3.

Domain Growth and Freezing on a Triangular Lattice

This chapter has been accepted for publication as a paper by H.C. Kang and W.H. Weinberg, in *The Physical Review* B.

ABSTRACT

We have performed Monte-Carlo simulations of domain growth at zero temperature of a lattice gas with nearest-neighbor repulsive interactions on a triangular lattice. Kawasaki dynamics were used with a fractional surface coverage of one-third. We studied both the case in which the second nearest-neighbor interaction is attractive and the case in which it is zero. The effect of increasing the range of allowed hops from nearest neighbor to third nearest neighbor was investigated. We find that domain growth freezes in the case in which the second nearest-neighbor interaction is attractive and only nearest-neighbor hops are allowed. Domain freezing is released when longer range hops are allowed or when the second nearest-neighbor interaction is zero. Allowing only nearest-neighbor hops, the growth exponent when there is no second nearest-neighbor interaction is consistent with the Lifshitz-Slyozov theory. We conclude that the range of particle hops is an important parameter to consider when classifying growth kinetics.

I. Introduction

The kinetics of domain growth in systems which have been quenched below an ordering temperature T_c has been studied widely **(1)**. There has been considerable interest recently in the kinetics of domain growth at zero temperature, with particular focus on the freezing of domain sizes **(2-6)**. A combination of Monte-Carlo simulations and renormalization-group methods was employed **(3)** to study the ferromagnetic Ising model, $H = J_{nn} \sum_{(i \neq j)_{nn}} s_i s_j$ **(7)**. Using Kawasaki dynamics, it was found that the domain size freezes at zero temperature. A similar method was used **(4)** to study the eight-state Potts model on a square lattice, with the Hamiltonian $H = J_{nn} \sum_{(i \neq j)_{nn}} \delta_{s_i s_j} + J_{nnn} \sum_{(i \neq j)_{nnn}} \delta_{s_i s_j}$ **(8)**. Two 'fixed points' at $T = 0$ were found; one is a freezing 'fixed point' for $J_{nnn}/J_{nn} \neq 1$, and the other is the equilibration 'fixed point' for $J_{nnn}/J_{nn} = 1$. It was concluded that the attractive 'fixed point' for quenches to finite temperatures is the equilibration 'fixed point.' Another Hamiltonian which has been investigated is $H = J_{nn} \sum_{(i \neq j)_{nn}} s_i s_j + J_{nnn} \sum_{(i \neq j)_{nnn}} s_i s_j$ on a square lattice with J_{nn} and J_{nnn} both positive. Using Glauber dynamics, it was found that for $\alpha = J_{nnn}/J_{nn} < 1$, domain freezing occurs; whereas for $\alpha \geq 1$, the growth exponent x is approximately $1/2$ **(5)**. At finite temperatures, the domain growth freezing is released. Using the same Hamiltonian with $\alpha = 1$, but using spin exchange dynamics, it was found that the domain size freezes when only nearest-neighbor spin exchanges are allowed **(6)**. If second nearest-neighbor spin exchanges are also allowed, the freezing is released.

Some general conclusions concerning domain growth have been drawn from these studies. It was suggested that the freezing of domain growth at zero temperature implies that the growth law at finite temperatures below the critical temperature is $l \sim ln\, t$ **(3)**. However, this has not been observed in simulations either for (2x1) ordered domains on a square lattice **(9)** or for $(\sqrt{3}\text{x}\sqrt{3})$ **(10)** ordered domains on a triangular lattice **(11)**. The simulations of the growth of (2x1) domains on a square lattice show $l \sim t^x$, with a temperature dependent x for temperatures

close to zero. This temperature dependence has been interpreted in two different ways. Sadiq and Binder **(9,12)** concluded that there is a 'crossover' from $x = 0$ at zero temperature to a finite value, probably $x = 1/3$, for all nonzero temperatures. The temperature dependence that is observed in simulations is thought to arise because the simulations have not yet reached the asymptotic regime in which the true growth exponent would be observed, and the time it would take to reach this asymptotic regime becomes longer as the temperature becomes lower. Using a precursor-mediated mechanism for domain growth, it has been found that the growth exponents obtained from Monte-Carlo simulations are strongly dependent on the mobility of the precursors **(13)**. It has also been found that the freezing of the growth of (2x1) domains, using Kawasaki dynamics, on a square lattice at zero temperature is released if second nearest-neighbor hops are allowed **(6)**. The growth exponent that was obtained is close to 1/2, and it was suggested that the actual growth exponent for (2x1) domains on a square lattice is 1/2. It was argued that the conflicting observations of Sadiq and Binder **(9)** resulted because their simulations were not sufficiently long to probe the asymptotic regime. Since the density is conserved in the simulations allowing second nearest-neighbor hops with Kawasaki dynamics, the value of approximately 1/2 for the growth exponent of (2x1) domains on a square lattice led to the conclusion **(6)** that density conservation is irrelevant for degeneracies greater than two.

Recent work **(2)** using a renormalization group method has proposed the classification of the growth kinetics of many systems in four classes. In class I, the only influence temperature has on the growth kinetics is through the determination of the correlation length and hence the width of the domain boundaries. In this class the zero temperature kinetics for sufficiently long time scales and sufficiently large length scales is the same as the finite temperature kinetics. In class II systems domain growth freezing occurs when the temperature is zero, but the growth kinetics follow a power law behavior at finite temperatures. Such behavior can result

from a time scale τ which depends strongly on the temperature in such a way that $\tau = \tau_0 \exp(-E/T)$, where tau_0 is weakly dependent on the temperature T, and E is a local barrier, independent of the domain length. In class III and IV systems, the energy barrier E is dependent on the domain length and there is evidence for logarithmic growth kinetics.

In this investigation we will investigate the zero temperature growth kinetics for lattice gases with repulsive nearest-neighbor and either attractive or zero second nearest-neighbor interactions on a triangular lattice and discuss the recently proposed classification **(2)** as applied to these lattice gases. In previous work it was found that the freezing of domain growth in the eight-state Potts model **(4)** or the superantiferromagnetic Ising model on square lattice **(5)** is caused by the impossibility of kink creation and annihilation for certain values of the interaction parameters. Similar to the eight-state Potts lattice gas on a square lattice, we find two stable 'fixed points' at zero temperature. One of them is a freezing 'fixed point,' and the other is an equilibration 'fixed point.' These systems exhibit class II behavior in the scheme proposed recently. **(2)**. We find that freezing of domain growth in the model we study here is caused by fluctuations in the local fractional coverage which can result in the formation of locally stable configurations. These 'defects' then pin the domain walls or act as traps for excess local fractional coverage, causing the freezing of domain growth. We also investigated the effect of allowing hops of range longer than nearest neighbor. We used Kawasaki dynamics **(14)**, and in some simulations allowed not only nearest-neighbor hops but also hops to second and third nearest neighbors. The freezing 'fixed point' is rendered unstable by allowing hops of longer range, as in the case of (2x1) domains on a square lattice. Interestingly, we find a growth exponent x of approximately 1/3 for the equilibration 'fixed point.' For this model, $x = 1/3$ was conjectured by Sadiq and Binder **(9)**.

II. Simulations

Since we used Kawasaki dynamics, the probability of a hop is given by

$$P = \begin{cases} 0, & \delta E > 0 \\ 1/2, & \delta E = 0 \\ 1, & \delta E < 0 \end{cases} \tag{1}$$

where δE is the change in energy caused by the hop. Time is measured in Monte-Carlo steps (MCS) per site. The Hamiltonian of the lattice gases that were simulated is

$$H = J_{nn} \sum_{(i \neq j)_{nn}} c_i c_j + J_{nnn} \sum_{(i \neq j)_{nnn}} c_i c_j. \tag{2}$$

The occupation variable c_i is unity if site i is occupied and zero if it is vacant. The interaction strength of a particle with each of its nearest neighbors is J_{nn}. The second nearest-neighbor interaction strength is J_{nnn}. We stipulate that J_{nn} is positive, i.e., the nearest-neighbor lateral interaction is repulsive, and the cases $J_{nnn} = 0$ and $J_{nnn} = -J_{nn}$ have been studied. The fractional surface coverage used in all the simulations was 1/3, and at this fractional surface coverage the equilibrium configuration is a single $(\sqrt{3}\text{x}\sqrt{3})$ ordered domain with a degeneracy $p = 3$. The phase diagram for $J_{nnn} = -J_{nn}$ has been obtained using Monte-Carlo simulations **(17)**. We allowed three different ranges of particle hops, namely, only hops to nearest neighbors; hops to nearest and second nearest neighbors; and hops to nearest, second and third nearest neighbors. Only hops to vacant sites are allowed. We used lattices which are parallelograms with L sites on each side. The sizes of the lattices used are commensurate with the $(\sqrt{3}\text{x}\sqrt{3})$ structure, and periodic boundary conditions are employed. For each configuration, the individual domain sizes were measured by counting the area occupied by each domain. The average domain size is then calculated, and the square root of this average area is taken to be the characteristic domain length l. For each set of parameters, thirty

runs were performed on lattices of size LxL=99x99 and five runs were performed on lattices of size LxL=201x201. This was done to determine whether the simulations were affected by the finite lattice sizes. For the final domain sizes we obtained, no finite-size effects were observed. Initial configurations were generated by randomly populating the lattices.

III. Results and Discussion

The results of the simulations employing the Hamiltonian of Eq. (2) with $J_{nnn} = -J_{nn}$ are shown in Fig. 1. Each curve is obtained from simulations in which a different range of allowed hops is used. Curve A shows results from simulations where only nearest-neighbor hops are allowed; curve B shows results from simulations in which hops up to second nearest neighbor in range are allowed; and curve C shows results from simulations in which hops up to third nearest neighbor in range are allowed. The asymptotic domain size for the simulations allowing only nearest-neighbor hops is $l \sim 16$, and it is independent of the lattice size. The decrease in the growth exponent is perceptibly slower for curves B and C than it is for curve A. Step-like increases in the domain size become apparent toward the end of the runs for the simulations in which hops of up to third nearest neighbor in range are allowed. As we will argue later, *domain growth is not frozen if hops of range greater than nearest neighbor are allowed.* Simulations were also performed employing the Hamiltonian of Eq. (2) with a weaker second nearest-neighbor attractive interaction, $J_{nnn} = -0.1J_{nn}$. In this case only simulations allowing nearest-neighbor hops were performed. The results of these simulations are shown in Fig. 2. The domain growth is frozen as in curve A of Fig. 1. The asymptotic domain size is approximately 18, which is slightly larger ($\sim$ 10-15%) than the aysmptotic domain size for $J_{nnn} = -J_{nn}$.

The results of simulations employing the Hamiltonian of Eq. (2) with zero second nearest-neighbor attraction are shown in Fig. 3, where the curves are

labelled according to their allowed hopping ranges as in Fig. 1. The domain growth kinetics are well described by $l \sim t^x$, with x asymptotically constant in time for all cases. However, as shown in Fig. 3, the value of the growth exponent x increases as the range of allowed hops increases. With only nearest-neighbor hops, the growth exponent is $x \sim 0.33 \pm 0.01$. Increasing the range of allowed hops to include both nearest-neighbor and second nearest-neighbor hops increases the growth exponent to $x \sim 0.38 \pm 0.01$. Finally, also allowing third nearest-neighbor hops increases the growth exponent to $x \sim 0.41 \pm 0.01$. Each uncertainty reported here is one standard deviation. The arrows in Fig. 3 indicate the range of data used to fit the growth law for each case.

In Figs. 4(a-d) we show typical configurations that were obtained from the simulations. Each of these configurations was obtained after 1350 MCS per site. The configurations shown in Fig. 4(a-c) were obtained from simulations in which there is an attractive second nearest-neighbor interaction $J_{nnn} = -J_{nn}$. The configuration shown in Fig. 4(a) is obtained from simulations in which only nearest-neighbor hops are allowed, while the configuration shown in Fig. 4(b) is obtained from simulations in which both nearest-neighbor and second nearest-neighbor hops are allowed, and the configuration shown in Fig. 4(c) is obtained from simulations in which nearest-neighbor, second nearest-neighbor and third nearest-neighbor hops are allowed. These correspond to curves A, B and C in Fig. 1, respectively. The configuration shown in Fig. 4(d) is obtained from simulations in which the second nearest-neighbor interaction is zero, and hops of up to third nearest neighbor in range are allowed. The configurations from simulations allowing only nearest-neighbor or second nearest-neighbor hops are similar.

As the system is quenched to below T_c, $(\sqrt{3}\mathrm{x}\sqrt{3})$ ordered domains form in regions of the lattice where the local fractional coverage is $1/3$. The degeneracy of this structure is $p = 3$, and domain walls form between domains which are out of phase with each other. The local configurations at the domain walls are not $(\sqrt{3}\mathrm{x}\sqrt{3})$

superstructures, and the domains will grow to minimize such regions. With second nearest-neighbor attraction, however, regions which have local fractional coverages greater than 1/3 will phase separate into domains which are ordered $(\sqrt{3}x\sqrt{3})$ and clusters which are ordered $(\sqrt{3}x\sqrt{3})^*$ **(10)**. Similarly, regions in which the local fractional coverages are less than 1/3 will phase separate into ordered $(\sqrt{3}x\sqrt{3})$ domains and clusters of vacant lattice sites. This would be expected by considering the phase diagram shown in Fig. 5 **(17)**. The abscissa is the total fractional coverage and the ordinate is the temperature. There is a cusp at the point where the temperature is zero and the total fractional coverage is 1/3. The equilibrium state at this point is a single ordered $(\sqrt{3}x\sqrt{3})$ phase, whereas on either side of this point the equilibrium states consist of two phases. When the coverage is less than 1/3, an ordered $(\sqrt{3}x\sqrt{3})$ phase is in equilibrium with vacant lattice sites, and when the coverage is greater than 1/3, an ordered $(\sqrt{3}x\sqrt{3})$ phase is in equilibrium with an ordered $(\sqrt{3}x\sqrt{3})^*$ phase. Fluctuations in the local fractional coverage cause excursions into the two-phase regions of the phase diagram. At zero temperature, these fluctuations are shown schematically by arrows in Fig. 5.

Consider the configurations shown in Figs. 4(a-c). These configurations were obtained from simulations in which there is an attractive second nearest-neighbor interaction between the lattice-gas particles. Clusters of particles showing $(\sqrt{3}x\sqrt{3})^*$ order as well as clusters of vacant lattice sites are clearly observed. These 'defects,' which are locally stable, are formed via fluctuations in the local fractional coverage as discussed above. It can be seen in Figs. 4(a-c) that some of the 'defects' are adsorbed at the interface between different $(\sqrt{3}x\sqrt{3})$ domains, whereas others are completely embedded in a domain of one phase. For the domain size to grow continuously, it must be possible for a particle to move away from a $(\sqrt{3}x\sqrt{3})^*$ cluster to regions where there is a deficit in the local fractional coverage. However, to do so a particle must traverse regions which are ordered $(\sqrt{3}x\sqrt{3})$. The change in energy due to a particle moving away from a $(\sqrt{3}x\sqrt{3})^*$ cluster into an ordered

($\sqrt{3}$x$\sqrt{3}$) domain is positive, however, and the probability of such a move is zero at $T = 0$. Similarly, the probability of particles moving from a region which is an ordered ($\sqrt{3}$x$\sqrt{3}$) to fill a cluster of vacant sites is zero.

However, if hops of range longer than nearest neighbor are allowed, it becomes possible for a cluster of ordered ($\sqrt{3}$x$\sqrt{3}$)* particles or a cluster of vacant lattice sites to move as a whole even though no single particle may break away from it. Therefore, in the late stages of the runs, the transport mechanism that enables the domain size to increase is the diffusion of these 'defects.' As a result of this, the size of a domain will increase in steps of more than one particle each time a cluster of ordered ($\sqrt{3}$x$\sqrt{3}$)* particles 'collides' with a cluster of vacant lattice sites. The effect of such discontinuities can be clearly observed, toward the end of the runs, in curve C of Fig. 1. Hence, even allowing only finite-range hops, domain growth is not frozen so long as hops of range longer than nearest neighbor are allowed. The diffusivity of the 'defects' is larger in the case in which third nearest-neighbor hops are allowed than in the case in which second nearest-neighbor hops are allowed. Thus, the configuration shown in Fig. 4(c) is more 'aged' than that shown in Fig. 4(b) even though both were obtained after the same number of Monte-Carlo moves in the simulations. Consequently, the latter configuration shows a larger number of smaller 'defect' clusters which are separated by shorter distances. It is possible that both of curve B and curve C of Fig. 1 shows $l \sim t^x$ behavior for long times. However, our simulations are not sufficiently long to verify this. There is, however, no reason to expect that $x \sim 1/3$ since the mechanism of growth is not diffusion of single particles but rather of 'defects,' the sizes of which must increase with time, and the diffusivity of which must decrease with size. With an infinite range of allowed hops, particles can go from the ($\sqrt{3}$x$\sqrt{3}$)* clusters directly to the clusters of vacant lattice sites. Since the change in energy for such a move is not positive, the probability is not zero. Hence, with a range of allowed hops extending to infinite distance, domain freezing does not occur.

Since it is the second nearest-neighbor attractive interaction which is responsible for the formation of the 'defects,' it is interesting to consider the case in which this interaction is set to a weaker attraction or to zero. From the above considerations, we expect that, for simulations in which only nearest-neighbor hops are allowed, domain growth will be frozen as long as the second nearest-neighbor interaction is attractive. This is because the clusters of vacant lattice sites and the clusters of particles in the ordered $(\sqrt{3}x\sqrt{3})^*$ domains are locally stable as long as J_{nnn} is negative. Furthermore, with only nearest-neighbor hops allowed, these clusters are not mobile. The results shown in Fig. 2 support this conclusion. The domain size is frozen at $l \sim 18$.

With zero second nearest-neighbor attraction, clusters of $(\sqrt{3}x\sqrt{3})^*$ and clusters of vacant lattice sites are not locally stable. Consider the configuration shown in Fig. 4(d), which is obtained from simulations in which the lattice-gas particles have zero second nearest-neighbor interaction. In contrast to Figs. 4(a-c), we do not observe clusters of ordered $(\sqrt{3}x\sqrt{3})^*$ particles or clusters of vacant lattice sites. Thus there are no 'defects,' as in the case of $J_{nnn} < 0$, to pin the domain walls or to trap excess or deficit local fractional coverage. *Hence, domain freezing is released by decreasing the second nearest-neighbor interaction to zero.* It can be seen that the boundaries between domains consist of *walls* with either excess or deficit fractional local coverage, and it is interesting to note that the growth exponent is $x \sim 1/3$ for the case in which only nearest-neighbor hops are allowed, cf. curve A of Fig. 3. This value for the growth exponent was conjectured by Sadiq and Binder **(9)** on the basis of their simulations which indicated that when there are domain walls with excess or deficit local fractional coverage, the redistribution of the excess and deficit density over a length scale of l results in $x \sim 1/3$. Our results support this conjecture. It has been suggested that the true density-conserved growth exponent for (2x1) domains on a square lattice is $x \sim 1/2$, and the values obtained by Sadiq and Binder **(9)** resulted from a 'crossover' between $x = 0$ and $x \sim 1/2$ **(6)**. For the

lattice gas that we studied, there is no freezing of domain growth at zero temperature without second nearest-neighbor attraction. Thus, the simulation result of $x \sim 1/3$ can be a true growth exponent and does not have to arise from a crossover effect between $x = 0$ and $x = 1/2$.

For simulations in which $J_{nnn} = 0$, increasing the range of allowed hops from nearest neighbor to third nearest neighbor increases the measured growth exponent from ~ 0.33 to ~ 0.41, cf. Fig. 3. This is similar to the increase in the growth exponent from $x = 0$ to $x \sim 0.5$ that was observed for the ordering of (2x1) domains on a square lattice when the range of allowed hops is increased from nearest neighbor to second nearest neighbor **(6)**. The latter result led to the conclusion that the growth exponent for density-conserved growth is 1/2, regardless of the degeneracy of the ground state. It was also suggested that earlier work **(9)** obtained $x \sim 1/3$ because of the influence of 'crossover' from $x = 0$ at zero temperature when only nearest-neighbor hops are allowed, and that the simulations had not reached the asymptotic regime where $x = 1/2$, this regime being reached faster when hops of longer range are allowed **(6)**. However, even for the case in which only nearest-neighbor hops are allowed, we have found that domain growth for the Hamiltonian with $J_{nnn} = 0$ is not frozen at zero temperature. There is thus no possibility of a 'crossover' from $x = 0$ to $x = 1/2$ as the range of hops is increased. Hence, if the density-conserved growth exponent is $x = 1/2$, even for $p > 2$, then this is the value that would be observed even for the case in which only nearest-neighbor hops are allowed. However, we actually observed $x \sim 0.33$.

Our results for the growth of $(\sqrt{3}\text{x}\sqrt{3})$ domains on a triangular lattice and those obtained earlier **(6,9)** for the growth of (2x1) domains on a square lattice may be interpreted better as follows. If there is a need for redistribution of either excess or deficit local density then, as suggested by Sadiq and Binder **(9)**, the growth exponent is $x \sim 1/3$, allowing only nearest-neighbor hops. If the Hamiltonian is such that freezing occurs at zero temperature, then the growth exponent at

temperatures close to zero is affected by 'crossover' from $x = 0$ **(9)**. Increasing the range of allowed hops changes the mechanism of transport from diffusion to evaporation-condensation. This is because the limit in which hops of all possible lengths up to infinity are allowed in Kawasaki dynamics is equivalent to Glauber dynamics **(13)**.

For the simulations that we performed, the largest lattice size was 201x201, and there is certainly some doubt as to whether the values of x obtained are the asymptotic growth exponents. It is, however, suggestive that the growth exponent obtained from simulations allowing only nearest-neighbor hops is in excellent agreement with the Lifshitz-Slyozov result of $x = 1/3$ for diffusion driven coarsening during the late stages of phase separation in solid solutions **(18,19)**. Furthermore, it is not clear how a change in the length scale of the hops from nearest neighbor to second nearest neighbor can produce a 'crossover' from $x \sim 1/3$ to $x = 1/2$. Therefore, we conclude that the growth exponent for density-conserved growth is not $1/2$, but changes continuously from $x \sim 1/3$ to $x = 1/2$ as the length of allowed hops increases from nearest neighbor to infinity.

It is clear that the case in which $J_{nnn} = 0$ falls into class I **(2)** systems, whereas the case in which $J_{nnn} = -J_{nn}$ exhibits class II behavior. Without next nearest-neighbor attraction the time scale of the lattice gas is not strongly dependent on the temperature through and energy barrier. On the other hand, with next nearest-neighbor attraction, the time scale is dependent on the temperature through an energy barrier which is not a function of the domain size. Consider the configuration space of the system. The local stability of clusters of vacant sites and clusters of ordered $(\sqrt{3}\text{x}\sqrt{3})^*$ particles imply that there are points in configuration space which have energies lower than all other points that it can access if only nearest-neighbor hops are allowed. Thus, in order for the system to 'escape' from such traps an energy barrier, independent of the domain size, has to be overcome. Therefore, the time scale for such a lattice gas would be strongly dependent on the temperature,

and freezing occurs when the temperature is zero. Therefore, the triangular lattice gas with $J_{nn} = -J_{nnn}$ is a class II system (2) when only nearest-neighbor hops are allowed. When hops of longer range are allowed, from any point in configuration space there are always accessible points with lower or equal energies. Hence, freezing does not occur, and the lattice gas is a class I system. Therefore, the range of hops that is allowed for a lattice gas particle can subtly influence the dynamical connectivity of points in configuration space, and is an important parameter to consider in classifying growth kinetics.

IV. Conclusions

We have found that for a triangular lattice gas with a fractional surface coverage of one third and with nearest-neighbor repulsions, the nature of domain growth of $(\sqrt{3}\text{x}\sqrt{3})$ superstructures is sensitively dependent upon whether the second nearest-neighbor interaction is zero or attractive. When the second nearest-neighbor interaction is attractive, fluctuations in the local fractional coverage lead, upon quenching to zero temperature, to the formation of locally stable clusters with a $(\sqrt{3}\text{x}\sqrt{3})^*$ superstructure (two particles per unit cell) and clusters of vacant lattice sites. In simulations allowing only nearest-neighbor hops, single lattice-gas particles cannot break away from the ordered $(\sqrt{3}\text{x}\sqrt{3})^*$ clusters, and single vacant sites cannot break away from the clusters of vacant lattice sites because both these clusters are locally stable. As a result, domain growth freezes. However, when hops of range longer than nearest neighbor are allowed, the freezing is released. In this case it is also true that single particles cannot break away from the ordered $(\sqrt{3}\text{x}\sqrt{3})^*$ clusters and single vacant sites cannot break away from the clusters of vacant sites. However, both the ordered $(\sqrt{3}\text{x}\sqrt{3})^*$ clusters and the clusters of vacant lattice sites are mobile. This is because single particles at the boundary of an ordered $(\sqrt{3}\text{x}\sqrt{3})^*$ cluster can move along the boundary, by hopping from their original sites to second nearest-neighbor sites, and still remain part of the cluster. Such

hops, which do not result in a change in the total energy and hence have a probability of 1/2, are forbidden when only nearest-neighbor hops are allowed. Similarly, single vacant sites can hop along the boundary of the clusters of vacant lattice sites. Toward the end of the simulation runs that we performed, the 'coalescence' of these 'defect' clusters to form ordered ($\sqrt{3}$x$\sqrt{3}$) superstructures contributes significantly to domain growth. In the classification of growth kinetics, it is thus important to consider the range of hops that are allowed for lattice gas particles (or the range of spin exchange for Ising systems). In the systems we have studied here, a change of hop range from nearest-neighbor to merely next nearest-neighbor can change the domain growth behavior from class I to class II in the scheme proposed in Ref. 2.

Without an attractive second nearest-neighbor interaction, domain growth is not frozen even at zero temperature. We find a growth exponent of $x \sim 1/3$ when only nearest-neighbor hops are allowed, in agreement with the conjecture by Sadiq and Binder **(9)**. It has been argued that the value of $x \sim 1/3$ for the growth of (2x1) domains on a square lattice results from a crossover effect between $x = 0$ at zero temperature and $x = 1/2$ at finite temperatures **(6)**. Our results indicate that even without the freezing of domain growth at zero temperature, it is possible to have a growth exponent of $x \sim 1/3$. In agreement with results for the growth of (2x1) domains on a square lattice **(6)**, we find that the observed growth exponent depends on the range of allowed hops. However, we interpret this as a continuous dependence of the growth exponent on the hopping range rather than a crossover effect. This is more consistent because we do not observe domain freezing even in the case in which we allow only nearest-neighbor hops. We also note that in the case in which density is conserved (Kawasaki dynamics), allowing the range of hops to be infinitely long causes the system effectively to evolve according to Glauber dynamics, since simulations are always done on finite lattices. Therefore, $x = 1/2$ when the range of allowed hops is infinitely long, even though density is conserved. We conclude that by increasing the range of allowed hops from nearest neighbor to

infinity, the growth exponent changes from $x \sim 1/3$ to $x = 1/2$.

Acknowledgment: This research was supported by the National Science Foundation under Grant No. CHE-8617826. We acknowledge partial support by the Donors of the Petroleum Research Fund (PRF 19819-AC5-C).

References

1. K. Binder and D.W. Heermann, in **Scaling Phenomena in Disordered Systems**, edited by R. Pym and A. Skjeltorp (Plenum, New York, 1985); K. Binder, D.W. Heermann, A. Milchev and A. Sadiq, in **Heidelberg Colloquium on Glassy Dynamics and Optimization**, edited by J.L. van Hemmen and I. Morgenstern (Springer, Berlin, 1987).
2. Z.W. Lai, G.F. Mazenko and O.T. Valls, Phys. Rev. B **37**, 9481 (1988).
3. G.F. Mazenko, O.T. Valls and F.C. Zhang, Phys. Rev. B **31**, 4453 (1985).
4. J. Vinals and J.D. Gunton, Phys. Rev. B **33**, 7795 (1986).
5. A. Host-Madsen, P.J. Shah, T.V. Hansen and O.G. Mouritsen, Phys. Rev. B **36**, 2333 (1987).
6. H.C. Fogedby and O.G. Mouritsen, Phys. Rev. B **37**, 5962 (1988).
7. Here J_{nn} is the nearest-neighbor interaction energy, and $s_i = \pm 1$ is the spin of the ith lattice site.
8. Here J_{nnn} is the next nearest-neighbor interaction energy, and δ is the Kronecker delta.
9. A. Sadiq and K. Binder, J. Stat. Phys. **35**, 517 (1984).
10. We use $(\sqrt{3}\mathrm{x}\sqrt{3})$ as an abbreviation for the $(\sqrt{3}\mathrm{x}\sqrt{3})R30°$ superstructure. The structure with two particles and one vacancy rather than two vacancies and one particle per unit cell is denoted by $(\sqrt{3}\mathrm{x}\sqrt{3})^*$.
11. H.C. Kang and W.H. Weinberg, in preparation.
12. K. Binder, Ber. Bunseges. Phys. Chem. **90**, 257 (1986).
13. H.C. Kang and W.H. Weinberg, Phys. Rev. B **38**, 11543 (1988).
14. Kawasaki dynamics, rather than a proper energy-barrier model **(15,16)**, were employed since the case of zero temperature is being investigated.

15. E.S. Hood, B.H. Toby and W.H. Weinberg, Phys. Rev. Letters **55**, 2437 (1985).

16. H.C. Kang and W.H. Weinberg, J. Chem. Phys. **90**, 2824 (1989).

17. D.P. Landau, Phys. Rev. B **27**, 5604 (1983).

18. I.M. Lifshitz and V. Slyozov, J. Phys. Chem. Solids **19**, 35 (1961).

19. I.M. Lifshitz, Sov. Phys. JETP **15**, 939 (1962). (1961).

Figure Captions

Figure 1. Results of simulations for domain growth with $J_{nnn} = -J_{nn}$ at $T = 0$. The results from simulations with only nearest-neighbor hops allowed are plotted as curve A. The results from simulations with nearest and second nearest-neighbor hops allowed are plotted as curve B. The results from simulations with nearest, second and third nearest-neighbor hops allowed are plotted as curve C. The ordinate is the average domain length in units of the lattice constant, and the abscissa is the time in units of Monte-Carlo steps per site.

Figure 2. Results of simulations for domain growth with $J_{nnn} = -0.1J_{nn}$ at $T = 0$. Only nearest-neighbor hops are allowed. The ordinate is the average domain length in units of the lattice constant, and the abscissa is the time in units of Monte-Carlo steps per site. Notice the freezing of domain growth at an asymptotic domain length slightly larger than that of curve A in Fig. 1.

Figure 3. Results of simulations for domain growth with $J_{nnn} = 0$ at $T = 0$. The results from simulations with only nearest-neighbor hops allowed are plotted as curve A. The results from simulations with nearest and second nearest-neighbor hops allowed are plotted as curve B. The results from simulations with nearest, second and third nearest-neighbor hops allowed are plotted as curve C. The ordinate and abscissa are the same as those in Fig. 1. For curve B the average domain length l has been multiplied by a factor of two, and for curve C l has been multiplied by a factor of four, so that the results can be presented more clearly.

Figure 4(a). Typical configuration at a time of 1350 MCS for simulations in which only nearest-neighbor hops are allowed. The second nearest-neighbor interaction is $J_{nnn} = -J_{nn}$. Note the clusters of ordered $(\sqrt{3}\text{x}\sqrt{3})^*$ particles and clusters of vacant lattice sites. This map corresponds to curve A of Fig. 1.

Figure 4(b). Typical configuration at a time of 1350 MCS for simulations in which both nearest and second nearest-neighbor hops are allowed. The second nearest-neighbor interaction is $J_{nnn} = -J_{nn}$. The clusters of ordered $(\sqrt{3}x\sqrt{3})^*$ particles and clusters of vacant lattice sites are farther apart than in the configuration in Fig. 4(a). The clusters are mobile in this case because second-nearest neighbor hops are allowed. This map corresponds to curve B of Fig. 1.

Figure 4(c). Typical configuration at a time of 1350 MCS for simulations in which first, second and third nearest-neighbor hops are allowed. The second nearest-neighbor interaction is $J_{nnn} = -J_{nn}$. The clusters of ordered $(\sqrt{3}x\sqrt{3})^*$ particles and clusters of vacant lattice sites are farther apart than in the configurations in Figs. 4(a,b). The mobility of the clusters is larger here than in Fig. 4(b). This map corresponds to curve C in Fig. 1.

Figure 4(d). Typical configuration at a time of 1350 MCS for simulations in which hops of up to third nearest-neighbor sites are allowed. The second nearest-neighbor interaction is $J_{nnn} = 0$. This map corresponds to curve C of Fig. 3.

Figure 5. Schematic of the phase diagram for the lattice gas with $J_{nnn} = -J_{nn}$ on a triangular lattice **(17)**. The arrows indicate the fluctuations in the local fractional coverage about a value of 1/3 at zero temperature, which could produce locally stable clusters of ordered $(\sqrt{3}x\sqrt{3})^*$ particles or locally stable clusters of vacant sites. The three types of diagrams that are shown indicate local fractional coverages of 2/3, 1/3, and zero.

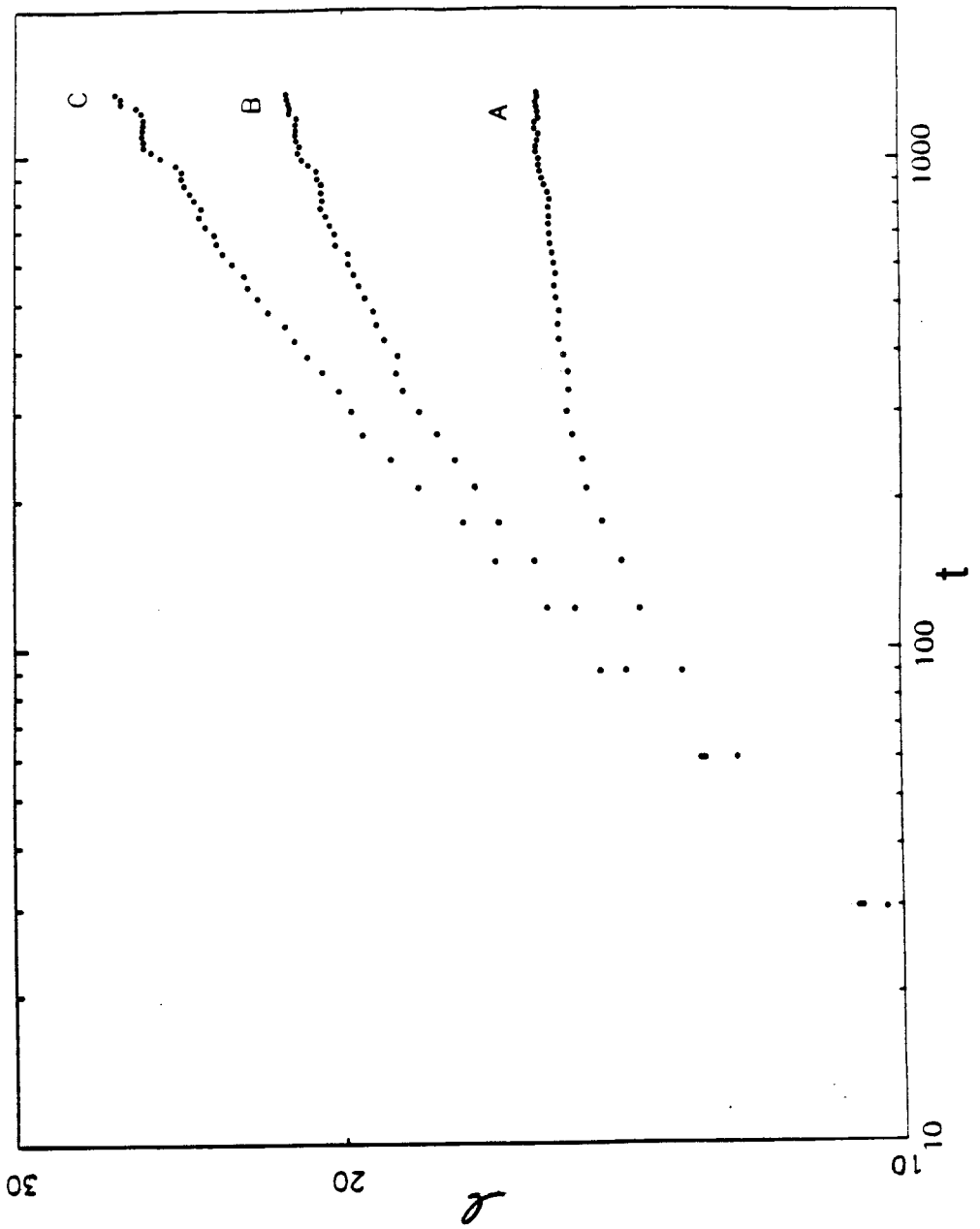

Figure 1

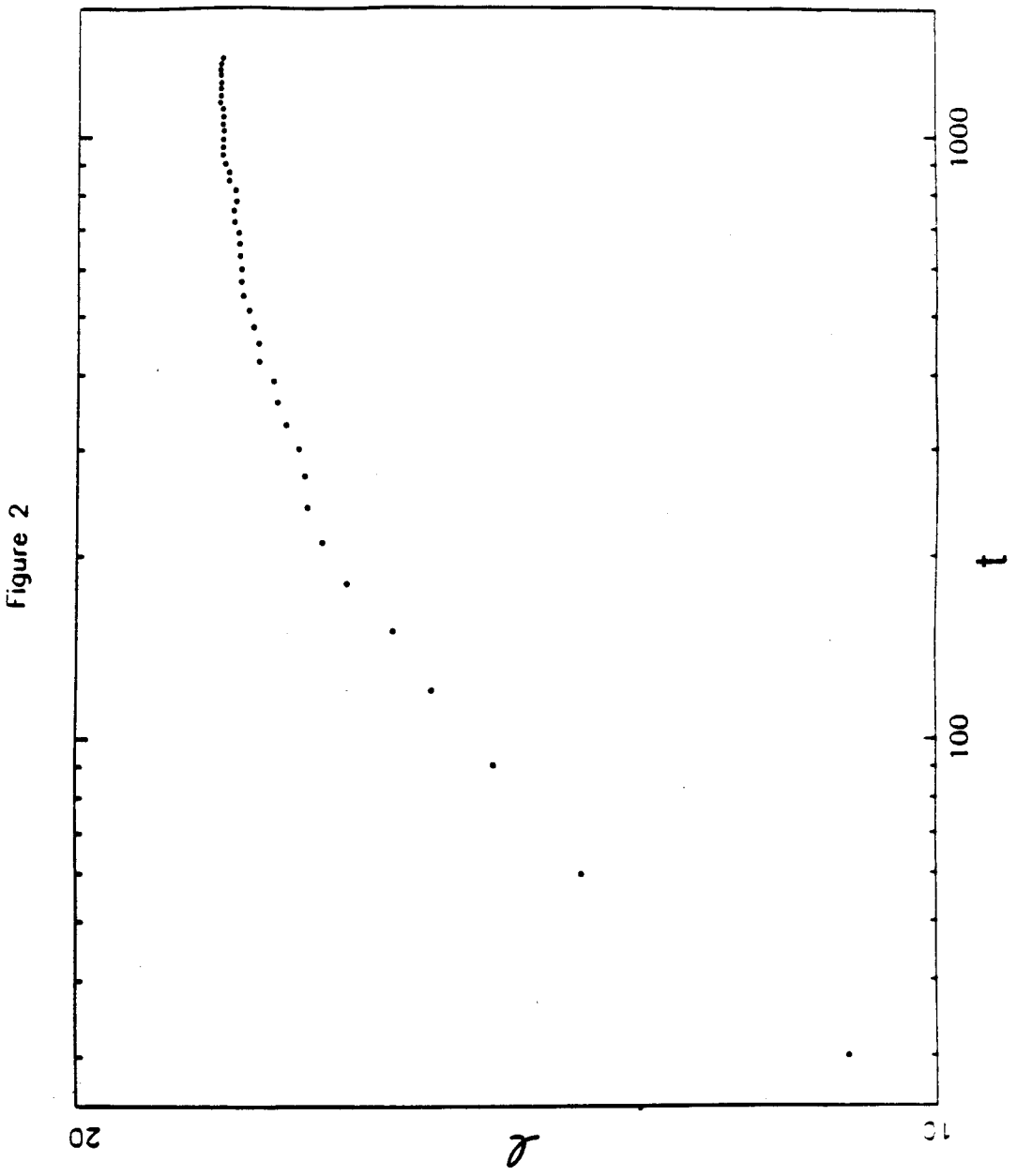

Figure 2

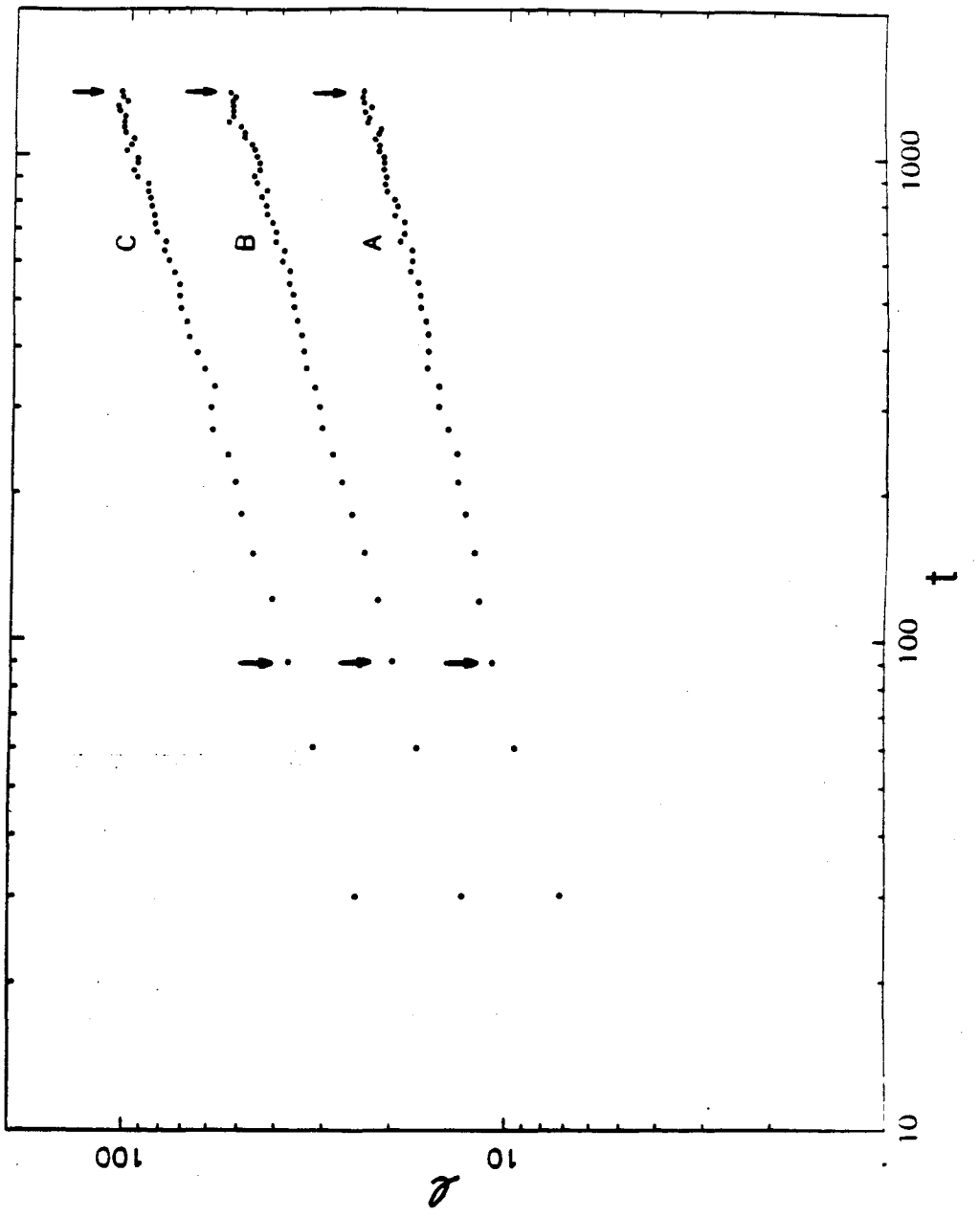

Figure 3

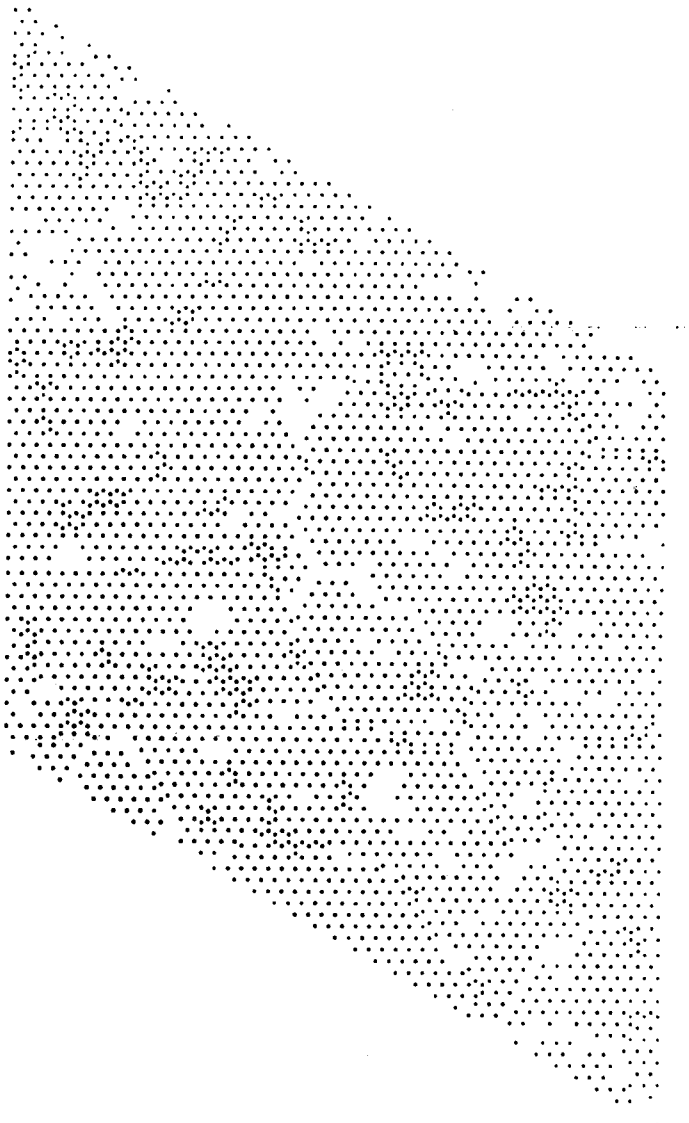

(a)

Figure 4

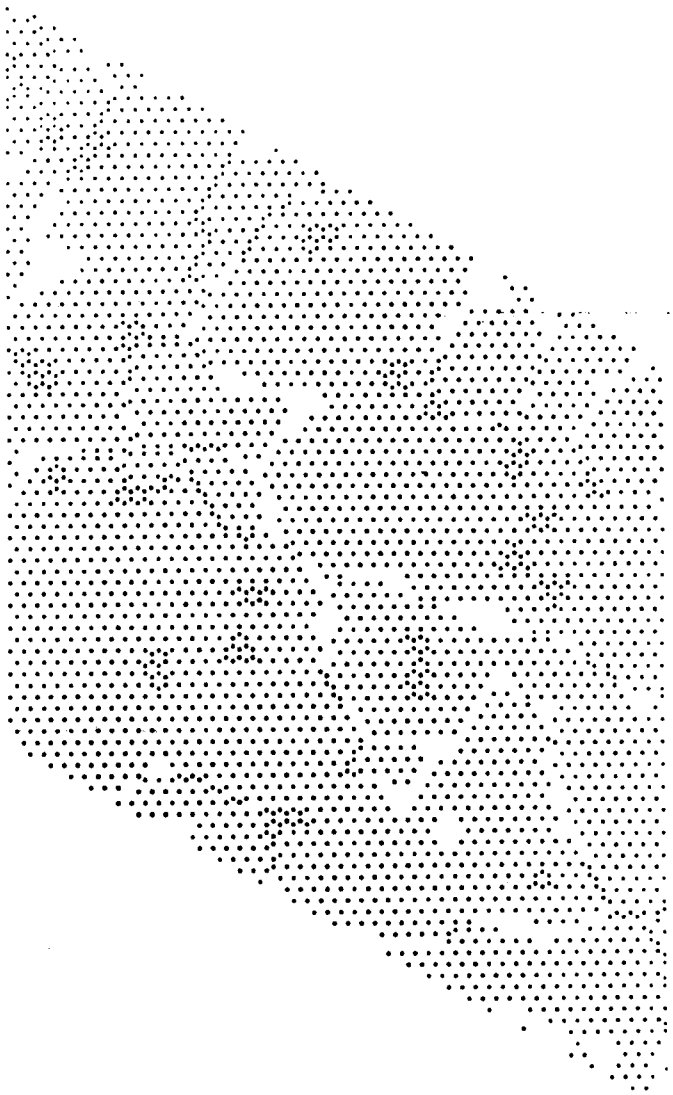

(b)

Figure 4

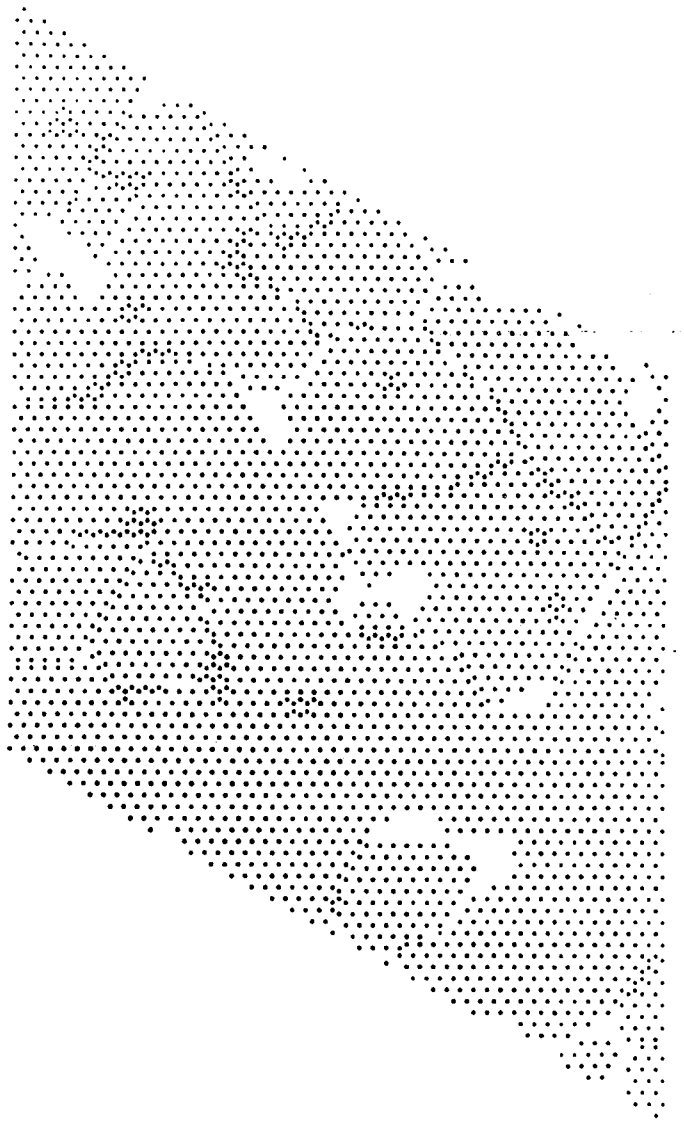

(c)

Figure 4

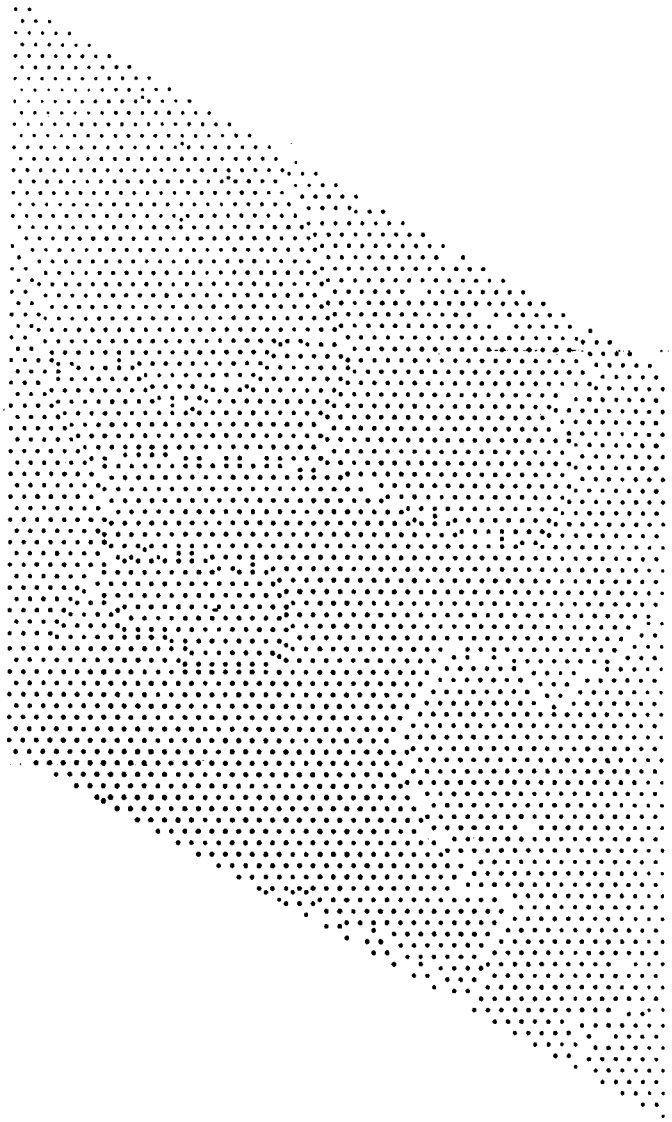

(d)

Figure 4

Figure 5

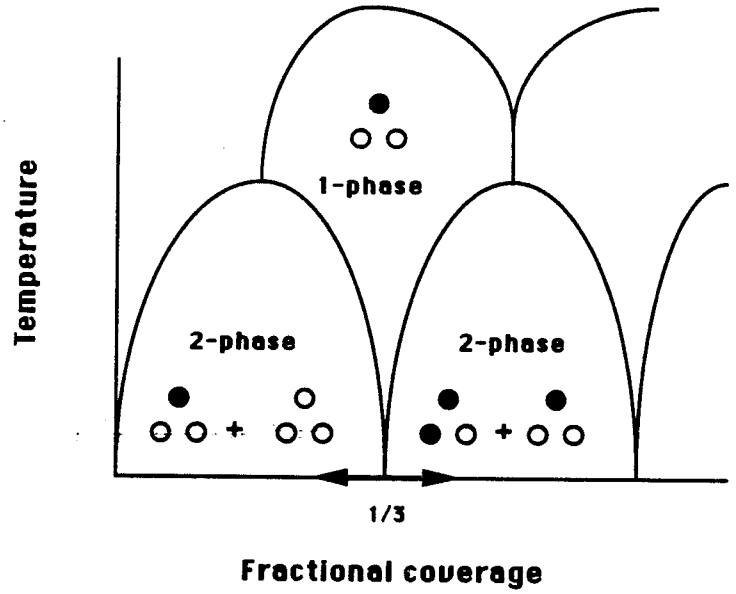

Chapter 4.

Precursor-Mediated Kinetics of Domain Growth

This chapter has been submitted as a paper by H.C. Kang and W.H. Weinberg, to *The Physical Review.*

ABSTRACT

Lattice-gas models that allow the influence of precursor states on the kinetics of domain growth to be studied are presented and discussed. Monte-Carlo simulations are performed on a square lattice with these models for the case of equal and repulsive lateral interactions between nearest and next-nearest neighbors. The dynamics used in the simulations incorporate the energy barrier that an adsorbed molecule must surmount in order to migrate on a crystal surface. We find that domain growth is well described by $l \sim At^{1/2}$, although during early stages of growth smaller exponents may be observed. The growth exponent of 1/2 holds regardless of the mobility of the precursor. We also find that the coefficient A in the growth law is proportional to the square root of the diffusion coefficient of the adsorbate particles.

1. INTRODUCTION

There has been, and continues to be, a great deal of interest in the kinetics of domain growth **(1-33)**. This represents an important problem in materials science because the macroscopic properties of materials can be influenced strongly by their microcrystalline structure. In the manufacture of microelectronic devices, for instance, it is of interest to know how the lattice structure of an epitaxially grown material develops layer-by-layer into its bulk lattice structure. It is also important in surface science where the microscopic structure of an adsorbed layer influences strongly the diffusion, desorption or reaction of the adsorbed molecules. Adsorbed atoms or molecules can exhibit a wide variety of ordered overlayer superstructures which result from the lateral interactions that exist between them. The observable properties of the ordered overlayers provide a means of studying these lateral interactions. Typically, when a layer of adsorbed atoms or molecules is quenched below an order-disorder transition temperature, ordered domains begin to form, and the ground state may be degenerate. Hence, even though within each domain the local configuration is that with the lowest free energy, at the boundaries between domains the local configurations are not the most favorable thermodynamically. To reduce the total free energy of the system, the lengths of these boundaries must be reduced, and hence the domain sizes become larger. By analogy to critical phenomena, it has been proposed **(5-7)** and observed **(14-16)** that at late stages of growth, when the domain sizes are much larger than all microscopic lengths, the growth law has the power-law form $l \sim t^z$, and the structure factor has the scaling form $S(q,t) \sim l^d S(kl(t))$. Here l is the length scale of the domains, d is the spatial dimension of the system, q is the wave vector, and k is the wave vector relative to the Bragg peak of the ordered superstructure. The size of the ordered domains is accessible experimentally, and there have been several experimental studies of the kinetics of domain growth using low-energy electron diffraction **(27-32)**. There have also been many investigations of domain growth using Monte-Carlo simula-

tions **(5-11,15-26)**, where the adsorbate particles are modelled by two-dimensional lattice gases. One of the major goals in the study of the kinetics of domain growth is to determine the value of the growth exponent x and to establish the factors that affect its magnitude.

One of the factors upon which much attention has been focussed is the underlying density conservation law that is supported by the dynamics used in the simulation of the ordering process. In studying the kinetics of domain growth in lattice-gas models using Monte-Carlo simulations, two types of dynamics have been widely used: Kawasaki dynamics and Glauber dynamics **(34-36)**. The former simulates ordering in a closed system, while the latter simulates ordering in an open system. In Kawasaki dynamics, particles migrate from one lattice site to a vacant nearest-neighbor lattice site, and domain growth occurs by means of this migration. In Glauber dynamics, the system is allowed to exchange particles with an external reservoir, and this is the mechanism by which domain growth occurs. When Kawasaki dynamics are used, the system is said to evolve with conserved density, whereas this is not so when Glauber dynamics are used. In the case of the latter, the number of adsorbed particles is allowed to fluctuate, while the *average* density remains constant with time. As a result of the conservation laws supported by these dynamics, Glauber dynamics have been regarded as simulating the dynamics of weakly adsorbed overlayers for which $\nu e^{-E/k_B T} \sim 1\,\mathrm{s}^{-1}$, where E is the energy barrier for desorption and ν is the vibrational frequency along the direction of desorption, so that exchange of adsorbed molecules with the gas phase is facile. On the other hand, Kawasaki dynamics have been regarded as simulating the dynamics of strongly adsorbed overlayers for which $\nu e^{-E/k_B T} \ll 1\,\mathrm{s}^{-1}$, so that the exchange of adsorbed molecules with the gas phase is not facile.

Another factor that can affect the ordering kinetics is the degeneracy of the ordered structure. For a square lattice gas that orders into a $(\sqrt{2}\mathrm{x}\sqrt{2})R45°$ superstructure, the degeneracy is $p = 2$, and the growth exponent is $x = 1/2$, independent

of whether the dynamics support conservation of density or not **(1-3,8-13,17,18)**. The situation is not so clear for $p > 2$ which occurs, for example, in the case of a lattice gas with equal repulsive nearest and next-nearest neighbor interactions on a square lattice **(19)**. In this case, a (2x1) superstructure with $p = 4$ occurs when the lattice gas is quenched below the transition temperature. For a fractional coverage of 0.5, this transition temperature is $T_c \sim 0.525\phi/k_B$, where ϕ is the lateral interaction strength **(37)**. Sadiq and Binder **(19)** have studied this system in detail, showing that $x \sim 0.35$ for Kawasaki dynamics and $x \sim 1/2$ for Glauber dynamics. In the case of Kawasaki dynamics, they argued that domain growth is governed by the diffusion of an excess (or deficit) fractional coverage at the domain walls. It was suggested that diffusion of the adsorbed particles from regions of excess to regions of deficit fractional coverage is necessary for domain growth, and that such a mechanism gives rise to $x \sim 1/3$. An investigation by Vinals and Gunton of a lattice-gas model for hydrogen chemisorbed on Fe(110) was not able, however, to verify this conjecture **(20)**. This system has both a (2x1) and a (3x1) phase. The (2x1) phase has degeneracy $p = 2$, and the (3x1) phase has degeneracy $p = 3$. Although domain walls with excess fractional coverage exist for both phases, it was found that $x = 1/2$ for the (2x1) phase, whereas the value of x ranged from approximately 0.14 to approximately 0.25 for the (3x1) phase. Another recent Monte-Carlo study has suggested that the Sadiq-Binder result of $x \sim 1/3$ is due to a 'crossover' from zero to the true asymptotic value which is 1/2 **(24)**. Using Kawasaki dynamics, the growth exponent for threefold-degenerate $(\sqrt{3}\text{x}\sqrt{3})R30°$ domains was found to be 1/2 **(38)** even with only nearest-neighbor hops. These simulations were performed with a triangular lattice gas with a nearest-neighbor repulsive interaction and a next nearest-neighbor attractive interaction of equal magnitude. At zero temperature domain growth is frozen in this system **(39)**.

Most studies of the kinetics of domain growth have utilized either Kawasaki or Glauber dynamics. These dynamical models do not allow for the possibility

of a precursor state. In many real systems, however, precursor states are important intermediates for surface diffusion **(40)**; adsorption, desorption and reaction **(41-44)**; and island formation **(42,45)**. An example is the diffusion of hydrogen adatoms on the Pt(111) surface. At a fractional coverage of 0.24, the preexponential factor for diffusion is 1.0 cm^2-s^{-1} **(40)**. If the lattice constant λ is 3 Å and the frequency of frustrated translational motion parallel to the surface is 10^{13} s^{-1}, then the value of the preexponential factor for diffusion for a random walk between sites is $D_0 = \lambda^2\nu/4 = 2.2 \times 10^{-3} cm^2$-$s^{-1}$. The large experimental value, compared to that which would be expected for the case of single 'hops,' is strong evidence for the existence of a stable precursor particle that executes many 'hops' prior to deexcitation into a chemisorbed state. Therefore, we have investigated domain growth in lattice-gas models which have both a strongly bound, chemisorbed state and a weakly bound, mobile precursor state at each lattice site.

2. MODEL

We have performed Monte-Carlo simulations of two models, referred to as model I and model II. In both models two adsorption states exist at each site of the lattice: a strongly bound chemisorption state and a weakly bound precursor or physically adsorbed state. A chemisorbed lattice-gas particle can only be excited into the precursor state at the same site. On the other hand, a lattice-gas particle in the precursor state can either be deexcited into the chemisorbed state at the same site if there is not another particle already chemisorbed there, desorb from the lattice if the system is open, or migrate to the precursor state of a nearest-neighbor site. We allow adsorption from the gas phase into the precursor state at any site when an open system is being modelled. There are five microscopic processes the rates of which we have to consider: (1) excitation from a chemisorbed state to a precursor state at the same site; (2) deexcitation from a precursor state to a chemisorbed state at the same site; (3) migration from a precursor state at any site to the precursor state at a nearest-neighbor site; (4) desorption from a

precursor state; and (5) adsorption into a precursor state.

In model I the excitation-deexcitation potential is modelled by two intersecting parabolae **(46)**,

$$E_1 = k_1\zeta^2/2 + \alpha_1,$$

and

$$E_2 = k_2(\zeta - \zeta_0)^2/2 + \alpha_2,$$

as may be seen in Fig. 1. The well described by E_1 is the chemisorption well, and that described by E_2 is the precursor well. The top of the barrier is the point of intersection of the two parabolae, and the barriers for excitation E_{exc} and deexcitation E_{dex} are the differences in energy between this point of intersection and the bottoms of the chemisorption and precursor wells, respectively. The variable ζ is the excitation coordinate with the origin at the equilibrium position of the chemisorbed particle. The equilibrium position of a particle in the precursor state is ζ_0. The parameters k_1 and k_2 are, respectively, the force constants of the chemisorption well and the precursor well; and the energies of the bottoms of these wells are α_1 and α_2, respectively. The role of the lateral interactions, which we assume exist only between chemisorbed particles, is to shift the chemisorption potential of a particle according to the lattice-gas configuration of its neighborhood. This shift in the chemisorption potential is modelled by $\alpha_1 = \phi_{nn}N_{nn} + \phi_{nnn}N_{nnn}$, where ϕ_{nn} and ϕ_{nnn} are the strengths of the nearest and next-nearest neighbor lateral interactions, and N_{nn} and N_{nnn} are the number of occupied nearest and next-nearest neighbor sites. The zero of energy is thus chosen to be the bottom of the chemisorption potential for a lattice-gas particle with no nearest or next-nearest neighbors, i.e., an isolated lattice-gas particle. The energy barrier for excitation is therefore a function of the local configuration of the *chemisorbed* particles. The height of the bottom of the precursor well α_2 is taken to be constant, i.e. we have assumed that only chemisorbed particles experience lateral interactions, whereas precursor particles do not. Although this may not be valid in general, we investigate only cases in

which the precursor density is vanishingly small, and hence do not need to consider the interaction between two precursor particles. We assume that the interaction between the precursor particles and the chemisorbed particles may be neglected since most lateral interactions are mediated by the substrate, and the coupling of the precursor particle to the substrate is weak. The migration and desorption barriers are E_{mig} and E_{des}, and they are assumed to be constant, independent of the local configuration. The probabilities of success for each attempt of a microscopic event are assumed to be given by the Boltzmann factors with the respective energy barriers, i.e.,

$$p_{exc} = \exp(-E_{exc}/k_BT),$$

$$p_{dex} = \exp(-E_{dex}/k_BT),$$

$$p_{mig} = \exp(-E_{mig}/k_BT),$$

and

$$p_{des} = \exp(-E_{des}/k_BT).$$

The probability of adsorption is also a constant which depends on the pressure of the gas-phase reservoir and the trapping probability into the precursor state. In our simulations of open systems, the probabilities of adsorption and desorption are chosen so that the time average of the fractional coverage is maintained constant.

We studied a square lattice gas with equal nearest and next-nearest neighbor repulsive interactions, i.e., $\phi_{nn} = \phi_{nnn} \equiv \phi$. The domain growth kinetics for this model have been studied by Sadiq and Binder using both Kawasaki and Glauber dynamics **(19)**. At a fractional coverage of 0.5, the critical temperature is $T_c \sim 0.525\phi/k_B$ **(37)**, where the strength of the repulsive lateral interaction is given by ϕ. We simulated the lattice gas at a temperature of $T = 0.3325\phi/k_B$, i.e., $T/T_c \sim 0.633$. This temperature was chosen to be equal to the temperature that was used by Sadiq and Binder in their simulations **(19)**, allowing direct comparisons

to be made between Kawasaki and Glauber dynamics and our model for precursor-mediated ordering.

The energy of the bottom of the precursor well was chosen to be 10ϕ. For model I we simulated systems in which $k_1\zeta_0^2 = 20\phi$ and systems in which $k_1\zeta_0^2 = 40\phi$. If the reduced mass of the adsorbed particle is $\mu = 10$ AMU, the lateral interaction strength is $\phi = 5$ kcal/mol, and the displacement between the equilibrium positions of the chemisorption well and the precursor well is $\zeta_0 = 1$ Å , then these values for the force constants correspond to frequencies of approximately $343\,\mathrm{cm}^{-1}$ and $485\,\mathrm{cm}^{-1}$, respectively, for the vibrational motion of the chemisorbed particle perpendicular to the surface of the solid. Similarly, the assumed force constants of the precursor well, $k_2\zeta_0^2 = \phi$ and $k_2\zeta_0^2 = 10\phi$, correspond to frequencies of approximately $77\,\mathrm{cm}^{-1}$ and $243\,\mathrm{cm}^{-1}$, respectively, for vibrational motion of the precursor perpendicular to the surface. The values of the force constants of the model excitation-deexcitation potentials for each set of simulations are summarized in Table 1.

Since the lateral interactions are restricted to equal nearest and next-nearest neighbor chemisorbed particles, a chemisorbed particle can have one of nine different values for the probability of successful excitation, depending on the number of nearest and next-nearest neighbor occupied sites that it possesses. Similarly, there are nine different values for the probability of successful deexcitation of a precursor particle. The probabilities of success of excitation and deexcitation for each particular local configuration are summarized in Tables 2 to 4. These are given by the Boltzmann factors with the energy barriers for excitation E_{exc} and deexcitation E_{dex}, respectively. The probabilities of success of migration, desorption and adsorption are also summarized in Table 1. For these microscopic events we choose the values of the probabilities of success directly, rather than choosing the values for the energy barriers and then calculating the corresponding Boltzmann factors. The probabilities of adsorption into and desorption from the precursor state are

chosen so that the average fractional coverage on the surface is $\theta = 0.5$. The probabilities of all possible microscopic events that each precursor particle can undergo are normalized according to $(p_{dex} + p_{des} + 4p_{mig} + p_0)/6 = 1$, where p_0 is the sum of the probabilities of *failure* of deexcitation, desorption, and migration in each of the four different directions.

Model II is a simpler model which has the same essential features as model I, i.e., a precursor state in which the particle is mobile and a chemisorbed state in which the particle is not mobile are present. The probability of excitation of a chemisorbed particle is again given by

$$p_{exc} = \exp(-E_{exc}/k_B T),$$

but now E_{exc} is simply set equal to $E_0 - \phi_{nn}N_{nn} - \phi_{nnn}N_{nnn}$, where E_0 is the energy barrier for excitation of an isolated chemisorbed particle. For all the simulations of model II that we performed, we set E_0 to be equal to 8ϕ. Again both lateral interaction strengths are equal ($\phi_{nn} = \phi_{nnn} = \phi$) and repulsive, and the system was simulated at the same temperature T, approximately equal to $0.633T_c$, as in model I. With these parameters, the probability of successful excitation of a chemisorbed particle ranged from 3.55×10^{-11} to unity for each attempt. The probability of deexcitation is set equal to a constant, $p_{dex,II}$, independent of the neighborhood into which the precursor particle attempts to deexcite. The probability of migration is also set equal to a constant, $p_{mig,II}$. These probabilities are normalized such that

$$p_{dex,II} + 4p_{mig,II} = 1,$$

i.e., model II was only used to examine closed systems.

Precursors are frequently observed in real adsorbed systems **(40-43)**. These lattice-gas models enable us to study the consequences resulting from the presence of a precusor state on the kinetics of ordering **(45)**. By varying the ratio of deexcitation probabilities to excitation probabilities, the precursor can be made

to be either 'long-lived' or 'short-lived.' This is done in model I by varying the force constants of the chemisorption and precursor wells, which in turn determine the magnitudes of the energy barriers for excitation and deexcitation, as discussed earlier in this section; and in model II by varying the ratio of the probability of deexcitation to migration. Therefore, it is possible to vary the average number of hops n_s taken by a precursor particle prior to its deexcitation, which turns out to be an important factor in determining the growth kinetics. We also allow in model I both migration of adsorbed particles and exchange of adsorbed particles with an external gas reservoir to occur simultaneously. This is in contrast to both Kawasaki dynamics where only particle migration occurs and Glauber dynamics where only adsorption and desorption occur. We can therefore vary the effective contributions to the ordering process due to particle migration (spin exchange in the language of spin systems) and particle adsorption and desorption (spin flip in the language of spin systems).

3. ALGORITHM AND DYNAMICS

The probabilities of success of the various microscopic events in model I are shown in Tables 2 to 4. It can be seen that these probabilities vary over many orders of magnitude, and thus a conventional Monte-Carlo simulation would not be practical. We use an approximation to circumvent this problem of diversity of time scales. The deexcitation rates are much higher than the excitation rates, which implies that at any instant there are either none or only one precursor particle. We can justify this statement with a simple kinetic argument which leads to the following expression for the fraction of precursor particles:

$$\langle n \rangle / N = \epsilon / (1 + \epsilon).$$

Here $\langle n \rangle$ is the average number of precursor particles, N is the total number of particles (5000 for most of our runs), and ϵ is the ratio of an average probability of

excitation to an average probability of deexcitation. As the lattice gas is quenched below the critical temperature, the initial, random configurations form ordered (2x1) domains separated by walls from ordered (2x1) domains of other phases. The types of walls which can occur are illustrated in Fig. 2(a-f). To obtain an estimate for ϵ, we need to consider only the local configurations within the ordered domains and those at the domain walls. Within the ordered (2x1) domains, the local configurations are thermodynamically the most favorable. This, however, is not the case at the domain walls. Thus, precursor particles are formed mainly by the excitation of particles chemisorbed at the domain walls. The local configuration that gives rise to the largest value for ϵ is the type of wall shown in Fig. 2(a). However, the walls in Fig. 2(a,b) are quite unfavorable thermodynamically and do not occur after a short transient period. This was also observed in the simulations by Sadiq and Binder **(19)**. Of the remaining types of walls, the one with the largest value of ϵ is shown in Fig. 2(c). At this type of wall, there are chemisorbed particles which have a total of four nearest and next-nearest neighbors. Using Table 4, which corresponds to the set of force constants that gives rise to the highest concentration of precursor particles, the value of ϵ for the local configuration at these types of walls is approximately 1.4×10^{-8}. Therefore, we expect to find, at most, only one precursor particle at any instant of time, i.e., with this numerology $\langle n \rangle = 5 \times 10^{-5}$.

Since the concentration of precursor particles is extremely low, the simulations can be carried out with two time scales. Excitation and adsorption (when open systems are simulated) are much slower events compared to migration, deexcitation and desorption (when open systems are simulated). For the slow processes, an adsorption event or an excitation event is chosen according to its relative probability, as in the 'n-fold' way **(47)**. We shall discuss in detail, presently, how this choice is made and by how much the time is incremented for each Monte-Carlo step. Once either one of these slow events occurs, there is a particle in a precursor state. The interaction of the precursor particle with the heat bath is then modelled as

follows. There are four directions in which the precursor particle may migrate, each corresponding to each direction on the square lattice. The precursor particle may also desorb or deexcite. Hence, there are six 'directions' available to the precursor particle. We assume that the heat bath excites the precursor particle with equal probability in each of these directions. Having chosen the direction of excitation, the probability of success of that event is then compared to a random number between zero and one. Only if the probability of success is larger than or equal to the random number does the event occur. This procedure is succinctly expressed in the normalization condition which we discussed in the previous section. It is repeated until the precursor particle either deexcites into a chemisorbed state or desorbs into the external gas-phase reservoir. Then we return to the slow time scale, and another precursor particle is generated by either excitation of a chemisorbed particle or adsorption from the external reservoir.

With τ^{-1} equal to the frequency with which the heat bath excites the precursor particles, and the probabilities of success for migration, deexcitation and desorption as defined earlier, the time increment for each step in the fast time scale is simply τ. Typically, τ^{-1} ranges approximately from $5 \times 10^{12}\,\mathrm{s}^{-1}$ to $1 \times 10^{13}\,\mathrm{s}^{-1}$. To calculate the time increment for each slow time-scale step, we group the slow events of excitation and adsorption into classes i, each corresponding to a probability of success p_i for each attempt; and m_i is the number of potential events in class i. For instance, if there were a total of n_i chemisorbed particles with a certain type of neighborhood such that the probability of success of excitation were p_i, then $m_i = n_i$. For adsorption, $m_i = L^2$, the total number of lattice sites, all of which are able to receive a particle from the external reservoir. Then an event in class i is chosen with relative probability

$$R_i = m_i p_i / \sum_i m_i p_i .$$

Having chosen an event in class i, the time is increased by $6\tau/p_i$. The factor of six

is due to the assumption that the heat bath excites a chemisorbed particle with equal probability in six directions, and only one of these directions can produce a precursor particle. For adsorption, as we have mentioned earlier, the probability is chosen so that the average fractional coverage is maintained at 0.5. Corresponding to each particular value of p_{ads}, a rate at which gas-phase particles are impinging upon the surface can be calculated, taking into consideration the factor of six that we have introduced to model the excitation. Thus, the simulations are performed as a series of slow events, widely separated in time, each of which is followed immediately by a series of fast events which terminate long before the next slow event occurs.

In model II, the algorithm is similar. The chemisorbed particle which is to be excited into the precursor state is chosen by considering the relative probabilities R_i as above. The time is incremented by $6\tau/p_i$ for each excitation of a chemisorbed particle from class i. Once there is a precursor particle, it is allowed either to migrate to a nearest-neighbor site or to deexcite. A random number r between zero and one is generated and compared to $p_{dex,II}$. If r is greater than $p_{dex,II}$ the particle is moved to a randomly chosen nearest-neighbor site. Otherwise, the site in which the precursor is located is checked for its occupancy. If the site is not already occupied by a chemisorbed particle, then the precursor is deexcited into it. If the site is already occupied by a chemisorbed particle, then the precursor particle remains where it is and the procedure is repeated. As in the algorithm for model I, the time is incremented by τ for each deexcitation or migration event.

4. RESULTS AND DISCUSSION

For each of the sets of parameters for model I shown in Table 1, 20 runs on a lattice of size (100x100) and five runs on a lattice of size (120x120) were performed. Periodic boundary conditions were used. For each set of simulations, the average domain size in units of the lattice constant is plotted as a function of time in units

of τ in Figs. 3 and 4. For each of the curves A through J in Figs. 3 and 4, the parameters used in the simulations have been summarized in the corresponding row in Table 1. Although we did not observe any finite-size effects in the simulations of model I, this could be due to the similarity in size of the two lattices that were employed. For the simpler model II, we were able to perform longer simulations on larger lattices. We performed simulations in which $p_{dex,II} = 0.5$, $p_{dex,II} = 0.8$ and $p_{dex,II} = 0.9$. Lattices of size (400x400) were used and we performed five runs for each value of $p_{dex,II}$. The domain size as a function of time is shown in Fig. 5, with the domain size in units of the lattice constant and the time in units of τ. In the simulations, we allowed the average domain size to grow until it reached $\sim L/3$, which is comparable to the average sizes obtained in simulations by Sadiq and Binder **(19)**. Each of the initial configurations was generated by populating the lattice at randomly selected sites until a fractional coverage of 0.5 was reached. For each set of parameters, the data points between the arrows (relatively late stages of growth) were fitted by a least-squares procedure to obtain the growth exponents. The values obtained are shown on the corresponding curves in Figs. 3 to 5. If $1/\tau \sim 10^{13}\,\mathrm{s}^{-1}$, this corresponds to domain growth at $0.5 < t < 200$ s for model I and $10^{-3} < t < 1$ s for model II. Experimentally, the initial configurations can be obtained by adsorbing molecules on a solid surface at very low temperatures so that the random configurations are frozen-in. The simulations then correspond to raising the temperature suddenly, allowing the particles to migrate.

The results of Sadiq and Binder **(19)** indicate that Kawasaki dynamics give a value of $\sim 1/3$ while Glauber dynamics give a value of $\sim 1/2$ for the growth exponent for this system. The difference between these two dynamics, as mentioned earlier, is that Glauber dynamics allow particle exchange, but Kawasaki dynamics do not. Hence, Glauber dynamics have frequently been associated with systems in which adsorption and desorption occur, and Kawasaki dynamics with systems in which only particle migration occurs. Thus, Glauber dynamics are frequently

considered to simulate the dynamics in weakly (physically) adsorbed systems, while Kawasaki dynamics are frequently considered to simulate the dynamics in strongly (chemically) adsorbed systems. In real adsorbed systems, however, it is obviously possible that adsorption and desorption occur along with particle migration on the surface. For domain sizes which are not extremely large, it is not certain that the observed growth exponents for open systems are equal to 1/2. Indeed, our simulations show that it is possible to observe growth exponents smaller than 1/2 for open systems. Consider the results for sets A, B and C in Fig. 3. The parameters for these sets of runs are all the same except for the rates of adsorption and desorption. It is clear that for the domain sizes accessible to our simulations the growth exponent decreases from $\sim 1/2$ to $\sim 1/3$ as the rate of particle exchange with the external reservoir decreases. Consider the ratio of the rate of exchange of particles between the precursor state and the external gas reservoir to the rate of exchange of particles between the precursor state and the chemisorption state. The results from the simulations in sets A, B and C show that as this ratio increases, the growth exponent x tends to the value given by Glauber dynamics. The same effect is observed by comparing set D with set E, and by comparing set J with set H. In each pair the parameters controlling the values of p_{exc} and p_{dex} are the same for both sets. However, sets D and J are open systems while sets E and H are closed systems. The observed growth exponents are higher for the open systems than for the closed systems. It is probable that as the domains get extremely large, the growth exponent observed for open systems tends to 1/2, regardless of the ratio of the rate of adsorption and desorption compared to the rate of migration. There are two possible ways in which this can occur. If the rate of domain growth due to particle migration decreases faster with domain size than the rate of domain growth due to particle adsorption and desorption, then when the domains are sufficiently large, domain growth is due mainly to adsorption and desorption, even when the probability of particle exchange between the precursor state and the gas phase is

smaller than the probability of particle exchange between the precursor state and the chemisorbed state. In this case the growth exponent of open systems will show a crossover from 1/3 to 1/2 when the domain size is sufficiently large that the contribution due to particle migration becomes very small. The results of sets A and B would then indicate that for the domain sizes reached in the simulations this crossover has occurred for set A but not for set B. However, it is also possible that the growth exponent for a closed system is also 1/2 and not 1/3, and that for two otherwise identical systems the growth exponent reaches its asymptotic limit earlier for an open system than for a closed system. Hence, the observed growth exponents for systems in which the rates of adsorption and desorption are higher would be larger because these systems would be closer to the asymptotic limit even though the domain sizes are the same.

A gradual increase in the observed growth exponent also occurs when the 'lifetime' of the precursor increases. It can be seen that as the allowed length of hops in a simulation using Kawasaki dynamics tends to infinity, the simulation is effectively being performed with Glauber dynamics. As the 'lifetime' of the precursor increases, the precursor particle is able to probe a larger area of the lattice prior to its deexcitation. Therefore, precursor-mediated migration is a physically realistic dynamic, which in the limit of infinite precursor 'lifetime' becomes Glauber dynamics. As the 'lifetime' of the precursor increases, the observed growth exponent also increases. This can be seen by comparing set F with set I, and set H with set G. Sets F and I have the same values of p_{exc} and p_{dex}. However, p_{mig} for set F is twice as large as p_{mig} for set I. A similar comparison holds for sets H and G. In both cases, the simulations in which the value of p_{mig} is larger gives the larger observed growth exponent. These results indicate that the exponent for the growth of (2x1) domains on a square lattice is probably 1/2. That the observed growth exponent is less than 1/2 for sets I and G could be an indication that the asymptotic limit has not been reached for these simulations. The experimental growth exponent for

oxygen adatoms on W(110), which orders into (2x1) domains which may have a degeneracy of $p = 4$, is $x \sim 0.28 \pm 0.05$ **(28,31)**. This could be due to the same effect that we see in our simulations. In order to verify that the growth exponent is 1/2, we have performed simulations of model II on larger lattices.

Note that although the essential features of precursor-mediated migration is preserved in model II, the details of the dynamics are quite different because in model II the probability of deexcitation of a precursor into a vacant site is independent of the neighborhood of the site, and the probability of excitation of a chemisorbed particle is computed differently. Regardless of these differences, however, the equilibrium distribution of the configurations of the chemisorbed particles is the same for both models because the Hamiltonians for the two models are identical. The results presented in Fig. 5 show that the growth exponent for (2x1) domains on a square lattice is 1/2 even for closed systems. This result has been suggested by previous simulations of the same system using Kawasaki dynamics and allowing next nearest-neighbor hops **(24)**. Our results show that even for $p_{dex,II} = 0.9$, which gives an average of approximately 0.222 step taken by a precursor particle prior to deexcitation, the growth exponent of 1/2 is observed. It is not clear why this value of the growth exponent is observed in model II even for domain sizes of only 10 lattice constants, while for some sets of parameters used in model I the observed growth exponent is not 1/2 even though domain sizes of up to approximately 30 lattice constants are obtained. This, however, must be due to differences in the details of the dynamics.

If we fit the simulation results with $l \sim At^{1/2}$, we observe that the value of A increases as $p_{dex,II}$ decreases, i.e., as the probability of migration of the precursor particles increases. The values of A obtained from the simulations are $(3.16 \pm 0.20) \times 10^{-5}$, $(1.58 \pm 0.10) \times 10^{-5}$ and $(1.05 \pm 0.10) \times 10^{-5}$ for $p_{dex,II}$ equal to 0.5, 0.8 and 0.9, respectively. The quantity A is in units of lattice constant per $\tau^{1/2}$. It is rather interesting that the ratio of the values of A, namely, 3.16 : 1.58 : 1.05

for the three values of $p_{dex,II}$ agrees rather well with the analogous ratio of the square root of the average number of hops taken by a precursor particle prior to deexcitation. This latter ratio, obtained from the simulations, is approximately $2.0^{1/2} : 0.5^{1/2} : 0.222^{1/2}$ (48). This can be understood as follows. Obviously, the quantity A has the dimensions of the square root of a diffusion coefficient, as has been found in the Lifshitz-Allen-Cahn theory for phase coarsening (4). We, therefore, consider the diffusion coefficient of the adsorbate particles. A particle in the precursor state executes a random walk. Hence, the mean square displacement $\langle s^2 \rangle$ experienced by a particle from the time it is excited from a chemisorbed state to the time it becomes deexcited back into a chemisorbed state is proportional to the average number of steps n_s taken by a precursor particle, because n_s plays the role of time for the random walk executed by each precursor particle. If we consider the excitation of a particle into a precursor state, its migration and then its subsequent deexcitation into a chemisorbed state to be a single 'hop' of variable length λ, then λ is equal to $\langle s^2 \rangle^{1/2}$ and, therefore, proportional to $n_s^{1/2}$. Since the diffusion coefficient in the random walk approximation is $D \sim \Gamma\lambda^2$, where Γ is the rate of hopping and λ is the hop length, it can be seen that the diffusion coefficient of the adsorbate particles is proportional to n_s. Thus, A must scale as $n_s^{1/2}$. In model II, the probability of deexcitation of a precursor particle is independent of the neighborhood of the chosen site. The only constraint is that the site must not already be occupied. In the more complicated model I, the probability of deexcitation differs from one vacant site to another, depending on the neighborhood configuration. Hence, a random walk approximation is expected to apply better to model II than to model I. Therefore, it is not obvious that the scaling relation $A \sim D^{1/2}$ is applicable to model I or to a model in which particles migrate not through a precursor state but from one chemisorption site to a nearest-neighbor chemisorption site.

5. CONCLUSIONS

We have investigated the kinetics of ordering of a model adsorbate system which has four degenerate (2x1) ordered phases on a square lattice. The use of dynamical models which have a precursor state enables us to study the influence that precursor-mediated migration has on the growth kinetics. We find that in the limit of large domain size, the growth law is $l \sim At^x$, where x is $1/2$, regardless of the mobility of the precursor particles. The observed growth exponent is, however, affected by the size of the domains reached in the simulations. If the large domain limit is not reached, smaller values of the growth exponent are observed. This limit is reached earlier in time for systems which have a higher ratio of the rate of particle exchange with the gas phase to the rate of particle migration on the lattice. For simulations of model II, which reach the large domain limit, we were able to extract values of A from the results. It was found that A is proportional to the square root of the average number of steps n_s taken by a precursor particle prior to deexcitation. This latter quantity is proportional to the diffusion coefficient D of the adsorbate particles in model II. A similar result might not be expected to hold for particle migration by nearest-neighbor hops.

Acknowledgment: This research was supported by the National Science Foundation under Grant No. CHE-8617826.

References

1. I.M. Lifshitz and V. Slyozov, J. Phys. Chem. Solids **19**, 35 (1961).
2. I.M. Lifshitz, Sov. Phys. JETP **15**, 939 (1962).
3. M. Hilbert, Acta. Metall. **13**, 227 (1965).
4. J.W. Cahn and S.M. Allen, Acta. Metall. **27**, 1085 (1979).
5. K. Binder and D. Stauffer, Phys. Rev. Lett. **33**, 1006 (1974).
6. K. Binder, Phys. Rev. B **15**, 4425 (1977).
7. K. Binder, C. Billotet and P. Mirold, Z. Phys. B **30**, 183 (1978).
8. P.S. Sahni and J.D. Gunton, Phys. Rev. Lett. **45**, 369 (1980).
9. S.A. Safran, Phys. Rev. Lett. **46**, 1581 (1981).
10. P.S. Sahni and J.D. Gunton, Phys. Rev. Lett. **47**, 1754 (1981).
11. P.S. Sahni, G. Dee, J.D. Gunton, M.K. Phani, J.L. Lebowitz and M.H. Kalos, Phys. Rev. B **24**, 410 (1981).
12. H. Furukawa, Phys. Rev. A **23**, 1535 (1981).
13. H. Furukawa, Phys. Rev. A **28**, 1717 (1983).
14. C.M. Knobler and N.C. Wong, J. Chem. Phys. **85**, 1972 (1981).
15. J. Marro, J.L. Lebowitz and M.H. Kalos, Phys. Rev. Lett. **30**, 282 (1979).
16. P.S. Sahni, J.D. Gunton, S.L. Katz and R.H. Timpe, Phys. Rev. B **25**, 389 (1982).
17. P.S. Sahni, G.S. Grest and S.A. Safran, Phys. Rev. Lett. **50**, 60 (1983).
18. S.A. Safran, P.S. Sahni and G.S. Grest, Phys. Rev. B **28**, 2693 (1983).
19. S. Sadiq and K. Binder, J. Stat. Phys. **35**, 517 (1984).
20. J. Vinals and J.D. Gunton, Surf. Sci. **157**, 473 (1985).
21. G.F. Mazenko, O.T. Valls and F.C Zhang, Phys. Rev. B **31**, 4453 (1985).

22. J. Vinals and J.D. Gunton, Phys. Rev. B **33**, 7795 (1986).

23. A. Host-Madsen, P.J. Shah, T.V. Hansen and O.G. Mouritsen, Phys. Rev. B **36**, 2333 (1987).

24. H.C. Fogedby and O.G. Mouritsen, Phys. Rev. B **37**, 5962 (1988).

25. Z.W. Lai, G.F. Mazenko and O.T. Valls, Phys. Rev. B **37**, 9481 (1988).

26. J.G. Amar, F.E. Sullivan and R.D. Mountain, Phys. Rev. B **37**, 196 (1988).

27. P.K. Wu, J.H. Perepezko, J.T. McKinney and M.G. Lagally, Phys. Rev. Lett. **51**, 1577 (1983).

28. M.C. Tringides, P.K. Wu and M.G. Lagally, Phys. Rev. Lett. **59**, 315 (1987).

29. M.C. Tringides, P.K. Wu, W. Moritz and M.G. Lagally, Ber. Bunseges Phys. Chem. **90**, 227 (1986).

30. W. Witt and E. Bauer, Ber. Bunseges Phys. Chem. **90**, 248 (1986).

31. M.G. Lagally and M.C. Tringides, in **Solvay Conference on Surface Science**, F.W. de Wette, Ed.,Springer-Verlag, Heidelberg, 1987, p. 181.

32. P.K. Wu, M.C. Tringides and M.G. Lagally, Phys. Rev. B **39**, 7595 (1989).

33. J.K. Zuo, G.C. Wang and T.M. Lu, Phys. Rev. B **39**, 9432 (1989).

34. **Monte-Carlo Methods in Statistical Physics**, K. Binder, Ed., Topics in Current Physics, Vol. 7, Springer-Verlag, Heidelberg, 1979.

35. **Applications of the Monte-Carlo Methods in Statistical Physics**, K. Binder, Ed., Topics in Current Physics, Vol. 36, Springer-Verlag, Heidelberg, 1983.

36. **Computer Studies of Phase Transitions and Critical Phenomena**, O.G. Mouritsen, Springer-Verlag, Heidelberg, 1984.

37. K. Binder and D.P. Landau, Phys. Rev. B **21**, 1941 (1980).

38. H.C. Kang and W.H. Weinberg, (unpublished).

39. H.C. Kang and W.H. Weinberg, Phys. Rev. B (ms BZ3616).

40. E.G. Seebauer and L.D. Schmidt, Chem. Phys. Lett. **123**, 129 (1986).

41. W.H. Weinberg, in **Kinetics of Interface Reactions**, M. Grunze and H.J. Kreuzer, Eds., Springer-Verlag, Heidelberg, 1987, p. 94; and references therein.

42. E.S. Hood, B.H. Toby and W.H. Weinberg, Phys. Rev. Lett. **55**, 2437 (1985).

43. K. Sinniah, M.G. Sherman, L.B. Lewis, W.H. Weinberg, J.T. Yates, Jr. and K.C. Janda, Phys. Rev. Lett. **62**, 567 (1989).

44. O.M. Becker and A. Ben-Schaul, Phys. Rev. Lett. **61**, 2859 (1988).

45. H.C. Kang and W.H. Weinberg, Phys. Rev. B **38**, 11543 (1988).

46. H.C. Kang and W.H. Weinberg, J. Chem. Phys. **90**, 2824 (1989).

47. A.B. Bortz, M.H. Kalos, J.L. Lebowitz, J. Comp. Phys. **17**, 10 (1975).

48. The value of n_s can be obtained from simulations, but it can also be shown that $n_s = 0.5p_{dez,II}(1 - p_{dez,II})/[1 - 0.5(2 - p_{dez,II})]^2$.

Set	$k_1\zeta_0^2/\phi$	$k_2\zeta_0^2/\phi$	p_{mig}	p_{des}	p_{ads}
A	20	10	0.3	0.30	4.32×10^{-9}
B	20	10	0.3	0.06	8.64×10^{-10}
C	20	10	0.3	0.00	0.00
D	20	10	0.6	0.30	4.32×10^{-9}
E	20	10	0.6	0.00	0.00
F	40	10	0.6	0.00	0.00
G	20	1.0	0.3	0.00	0.00
H	20	1.0	0.6	0.00	0.00
I	40	10	0.3	0.00	0.00
J	20	1.0	0.6	0.30	4.32×10^{-9}

Values of parameters used in simulations.

Table 1

α_1/ϕ	p_{exc}	p_{dex}
0	8.68×10^{-14}	1.00
1	1.70×10^{-12}	0.96
2	3.03×10^{-11}	0.85
3	4.99×10^{-10}	0.69
4	7.45×10^{-9}	0.51
5	1.00×10^{-7}	0.34
6	1.20×10^{-6}	0.20
7	1.26×10^{-5}	0.10
8	1.24×10^{-4}	0.05

Probabilities of success for excitation and deexcitation for sets A, B, C, D and E at temperature $T = 0.3325\phi/k_B$

Table 2

α_1/ϕ	p_{exc}	p_{dex}
0	2.69×10^{-14}	0.310
1	4.09×10^{-13}	0.232
2	5.97×10^{-12}	0.168
3	8.31×10^{-11}	0.116
4	1.10×10^{-9}	0.076
5	1.38×10^{-8}	0.047
6	1.61×10^{-7}	0.027
7	1.75×10^{-6}	0.015
8	1.75×10^{-5}	0.007

Probabilities of success for excitation and deexcitation for sets F and I at temperature $T = 0.3325\phi/k_B$.

Table 3

α_1/ϕ	p_{exc}	p_{dex}
0	8.68×10^{-14}	1.00
1	1.75×10^{-12}	0.99
2	3.50×10^{-11}	0.98
3	6.91×10^{-10}	0.96
4	1.35×10^{-8}	0.93
5	2.60×10^{-7}	0.88
6	4.89×10^{-6}	0.82
7	8.98×10^{-5}	0.74
8	1.58×10^{-3}	0.65

Probabilities of success for excitation and deexcitation for sets G, H and J at temperature $T = 0.3325\phi/k_B$.

Table 4

Figure Captions

Figure 1. Excitation-deexcitation potential for model I.

Figure 2. Types of domain walls for ordered (2x1) domains on a square lattice.

Figure 3. The results of simulations of model I for parameter sets A through E in Table 1. The value of $l(t)$ for each set has been multiplied by an offset factor, f, for clarity. The value of f is 1, 2, 4, 8 and 16 for sets A, B, C, D and E, respectively. For each of these sets, $k_1\zeta_0^2/\phi = 20$ and $k_2\zeta_0^2/\phi = 10$; t is in units of τ; and l is in units of the lattice constant. The growth exponents are shown beside each line and were evaluated by a least-squares fit to the data delimited by the arrows. The uncertainties represent one standard deviation.

Figure 4. The results of simulations of model I for parameter sets F through J in Table 1. The value of $l(t)$ for each set has been multiplied by an offset factor, f, for clarity. The value of f is 1, 2, 4, 6 and 16 for sets F, G, H , I and J, respectively. For sets F and I, $k_1\zeta_0^2/\phi = 40$ and $k_2\zeta_0^2/\phi = 10$. For sets G, H and J, $k_1\zeta_0^2/\phi = 20$ and $k_2\zeta_0^2/\phi = 1$. The value of t is in units of τ; and l is in units of the lattice constant. The growth exponents are shown beside each line and were evaluated by a least-squares fit to the data delimited by the arrows. The uncertainties represent one standard deviation.

Figure 5. The results of simulations of model II for $p_{dex,II}$ ranging from 0.5 to 0.9. Each plot is labeled with its corresponding value of $p_{dex,II}$ and the best least-squares fit value of the growth exponent which was evaluated using the data delimited by the arrows. Each of the quoted uncertainties is one standard deviation. The domain size is in units of the lattice constant, and the time is in units of τ.

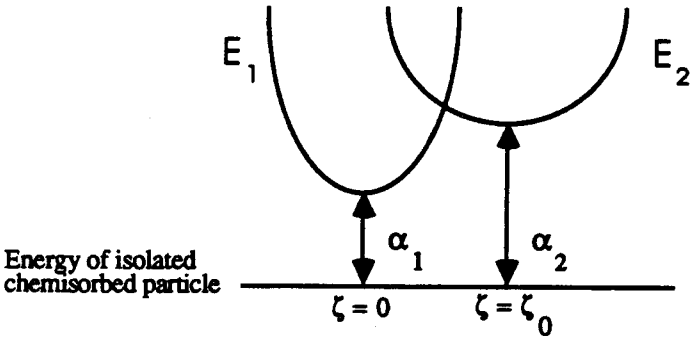

Figure 1. Model for excitation-deexcitation potential

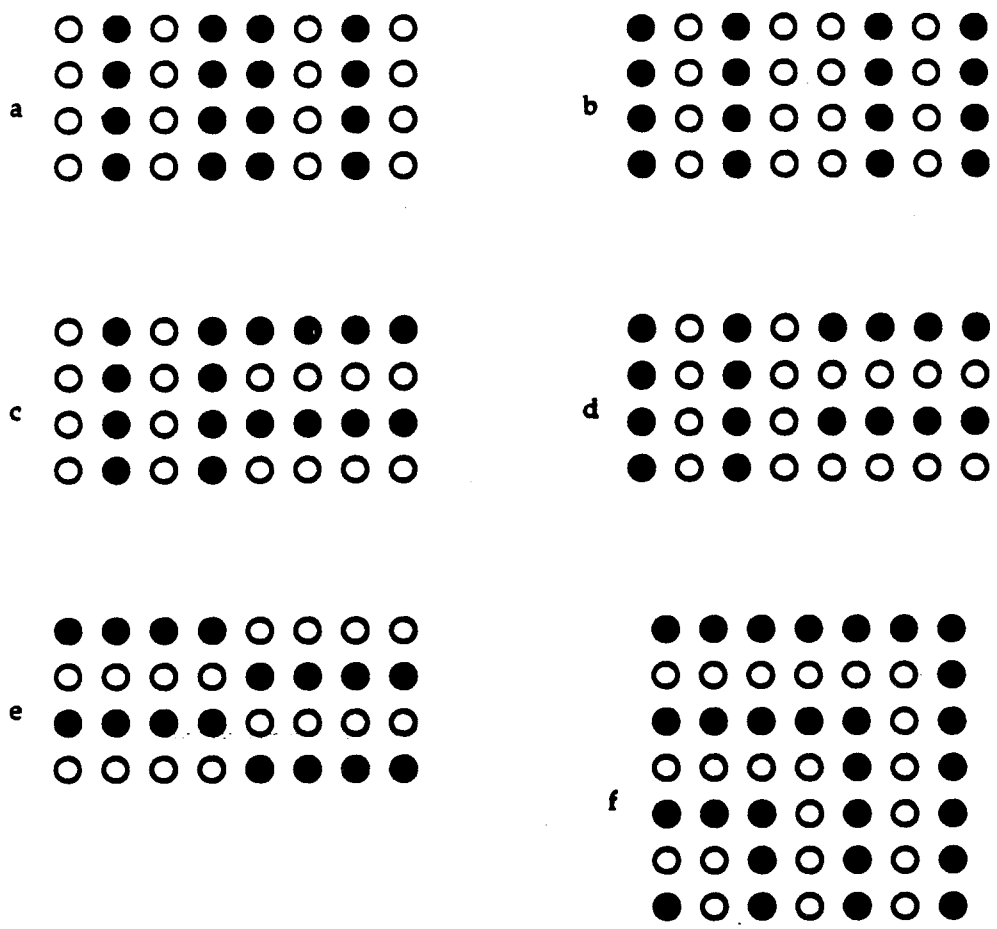

Figure 2

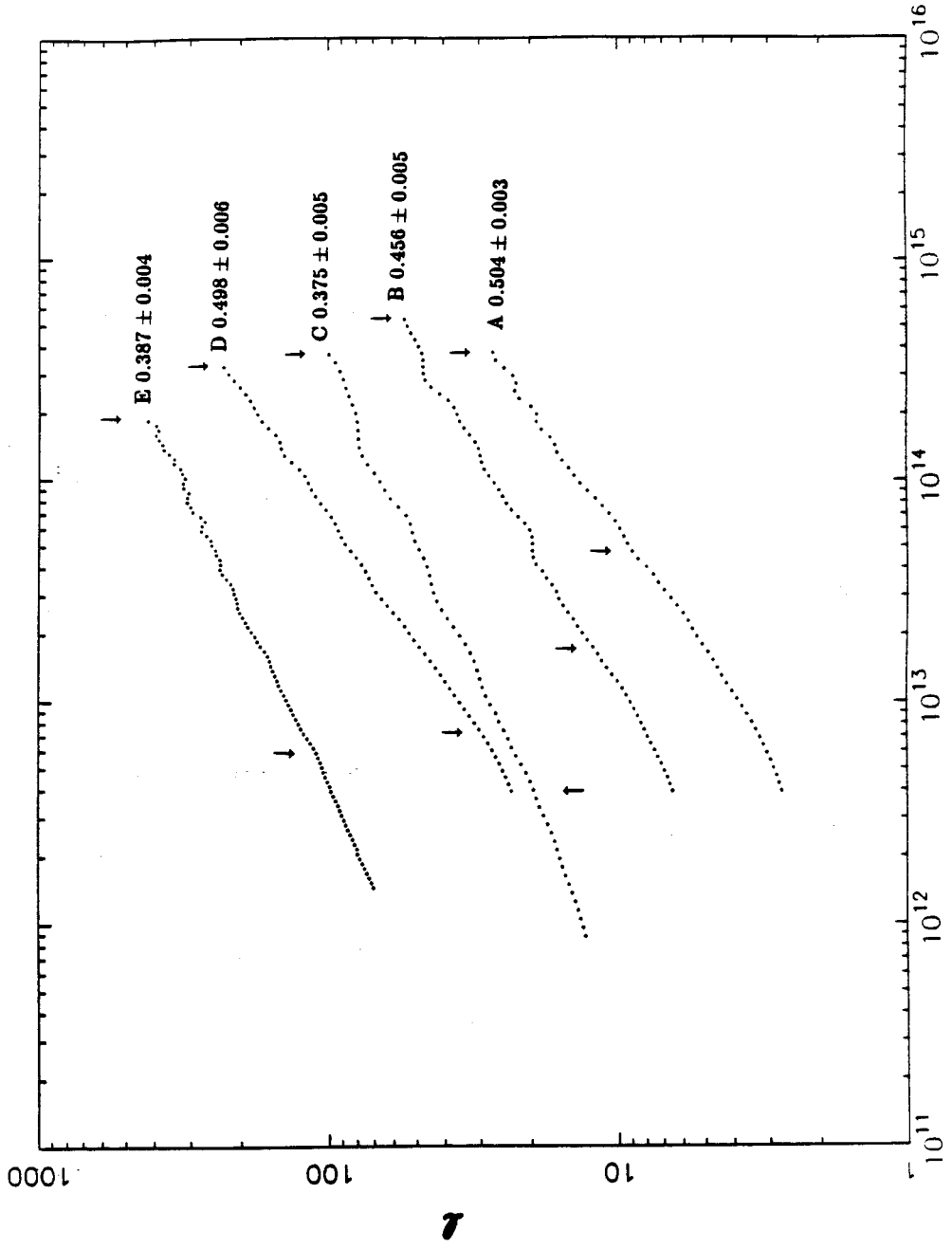
E 0.387 ± 0.004
D 0.498 ± 0.006
C 0.375 ± 0.005
B 0.456 ± 0.005
A 0.504 ± 0.003
1000
100
10
τ
10^{11}
10^{12}
10^{13}
10^{14}
10^{15}
10^{16}
t

Figure 3

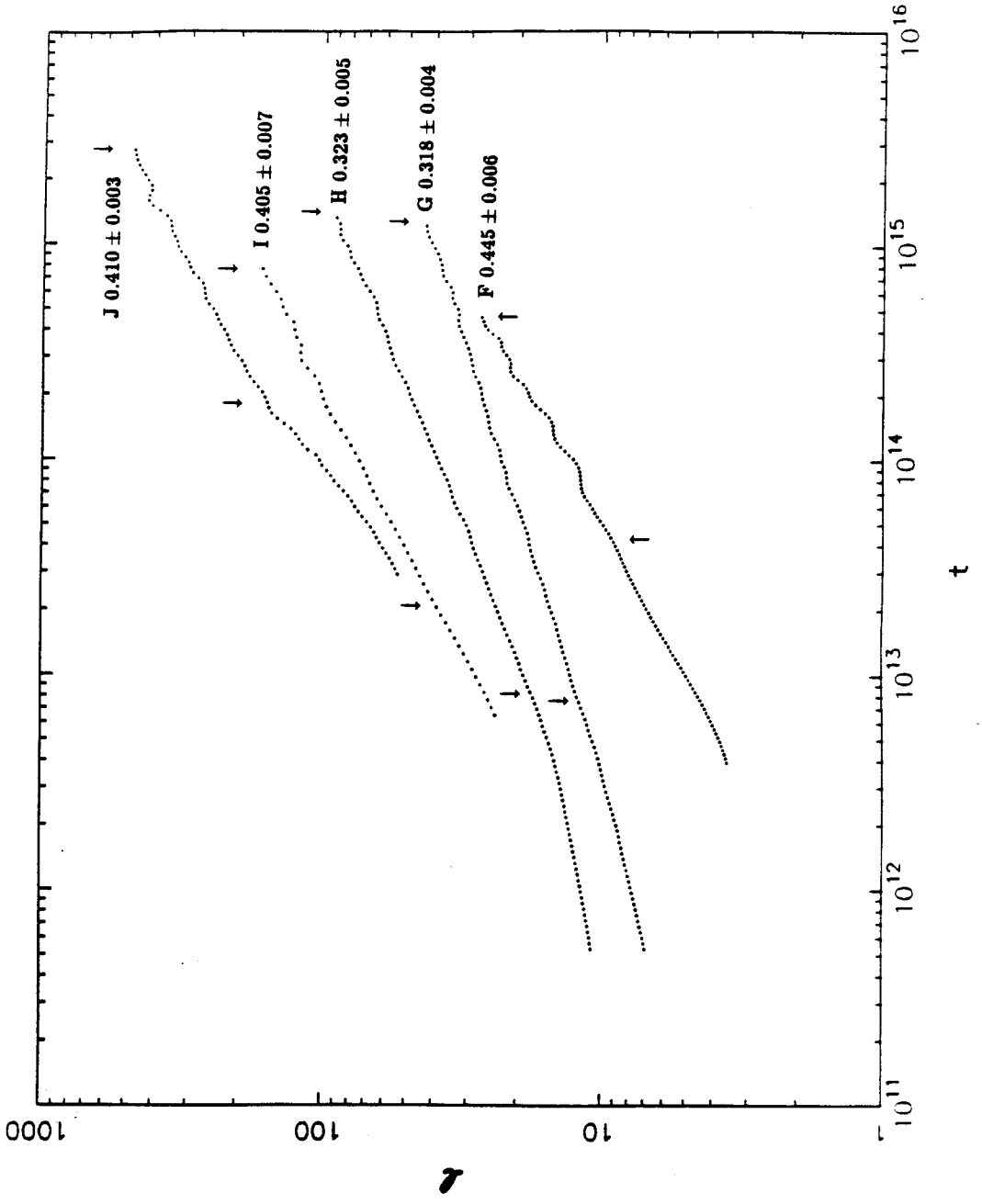
J 0.410 ± 0.003
I 0.405 ± 0.007
H 0.323 ± 0.005
G 0.318 ± 0.004
F 0.445 ± 0.006
1000
100
10
1
10^{11}
10^{12}
10^{13}
10^{14}
10^{15}
10^{16}
t

Figure 4

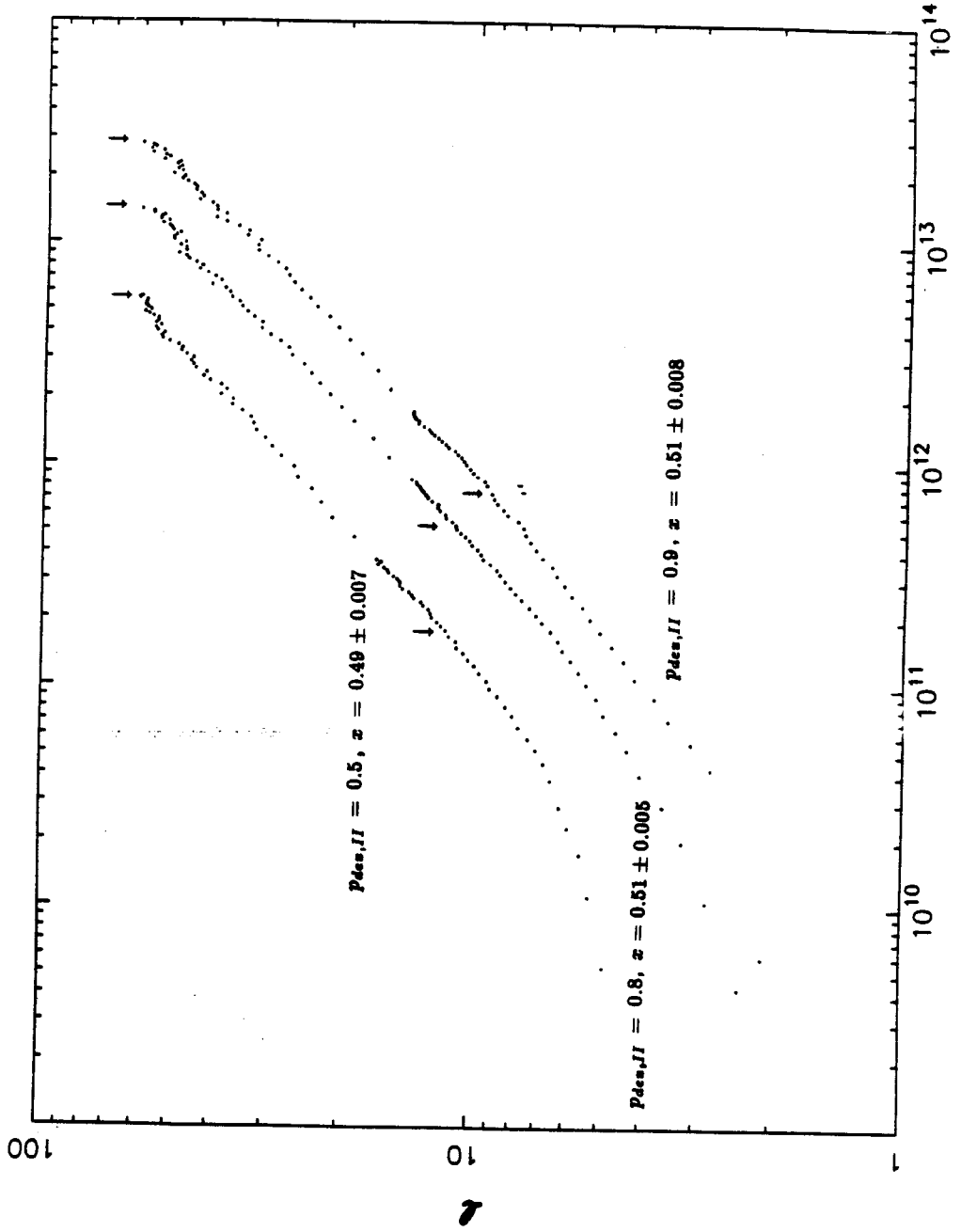
100
10
1
τ
10^{10}
10^{11}
10^{12}
10^{13}
10^{14}
t
$P_{des,II} = 0.5$, $x = 0.49 \pm 0.007$
$P_{des,II} = 0.8$, $x = 0.51 \pm 0.005$
$P_{des,II} = 0.9$, $x = 0.51 \pm 0.008$

Figure 5

Chapter 5.

Molecular Adsorption of Ethane on the Ir(110)-(1x2) Surface: Monte-Carlo Simulations and Molecular Beam Reflectivity Measurements

This chapter has been submitted as a paper by H.C. Kang, C.B. Mullins and W.H. Weinberg, to *The Journal of Chemical Physics.*

ABSTRACT

Experimental results, obtained using a molecular beam reflectivity method, for the probability of molecular physical adsorption of ethane on the Ir(110)-(1x2) surface are presented. We analyze these results using Monte-Carlo simulations and show that molecular adsorption can occur either "directly" or through a precursor state in which an ethane molecule is trapped in a second layer of molecularly adsorbed ethane with subsequent migration to a vacant site. From the Monte-Carlo simulations, we are able to establish that the energy barrier for the desorption of an ethane molecule from the precursor state is approximately 4.5 kcal/mol. We also find that the energy barrier for diffusion of an ethane molecule on top of a monolayer of ethane molecularly adsorbed on the Ir(110)-(1x2) surface is approximately 3.7 kcal/mol.

1. Introduction

The adsorption of a molecule from the gas phase onto a solid surface does not necessarily occur in one direct step. The impinging molecule may be trapped temporarily in a weakly bound precursor well before it reaches the adsorption well. For example, a physically adsorbed molecule could be a precursor to either molecular or dissociative chemisorption (**1**). Likewise, condensed molecules in a second layer could be precursors to adsorption on the surface, depending on the relative rates of migration in the second layer and desorption from the second layer (**1**). The concept of such precursor states, first proposed by Langmuir (**2,3**), is rather important in understanding the kinetics of a variety of surface phenomena. If, for instance, chemisorption is mediated by a precursor state in which the adsorbing molecule accommodates thermally to the surface, then the probability of chemisorption would be strongly affected by the surface temperature. This would not be true if chemisorption occurs directly, i.e. without passing through a precursor state. Descriptions of the kinetics of precursor-mediated adsorption have been presented by Becker (**4,5**), Ehrlich (**6**) and Kisliuk (**7**); and they have been reviewed by Weinberg (**1**). There have been important refinements of these macroscopic approaches by treating the microscopic configurations of the adsorbed layer in a statistical manner (**8-14**). Monte-Carlo modeling, taking into account the microscopic configuration of the adsorbed layer around each adsorbed molecule, and hence the lateral interactions by which each molecule is influenced, has also been formulated (**13**). In this paper we present evidence demonstrating that the molecular physical adsorption of ethane on the Ir(110)-(1x2) surface can be understood by drawing upon the concept of a precursor to molecular adsorption. We show that molecular adsorption can occur directly when an ethane molecule impinges upon the bare iridium surface or indirectly when an ethane molecule impinges upon already molecularly adsorbed ethane. The "extrinsic" precursor in this case is the mobile ethane molecule trapped on top of a layer of molecularly adsorbed

ethane **(15)**. We will refer, hereafter, to an ethane molecule in this precursor state as a trapped molecule, and an ethane molecule in the molecularly adsorbed state as a (physically) adsorbed molecule. The experimental results, which are obtained from reflectivity measurements performed using a molecular beam apparatus, are shown to be well described by Monte-Carlo simulations of a model which takes into account the two pathways delineated above.

2. Experimental and Algorithmic Details

Measurements of the probability of molecular adsorption of ethane on the Ir(110)-(1x2) surface have been made using the reflectivity method of King and Wells **(12)**, employing a molecular beam apparatus that will be described in detail elsewhere **(16)**. Briefly, the apparatus consists of a thrice differentially pumped, supersonic nozzle molecular beam source and an ultrahigh vacuum scattering chamber. Low-energy electron diffraction optics, Auger electron spectroscopy and an ion gun are mounted on the scattering chamber for obtaining and checking surface cleanliness and order. A quadrupole mass spectrometer is also mounted on the scattering chamber for thermal desorption mass spectrometry, reflectivity measurements and beam time-of-flight measurements. The source chambers contain the nozzle, a high-speed shutter and a chopper for beam modulation, as well as apertures for beam collimation. Beam energies are varied by a combination of seeding and variation of nozzle temperature and are measured by time-of-flight techniques. Both the scattering chamber and the third-beam chamber are pumped by turbomolecular pumps; the other two beam chambers are pumped by diffusion pumps. The iridium crystal is mounted on a manipulator which provides precise alignment. The manipulator is liquid nitrogen cooled, providing rapid cooling of the sample to below 80 K. The sample temperature is determined by a 0.003 in. W/5%Re-W/26%Re thermocouple spotwelded to the back of the crystal.

The partial pressure P_E of ethane, at time t, in the scattering chamber is

used as a measure of the flux of ethane molecules that do not adsorb. Hence, the probability of adsorption at time t is $(P_S - P_E)/P_S$, where P_S is the partial pressure of ethane in the chamber due to scattering from a saturated surface. Both P_E and P_S are corrected for a small effusive component of the flux **(16)**. This technique is particularly useful in measuring the adsorption probability as a function of time or coverage. The surface temperature T_s was maintained constant at approximately 77 K for all the measurements reported here. The experiments were performed with beam energies E_i ranging from approximately 2.2 kcal/mol to 10 kcal/mol, and with incident angles θ_i ranging from 0° to 45°. The incident energy and angle for each experiment are summarized in Table 1. For normal kinetic energies $E_i\cos^2\theta_i$ greater than approximately 8 kcal/mol, there is a non-zero component of direct dissociative chemisorption in the adsorption at 77 K **(16)**. As shown in Table 1, experiment *f* has a normal kinetic energy of approximately 8.5 kcal/mol and, hence, has a small component of direct dissociative chemisorption. The initial probability of dissociative chemisorption under these conditions is approximately 0.03, and this has been ignored. We can also ignore desorption of the molecularly adsorbed ethane, which only occurs at temperatures above 100 K **(17)**.

The Monte-Carlo simulations are carried out as follows. The surface is modelled by a square lattice of size 400x400. Each site is allowed to be in one of three possible states: the site can be vacant; the site can be occupied by a molecularly adsorbed particle; or the site can be occupied by a molecularly adsorbed particle *and* a particle trapped in the precursor state. A site *s* on the lattice is selected at random. If it is occupied by a trapped particle, then the particle is allowed either to hop to a nearest-neighbor site or to desorb. The choice is determined as follows. The trapped particle has a probability of 1/5 of *attempting* to move in each of five directions: the four lattice directions in the plane of the surface and the direction into the gas phase. If one of the lattice directions is chosen, the trapped particle successfully moves to the nearest-neighbor site in that direction with a probability

of p_m. If the direction into the gas phase is chosen, the trapped particle successfully desorbs with a probability of p_d. If the site s that is chosen is vacant, or is occupied by only a molecularly adsorbed particle, then a particle from the gas phase impinges upon it with a probability of p_f. If the site s is vacant, then the impinging particle is molecularly adsorbed with a probability p_0. If the site s chosen is occupied by a molecularly adsorbed particle, then the impinging particle is trapped with a probability p_1. Upon completion of this procedure, the time is increased by one Monte-Carlo step, another site is selected at random, and the procedure is repeated. When a gas-phase molecule impinges upon a trapped molecule the situation becomes more complicated than when it impinges upon either a vacant site or on top of a layer of adsorbed ethane. The trapped molecule may gain sufficient energy to desorb along with the impinging molecule, or the impinging molecule may be scattered from the trapped molecule and become trapped itself while desorbing the previously trapped molecule. However, we have simply neglected such events because the fractional coverage of the trapped ethane is vanishingly small most of the time, and even though it increases when the fractional coverage of adsorbed ethane approaches unity, the saturation value is less than approximately 0.06, as will be seen later.

The quantity measured in the reflectivity experiments is the partial pressure of ethane as a function of time. From the Monte-Carlo simulations, we obtain the values of n_i the number of particles impinging upon the lattice, and n_r the number of particles "reflecting" from the lattice in each Monte-Carlo step/site. The quantity n_r includes both the particles that impinge upon and fail to be adsorbed molecularly or trapped, and the previously trapped particles that desorb from the lattice. The quantity that is obtained from the reflectivity experiments is $(n_i - n_r)/n_i$. It should be noted that this is equal to the quantity n_a/n_i, where n_a is the number of particles molecularly adsorbing per Monte-Carlo step/site, only when the number of trapped ethane molecules in the second layer at any instant of time is vanishingly small.

There are five parameters in the simulations, namely p_0, p_1, p_m, p_d and p_f. The value of p_0 used in the simulations is obtained from the zero-coverage limit of the *experimentally measured* probability of molecular adsorption **(16)**. This is the probability with which an ethane molecule accommodates and adsorbs molecularly on the bare Ir(110)-(1x2) surface. At a particular surface temperature, it is strongly dependent on the energy of the incident beam of ethane. For the results that are presented here, the beam energy varies from $\sim$ 2.2 kcal/mol to $\sim$ 10 kcal/mol, and the corresponding values of p_0 vary from $\sim$ 0.95 to $\sim$ 0.45 at a surface temperature of 77 K. The value of p_1, the probability of accommodation of an ethane molecule on top of a physically adsorbed layer of ethane, is clearly larger than p_0 due to a better match of masses, facilitating momentum transfer, and the existence of a softer potential than in the case of a collision with the bare iridium surface **(18-20)**. In principle, both p_0 and p_1 are dependent on the beam energy. On the other hand, in our model p_m and p_d must not be dependent on the beam energy because the trapped particle is assumed to be completely accommodated thermally to the surface. In the experiments the surface temperature is kept constant at approximately 77 K. *Hence, for the simulations to be consistent physically, it is necessary that the same values of p_m and p_d successfully describe the experimental results at all beam energies.* We choose p_m to be unity, and vary the ratio of p_d/p_m. As a result, we have set the time-scale of the simulation to be the time-scale for a trapped ethane molecule to hop from one site to the next. The parameter p_f is the probability, in each Monte-Carlo step, that a a gas-phase molecule impinges upon each site. This parameter can, in principle, be determined from an accurate measurement of the flux of ethane in the molecular beam used in the experiments. If each Monte-Carlo step corresponds to a real time of τ_r, then the incident flux would be p_f/τ_r site^{-1}s^{-1}. A crude estimate of this flux in the experimental measurements is 0.1 σ^{-1}s^{-1}, where σ is the area occupied by one adsorbed ethane molecule when the surface is covered by one monolayer of ethane at 77 K. This is because the

experiments take approximately 10 s, and, as shown below, the final fractional coverages are only slightly greater than one monolayer. In the simulations, however, we used a range of values of p_f and chose the value that best fits the experimental results, cf. Table 1.

3. Results and Discussion

Before we compare the simulations with the experimental results, we discuss the simulation in the limiting case where p_f is set equal to zero, i.e., the limit of infinitesimally small flux. When p_f is zero no particles can be added onto the lattice from the gas phase because p_f is the probability of a gas particle impinging on each site of lattice per Monte-Carlo step. In this case the simulation cannot be carried out as we have discussed above. With $p_f = 0$, the Monte-Carlo procedure discussed above will not allow the number of particles on the surface to increase, because gas-phase particles impinge on the lattice with a probability of p_f per Monte-Carlo step per site. Hence, no new particles can be introduced onto the lattice with this procedure. When the flux is infinitesimally small, then any particle that impinges on the surface will have already adsorbed molecularly or desorbed before the next particle impinges on the surface. Hence, particles will have to be introduced one at a time onto the surface. Then the time in the simulations is not measured as before. In this case, the time is linearly proportional to the number of particles that are introduced onto the surface, regardless of the number of hops that each trapped particle takes before it desorbs or adsorbs. This is in contrast to the simulation procedure for the case in which p_f is not zero, where the time is increased by one Monte-Carlo step each time an attempt is made to hop, desorb or trap a particle. The simulations for $p_f = 0$ are done as follows. First, we determine the probability of molecular adsorption for a fixed coverage on the surface, and then we increase the coverage on the surface. The probability of molecular adsorption is determined by introducing test particles one at a time and counting the fraction

that adsorbs molecularly. If a test particle impinges on a vacant site, then molecular adsorption occurs with a probability of p_0. If the test particle impinges on a site which already has a molecularly adsorbed particle, then it traps with a probability of p_1. A trapped particle is allowed to attempt a move in one of the four lattice directions or in the direction into the gas phase. Each of these directions is picked with a probability of $1/5$. An attempted hop to a nearest-neighbor site is successful with a probability of p_m. If the test particle attempts to move into the gas phase, it desorbs with a probability of p_d. A test particle is allowed to migrate on the lattice by nearest-neighbor hops until it either desorbs or reaches a vacant lattice site whereupon it immediately adsorbs molecularly. Then the next test particle is introduced. In order to obtain the probability of molecular adsorption at a constant coverage, the configuration on the lattice is not updated even if a test particle molecularly adsorbs. For each datum point we introduce 2000 test particles. The configuration on the lattice is updated as follows. A certain number of test particles are introduced, again one at a time. However, now the positions of the test particles which adsorb molecularly are recorded. A test particle which adsorbs molecularly into a site at which an earlier test particle had adsorbed is not counted. After N particles have been introduced, the configuration is updated by using the recorded positions of the molecularly adsorbed test particles. Time is increased by N/FL^2, where F is the flux from the gas phase in units of site^{-1}s^{-1} and L^2 is the number of sites on the lattice. For our simulations we used $N = 1600$ so that we obtain the adsorption probabilities for every fractional surface coverage increment of 0.01. The procedure is then repeated with the new configuration. It should be noted that the time increment is not dependent upon the actual number of migration steps that are taken by the test particles, since the time for each migration step is infinitesimally small compared to that between subsequent particle impingements on the surface when $p_f = 0$.

The physical situation to which simulations with $p_f = 0$ can be applied is

when the rate at which particles from the gas phase impinge upon the surface is much smaller than $1/\tau$, where τ is the lifetime of a trapped particle. When the fractional coverage of molecularly adsorbed particles is not high, a trapped particle can find a vacant site in a time interval τ such that $1/\tau$ is much smaller than the rate at which particles impinge on the surface. In this case the quantity $(n_i - n_r)/n_i$ obtained from the simulations in which p_f is not zero would be equal to the fraction of molecularly adsorbed test particles in the simulations in which $p_f = 0$. In the simulations using $p_f = 0$, the lifetime of the trapped particles is infinitesimally small compared to the time between which particles impinge on the surface from the gas phase. Therefore, there is no accumulation of trapped particles. This means that the simulations in which $p_f = 0$ model the situation when a second adsorbed layer is not allowed. As a result, by comparing such simulations with experimental results, it is possible to infer the accumulation of a second adsorbed layer. Since both desorption and migration occur infinitely fast on the timescale of the particle flux onto the surface, it is not possible to establish, via comparison with experimental results, the absolute rates of desorption and migration. This, however, can be done with the simulations in which p_f is not zero.

The results of the reflectivity measurements are plotted as crosses in Figs. 1 and 2. The ordinate has been labelled as the probability of adsorption although for the experimental data it really corresponds to the quantity $(n_i - n_r)/n_i$. As mentioned earlier, this is equal to n_a/n_i only when the incident flux is extremely low. The abscissa is the time in units of 0.1 s. The experiments were not all performed with the same value of the incident angle θ_i. Thus, even though the beam intensities are the same for all the experiments, the incident fluxes are not. In order to correct for this we have scaled the time by $\cos\theta_i$. Although it would be interesting to perform the experiment at lower surface temperatures (this would give us an independent estimate of the difference between the desorption and migration barriers discussed below), we were not able to cool below the temperature

of liquid nitrogen. However, it should be noted that for this particular system, the temperature of $\sim$ 77 K is optimal. At higher temperatures the fractional coverage of the second layer and hence the 'tail' in the experimental data would not be so large, and at lower temperatures it might become necessary to consider the accumulation of more than two layers of ethane on the surface. A smaller 'tail' would lower the accuracy of the Monte-Carlo analysis, and the accumulation of multilayers would render it necessary to introduce additional parameters to describe the third or fourth layers and hence complicate the simulations.

The parameters that were fitted to the data are p_1, p_d/p_m and p_f/p_m. As explained earlier, p_0 is obtained directly from the experimentally measured adsorption probability at zero coverage. The parameters which best fit the experimental data are summarized in Table 1 where each row refers to the correspondingly labelled curves in Figs. 1 and 2. The results of simulations in which $p_f = 0$ are shown by the lines in Fig. 1, while the results of simulations in which p_f is not zero are shown by the circles in Fig. 2. Since the second layer does not accumulate until the first layer is close to saturation, the optimal values of p_1 and p_d/p_m can be determined from simulations in which p_f is zero. The values of p_1 used for each beam energy are shown in Table 1. It should be noted that these values are all rather close to unity, although there is a dependence on the beam energy as would be expected. Having determined the values for p_1 and p_d/p_m that best fit the experimental data except for values of the coverage close to saturation of the first layer, the same values of p_1 and p_d/p_m are used in simulations in which p_f is varied. In this systematic way, we have determined that the value of p_d/p_m is ~ 0.005 and the value of p_f is $\sim 6 \times 10^{-5}$. Note that the relationship between the incident flux and p_f is given by $F = p_f/\tau_r$. Thus, the simulations in which $p_f = 0$ are simulations of experiments in which the incident flux is infinitesimally small on the time scale for migration or desorption. These simulations are sufficiently sensitive that significant deviations between the experimental data and the simulation results are observed

if p_d/p_m is set less than 0.001 or greater than 0.01. Similarly, deviations between the experimental 'tail' and the simulation results are apparent if p_f is set greater than $\sim 1 \times 10^{-4}$ or less than 1×10^{-5}. From Fig. 1 it can be inferred that at 77 K a second layer of ethane accumulates on the surface (at least at coverages where the first layer is nearly saturated). This is indicated by the 'tail' in the experimental data which is not seen in the simulation results in which $p_f = 0$. It is possible that such a 'tail' can result from an equilibrium between the first monolayer of ethane and the gas phase rather than the second layer with the gas phase. However, the desorption barrier for a molecularly adsorbed ethane molecule from the Ir(110)-(1x2) surface is approximately 7.5 kcal/mol **(17)**. As will be seen below, this 'tail' indicates equilibration between the gas phase and a layer of adsorbed ethane with a desorption barrier of 4.5 kcal/mol. Hence, the 'tail' in the experimental data is much too long to be accounted for by desorption from the first monolayer. From Fig. 2 it can be seen that by simply allowing p_f to be non-zero, the simulations can produce the 'tail' observed in the reflectivity experiments. The accompanying accumulation of particles in the second layer in these simulations is shown in Fig. 3. The equilibrium second-layer coverage for the simulation parameters used is approximately 0.057.

By comparing the experimental data with the simulations in which p_f is not zero, it is possible to determine the real time τ_r that corresponds to each Monte-Carlo step/site. In many simulations, it is convenient to use ν^{-1}, the reciprocal of the frequency of the frustrated translational degree of freedom parallel to the surface, as the time scale so that each Monte-Carlo step corresponds to an attempted hop. However, we have set p_m to be unity so that the time scale in these simulations is not the time scale of the frustrated translational motion. Rather, it is the time scale at which successful hops occur. Therefore, τ_r can be much larger than ν^{-1} of which the latter has a typical value of approximately 10^{-13} s. The rate of desorption of a trapped particle is $p_d/5$ per Monte-Carlo step. The factor of 1/5

arises from allowing a trapped particle to attempt to move with equal probability in each of five directions, as discussed above; and desorption is allowed in only one of these directions. Hence, the rate of desorption from the second layer of ethane is given by $R_d = p_d/5\tau_r$. Similarly, as mentioned earlier, the flux incident upon the surface is given by p_f/τ_r. For each value of the beam energy, the values of the incident flux and the values of the energy barrier for desorption from the second layer E_d are summarized in Table 1 **(21)**. The simulation results presented in Fig. 2 are from simulations in which $p_f = 6 \times 10^{-5}$. As mentioned earlier deviations between the experimental 'tail' and the Monte-Carlo 'tail' begin to be apparent for p_f greater than 1×10^{-4}, the simulation results showing a longer 'tail' than is observed experimentally. This analysis indicates that the fluxes used in the reflectivity measurements are constant to approximately 20 percent, which is physically reasonable. This uncertainty in the value of flux is from the uncertainty in the value of τ_r. This same 20 percent uncertainty in τ_r implies an uncertainty of approximately 50 cal/mol in the value of E_d but, as noted earlier, there is a much greater uncertainty due to the lack of information concerning the preexponential factor for desorption **(21)**. For the simulation results shown in both Figs. 1 and 2, the value of p_d/p_m is 0.005. This is the ratio of the probability of success of desorption to the probability of success of migration. Hence the difference between the respective energy barriers $\delta E = E_d - E_m$ is approximately 800 cal/mol, assuming that the preexponential factors for these two processes are equal. If the preexponential factor for desorption is larger than that for migration, as might be expected, then δE would be somewhat larger than 800 cal/mol **(22)**. Simulations were also performed for $p_d/p_m = 0.01$ and $p_d/p_m = 0.001$ to estimate the sensitivity of the fit. These runs allow us to conclude that the uncertainty in δE is approximately 200 cal/mol.

In our model the fractional coverage of ethane in the first layer increases through both direct and precursor-mediated adsorption. In direct adsorption all vacant sites on the lattice have equal probabilities of being impinged upon by an

incident molecule. However, the probability that a trapped ethane molecule reaches a vacant site is not the same from one vacant site to another. In our simulations, the only lattice sites with a nonzero probability of being reached by a trapped ethane molecule are those that have at least one occupied nearest-neighbor site. Therefore, 'islands' of molecularly adsorbed ethane form as a result of precursor-mediated adsorption. The adsorbed layer of ethane, hence, consists of 'islands' due to precursor-mediated adsorption and randomly distributed ethane molecules due to direct adsorption. We have stipulated that the adsorption of a previously trapped ethane molecule occurs with unit probability when the molecule reaches a vacant site during its migration. We have assumed that this is the case because an ethane molecule trapped and thermally accommodated in the precursor state can be considered to be equivalent to an ethane molecule in an incident molecular beam which has an extremely low incident energy. The probability of direct adsorption p_0 for the latter case is very close to unity, as shown by the experimental data. If, however, a trapped ethane molecule is adsorbed with a probability lower than unity when it reaches a vacant site, as might occur if adsorption from the precursor state were activated, then the configuration of the adsorbed layer would become more characteristic of a random distribution of ethane molecules.

It is also possible to use the Kisliuk approach **(7)** to treat the adsorption kinetics in our model. In this approach the probability of occupancy, for each site sampled by the trapped ethane molecule, is assumed to be equal to the fractional coverage. The actual configuration of the adsorbed layer is, hence, approximated by a random configuration in calculating the probability of adsorption. The probability that a trapped ethane molecule reaches a vacant site before it desorbs is dependent, however, upon the configuration of the adsorbed layer. An ethane molecule that is trapped on top of the center of an 'island' of adsorbed ethane is less likely to reach a vacant site than another ethane molecule that is trapped near the edge of an 'island.' The former type of molecule will also have a lower probability of

reaching a vacant site compared to a trapped molecule in the Kisliuk approach. However, a molecule that is trapped sufficiently close to the edge of an 'island' will have a higher probability of reaching a vacant site than a trapped molecule in the Kisliuk approach. Thus, the probability of adsorption calculated using the Kisliuk approach will be different from that obtained from the simulations.

The probability of adsorption as a function of coverage for the simulations with p_f set equal to zero is compared with calculations using the Kisliuk approach in Fig. 4. The ordinate is the probability of adsorption, and the abscissa is the fractional coverage. In Fig. 5 the time dependence of the probability of adsorption from the simulations and from the Kisliuk approach are compared. The ordinate is again the probability of adsorption, while the abscissa is the time in units of 0.1 s. The simulation results, which are for the parameters in row d of Table 1, are denoted by the lines in these figures. The dots are the results calculated by the Kisliuk approach using the same parameters. For the probability of adsorption $P(\theta)$, the Kisliuk approach gives

$$P(\theta) = [\frac{p_0}{q_m} + \theta(p_1 - p_0 - \frac{p_0}{q_m}) + \theta^2(p_0 - p_1)]/(\frac{1}{q_m} - \theta),$$

where q_m, the probability that a precursor particle hops to a nearest-neighbor site relative to the total probability of hopping and desorption, is equal to $\frac{4}{5}p_m/(\frac{4}{5}p_m + \frac{1}{5}p_d)$. The dependence of the fractional coverage upon time is calculated from

$$\int_0^\theta \frac{dx}{P(x)} = ft,$$

where f is the incident flux.

The probability of adsorption as a function of the fractional coverage is the same for both the simulations and the Kisliuk approach when the fractional coverage is low. This is to be expected since the 'islands' formed in the simulations are not large at this stage. However, for fractional coverages above approximately 0.6,

the effect of using a random configuration in the Kisliuk approach becomes apparent. The probability of adsorption calculated using the Kisliuk approach is higher than that obtained from the simulations. This indicates that the probability of a trapped ethane molecule reaching a vacant site is lower than that which is obtained when a random configuration is assumed. As mentioned earlier, a higher probability of reaching vacant sites is computed for molecules trapped at the edge of the 'islands' when the actual configuration on the surface is used than when the random configuration assumed in the Kisliuk approach is used. However, for molecules trapped near the center of the 'islands,' this probability is lower when computed with the actual configuration than when computed with a random configuration. When the fractional coverage is high and the 'islands' are large, the latter effect dominates. Consider a circular 'island' with a radius of r. Then molecules trapped at a site (within the 'island') which is less than a distance l from the edge of the 'island' reach a vacant site at the edge with a probability that is greater than that obtained using the random configuration approximation in the Kisliuk approach. Those that are trapped at a site farther than a distance l from the edge have a probability of reaching a vacant site that is lower than the probability obtained using the Kisliuk approach. Then the number of sites for which it is 'favorable' for the trapped molecules to reach a vacant site increases as r while the number of sites for which it is 'unfavorable' increases as r^2. Hence, it is reasonable for the probability of adsorption obtained from the simulations to be less than that calculated using the Kisliuk approach. Since the value of the parameter l increases when the trapped molecules become more mobile, the difference in the probability of adsorption seen in Fig. 4 will be less if the trapped molecules are even more mobile than we have found, and conversely.

4. Conclusions

We have analyzed molecular beam reflectivity measurements by Monte-Carlo

simulations of a model in which ethane adsorption can occur through two routes: a direct molecular adsorption pathway, and a precursor-mediated adsorption pathway in which the precursor is an ethane molecule trapped above a previously adsorbed ethane molecule. We have performed simulations for the limiting case in which the flux incident upon the surface is infinitesimally small, and also for cases in which this flux is not zero. It is possible to infer from the discrepancy between the 'tail' of the experimental data and the simulations with infinitesimally small flux that some accumulation of a second layer of ethane occurs. The simulations with non-zero flux allow us to determine the real time corresponding to each Monte-Carlo step in these simulations. Thus, it is possible to determine the rate of desorption of ethane from the second layer and hence the energy barrier for this process. This is approximately 4.5 ± 0.3 kcal/mol, and the barrier to migration of trapped ethane molecules is approximately 3.7 ± 0.2 kcal/mol. The saturation coverage for the second layer is approximately 0.06 relative to the saturation coverage of the first monolayer at 77 K.

It is difficult to imagine a simpler and yet more intuitively reasonable model that would give rise to the experimentally observed maximum in the probability of adsorption. The essential ingredient in the model is the physically reasonable assumption that an incident ethane molecule accommodates better if it impinges on a previously adsorbed ethane molecule than if it impinges on the bare iridium surface. It should be noted that the use of a square lattice to simulate the Ir(110)-(1x2) surface, which is a rectangular lattice, is acceptable. The probable anisotropy of the Ir(110)-(1x2) surface to diffusion need not be considered because the hopping of trapped ethane molecules occurs on top of a layer of molecularly adsorbed ethane, which probably presents an isotropic surface to a trapped ethane molecule. The validity of using a square lattice is also indicated by the good agreement obtained. It is gratifying that using values of p_0 obtained from experiments, values of p_f that are consistent with the beam flux, and assuming (reasonably) that $p_1 \sim 1$, it is

possible to describe the probability of adsorption for the entire range of surface coverage from zero coverage to saturation using only a single value of p_d/p_m. This single value of p_d/p_m also describes the data obtained using beams of different incident energies, and is physically consistent with the idea that the trapped ethane molecules are completely accommodated thermally to the surface.

Acknowledgment: This research was supported by the National Science Foundation under Grant No. CHE-8617826. Acknowledgment is also made to the donors of the Petroleum Research Fund for partial support of this research under Grant No. PRF 19819-AC5-C.

References

1. W.H. Weinberg, in **Kinetics of Interface Reactions**, Eds., H.J. Kreuzer and M. Grunze, Springer-Verlag, Heidelberg, 1987, p. 94.
2. I. Langmuir, Chem. Rev. **6**, 451 (1929).
3. J.B. Taylor and I. Langmuir, Phys. Rev. **44**, 423 (1933).
4. J.A. Becker, in **Structure and Properties of Solid Surfaces**, Eds., R. Gomer and C.S. Smith (Univ. of Chicago Press 1953) p. 459.
5. J.A. Becker and C.D. Hartman, J. Phys. Chem. **57**, 157 (1953).
6. G. Ehrlich, J. Phys. Chem. **59**, 473 (1955).
7. P. Kisliuk, J. Phys. Chem. Solids **3**, 95 (1957); **5**, 78 (1958).
8. P.W. Tamm and L.D. Schmidt, J. Chem. Phys. **52**, 1150 (1970); **55**, 4253 (1971).
9. L.R. Clavenna and L.D. Schmidt, Surf. Sci. **22**, 365 (1970).
10. C. Kohrt and R. Gomer, J. Chem. Phys. **52**, 3283 (1970).
11. D.A. King and M.G. Wells, Surf. Sci. **29**, 454 (1972).
12. D.A. King and M.G. Wells, Proc. Roy. Soc. (Lond.) **A339**, 245 (1974).
13. E.S. Hood, B.H. Toby and W.H. Weinberg, Phys. Rev. Lett. **55**, 2437 (1985).
14. O.M. Becker and A. Ben-Shaul, Phys. Rev. Lett. **61**, 2859 (1988).
15. Since the product of the adsorption reaction is physically adsorbed ethane, there can be no "intrinsic" precursor to adsorption in the usual sense on the bare surface **(1)**.
16. C.B. Mullins and W.H. Weinberg, J. Chem. Phys. (submitted).
17. T.S. Wittrig, P.D. Szuromi and W.H. Weinberg, J. Chem. Phys. **76**, 3305 (1982).

18. C.B. Mullins, C.T. Rettner, D.J. Auerbach and W.H. Weinberg, to be published.

19. R.J. Hamers, P.L. Houston and R.P. Merrill, J. Chem. Phys. **88**, 6548 (1988).

20. L. Wilzen, S. Andersson and J. Harris, Surf. Sci. **205**, 387 (1988).

21. The values of E_d are calculated from $R_d = k_d^{(0)}\exp(-E_d/k_BT)$, where $k_d^{(0)}$ is assumed to be 10^{13} s^{-1}. If $k_d^{(0)}$ is assumed to be 10^{14} s^{-1}, the corresponding values of E_d would be about 0.4 kcal/mol greater than the values indicated in Table 1. A related issue is the use of the factor of 1/5 in choosing the direction of motion of the trapped ethane. If a trapped molecule can move toward the surface and then be reflected into the gas phase, a factor of 1/6 would be more appropriate. This would imply that the probability of successful desorption p_d that we have used is twice as large as it should be, and that the desorption energy barrier E_d is approximately 0.1 kcal/mol lower than the value reported in Table 1.

22. For example, if the ratio of the preexponential factors $k_d^{(0)}/k_m^{(0)}$ were equal to 100, then δE would be equal to 1500 cal/mol, and E_m would be 3.0 ± 0.2 kcal/mol.

Table 1

Set	E_i	θ_i	p_0	p_1	E_d	Flux
a	2.2	0	0.95	1.00	4.55	0.087
b	3.7	45	0.90	1.00	4.57	0.077
c	5.2	45	0.83	0.97	4.53	0.102
d	6.6	0	0.68	0.96	4.52	0.107
e	10.0	45	0.50	0.95	4.53	0.104
f	10.0	22.5	0.45	0.95	4.55	0.085

Values of parameters used in simulations and experiments. The energy of the beam E_i is in units of kcal/mol and the incident angle θ_i is in degrees. The energy barrier for desorption is in units of kcal/mol and the fluxes in units of $s^{-1}\ \sigma^{-1}$ for each beam energy, where σ is the area occupied by a molecularly adsorbed ethane molecule in a saturated first layer on the Ir (110)-(1x2) surface at 77 K. The probability of adsorption on the clean surface (in the limit of zero coverage) is p_0, and the probability of trapping on top of an adsorbed ethane molecule is p_1. The value of p_d/p_m, where p_d is the probability of success of an attempted desorption event and p_m is the probability of success of an attempted hop by a trapped particle, is 0.005 for all the simulation results shown here.

Figure Captions

Figure 1. The crosses indicate experimental data, and the lines indicate results from simulations in the zero-flux limit. The abscissa is time in units of 0.1 s. For each experiment, the time has been multiplied by $\cos\theta_i$, where θ_i is the angle of incidence in order to normalize the area of the surface upon which ethane molecules are incident. The parameters for each figure can be found in the corresponding rows of Table 1.

Figure 2. The crosses indicate experimental data as in Fig. 1. The circles indicate results from simulations in which the value of p_f, and thus the flux which is equal to p_f/τ_r, is not zero. The abscissa for the Monte-Carlo data has been converted from Monte-Carlo steps/site to real time. The conversion factor τ_r gives the number of seconds in real time to which each Monte-Carlo step/site corresponds. This, as explained in the text, enables an absolute determination of the desorption rate from the second layer. The units for the abscissa are 0.1 s.

Figure 3. Simulations in which p_f is not zero enable a second layer of particles to accumulate. The fractional coverage of this second layer is shown here as a function of time which, as in Fig. 2, has been converted from Monte-Carlo steps/site to real time.

Figure 4. The dependence of the probability of adsorption upon the fractional coverage of adsorbed ethane is plotted here. The line indicates the results from simulations in which p_f is equal to zero, and the dots indicate the results of calculations using the Kisliuk approach, as discussed in the text. The abscissa is the fractional coverage of adsorbed ethane, and the ordinate is the probability of adsorption.

Figure 5. The probability of adsorption as a function of time is plotted here. The line indicates the results from simulations in which p_f is equal to zero, and the dots indicate the results of calculations using the Kisliuk approach, as discussed in the text. The abscissa is time in units of 0.1 s, and the ordinate is the probability of adsorption.

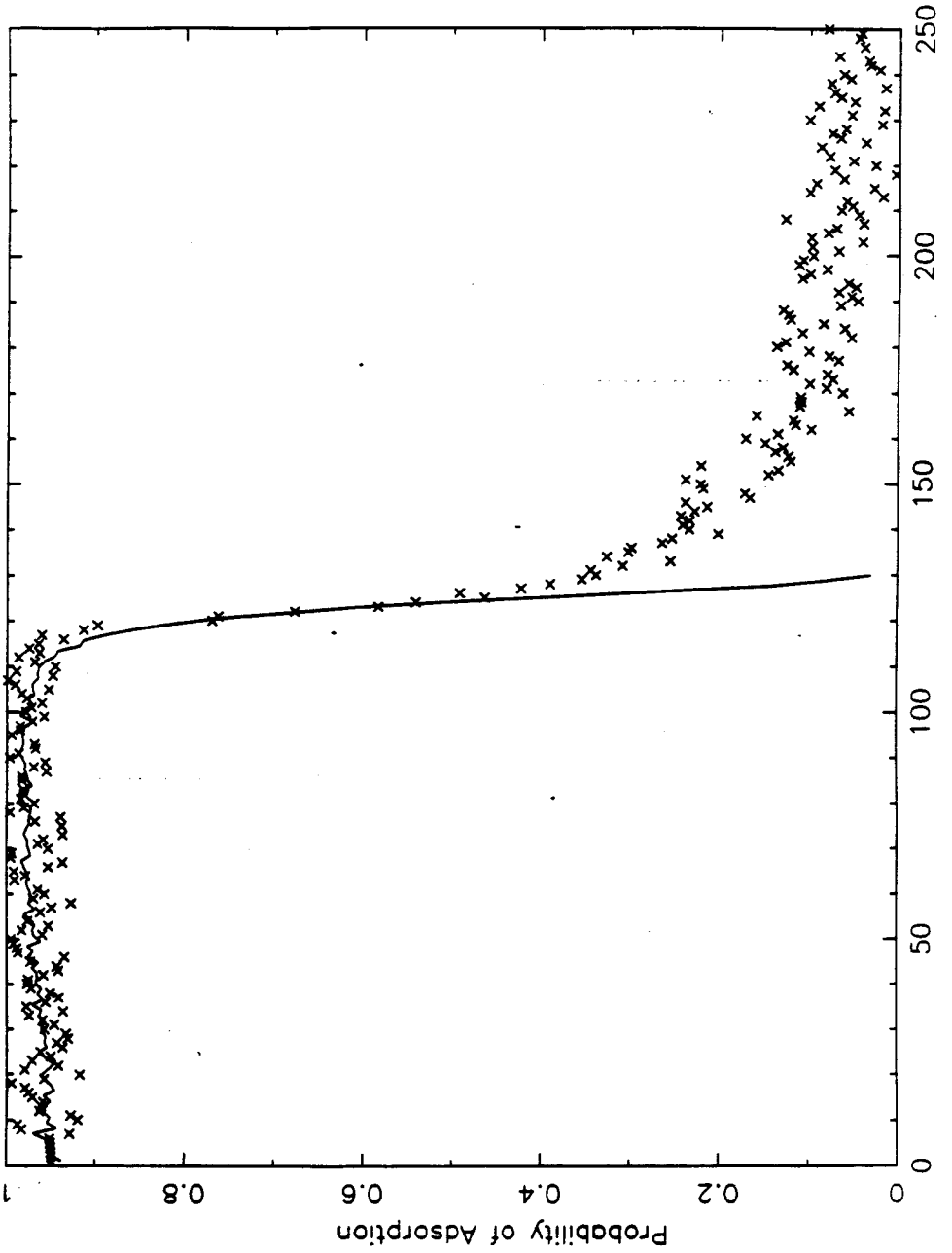
Probability of Adsorption
0
0.2
0.4
0.6
0.8
1
0
50
100
150
200
250
Time/ 0.1 s

Figure 1 a

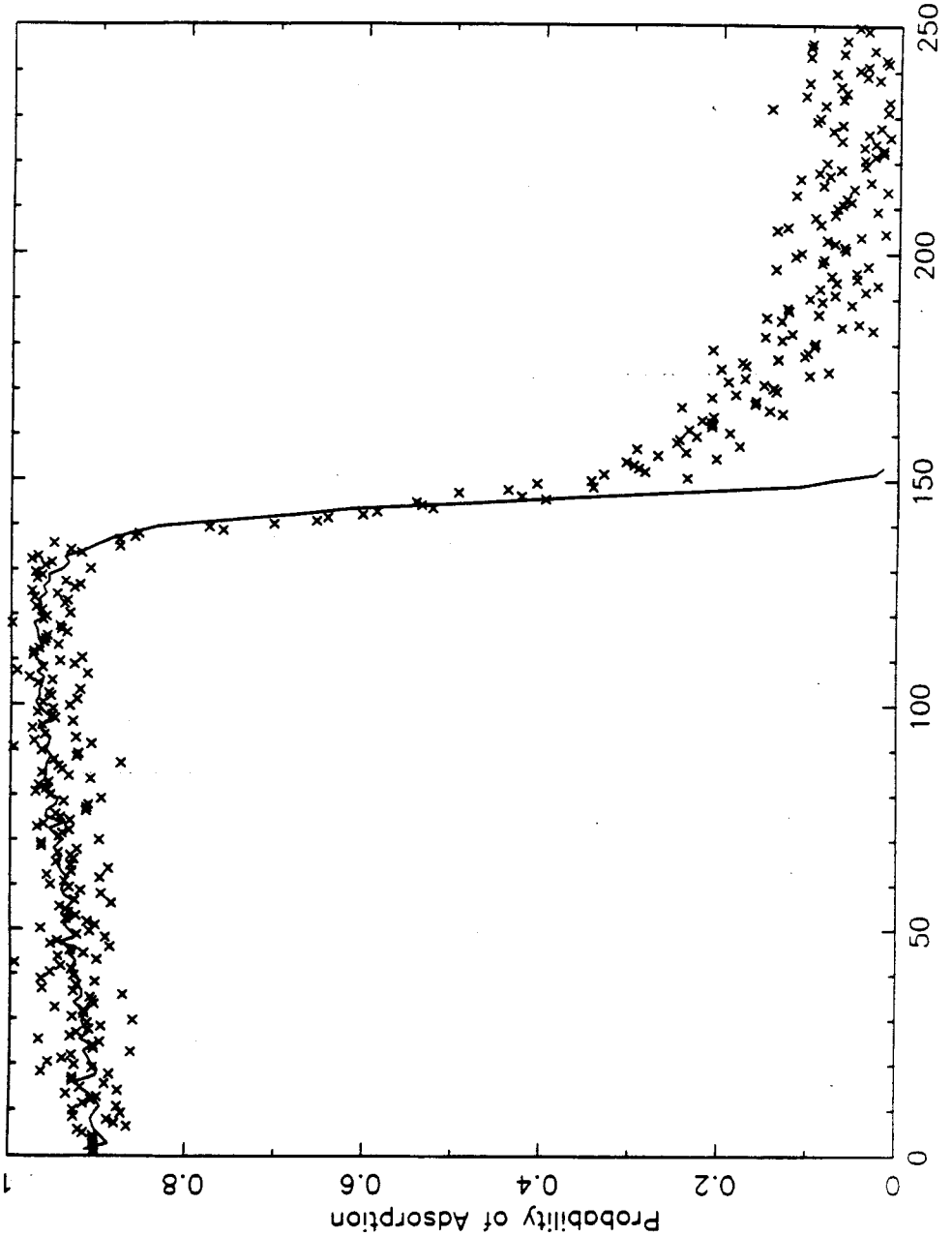
Probability of Adsorption
0
0.2
0.4
0.6
0.8
1
0
50
100
150
200
250
Time/ 0.1 s

Figure 1 b

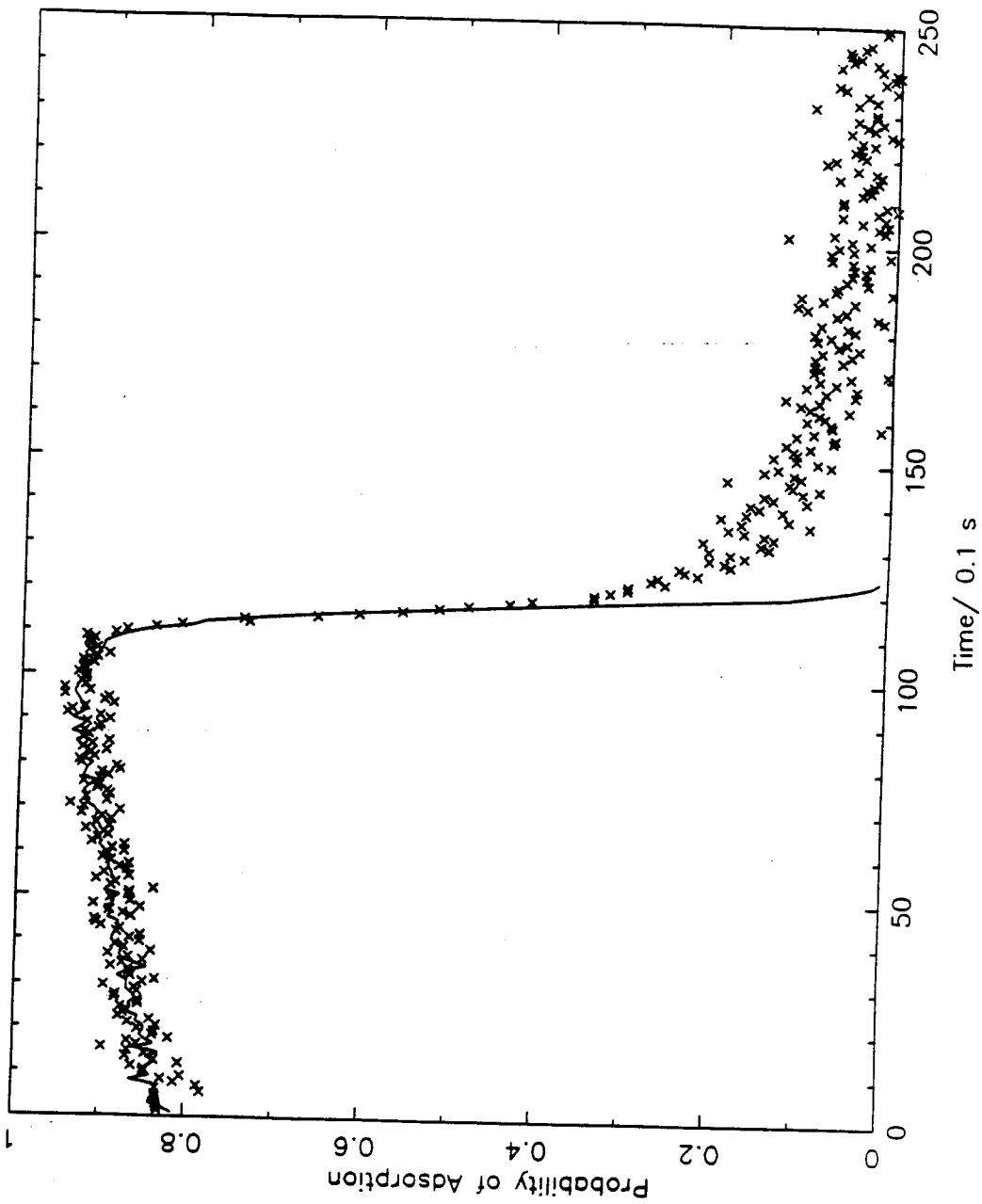
Probability of Adsorption
0
0.2
0.4
0.6
0.8
1
0
50
100
150
200
250
Time/ 0.1 s

Figure 1 c

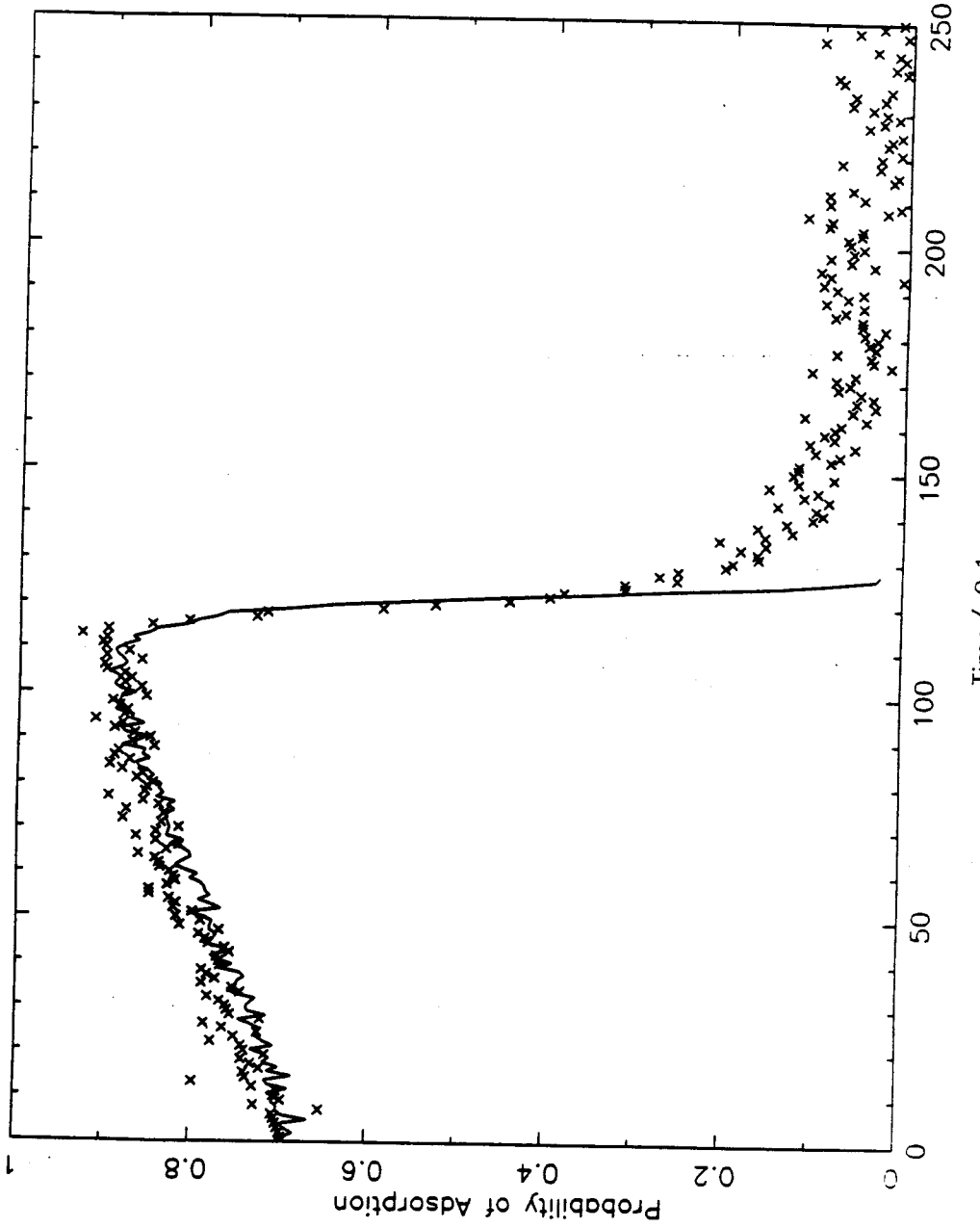
Probability of Adsorption
0
0.2
0.4
0.6
0.8
1
0
50
100
150
200
250
Time/ 0.1 s

Figure 1 d

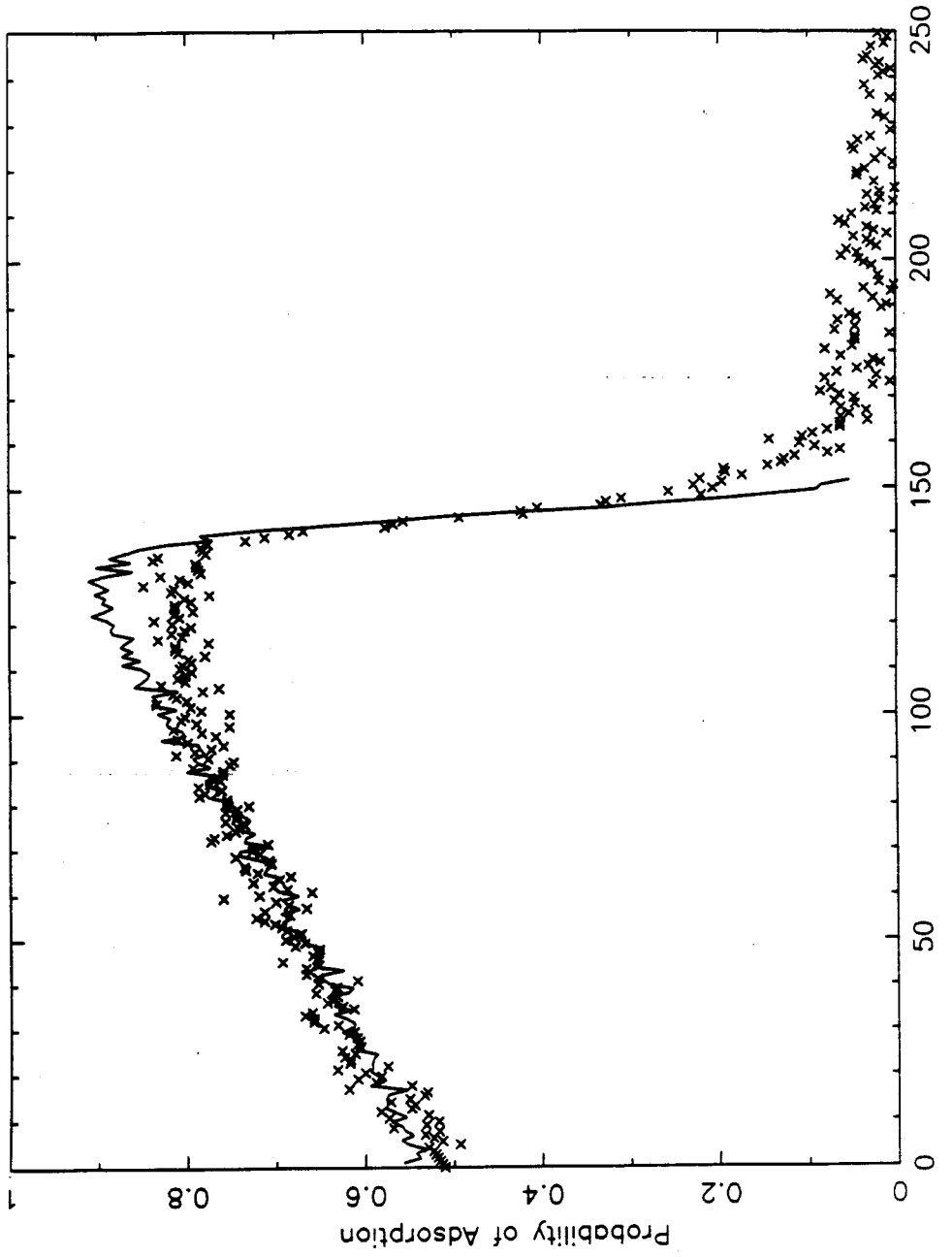
Probability of Adsorption
0
0.2
0.4
0.6
0.8
1
0
50
100
150
200
250
Time/ 0.1 s

Figure 1 e

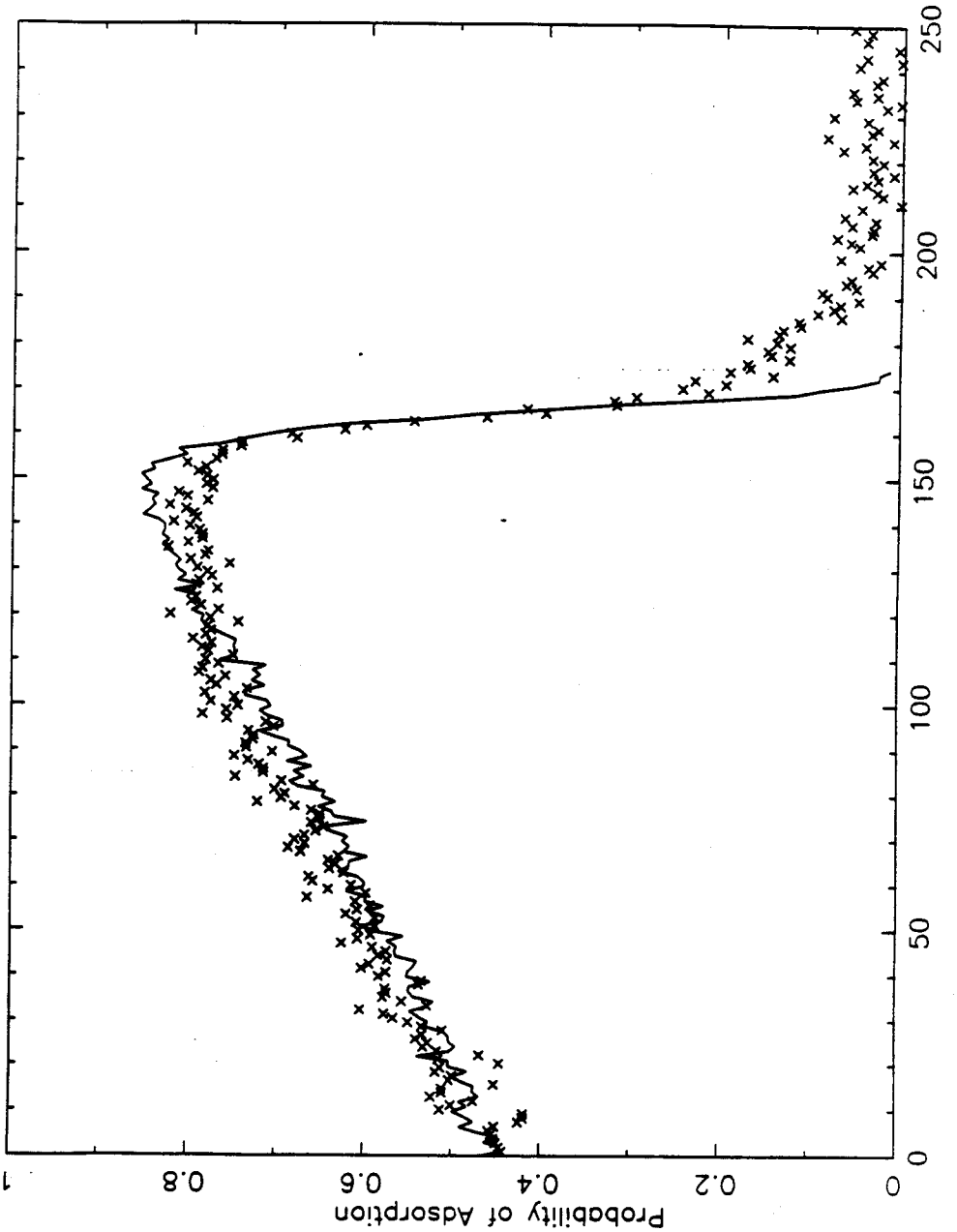
Probability of Adsorption
0
0.2
0.4
0.6
0.8
1
0
50
100
150
200
250
Time/ 0.1 s

Figure 1 f

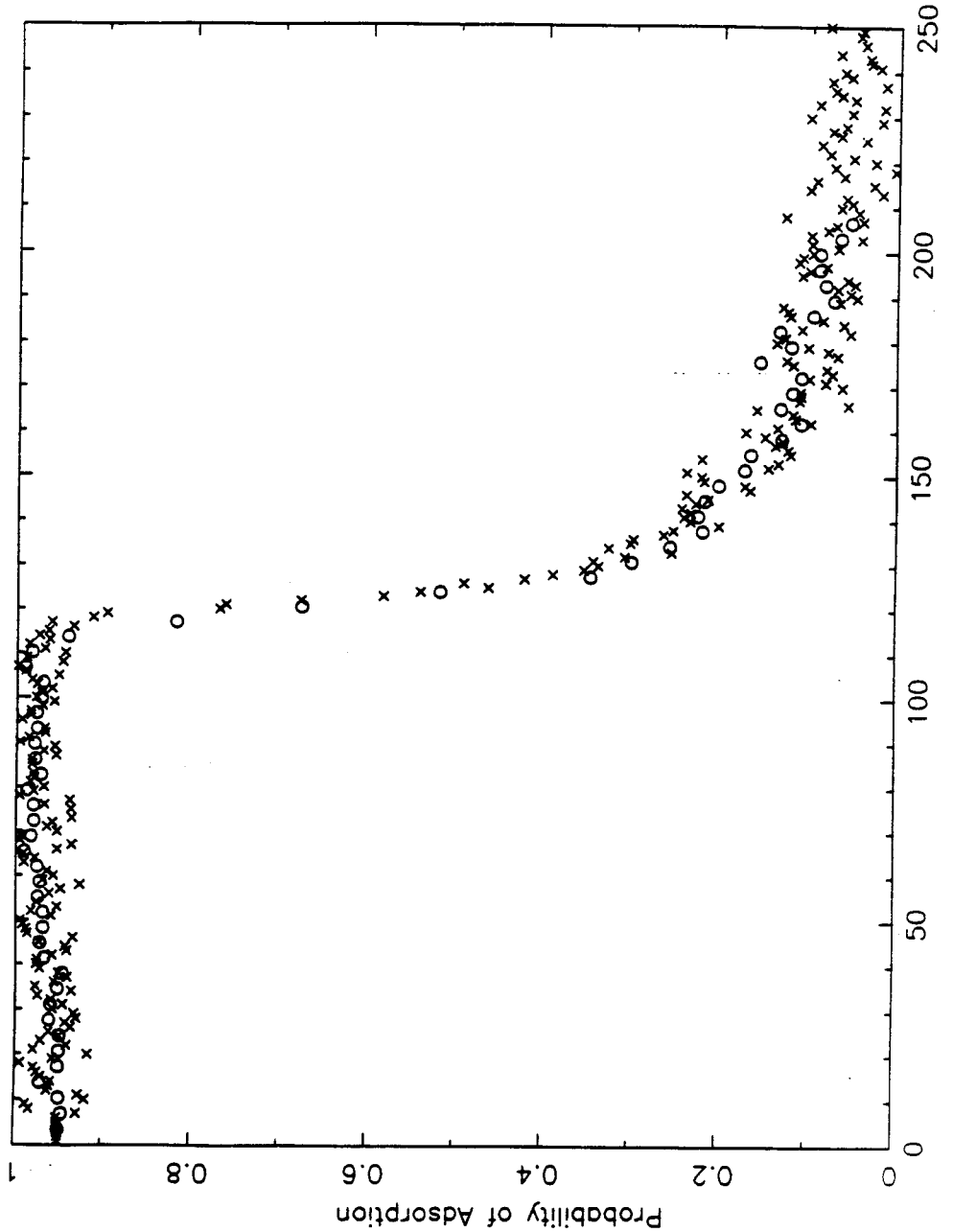
Probability of Adsorption
0
0.2
0.4
0.6
0.8
1
0
50
100
150
200
250
Time/ 0.1 s

Figure 2 a

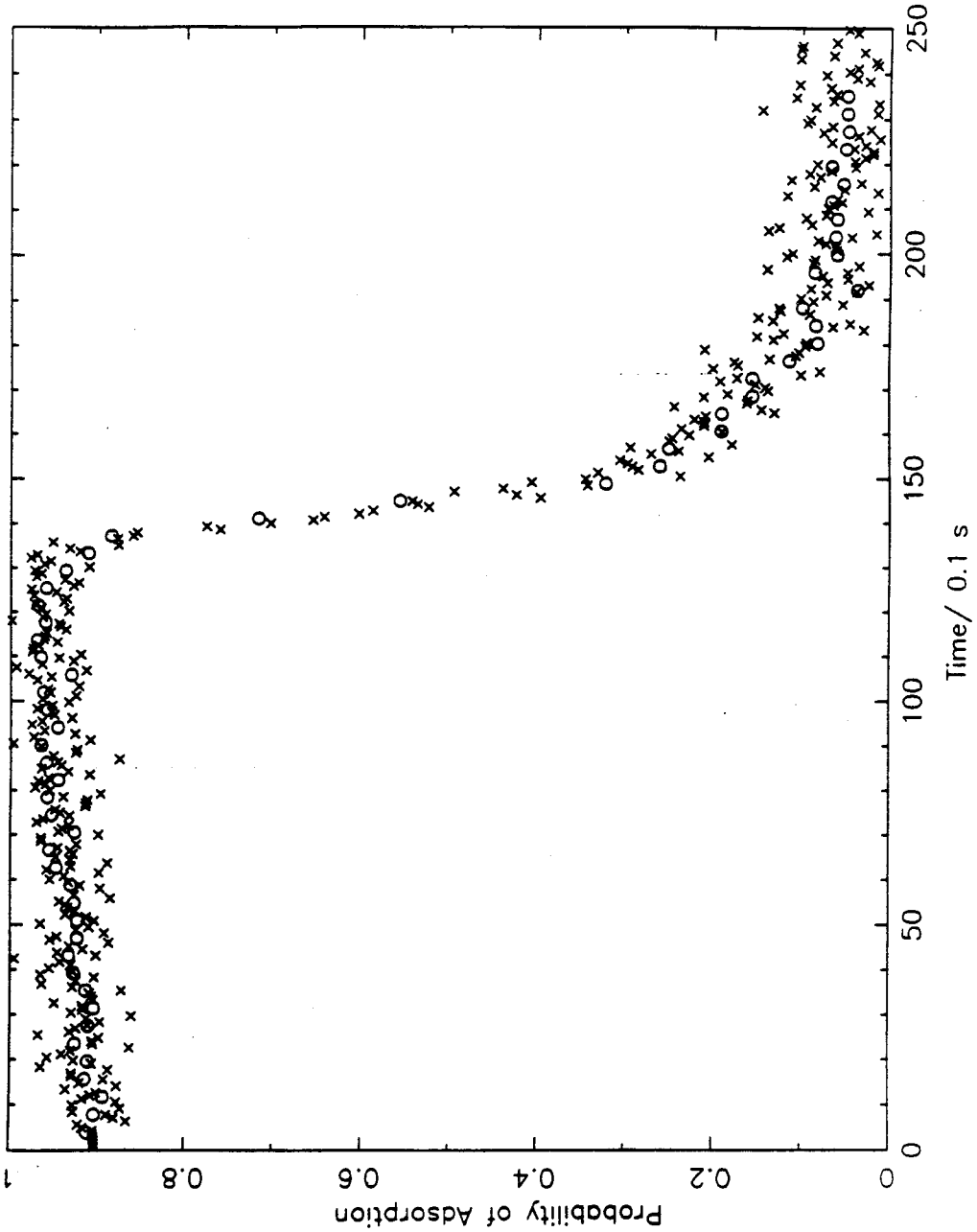
Probability of Adsorption
0
0.2
0.4
0.6
0.8
1
0
50
100
150
200
250
Time/ 0.1 s

Figure 2 b

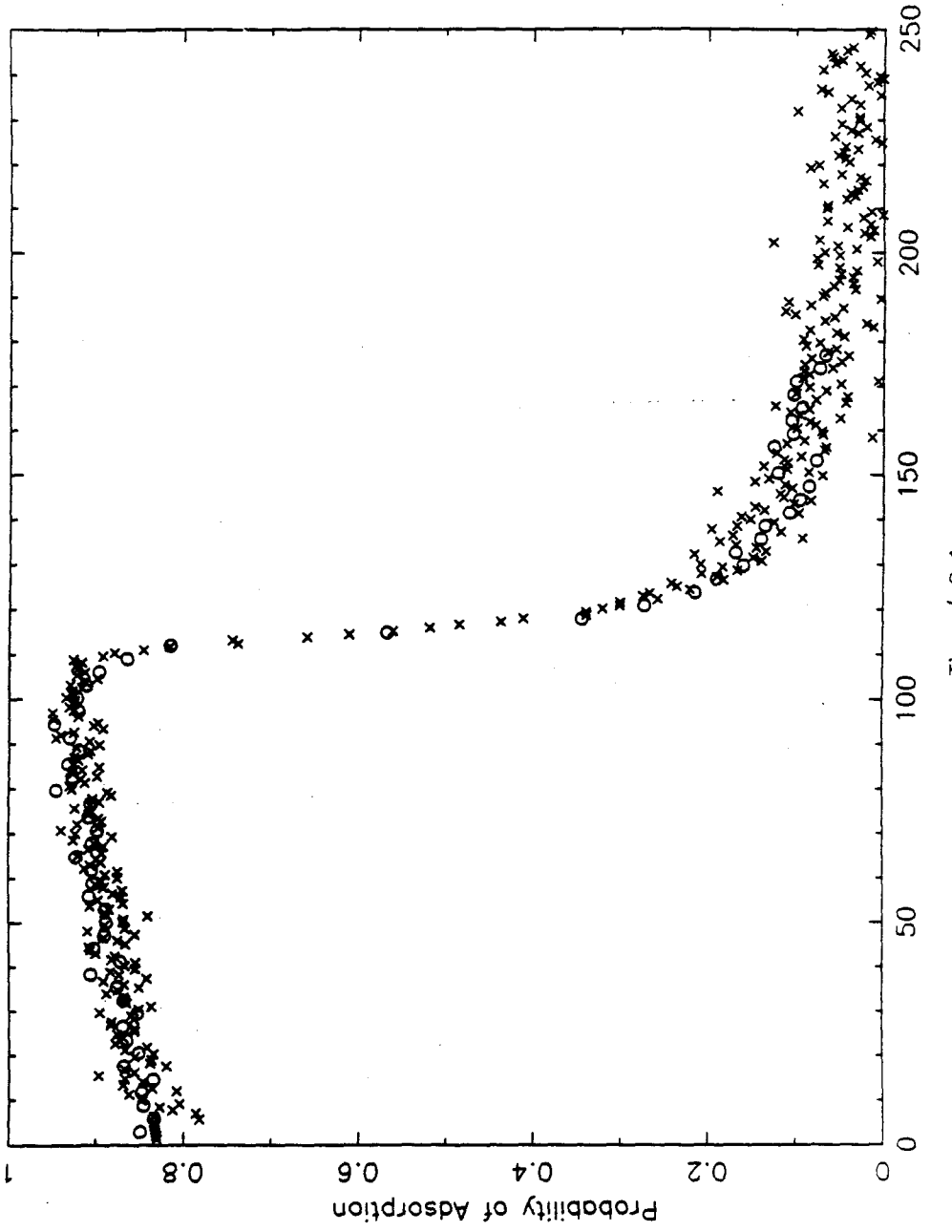
Probability of Adsorption
0
0.2
0.4
0.6
0.8
1
0
50
100
150
200
250
Time/ 0.1 s

Figure 2 c

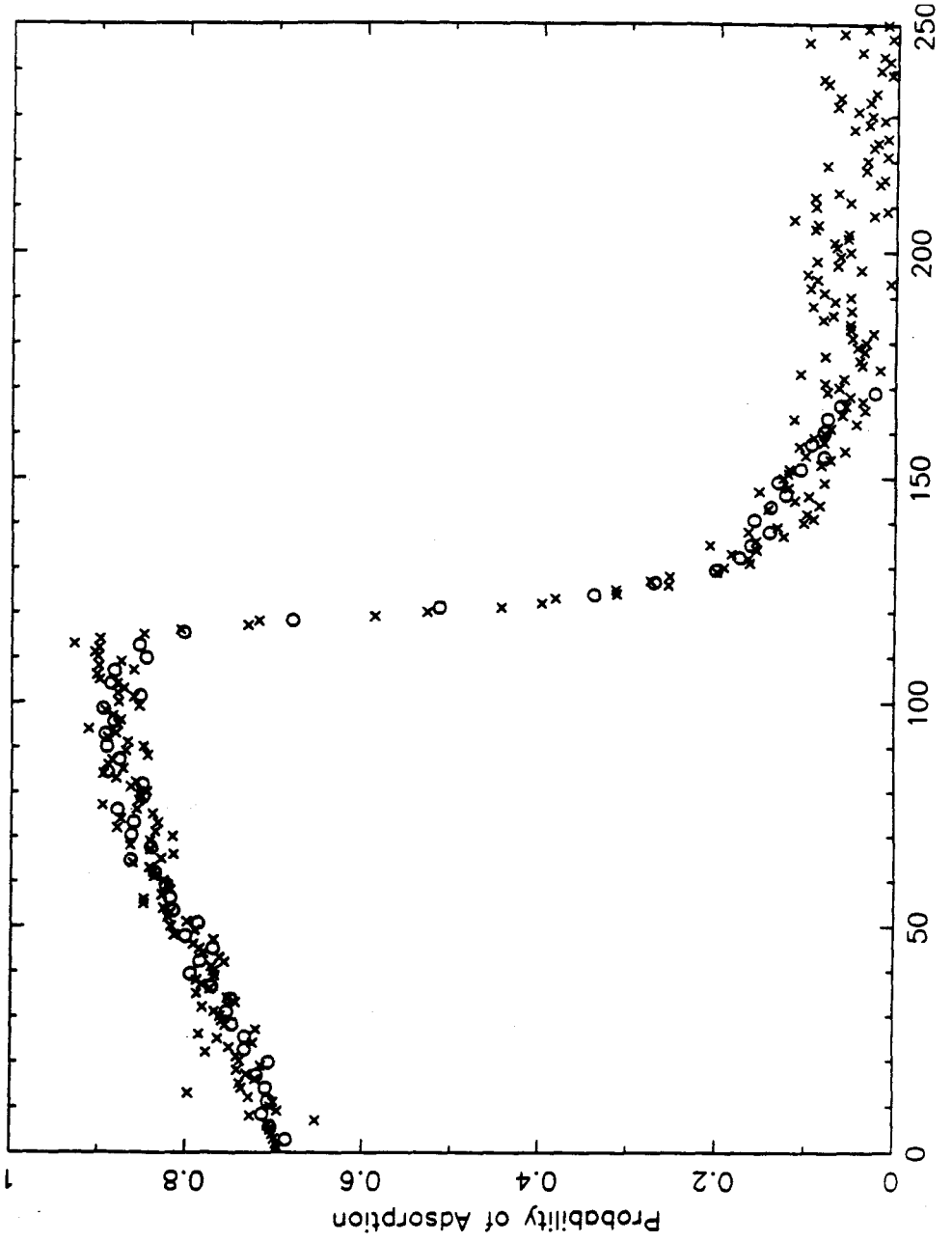
Probability of Adsorption
0
0.2
0.4
0.6
0.8
1
0
50
100
150
200
250
Time/ 0.1 s

Figure 2 d

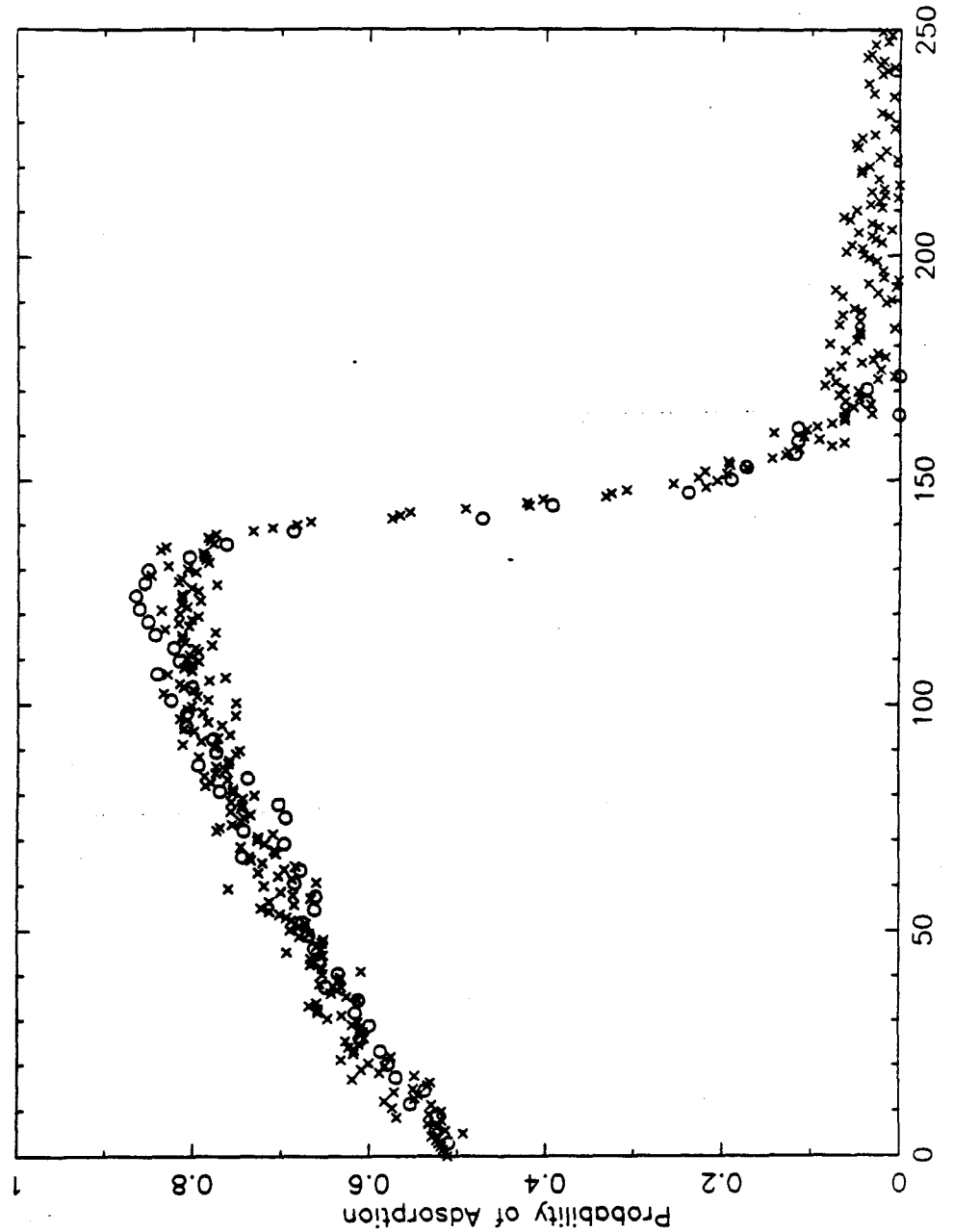
Probability of Adsorption
0
0.2
0.4
0.6
0.8
1
0
50
100
150
200
250
Time/ 0.1 s

Figure 2 e

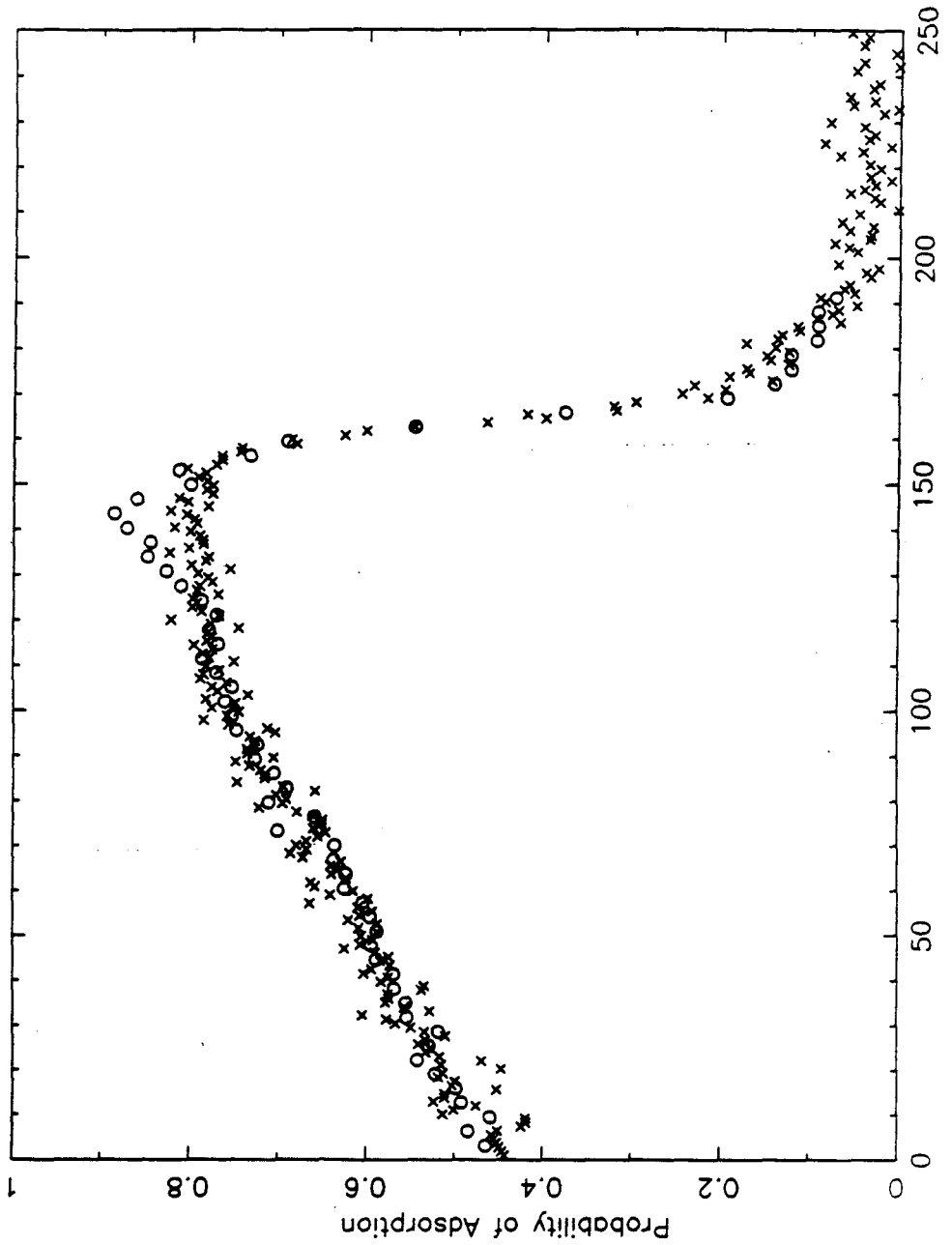
Probability of Adsorption
0
0.2
0.4
0.6
0.8
1
0
50
100
150
200
250
Time/ 0.1 s

Figure 2 f

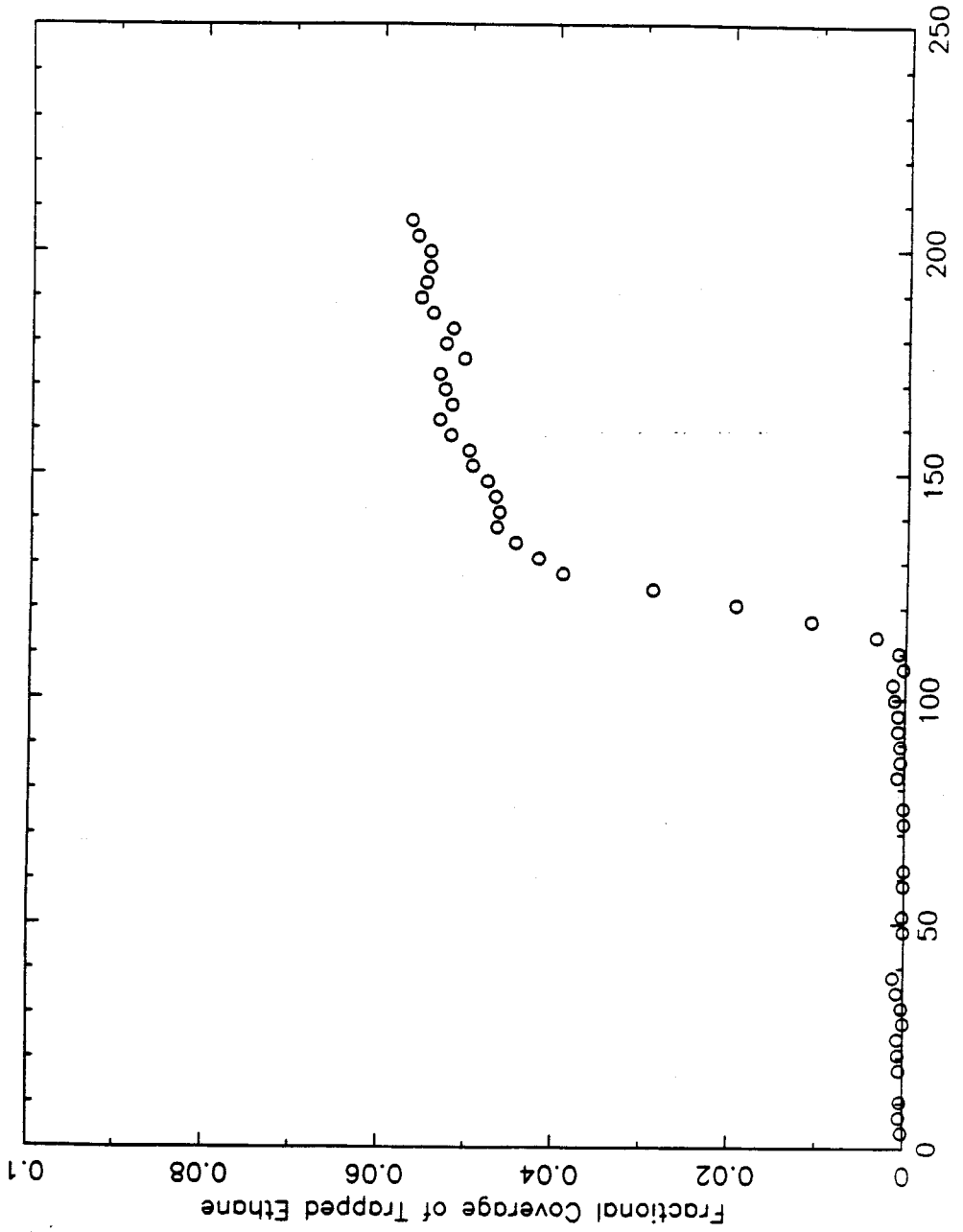
Fractional Coverage of Trapped Ethane
0.1
0.08
0.06
0.04
0.02
0
0
50
100
150
200
250
Time/ 0.1 s

Figure 3 a

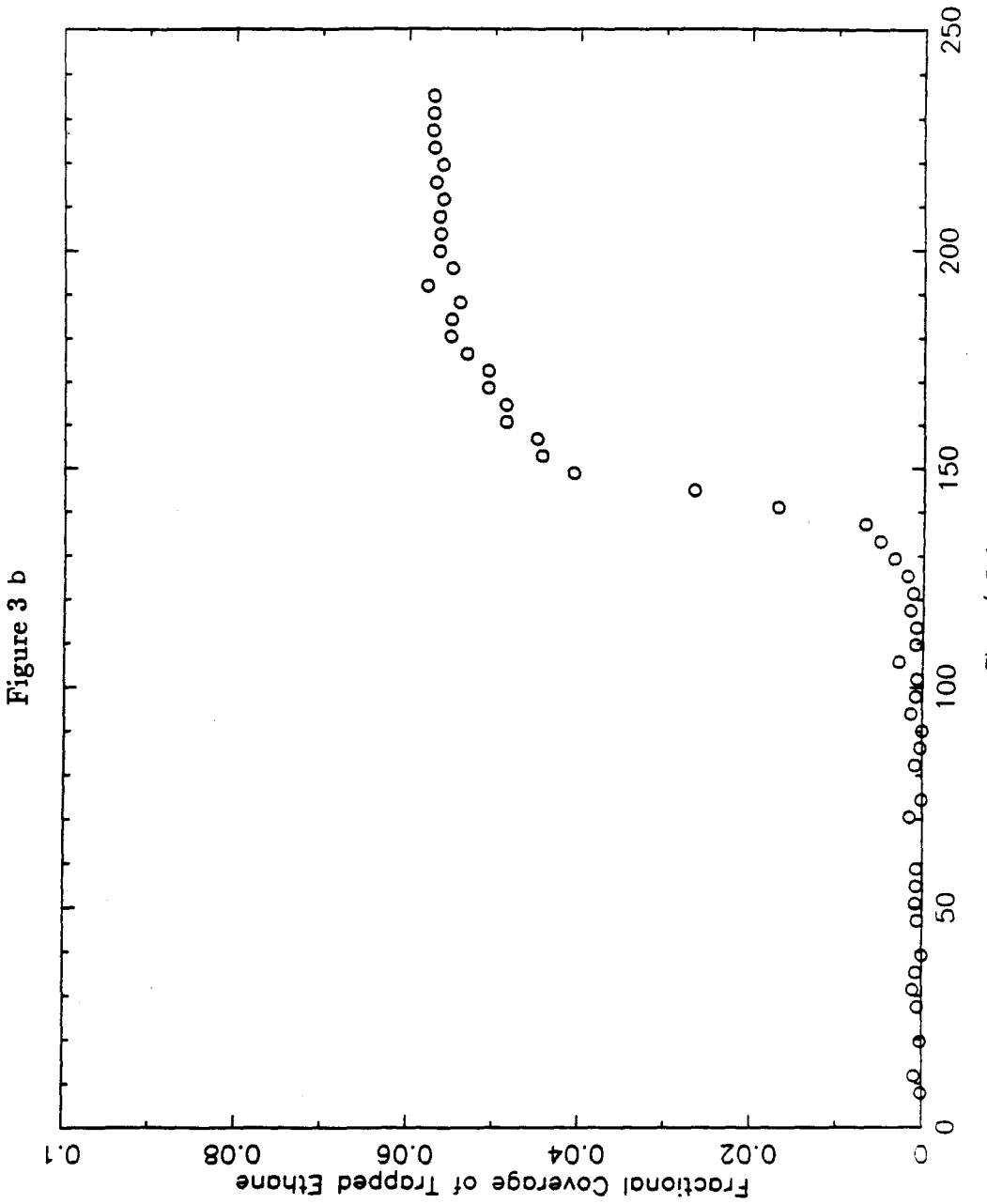
Fractional Coverage of Trapped Ethane
0
0.02
0.04
0.06
0.08
0.1
0
50
100
150
200
250
Time/ 0.1 s

Figure 3 b

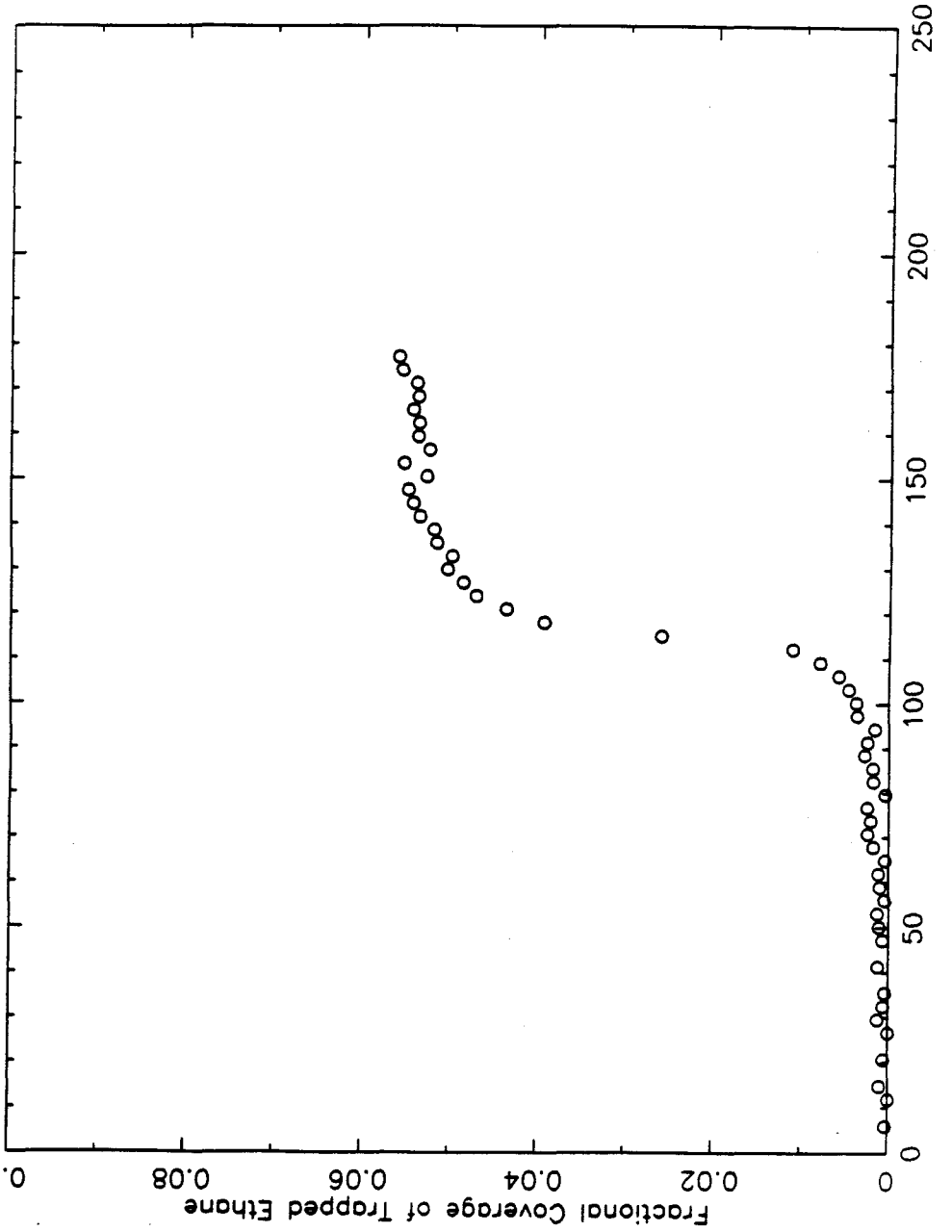
Fractional Coverage of Trapped Ethane
0
0.02
0.04
0.06
0.08
0.1
0
50
100
150
200
250
Time/ 0.1 s

Figure 3 c

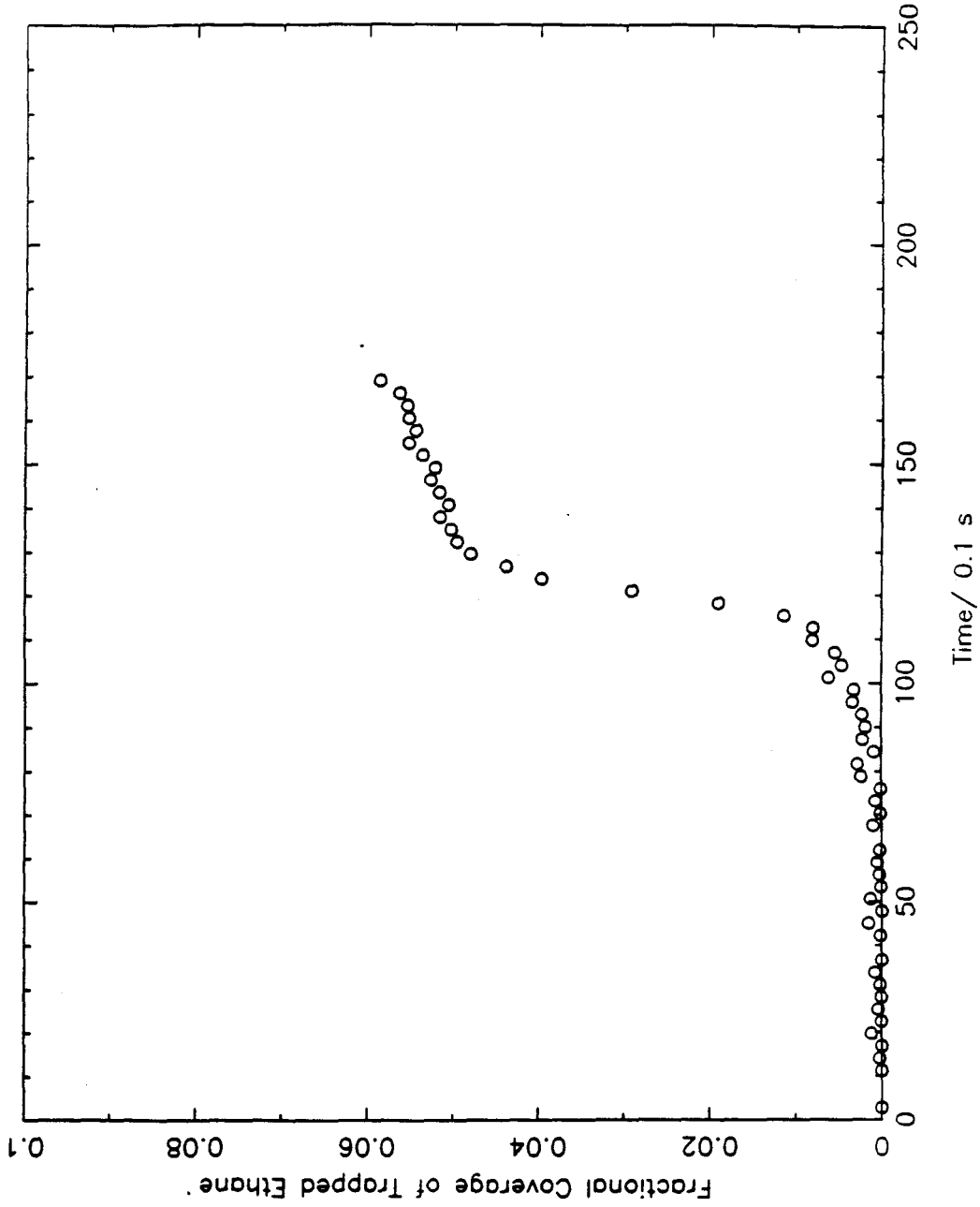
Fractional Coverage of Trapped Ethane
0
0.02
0.04
0.06
0.08
0.1
0
50
100
150
200
250
Time/ 0.1 s

Figure 3 d

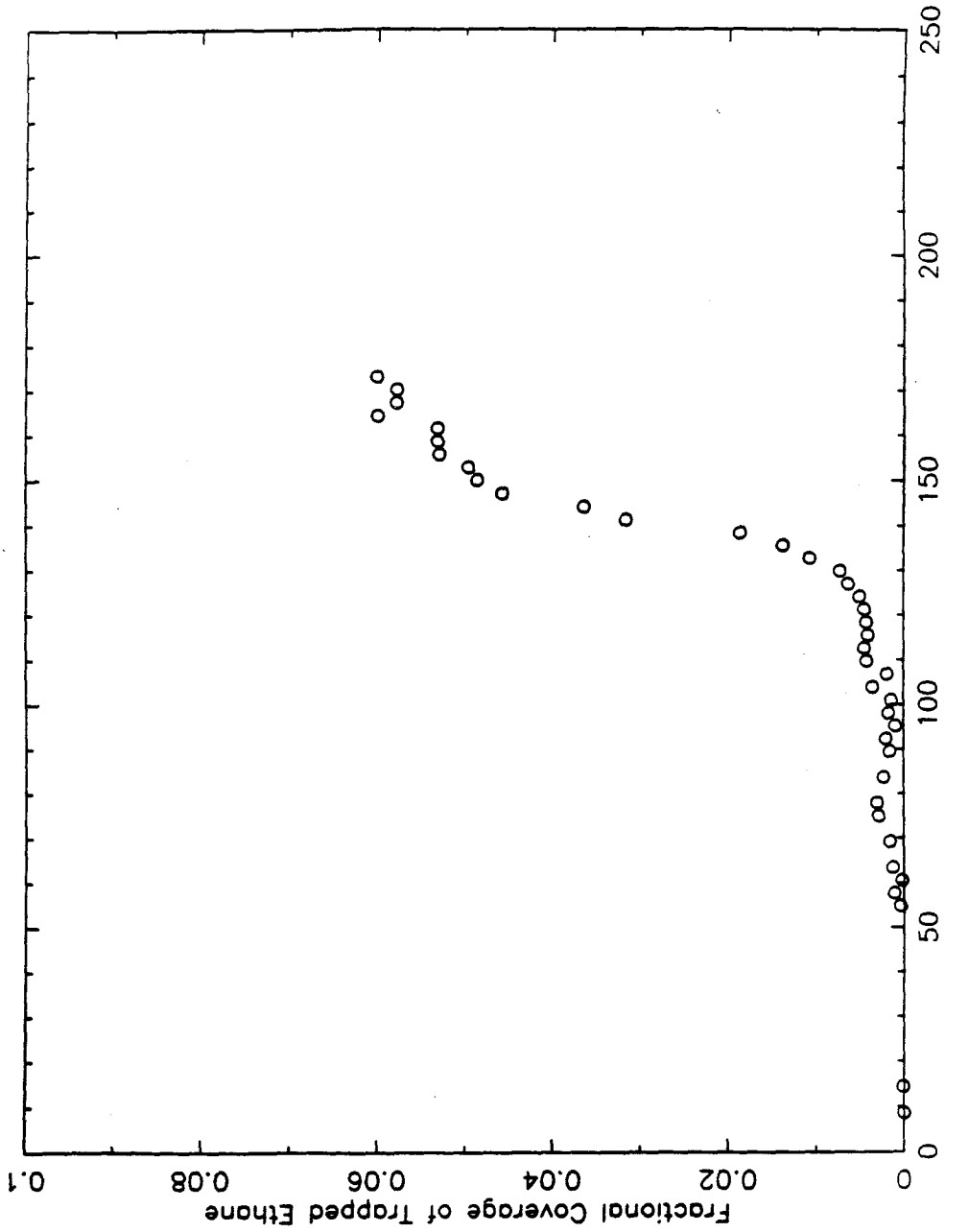
Fractional Coverage of Trapped Ethane
0
0.02
0.04
0.06
0.08
0.1
0
50
100
150
200
250
Time/ 0.1 s

Figure 3 e

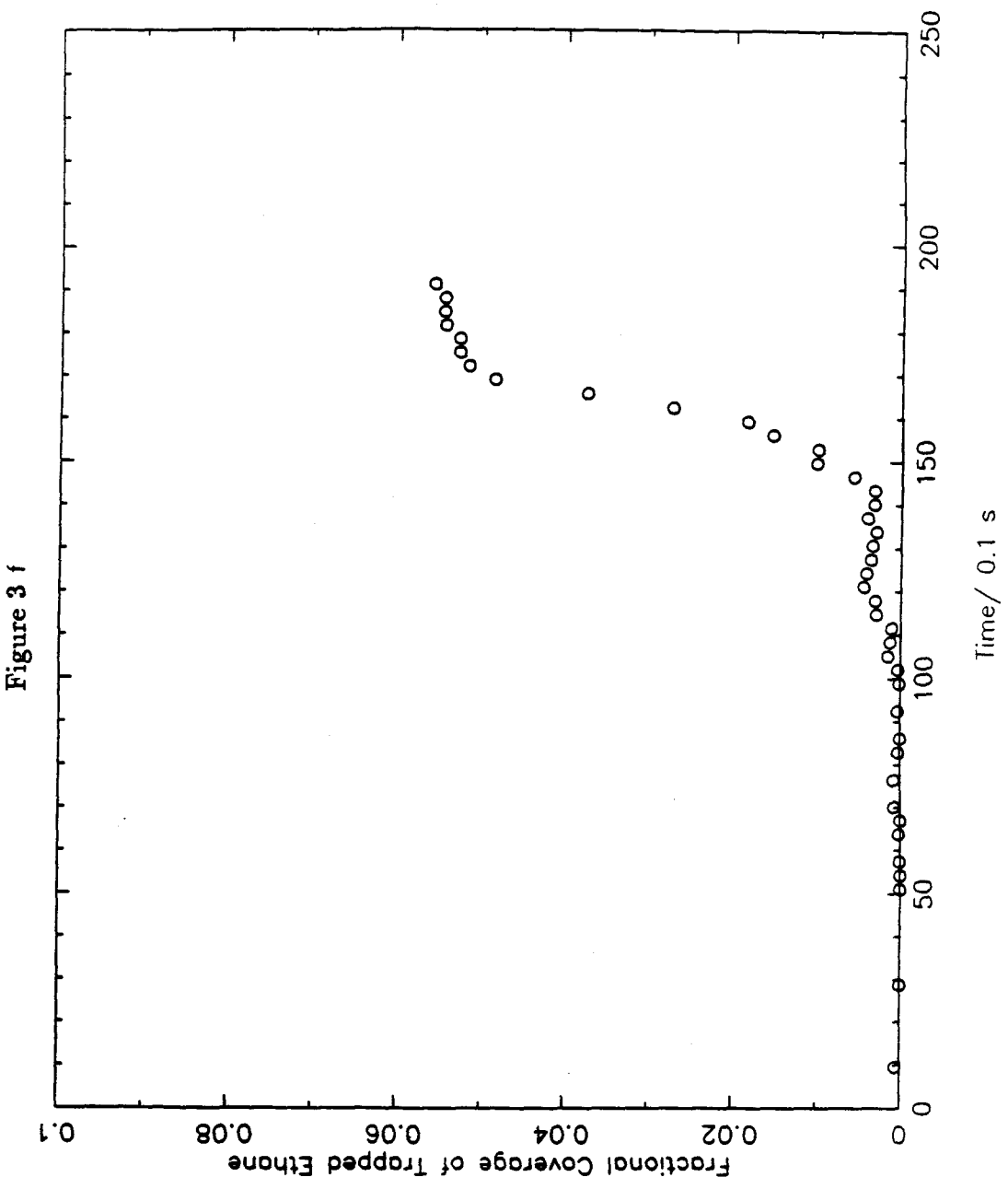
Fractional Coverage of Trapped Ethane
0
0.02
0.04
0.06
0.08
0.1
0
50
100
150
200
250
Time/ 0.1 s

Figure 3 f

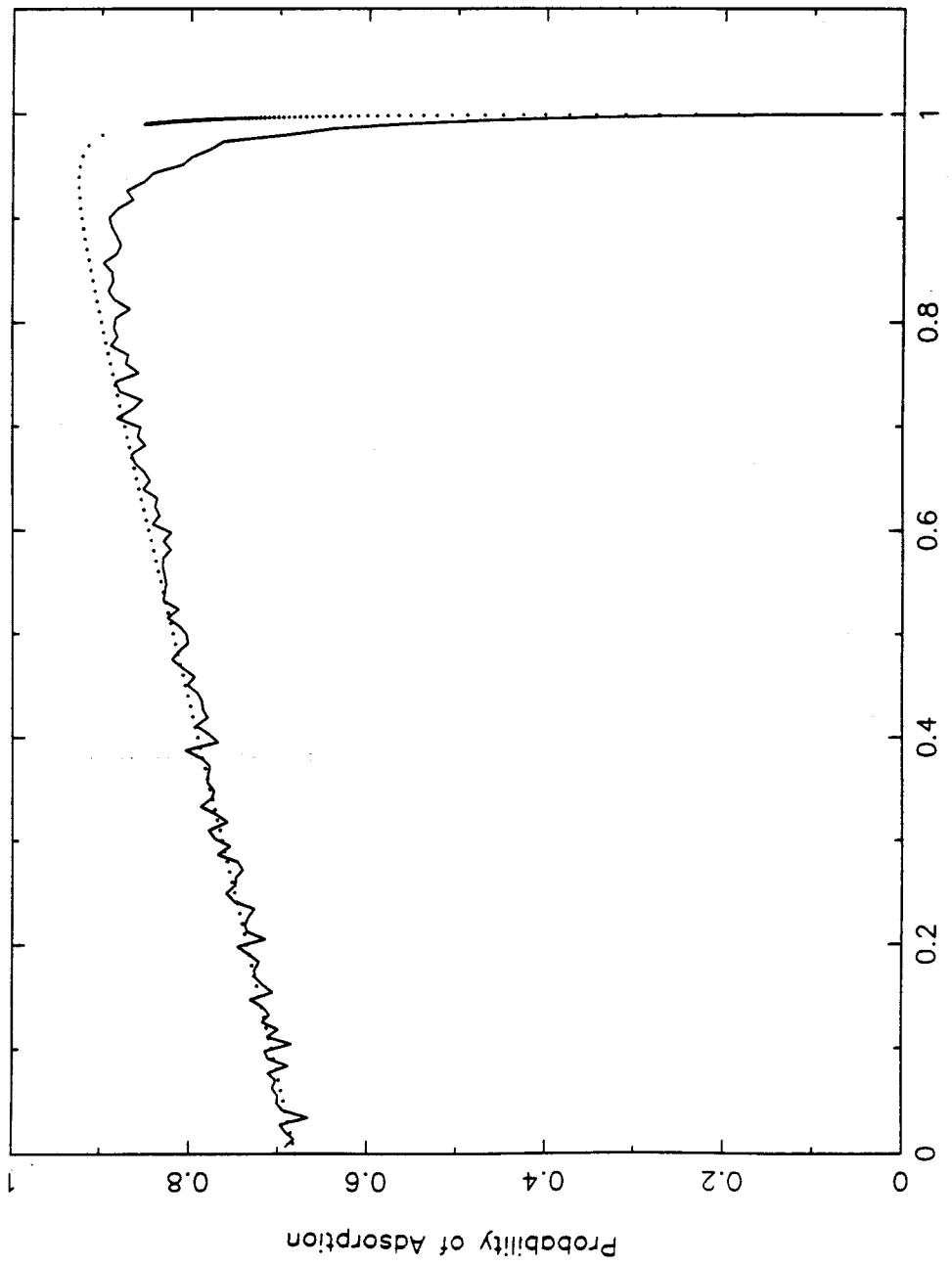
Probability of Adsorption
0
0.2
0.4
0.6
0.8
1
0
0.2
0.4
0.6
0.8
1
Fractional Coverage

Figure 4

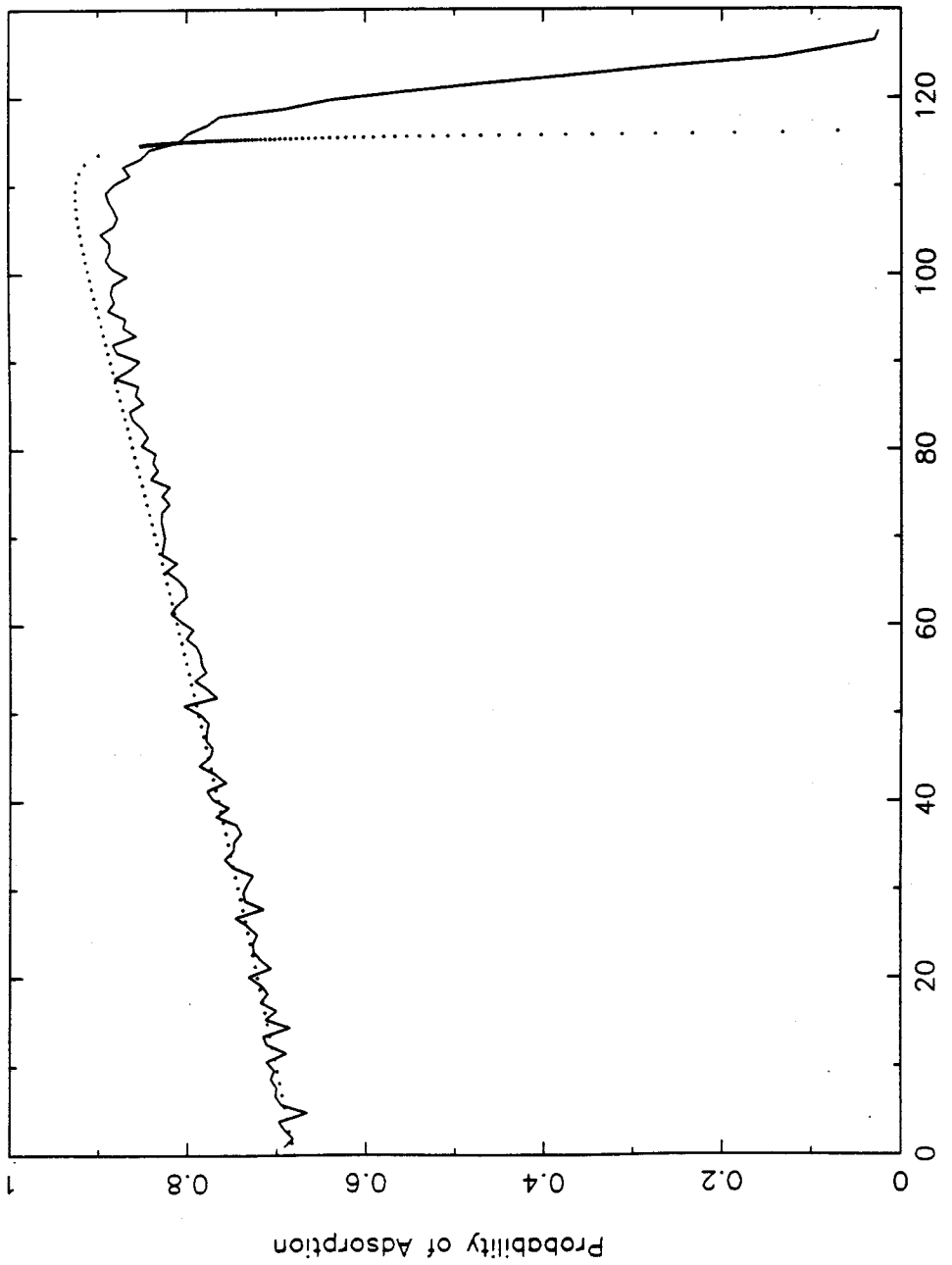
Probability of Adsorption
0
0.2
0.4
0.6
0.8
1
0
20
40
60
80
100
120
Time/ 0.1 s

Figure 5

Chapter 6.

Role of Local Configurations in a Langmuir-Hinshelwood Surface Reaction: Kinetics and Compensation

This chapter has been submitted as a paper by H.C. Kang, T.A. Jachimowski and W.H. Weinberg, to *The Journal of Chemical Physics*.

ABSTRACT

We have used Monte-Carlo sampling to calculate the rate coefficient for a Langmuir-Hinshelwood reaction between species A and B on a square lattice. The experimental situation that is simulated is the reaction between a *preadsorbed* overlayer of species A with species B. The preadsorbed overlayer of A is allowed to equilibrate prior to the adsorption of B. Upon the adsorption of B, the initial reaction rate is calculated assuming that A is irreversibly adsorbed and immobile, and that equilibrium between adsorbed B and gas-phase B is established much more rapidly than the timescale of the reaction between A and B. Reaction is allowed only between nearest-neighbor AB pairs. We examine the parametrization of the reaction rate coefficient into an effective activation energy and an effective preexponential factor. We find that correlations between nearest-neighbor particles affect the reaction rate coefficient significantly. We also find that if the distribution of local configurations of nearest-neighbor pairs of reactant particles changes with temperature, the corresponding Arrhenius plot is non-linear. The effective activation energy and the effective preexponential factor vary strongly with the fractional coverage of A and show a large compensation effect, similar to that observed experimentally in many desorption and surface-reaction systems. We conclude that variations in the distribution of local configurations of pairs of reactant molecules as a function of temperature and fractional surface coverage can be responsible for these experimentally observed compensation effects.

1. Introduction

The configuration of an overlayer of adsorbed molecules on a surface is generally a function of the fractional coverage and the temperature of the surface. Likewise, the kinetics of a surface chemical reaction can be strongly dependent upon the local configurations of the reactant molecules, as well as a function of the fractional coverage of the reactants and the temperature. The important role of the overlayer configuration of the reactant molecules on a catalytic surface has been established by many experimental investigations **(1-7)**. Similarly, the influence of the overlayer structure on the kinetics of thermal desorption has also been demonstrated **(8-13)**. Much work in this area has also been carried out using Monte-Carlo simulations **(14-28)** and mean-field approximations **(29-41)**. In particular, the formation of adsorbate 'islands' due to lateral interactions and their effects on the kinetics of a bimolecular Langmuir-Hinshelwood reaction have been investigated extensively using Monte-Carlo simulations **(14,15)**. An important feature of these simulations is that it is possible to obtain the correlation between the sites occupied by pairs of reactant molecules in Monte-Carlo simulations. As a consequence of the lateral interactions that exist between adsorbed molecules, the magnitude of these pair correlations may deviate from the values for a random distribution of molecules on the surface. For instance, with attractive nearest-neighbor interactions, the correlation between nearest-neighbor pairs of molecules is greater than when there are no lateral interactions. Such effects arising from lateral interactions have been referred to as 'topological' effects **(14,15)**. The energy barrier to reaction for each pair of reactant molecules depends upon the configuration of their neighboring sites, since each of the molecules in the reacting pair experiences lateral interactions with the molecules in the neighboring sites. The energy of the transition state for the reaction may also be affected by the configuration of the neighboring sites, but the change in the energies of the reactant molecules and the transition state are, in general, different because the lateral interactions experienced by the reactant

molecules are different from those experienced by the transition state. Hence, the energy barrier to reaction is dependent upon the number of occupied neighboring sites. This has been referred to as an 'energetic' effect **(14,15)**.

In Monte-Carlo simulations the positions of each of the particles on the surface are known. Therefore, it is possible to separate easily 'topological' effects from 'energetic' effects, in distinct contrast to the situation that obtains in laboratory experiments. In analyzing experimental data it is convenient to write the reaction rate per unit surface area as

$$F = f k^{(0)} \exp(-\beta E), \tag{1}$$

where f is the probability of finding a pair of molecules per unit surface area in a suitable configuration for reaction, e.g., in nearest-neighbor sites on the surface and β is defined to be $1/k_B T$, where T is the temperature of the surface. *Indeed Eq. (1) can be considered to be merely a formal parametrization of the reaction rate* into an effective 'topological' factor f, an effective preexponential factor $k^{(0)}$ and an effective activation energy E. Generally, f, $k^{(0)}$ and E are each dependent upon the fractional coverages and the temperature of the surface. It is, therefore, not easy to extract the temperature and coverage dependence of each of these factors from experimentally measured reaction rates.

If we consider all the different types of local configurations in which a nearest-neighbor pair of molecules can be found, we can write the total reaction rate per pair of nearest-neighbor sites on the lattice as a sum of the reaction rates of the elementary bimolecular reactions occurring between each pair of reactant molecules, i.e.,

$$F = \sum_i f_i \nu_i \exp(-\beta E_i), \tag{2}$$

where ν_i is the 'attempt' frequency and E_i is the activation energy to reaction for a pair of nearest-neighbor reactant molecules in a local configuration of type i. In the

simulations that we performed we set the 'attempt' frequency for all local configurations to be constant and equal to ν_0. The distribution of local configurations of nearest-neighbor pairs of reactant molecules is given by the probability of finding a nearest-neighbor pair of reactant molecules per pair of nearest-neighbor sites on the lattice f_i for each i. The sum of f_i over all i is the probability of finding a pair of reactant molecules in each pair of nearest-neighbor sites. It is usually the case that when Eq. (2) is reduced to the parametrization which is implicit in Eq. (1), each of the *macroscopic* quantities f, $k^{(0)}$ and E are determined by all the *microsocpic* quantities f_i, ν_i and E_i. In particular, it is usually not possible to parametrize the reaction rate in the form of Eq. (1) without including the influence of the distribution of overlayer configurations on the quantities E and $k^{(0)}$. One case in which this is possible is when the 'attempt' frequency and the activation energy are not dependent on the type of local configurations. However, as a consequence of the lateral interactions between adsorbed molecules, this is not generally true. Hence, the values of $k^{(0)}$ and E obtained when Eq. (1) is used to analyze experimental data include not only the effects due to the dynamics of the elementary bimolecular reaction but also the effects due to the statistics of the overlayer configuration.

In this paper we will show that by using the parametrization suggested by Eq. (1) it is possible to observe a compensation occurring between the variation of $k^{(0)}$ and E with coverage when the distribution of local configurations, given by the quantities f_i, changes significantly with temperature. Numerous experimental **(8-13)** and theoretical **(29-41)** studies have been conducted on similar a compensation effect in thermal desorption. Experimental studies **(8-13)** have indicated that the preexponential factor for desorption is generally not constant with coverage and may vary by up to eleven orders of magnitude. The change of the preexponential factor with coverage generally occurs in the direction which compensates for the change in the desorption activation energy. Mean-field approximations of lattice gases have been used to model this behavior **(29-41)**. The energy barrier and

the preexponential for the desorption of CO from the Ru(001) surface has been shown to be well described by mean-field approximations in which the overlayer undergoes a transition from a disordered lattice gas to an ordered $(\sqrt{3}x\sqrt{3})R30°$ domains when the coverage is 1/3. The anomalously high preexponential factor for desorption which is observed when the coverage is increased to close to 1/3 can be considered to arise from the large decrease in the overlayer entropy when the ordering transition is approached. A recent review of the work in this area may be found in Ref. 40. In this paper we show that compensation can arise because of the parametrization implicit in Eq. (1) when the distribution of the local configurations of the overlayer in the neighborhood of a pair of reacting molecules changes with temperature.

2. Model

Without loss of generality we choose to model the following particular experimental situation. The surface is exposed to species A until the fractional coverage has reached a desired value. The overlayer configuration is allowed to equilibrate, and the gas-phase A is pumped away. The surface is then exposed to species B, and the initial reaction rate is measured. As the reaction proceeds, the coverage of A on the surface decreases due to consumption by the reaction. The coverage of B will, in general, also change as a result of both the change in the coverage of A and the reaction itself. As a consequence the overlayer configuration will change. The reaction rate at any time will be strongly dependent on the overlayer configuration at that time, and this, in turn, is determined by the rate of relaxation of the configuration of the overlayer. In this paper we do not attempt to simulate this complicated situation, but rather we focus on the *initial reaction rate*. We simulate the case in which the rates of adsorption and desorption of species B are much greater than the reaction rate. Hence, by the time the reaction "begins"

equilibrium has already been established between gas-phase B and adsorbed B, i.e. we avoid having to consider the effect of a transient due to the adsorption of B. In other words, we assume that species B is quite mobile on the surface. On the other hand, we set the diffusion rate of species A to be zero in order to avoid having to consider the effect of relaxation of the preadsorbed overlayer of A. A similar situation occurs, for instance, during the oxidation of CO on the Pt(110)-(1x2) surface **(42)**. In this case, CO is rather weakly bound to the surface compared to the oxygen and is considerably more mobile than the oxygen atoms (which have been preadsorbed and equilibrated). However, it is probably the case that the oxygen overlayer configuration can relax on the time scale of the reaction, and any initial reaction rate calculated using a model which does not permit this relaxation will probably be too high. This is because relaxation of the overlayer will drive the adsorbed oxygen into configurations with higher binding energy. However, as will be seen, this does not qualitatively affect the conclusions that are drawn here.

We use a lattice gas to simulate species A. First, a square lattice is populated to a specific fractional coverage with particles of species A. We used lattices of size (100x100) in all our simulations. These particles are allowed to interact with each other through nearest- and next-nearest-neighbor interactions of strength E_{nn} and E_{nnn}, respectively. The values used in the simulations are $E_{nn} = 2$ kcal/mol and $E_{nnn} = 1$ kcal/mol. In the simulations, the fractional coverage of A ranged from 0.1 to 0.6, and the temperature ranged from 300 to 400 K. For these lateral interaction strengths, fractional coverages and temperatures, the equilibrium phase for the preadsorbed overlayer of A is a *disordered* lattice gas **(43)**. Indeed, this situation is chosen to be somewhat similar to the conditions in a recent experimental study of CO oxidation in which no overlayer low-energy electron diffraction spots were observed **(42)**. It should be noted, however, that steady-state reaction rates between CO and oxygen were measured in the experiments; whereas here only the initial reaction rates upon adsorption of species B onto a preadsorbed overlayer of

species A are modeled. In those experiments, the fractional coverage of CO ranged from approximately 0.25 to approximately 0.003. Although it is possible to use a lattice gas to model species B also, we find it more convenient for the range of fractional coverages that we wish to study to assume a Langmuir-adsorption isotherm for species B, and to allow the interspecies interaction E_{A-B} to be expressed by requiring a different binding energy for B at each adsorption site, depending upon the local configuration of the site. We allow an interspecies interaction E_{A-B} only between nearest-neighbor AB pairs. The values of E_{A-B} used in the simulations are -2, -1, 0, 1, and 2 kcal/mol, where negative interaction strengths indicate an attractive interaction and positive interaction strengths indicate a repulsive interaction. We assume that particles of species B do not interact with each other.

The probability that each site n is occupied by a particle of species B is determined by

$$p_n = \frac{p_{ad}\alpha\exp(\beta E_{d,n})}{1 + p_{ad}\alpha\exp(\beta E_{d,n})}, \tag{3}$$

where $E_{d,n}$ is the desorption barrier for species B from site n, p_{ad} is the probability of adsorption for a gas phase molecule incident upon the surface and the quantity α is the ratio of the rate at which particles of species B are impinging upon each site of the lattice to the preexponential factor for desorption. The value of $E_{d,n}$ for an isolated molecule of species B is chosen to be 36 kcal/mol in order to agree with the experimentally measured value for CO desorption from Pt(110) at low fractional coverages. For a site which has N_A nearest-neighbor particles of species A, the desorption energy barrier for species B is given by

$$E_{d,n} = E_d - N_A E_{A-B}, \tag{4}$$

where N_A is the number of nearest-neighbor sites of n occupied by particles of species A. The value of α used in the simulations is 1×10^{-26}. If the probability of adsorption p_{ad} is unity and the preexponential factor for desorption of B is assumed to be 1×10^{-14} s^{-1} then this value of α corresponds to a pressure of approximately

3×10^{-18} torr. This pressure is necessarily quite low because we have chosen to allow the gas-phase B to equilibrate with the adsorbed B, and we want the range of the equilibrium fractional coverage of B to include very low values. If the interspecies interaction E_{A-B} is zero and the temperature ranges from 300 to 400 K, then the fractional coverage of B ranges from approximately 5×10^{-7} to approximately 0.6.

The simulations were carried out by allowing the particles of species A to equilibrate on the surface. In order to ensure that a sufficiently large number of Monte-Carlo steps have been performed so that the configuration of the preadsorbed A has equilibrated, we monitor the energy of the lattice gas and sample the configurations only when the average energy has reached a constant asymptotic value. For each set of parameter values, we sampled 100 different configurations which had been obtained by using this procedure. Recall that the equilibrium phase for A for the lateral interaction strengths, coverages and temperatures used in the simulations is a disordered lattice gas. Hence, there are no complications arising from the slow dynamics associated with ordered domain growth. For the same reason, the (100x100) lattice that we used is almost certainly sufficiently large to avoid finite-size effects although we did not verify this explicitly.

After it has been established that the configuration has equilibrated, the probability of occupancy by species B of each vacant site p_n is calculated using Eq. (3). Then the reaction rate per nearest-neighbor pair of sites on the lattice is calculated by performing the sum

$$F = (2L)^{-2} \sum_{m,n} \sigma_m p_n \nu_{mn} \exp(-\beta E_{r,mn}), \tag{5}$$

where m and n denote a pair of nearest-neighbor sites, and L is the length of each side of the square lattice in units of the lattice constant. The occupancy of a site m by species A is denoted by σ_m, which has the value zero when the site is vacant and the value unity when it is occupied by a particle of species A. The energy barrier

for reaction for a pair of particles, A situated at site m and B situated at site n, is given by $E_{r,mn}$. This is determined by the local configurations of the pair by

$$E_{r,mn} = E_r - N_{nn}E_{nn} - N_{nnn}E_{nnn} - E_{A-B}(M_B + N_A), \tag{6}$$

where E_r is the energy barrier for reaction for an isolated nearest-neighbor pair of A and B. The 'attempt' frequency for the same pair is given by ν_{mn}. The quantities N_{nn} and N_{nnn} are, respectively, the number of nearest-neighbor and next-nearest-neighbor sites of m occupied by particles of species A. Similarly, N_A is the number of nearest-neighbor sites of n occupied by particles of species A. The quantity M_B is the sum over the nearest-neighbor sites of m of the probability of occupancy by a particle of species B at each of these sites. In computing M_B and N_A the particle of species A in site n and the particle of species B in site m are not counted. Recall that we have assumed no interactions between pairs of particles of species B. The reaction barrier for an isolated pair is chosen to be 22 kcal/mol, again to reflect a typical experimental value for CO oxidation on platinum. We can also obtain the distribution of nearest-neighbor AB pairs from the simulations. We denote this by f_i as in Eq. (2). In order to extract a rate coefficient k from the reaction rate in Eq. (5), we divide by the quantity

$$N_r = (2L)^{-2} \sum_{m,n} \sigma_m p_n, \tag{7}$$

where m and n are nearest-neighbor pairs of sites. This sum is simply the probability of finding a nearest-neighbor AB pair per nearest-neighbor pair of sites on the lattice. Another reaction rate coefficient, k_0 can also be obtained by dividing the reaction rate by $2\theta_A\theta_B$, i.e. the probability of finding a nearest-neighbor AB pair per nearest-neighbor pair of sites on the lattice, *if the distribution of particles were random.*

We have assumed that only AB pairs of which are nearest neighbor to each other can react. This is not necessarily the case in a real surface chemical reaction,

even if the surface were well modeled by a square lattice because the distance between the reactant molecules probably has to be less than one lattice constant for reaction to occur. This, however, will not change the nature of the results since the important factor here is the distribution of the local configurations around a reacting pair, and not whether these pairs can be considered to be nearest-neighbor pairs. If we assume that the 'attempt' frequency ν_{mn} factor is independent of the local configuration and is given by ν_0 s^{-1}, then the reaction rate coefficient k is the probability per ${\nu_0}^{-1}$ s of an AB product molecule leaving a nearest-neighbor pair of sites on the lattice, given that the nearest-neighbor pair of sites is occupied by a particle of species A and a particle of species B. A similar interpretation applies to k_0. More importantly, we have not built into the model a preexponential factor which changes with the local configuration and compensates for changes in $E_{r,nm}$.

3. Results and Discussion

The results for the reaction rate coefficients k and k_0 are shown in Figs. 1(a)-(e) and in Figs. 2(a)-(e), respectively. The data points are plotted as circles, and the lines are merely guides to the eye. Each of these curves is an Arrhenius plot of the reaction rate coefficient at the fractional coverage of A which labels it. In each figure we have noted the value of the lateral interaction E_{A-B} between species A and species B that is used in the simulations. The difference between k and k_0 can be seen immediately by comparing the corresponding curves in Figs. 1(a)-(e) and Figs. 2(a)-(e). This arises from a non-random distribution of particles on the lattice. The fact that the distribution on the surface is not random can be observed clearly by plotting the ratio $N_r/2\theta_A\theta_B$ as a function of temperature. This is shown in Figs. 3(a)-(c) in which each curve is a plot of $N_r/2\theta_A\theta_B$ as a function of temperature for values of the interspecies lateral interaction E_{A-B} equal to 2 kcal/mol, zero and -2 kcal/mol. A value of unity for the quantity $N_r/2\theta_A\theta_B$ implies a random distribution of particles on the surface. We have not

shown the results of simulations for which $E_{A-B} = 1$ kcal/mol and simulations for which $E_{A-B} = -1$ kcal/mol, but the trends are the same as in Figs. 3(b) and 3(c) respectively. Again, the lines are merely guides to the eye. Each curve is labeled by the fractional coverage of A used in the simulations. As expected, a repulsive interaction between A and B decreases the probability of finding nearest-neighbor AB pairs and an attractive interaction between A and B increases that probability. However, even though there is a significant difference between the values of k and k_0 at each temperature and fractional coverage of A, the trends in each of the Arrhenius curves in Figs. 1(a)-(e) are the same as the corresponding curve in Figs. 2(a)-(e). This is important since the quantity N_r is not experimentally accessible, and in analyzing experimental data the reaction rate coefficient k_0 is frequently used. At least for the model investigated here, the use of k_0 rather than k does not lead to qualitatively different behavior of the parameters E and $k^{(0)}$ extracted from the Arrhenius plots. It should also be noted that the Arrhenius plots in Figs. (1a-c) and Figs. 2(a)-(c) are rather well approximated by straight lines, whereas those in Figs. 1(d,e) and Figs. 2(d,e) are not (*vide infra*).

The reaction rate, when written in the form of Eq. (2), clearly separates the dependence for each type of local configuration into a 'topological' factor f_i and an 'energetic' factor E_i. We have noted earlier that in our simulations the preexponential factor ν_i for each type of local configuration has been set equal to a constant ν_0. Indeed, E_i and ν_i may be more accurately termed dynamic factors because, for a given local environment the values of E_i and ν_i are determined by the dynamics of the elementary bimolecular reaction. On the other hand, f_i may be more accurately termed a thermodynamic factor, since it is determined only by the statistics of the overlayer. *Such a clear separation is possible only when the timescales of the dynamics of the elementary reaction and the dynamics that govern the relaxation of the overlayer configuration are vastly different.* Generally, the bimolecular reactions occur on a much shorter timescale than the relaxation of the overlayer

configuration. However, even when this is the case in order to obtain a complete picture of the effect that the statistics of the overlayer configuration has on a surface reaction, it is necessary to be able to measure separately the 'topological' factors and the energetic 'factors.' This separation can easily be achieved in a computer simulation, but it is not readily performed in an experiment. Indeed, the difficulty of experimentally obtaining, for instance, the nearest-neighbor pair correlation coupled with the parametrization implicit in Eq. (1) render the interpretation of the quantities E and $k^{(0)}$ obtained from an Arrhenius plot difficult.

Using the parametrization defined by Eq. (1) it is possible to extract the effective activation energy E and the effective preexponential factor $k^{(0)}$. Note that we have simply set the preexponential factors ν_i for all types of local configurations to be equal to ν_0. In the simulations, we set ν_0 equal to unity. Therefore, values of $k^{(0)}$ of unity would be considered 'normal.' The values of E obtained from simulations in which E_{A-B} is zero, from simulations in which $E_{A-B} = 2$ kcal/mol, and from simulations in which $E_{A-B} = -2$ kcal/mol are plotted as functions of the fractional surface coverage of A in Figs. 4(a)-(c), respectively. For each value of E_{A-B}, we have obtained the values of E and $k^{(0)}$ for three different ranges of temperatures. For the temperature range of 300 to 340 K, the results are plotted as circles; for the temperature range of 340 to 360 K, the results are plotted as crosses; and for the temperature range of 360 to 400 K, the results are plotted as squares. The lines are guides to aid the eye. The corresponding results for the preexponential factor $k^{(0)}$ are plotted in Figs. 5(a)-(c). Consider first the case in which we have set the interspecies lateral interaction E_{A-B} to be zero. The results for this case are shown in Figures 4(a) and 5(a). Note that even though E_{A-B} is zero, there are repulsive lateral interactions between the particles of species A. Hence, if the distribution of the particles on the lattice were completely random, the activation energy for the elementary bimolecular reaction should decrease linearly with the fractional coverage of A. At zero fractional coverage of A, the activation energy

will be 22 kcal/mol; and at a fractional coverage of A of 0.8, it will be 12 kcal/mol. Hence, if the overlayer configuration were random the activation energy in this case would be given by a straight line from 22 kcal/mol at zero coverage to 12 kcal/mol at a fractional coverage of 0.8. As may be seen in Fig. 4(a), the value of E does not decrease so fast as would be expected if the particles were randomly distributed on the surface. This indicates that even though the equilibrium phase for the preadsorbed overlayer of A is a disordered lattice gas, there is some correlation between the positions of the sites occupied by the particles of species A. This correlation is such that the nearest-neighbor sites to a particle of species A are not so likely to be occupied by another particle of species A as would obtain if there were no correlation. This is to be expected since the lateral interactions between particles of species A are repulsive. As the fractional coverage of A increases, the difference between the activation energy expected and the activation energy observed becomes less because the lattice becomes more crowded and the difference between the actual configuration on the surface and a random distribution diminishes. Hence, the configurational entropy of the overlayer is less than the entropy for a random configuration but approaches this latter quantity when the fractional coverage of A increases.

If we now consider the case in which the lateral interaction between A and B is repulsive, we obtain the results plotted in Figs. 4(b) and 5(b). Again, at low fractional coverages of A, the observed activation energy is higher than the activation energy which would be expected if the overlayer configuration were random and if there were no interspecies lateral interactions. However, values of the activation energy given by the straight line between 22 kcal/mol at zero coverage and 12 kcal/mol at a fractional coverage of 0.8 is higher than the observed activation energy for fractional coverages of A above 0.4. This is due to the interspecies lateral repulsion of 2 kcal/mol used here. In this case the value of E at low fractional coverages of A depends more strongly on the temperature than the case in which E_{A-B}

is zero. If we recall that here the lateral interactions between A and B are repulsive, the temperature dependence can be understood. As the temperature is raised, the coverage of B decreases, because of a higher desorption rate, but the Boltzmann factor for the interaction energy of an AB nearest-neighbor pair increases. The first factor tends to decrease the average number of nearest-neighbor particles of species B for each particle of species A while the second factor tends to increase this number. The temperature dependence of the activation energy observed in Fig. 4(b) can be understood as arising from the competition between these two factors. The activation energy at a fractional coverage of A of 0.1 is lowest for the temperature range of 360 to 400 K. For the temperature range of 340 to 360 K, the activation energy is highest, and it decreases by a small amount for the temperature range of 360 to 400 K.

For both the case in which E_{A-B} is zero and the case in which $E_{A-B} = 2$ kcal/mol, the trends in the effective activation energy can be understood simply in terms of the average local configuration. However, we have not considered the trends in the effective preexponential factor $k^{(0)}$ which, has a much smaller range of values in these cases than in the case in which $E_{A-B} = -2$ kcal/mol. Also note that all the values of k shown in Figs. 5(a) and 5(b) are close to unity, in contrast to some of the values of $k^{(0)}$ shown in Fig. 5(c). Considering the effective activation energy plotted in Fig. 4(c) and the effective preexponential factor plotted in Fig. 5(c), it can be seen that large variations in both E and $k^{(0)}$ as a function of the fractional coverage of A occurs and the variations in $k^{(0)}$ compensate for the variations in E. Indeed, the results for the temperature range of 340 to 360 K give typically observed ranges of variations of E and $k^{(0)}$ for CO oxidation reactions on the late transition metal surfaces. The effective activation energy decreases from approximately 26 kcal/mol at a fractional coverage of A of 0.1 to approximately 9 kcal/mol at a fractional coverage of A of 0.6. At the same time the preexponential factor decreases from approximately $10^2\nu_0$ to approximately $10^{-7}\nu_0$ over the same

fractional coverage range of A. The quantity ν_0 is the 'normal' preexponential factor for the elementary bimolecular reaction between an adsorbed particle of A and an adsorbed particle of B. This is in rather close agreement with the observed compensation effect in the oxidation of CO on Pt(110)-(1x2) **(43)**. However, it can be seen that for the temperature range 300 to 340 K, the value of E that is obtained from the Arrhenius plots has a value as high as approximately 46 kcal/mol when the fractional coverage of A is 0.1. For the same temperature range, it can be seen in the Arrhenius plot of Fig. 1(e) that a high effective activation energy and a high effective preexponential factor are also obtained for a fractional coverage of A of 0.2.

If we consider local configurations of a nearest-neighbor AB pair the highest activation energy E_i that is possible is 32 kcal/mol. In order to explain the anomalously high value of E obtained for the case in which $E_{A-B} = -2$ kcal/mol, it is necessary to compare the distribution of local configurations for the three different values of E_{A-B}. In Figs. 6(a)-(c) we plot these distributions as a function of the lateral interaction energy. In each of these figures, we plot the distributions at various temperatures obtained from simulations in which the fractional coverage of A is 0.4. The temperatures range from 320 to 400 K. Each curve is labeled with its corresponding temperature, and each figure is labeled with the value of E_{A-B} used in the simulations. Each distribution is the result of only one simulation. It can be seen that while the distributions in Figs. 6(a) and 6(b) do not change significantly with temperature, the distribution in Fig. 6(c), the case in which $E_{A-B} = -2$ kcal/mol, changes very significantly indeed with temperature. As the temperature is steadily decreased, a steadily larger fraction of nearest-neighbor AB pairs can be found in local configurations for which the activation energy E_i is high. This is due to the increased adsorption of particles of species B as the temperature is decreased. Similar features are observed for the distributions at other values of the fractional coverage of A.

From Eq. (2), it is clear that a temperature dependence in the distribution of local configurations will give rise to a temperature dependence in k (or k_0) which arises solely from 'topological' effects. This can be clarified by approximating the distribution of local configurations by delta-functions. For instance, we can approximate the distribution at 400 K by a delta-function at an activation energy of 24 kcal/mol and the distribution at 340 K by a delta-function at 27 kcal/mole. If these two data points were used in an Arrhenius plot, as shown schematically in Fig. 7, the effective activation energy E is approximately 44 kcal/mol. This value is higher than the maximum activation energy that can be expected by considering only the lateral interactions between the particles. The discrepancy is due to the 'extra' temperature dependence that is introduced into the Arrhenius plot as a result of the temperature dependence of the distribution of local configurations observed in Fig. 6(c). The corresponding effective preexponential factor $k^{(0)}$ is approximately $7 \times 10^{10}\nu_0$. Therefore, it is clear that intrepreting the quantity $k^{(0)}$ as an 'attempt' frequency can be quite incorrect when there is a temperature dependence of the overlayer configuration. Such a temperature dependence can result in an observed value of $k^{(0)}$ which is much larger than the 'normal' value of $10^{13}\mathrm{s}^{-1}$ simply because of the use of the Arrhenius parametrization in Eq. (1).

The distribution of local configurations is approximately independent of the temperature for the simulations in which E_{A-B} is either zero or repulsive and, thus, the 'average' activation energy in each of these cases is approximately independent of the temperature. When the interspecies interaction is zero, both the effective activation energy E and the effective preexponential factor decreases with coverage, although the change in E is dominant. The change in $k^{(0)}$ is less than one order of magnitude from the highest value to the lowest value. However, as we have discussed earlier, the configuration of the preadsorbed overlayer of A is not random but tends towards randomness as the fractional coverage of A is increased. Thus, at low fractional coverages of A the configurational entropy of the overlayer is higher

than the value that would be expected if the configuration were random. Therefore, there would be a decrease in the preexponential factor as the fractional coverage is increased. This effect is not large because the change in the configuration of the overlayer is not large, and accounts for the general trend, observed in Fig. 5(a), of $k^{(0)}$ decreasing with an increase in the fractional coverage of A.

When the interspecies interaction E_{A-B} is repulsive, we have noted the slight temperature dependence that arises in the activation energy at low fractional coverages of A. Consider the results for the temperature range of 300 to 340 K by comparing the corresponding curves in Figs. 4(a) and (b). The activation energy is lower in Fig. 4(b) than in Fig. 4(a) for all fractional coverages as a result of the interspecies repulsive interaction that occurs for Fig. 4(b). If we consider the fractional coverages of 0.1 and 0.2, it can be seen the difference in the activation energy is larger for the fractional coverage of 0.1. This is to be expected because at a fractional coverage of 0.1, the number of nearest-neighbor particles of species A for each site is lower and, consequently, the probability of occupation of each vacant site (after preadsorption of A) by a particle of species B is higher. Therefore, there is a larger number of nearest-neighbor particles of species B for each particle of species A at a fractional coverage of 0.1 than at a fractional coverage of 0.2. Now, assume that the effective preexponential that is obtained for the case in which E_{A-B} is zero is the same at these two fractional coverages. Then the decrease in the activation energy E implies that at both fractional coverages the intercept on the ordinate of the Arrhenius plot is lower for the case in which E_{A-B} is repulsive than for the case in which it is zero. But the decrease in the intercept for the fractional coverage of 0.1 is larger. Thus, there is an increase in the value of $k^{(0)}$ when the the fractional coverage of A increases from 0.1 to 0.2, as seen in Fig. 5(b). Similarly, the trend at higher fractional coverags can be understood.

The range of the variation in the effective preexponential $k^{(0)}$ that is observed in Figs. 5(a) and (b) is at most one order of magnitude. This is not the case,

however, when E_{A-B} is attractive since in this case the local distribution is a strong function of the temperature. The Arrhenius plots for simulations with these attractive values of the interspecies interaction would thus be expected to be rather nonlinear as was noted earlier and can be seen in Figs. 1(a)-(e) and Figs. 2(a)-(e). Hence, we conclude that it is the variation of the overlayer configuration which gives rise to the compensation effect that we have observed in the simulations for which $E_{A-B} = -2$ kcal/mol, cf. Figs. 4(c) and 5(c). The results from these simulations are qualitatively the same as the results of simulations for which $E_{A-B} = -1$ kcal/mol, and the same conclusion applies for that case as well. A compensation effect is observed in both these cases because of a change in the distribution of local configurations, the latter of which is caused by an increase in the fractional coverage of species B when the temperature is reduced. In Fig. 8 we show schematically the general situation in which a compensation effect arising from the temperature dependence of the overlayer configuration can be expected. In a steady-state bimolecular reaction, the fractional coverages of both reacting species are constant. If the reaction rate constant is measured over a range of temperatures, the Arrhenius plots of such results are shown by the solid lines a and b, where each line denotes the results obtained at constant fractional coverages of the reacting species. For the case in which there is no temperature dependence of the overlayer configuration and, consequently, no temperature dependence of the effective activation energy at a fixed fractional coverage, the effective preexponential factors obtained by extrapolation of the two lines a and b will be the same. We have ignored a possible dependence of the configurational entropy of the overlayer on the fractional coverage which may lead to a small compensation effect as was observed for the case in which E_{A-B} is zero. If, however, there is a temperature dependence of the overlayer configuration then the effective activation energy is expected to change with temperature for each Arrhenius plot. The Arrhenius plots that would be expected to be obtained in this case is denoted by the curves a^* and b^*. We have

assumed that at high temperatures, the temperature dependence is smaller than at low temperature so that the curves a^* and b^* asymptotically approach the straight lines a and b respectively. If there is a stronger dependence of the activation energy on the temperature for the case denoted by line a than for the case denoted by line b, then a compensation effect can be observed as the extrapolations denoted by the dotted lines show. We would expect from thermodynamic considerations that the lower activation energy indicates an overlayer configuration which has a lower correlation between the positions of the particles, i.e. a configuration which is 'more' random. The overlayer configuration in this case would be expected to show a smaller temperature dependence than an overlayer configuration in which there are stronger correlations between the particle positions. Therefore, in Fig. 8 we expect the temperature dependence to be greater for the case denoted by a than for the case denoted by b. Thus, in general, when there is a temperature dependence in the activation energy, we would expect it to result in a compensation effect. The same effect can also be expected to occur for desorption from an overlayer consisting of only one species. Judging from the extremely large variation of the effective preexponential factor and the effective activation energy that we have obtained for $E_{A-B} = -2$ kcal/mol, the magnitude of this attractive interspecies lateral interaction is evidently larger than the lateral interaction between CO molecules and oxygen atoms on the Pt(110)-(1x2) surface **(42)**. However, we conclude that the typically observed compensation between E and $k^{(0)}$ in numerous experimental studies **(8-13)** can result from the dependence of the overlayer statistics upon the temperature of the system.

As we noted earlier, we have focussed on the initial reaction rate and have not allowed the configuration of the preadsorbed A to relax. These constraints on the simulations should not affect the conclusions drawn here, however, because by allowing the adsorbed overlayer to relax, the distribution of local configurations will still be a function of temperature and coverage. Indeed, as the temperature and

coverage are changed such that the equilibrium phase of the system changes from a disordered lattice gas to an ordered phase, *the change in the distribution of local configurations will be even larger than in our simulations which did not allow the configuration of species A to relax when B is adsorbed.*

4. Conclusions

We have investigated using Monte-Carlo sampling a Langmuir-Hinshelwood reaction between two species A and B, of which A is irreversibly adsorbed to the surface and immobile, whereas B is mobile and can desorb from the surface at the temperatures of interest. In the simulations, which are performed on square lattices, nearest-neighbor and next-nearest-neighbor lateral interactions are allowed between pairs of particles of species A. Nearest-neighbor lateral interactions are allowed between AB pairs, but pairs of particles of species B are assumed not to interact with one another. These features, while not essential to the conclusions drawn, were chosen to be typical of the important catalytic reaction between CO and oxygen on the platinum metals. From the simulations we were able to calculate the reaction rate and to extract reaction rate coefficients. We obtained two different rate coefficients k and k_0, the former of which is the reaction rate divided by the number of nearest-neighbor AB pairs, while the latter of which is the reaction rate divided by the expected number of nearest-neighbor AB pairs if the particle distribution on the lattice were random. Although the values of k and k_0 differ significantly because of the non-random distribution of particles of the lattice, it was found that the trends in k and k_0 as a function of temperature and coverage are similar. From Arrhenius plots of the reaction rate coefficient R, we extracted the dependence of the effective activation energy E and the effective preexponential factor $k^{(0)}$ as a function of the coverage over various temperature ranges. We observed that in the cases in which the distribution of the local configurations around a nearest-neighbor AB pair changes significantly with temperature, there

is a compensation effect between E and $k^{(0)}$. We conclude that this behavior is typical of systems in which the overlayer configuration changes with temperature and coverage, and that such changes generally result in the compensation between the variations of E and of $k^{(0)}$ with coverage that is observed in both surface chemical reaction **(43)** and thermal desorption **(8-13)**.

Acknowledgment: This research was supported by the Office of Basic Energy Sciences of the Department of Energy.

References

1. H.P. Bonzel and R. Ku, Surf. Sci. **40**, 85 (1973).
2. T. Engel and G. Ertl, J. Chem. Phys. **69**, 1267 (1978).
3. M.A. Barteau, E.I. Ko and R.J. Madix, Surf. Sci. **104**, 161 (1981).
4. G.E. Bechthold, Surf. Sci. **115**, L125 (1982).
5. J.L. Gland and E.B. Kollin, J. Chem. Phys. **78**, 963 (1983).
6. E.M. Stuve, R.J. Madix and C. Brundle, Surf. Sci. **146**, 155 (1984).
7. S. Akhter and J.M. White, Surf. Sci. **171**, 527 (1986).
8. J.C. Tracy, J. Chem. Phys. **56**, 2736 (1972).
9. H. Pfnur, P. Feulner, H.A. Engelhardt and D. Menzel, Chem. Phys. Lett. **59**, 481 (1978).
10. J.L. Taylor, D.E. Ibbotson, W.H. Weinberg, J. Chem. Phys. **69**, 4298 (1978).
11. H. Ibach, W. Erley and H. Wagner, Surf. Sci. **92**, 29 (1980).
12. C.M.A.M. Mesters, A.F.H. Wielers, O.L.J. Gijzeman, J.W. Geus and G.A. Bootsma, Surf. Sci. **115**, 237 (1982).
13. H. Papp, Surf. Sci. **129**, 205 (1983).
14. M. Silverberg and A. Ben-Shaul, J. Chem. Phys. **83**, 6501 (1985).
15. M. Silverberg and A. Ben-Shaul, J. Chem. Phys. **87**, 3178 (1987).
16. M. Silverberg and A. Ben-Shaul, Chem. Phys. Lett. **134**, 491 (1987).
17. M. Silverberg and A. Ben-Shaul, J. Stat. Phys. **52**, 1179 (1988).
18. M. Silverberg and A. Ben-Shaul, Surf. Sci. **214**, 17 (1989).
19. E.S. Hood, B.H. Toby and W.H. Weinberg, Phys. Rev. Lett. **55**, 2437 (1985).
20. P. Araya, W. Porod, R. Sant and E.E. Wolf, Surf. Sci. **208**, L80 (1989).
21. M. Dumont and P. Dufour, Comp. Phys. Comm. **41**, 1 (1986).

22. M. Dumont, M. Poriaux and R. Dagonnier, Surf. Sci. **169**, L307 (1986).

23. J.L. Sales and G. Zgrablich, Phys. Rev. B **35**, 9520 (1987).

24. J.L. Sales and G. Zgrablich, Surf. Sci. **187**, 1 (1987).

25. D. Gupta and C.S. Hirtzel, Chem. Phys. Lett. **149**, 527 (1988).

26. D. Gupta and C.S. Hirtzel, Surf. Sci. **210**, 322 (1989).

27. M. Stiles and H. Metiu, Chem. Phys. Lett. **128**, 337 (1986).

28. G. Ertl and J. Kuppers, Surf. Sci. **21**, 61 (1970).

29. C.G. Goymour and D.A. King, J. Chem. Soc. Faraday Trans. I **69**, 736 (1973).

30. C.G. Goymour and D.A. King, J. Chem. Soc. Faraday Trans. I **69**, 749 (1973).

31. D.L. Adams, Surf. Sci. **42**, 12 (1974).

32. M.E. Bridge and R.M Lambert, J. Catal. **46**, 143 (1977).

33. M.E. Bridge and R.M Lambert, Surf. Sci. **63**, 315 (1977).

34. M.E. Bridge and R.M Lambert, Proc. Roy. Soc. A **370**, 545 (1980).

35. V.P. Zhdanov, Surf. Sci. **111**, L662 (1981).

36. V.P. Zhdanov, Surf. Sci. **123**, 106 (1982).

37. V.P. Zhdanov, Surf. Sci. **133**, 464 (1983).

38. V.P. Zhdanov, Surf. Sci. **137**, 515 (1984).

39. E. Goldys, Z.W. Gortel, and H.J. Kreuzer, Solid State Comm. **40**, 963 (1981).

40. P.K. Johansson, Chem. Phys. Lett. **65**, 366 (1979).

41. E.G. Seebauer, A.C.F. Kong and L.D. Schmidt, Surf. Sci. **193**, 417 (1988).

42. J.R. Engstrom and W.H. Weinberg, Surf. Sci. **201**, 145 (1988).

43. K. Binder and D.P. Landau, Phys. Rev. **B21**, 1941 (1980).

Figure Captions

Figure 1(a)-(e): Arrhenius plots for the reaction rate coefficient k are shown here. The abscissa is the reciprocal of the temperature in units of K^{-1}. The ordinate is k, which is the probability per ν_0^{-1} s of a product molecule AB leaving a nearest-neighbor pair of sites on the lattice, given that the nearest-neighbor pair of sites is occupied by a pair of reactant particles A and B. The interspecies lateral interaction E_{A-B} is shown in each panel, and each curve is labeled with its corresponding fractional coverage of A. For all simulations, the lateral interactions for pairs of particles of species A are 2 kcal/mol for nearest-neighbor pairs and 1 kcal/mol for next-nearest-neighbor pairs. The data points are denoted by circles and the lines are guides to the eye.

Figure 2(a)-(e): Arrhenius plots for the reaction rate coefficient k_0 are shown here. The abscissa is the reciprocal of the temperature in units of K^{-1}. The ordinate is k_0, which is the probability per ν_0^{-1} s of a product molecule AB leaving a nearest-neighbor pair of sites on the lattice divided by the probability that the nearest-neighbor pair of sites is occupied by a pair of reactant particles A and B if the particle distribution on the surface were random. The interspecies lateral interaction E_{A-B} is shown in each panel, and each curve is labeled with its corresponding fractional coverage of A. For all simulations, the lateral interactions for pairs of particles of species A are 2 kcal/mol for nearest-neighbor pairs and 1 kcal/mol for next-nearest-neighbor pairs. The data points are denoted by circles and the lines are guides to the eye.

Figure 3(a)-(c): The ratio of N_r to $2\theta_A\theta_B$ is plotted as a function of temperature. Each curve is labeled by the fractional coverage of A, and the interspecies lateral interaction E_{A-B} is shown in each panel. For all simulations, the lateral interactions for pairs of particles of species A are 2 kcal/mol for nearest-neighbor pairs and 1 kcal/mol for next-nearest-neighbor pairs. The data points are denoted by circles

and the lines are guides to the eye.

Figure 4(a)-(c): The effective activation energy E for reaction obtained from the Arrhenius plots in Fig. 1. The abscissa is the fractional coverage of species A and the ordinate is the effective activation energy in units of kcal/mol. The activation energy for reaction for an isolated pair of reactant particles has been set equal to 22 kcal/mol. The interspecies lateral interaction E_{A-B} is shown in each panel. For all simulations, the lateral interactions for pairs of particles of species A are 2 kcal/mol for nearest-neighbor pairs and 1 kcal/mol for next-nearest-neighbor pairs. Each curve is labeled by the range of temperature of the data points used to extract the effective activation energy. The lines are guides to the eye.

Figure 5(a)-(c): The effective preexponential factor k^0 for reaction obtained from the Arrhenius plots in Fig. 1. The abscissa is the fractional coverage of species A and the ordinate is the logarithm (base ten) of the effective preexponential factor in units of ν_0, the preexponential factor for the elementary bimolecular reaction. The interspecies lateral interaction E_{A-B} is shown in each panel. For all simulations, the lateral interactions for pairs of particles of species A are 2 kcal/mol for nearest-neighbor pairs and 1 kcal/mol for next nearest-neighbor pairs. Each curve is labeled by the range of temperature of the data points used to extract the effective activation energy. The lines are guides to the eye.

Figure 6(a)-(c): The distribution of local configurations for nearest-neighbor AB pairs of particles is plotted as a function of the lateral interaction energy. The distribution has been normalized to unity. The interspecies lateral interaction strength is shown in each panel, and each curve is labeled by the temperature at which the distribution is obtained. Each distribution is the result of only one simulation. The lines are guides to the eye.

Figure 7: A schematic diagram of the effect of the temperature dependence of the activation energy for the case in which E_{A-B} is -2 kcal/mol. The abscissa

is the reciprocal of the temperature and the ordinate is the natural logarithm of the reaction rate constant. We have approximated the distribution of activation energies E_i by a delta-function at 27 kcal/mol at a temperature of 340 K and a delta-function at 24 kcal/mol at a temperature of 400 K. The two circles denote the results of the simulations, and the line labeled *a* indicates the Arrhenius construction to obtain the effective activation energy and the effective preexponential factor for this temperature range given the two data points.

Figure 8: A schematic diagram of the reaction rate constants over a range of temperatures at two different fractional coverages. The abscissa is the reciprocal of the temperature and the ordinate is the natural logarithm of the reaction rate constant. The lines labeled *a* and *b* are the reaction rate constants, each at constant but different fractional coverages of the reacting species, when there is no temperature dependence of the overlayer configuration. The curves labeled a^* and b^* are the reaction rate constants when there is a dependence of the overlayer configuration upon the temperature. As we argue in the text, the temperature dependence is generally greater for the case denoted by *a* than for the case denoted by *b*. The Arrhenius constructions indicated by the broken lines show a compensation effect.

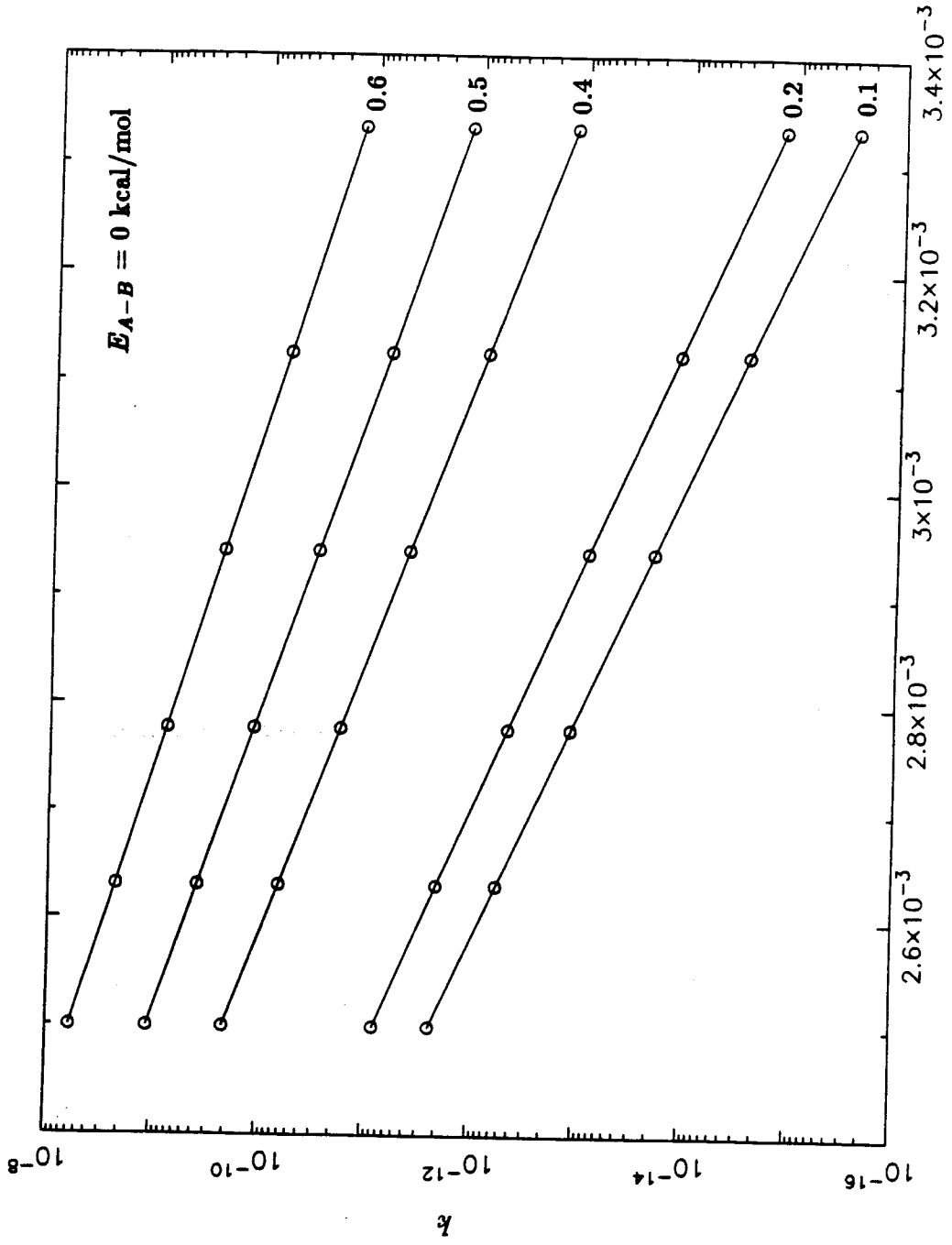
$E_{A-B} = 0$ kcal/mol
0.6
0.5
0.4
0.2
0.1
10^{-8}
10^{-10}
10^{-12}
10^{-14}
10^{-16}
k
2.6×10^{-3}
2.8×10^{-3}
3×10^{-3}
3.2×10^{-3}
3.4×10^{-3}
T^{-1}

Figure 1(a)

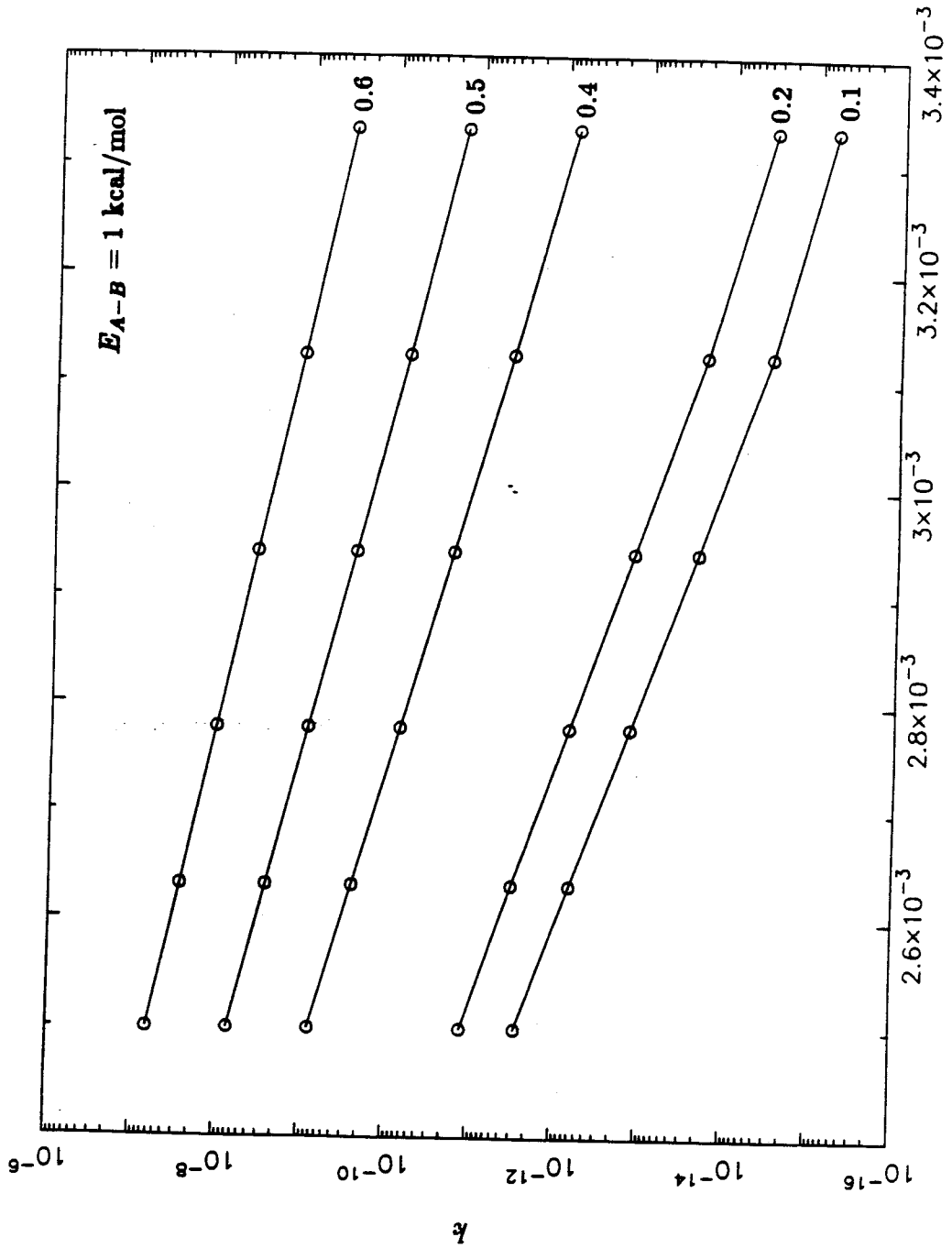
$E_{A-B} = 1$ kcal/mol
0.6
0.5
0.4
0.2
0.1
k
10^{-6}
10^{-8}
10^{-10}
10^{-12}
10^{-14}
10^{-16}
T^{-1}
2.6×10^{-3}
2.8×10^{-3}
3×10^{-3}
3.2×10^{-3}
3.4×10^{-3}

Figure 1(b)

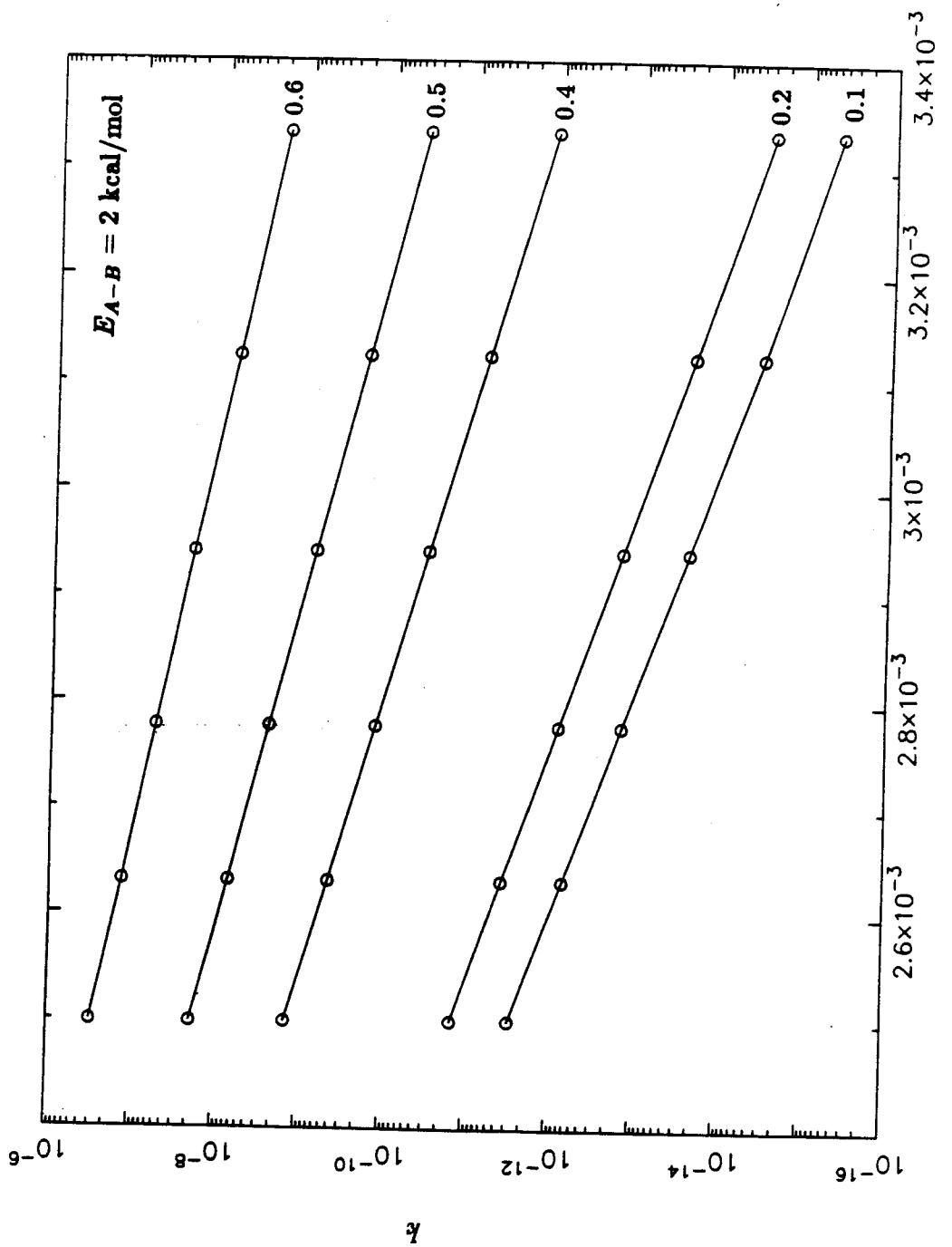
E_{A-B} = 2 kcal/mol
0.6
0.5
0.4
0.2
0.1
k
10^{-6}
10^{-8}
10^{-10}
10^{-12}
10^{-14}
10^{-16}
T^{-1}
2.6×10^{-3}
2.8×10^{-3}
3×10^{-3}
3.2×10^{-3}
3.4×10^{-3}

Figure 1(c)

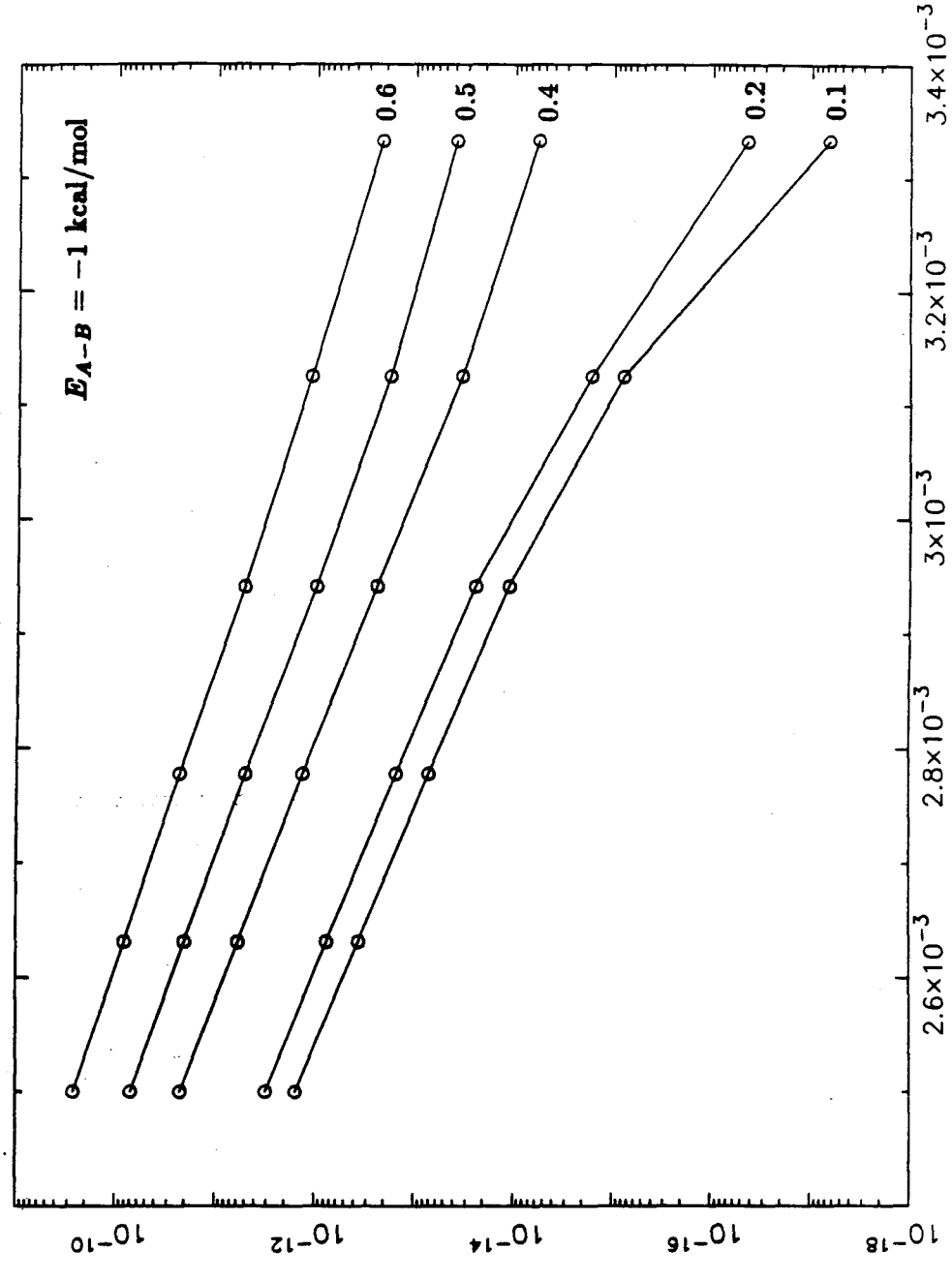
$E_{A-B} = -1$ kcal/mol
0.6
0.5
0.4
0.2
0.1
10^{-10}
10^{-12}
10^{-14}
10^{-16}
10^{-18}
2.6×10^{-3}
2.8×10^{-3}
3×10^{-3}
3.2×10^{-3}
3.4×10^{-3}
T^{-1}

Figure 1(d)

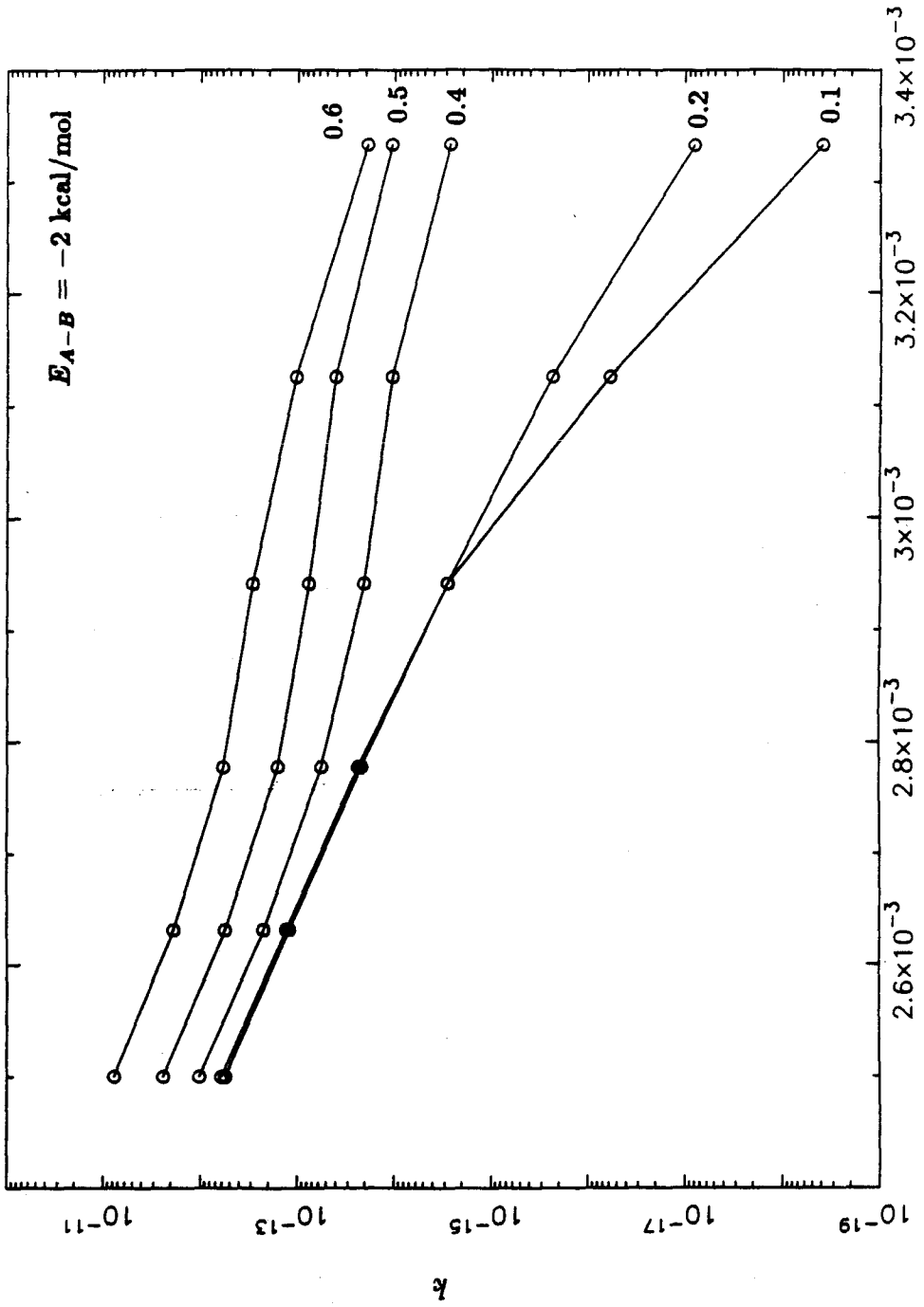
$E_{A-B} = -2$ kcal/mol
0.6
0.5
0.4
0.2
0.1
10^{-11}
10^{-13}
10^{-15}
10^{-17}
10^{-19}
k
2.6×10^{-3}
2.8×10^{-3}
3×10^{-3}
3.2×10^{-3}
3.4×10^{-3}
T^{-1}

Figure 1(e)

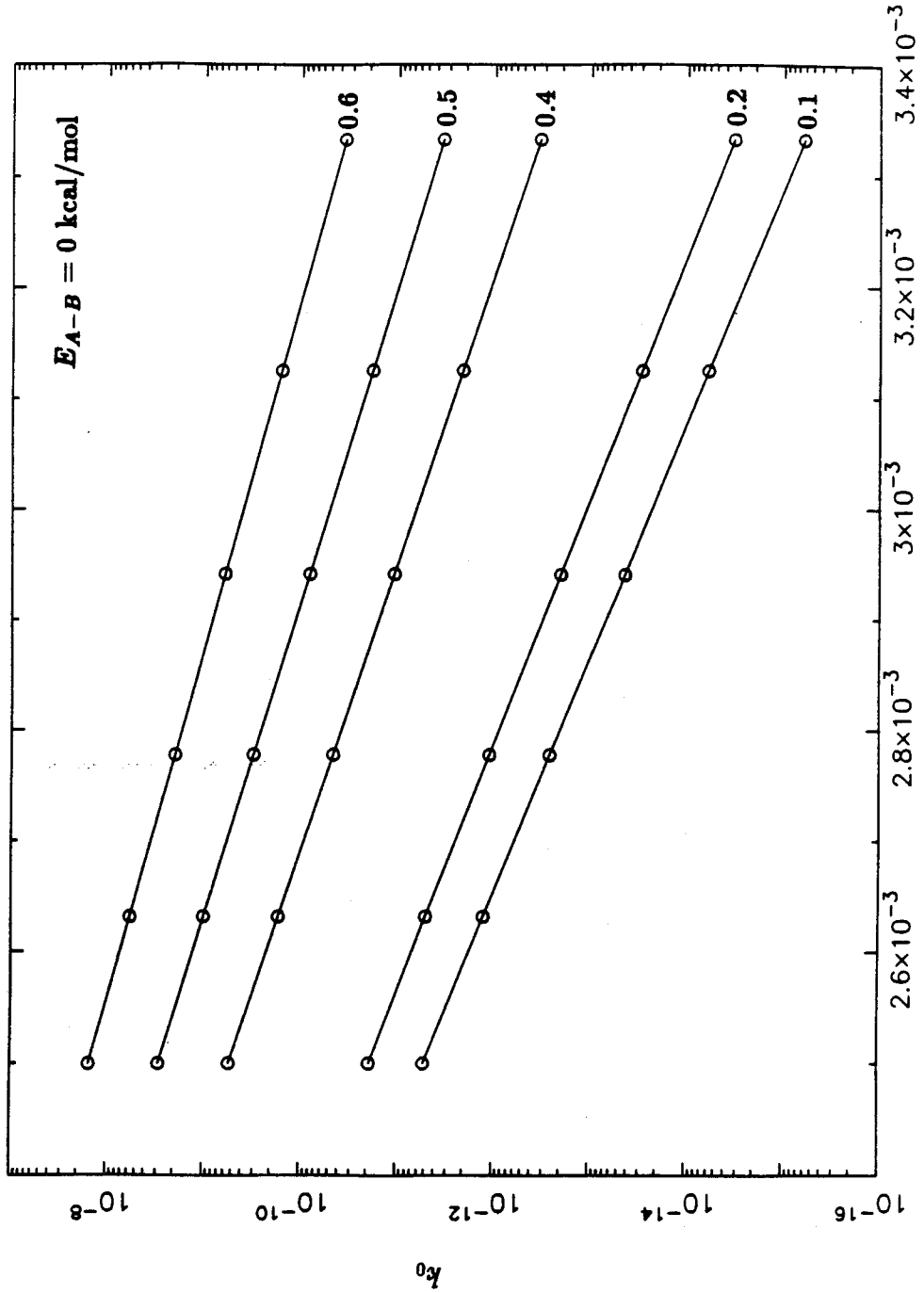
$E_{A-B} = 0$ kcal/mol
0.6
0.5
0.4
0.2
0.1
k_0
10^{-8}
10^{-10}
10^{-12}
10^{-14}
10^{-16}
2.6×10^{-3}
2.8×10^{-3}
3×10^{-3}
3.2×10^{-3}
3.4×10^{-3}
T^{-1}

Figure 2(a)

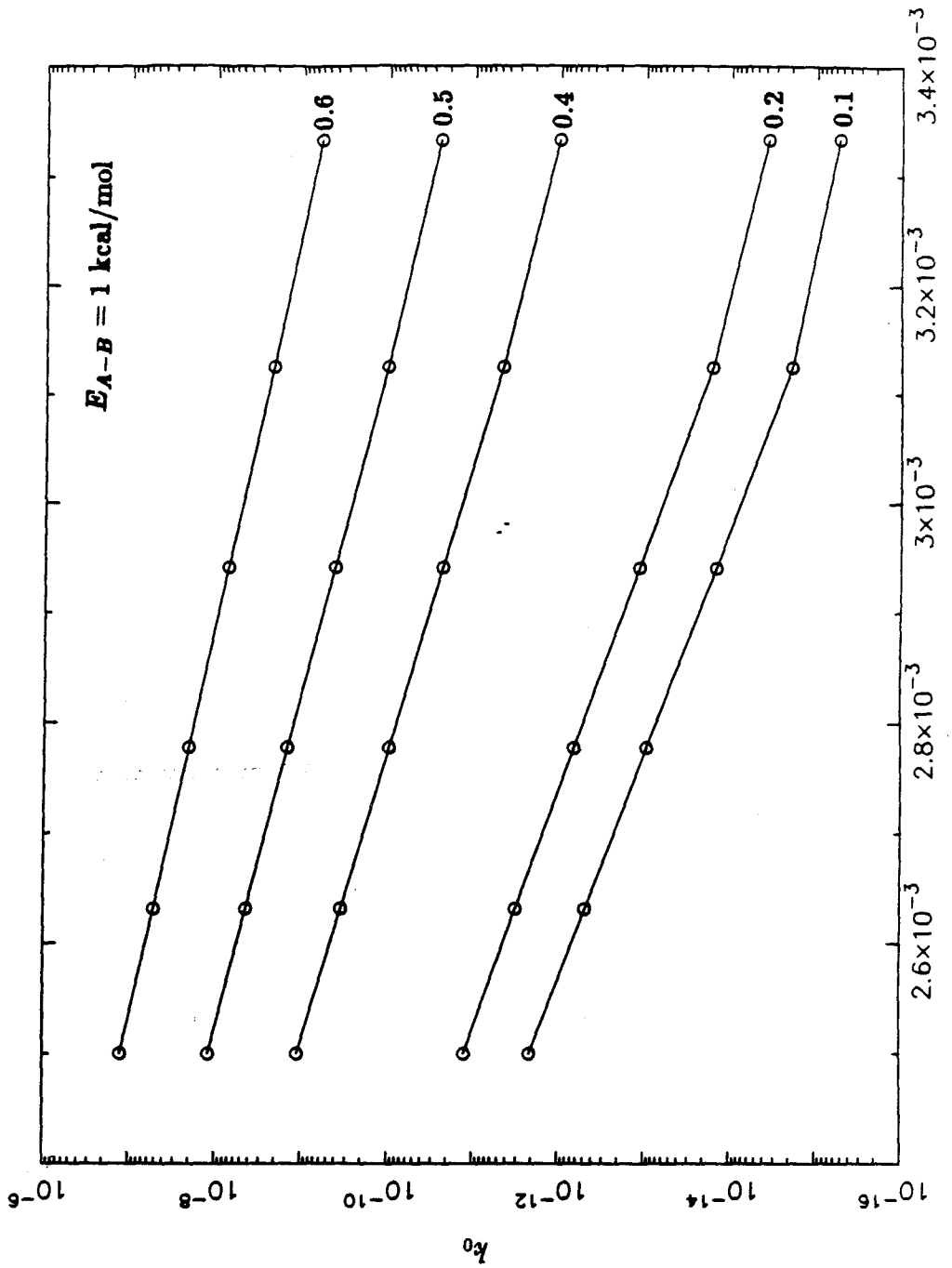
E_{A-B} = 1 kcal/mol
0.6
0.5
0.4
0.2
0.1
k_0
10^{-6}
10^{-8}
10^{-10}
10^{-12}
10^{-14}
10^{-16}
T^{-1}
2.6×10^{-3}
2.8×10^{-3}
3×10^{-3}
3.2×10^{-3}
3.4×10^{-3}

Figure 2(b)

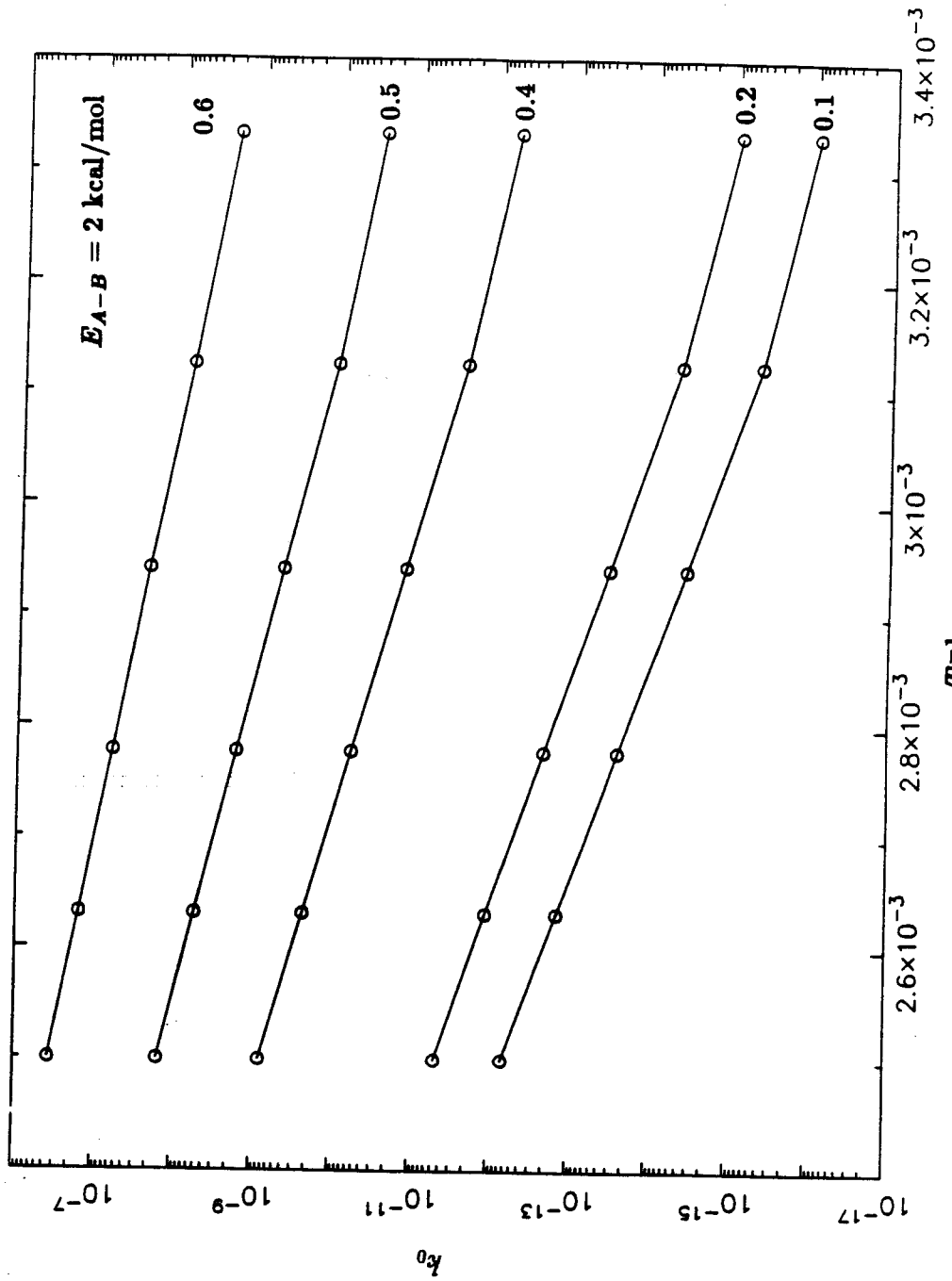
$E_{A-B} = 2$ kcal/mol
0.6
0.5
0.4
0.2
0.1
k_0
10^{-7}
10^{-9}
10^{-11}
10^{-13}
10^{-15}
10^{-17}
2.6×10^{-3}
2.8×10^{-3}
3×10^{-3}
3.2×10^{-3}
3.4×10^{-3}
T^{-1}

Figure 2(c)

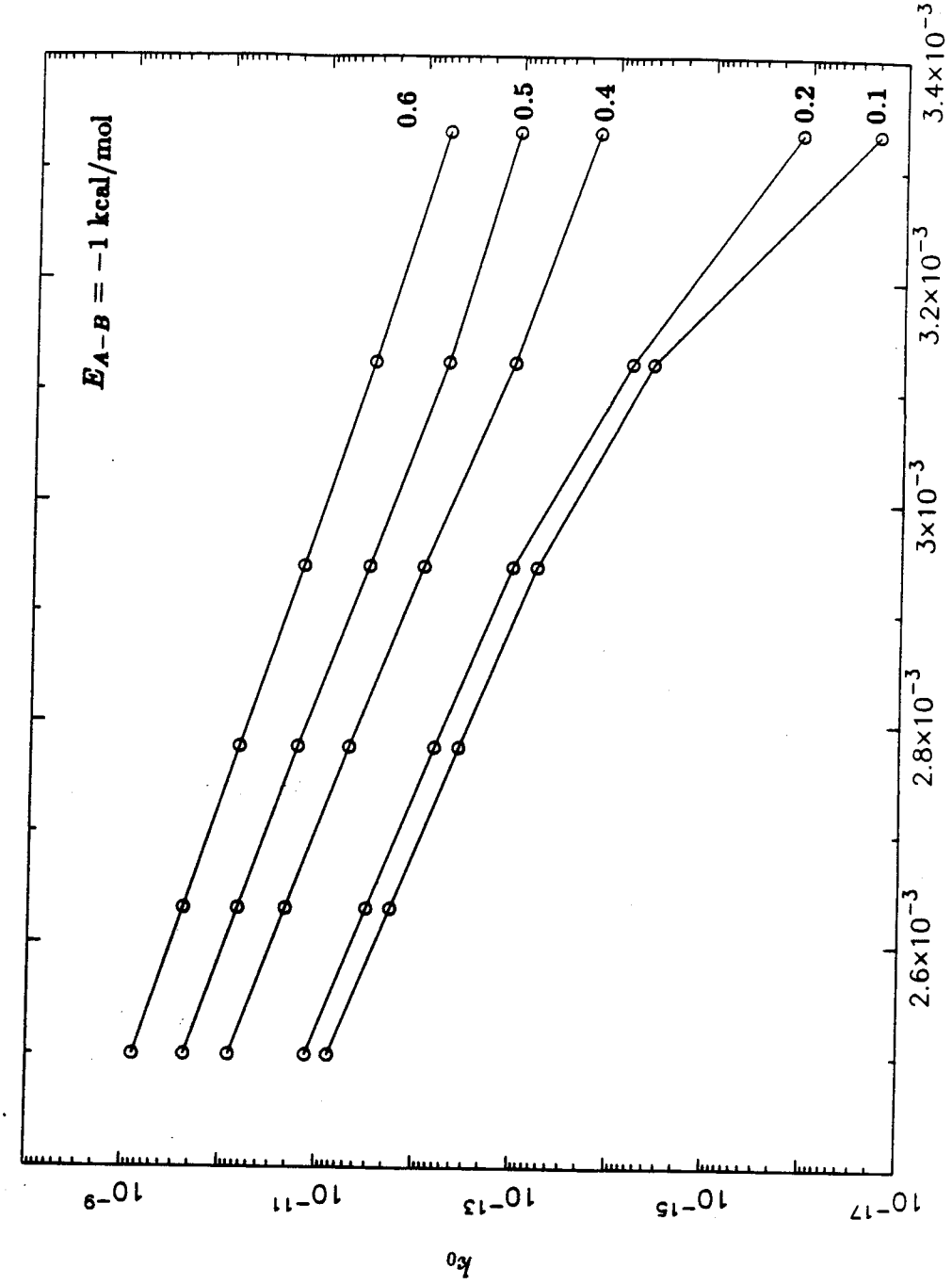
$E_{A-B} = -1$ kcal/mol
0.6
0.5
0.4
0.2
0.1
k_0
10^{-9}
10^{-11}
10^{-13}
10^{-15}
10^{-17}
T^{-1}
2.6×10^{-3}
2.8×10^{-3}
3×10^{-3}
3.2×10^{-3}
3.4×10^{-3}

Figure 2(d)

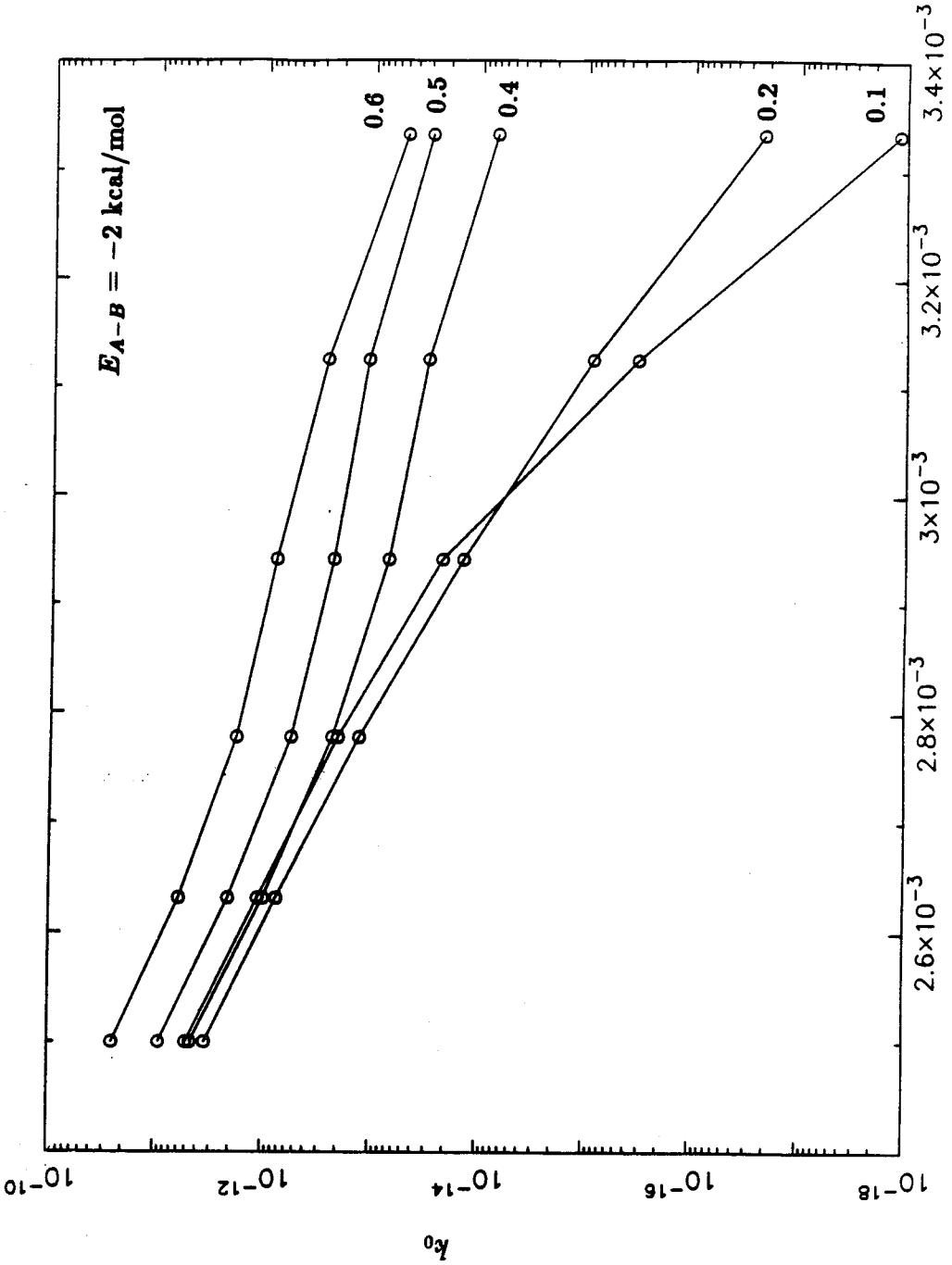
$E_{A-B} = -2$ kcal/mol
0.6
0.5
0.4
0.2
0.1
k_0
10^{-10}
10^{-12}
10^{-14}
10^{-16}
10^{-18}
T^{-1}
2.6×10^{-3}
2.8×10^{-3}
3×10^{-3}
3.2×10^{-3}
3.4×10^{-3}

Figure 2(e)

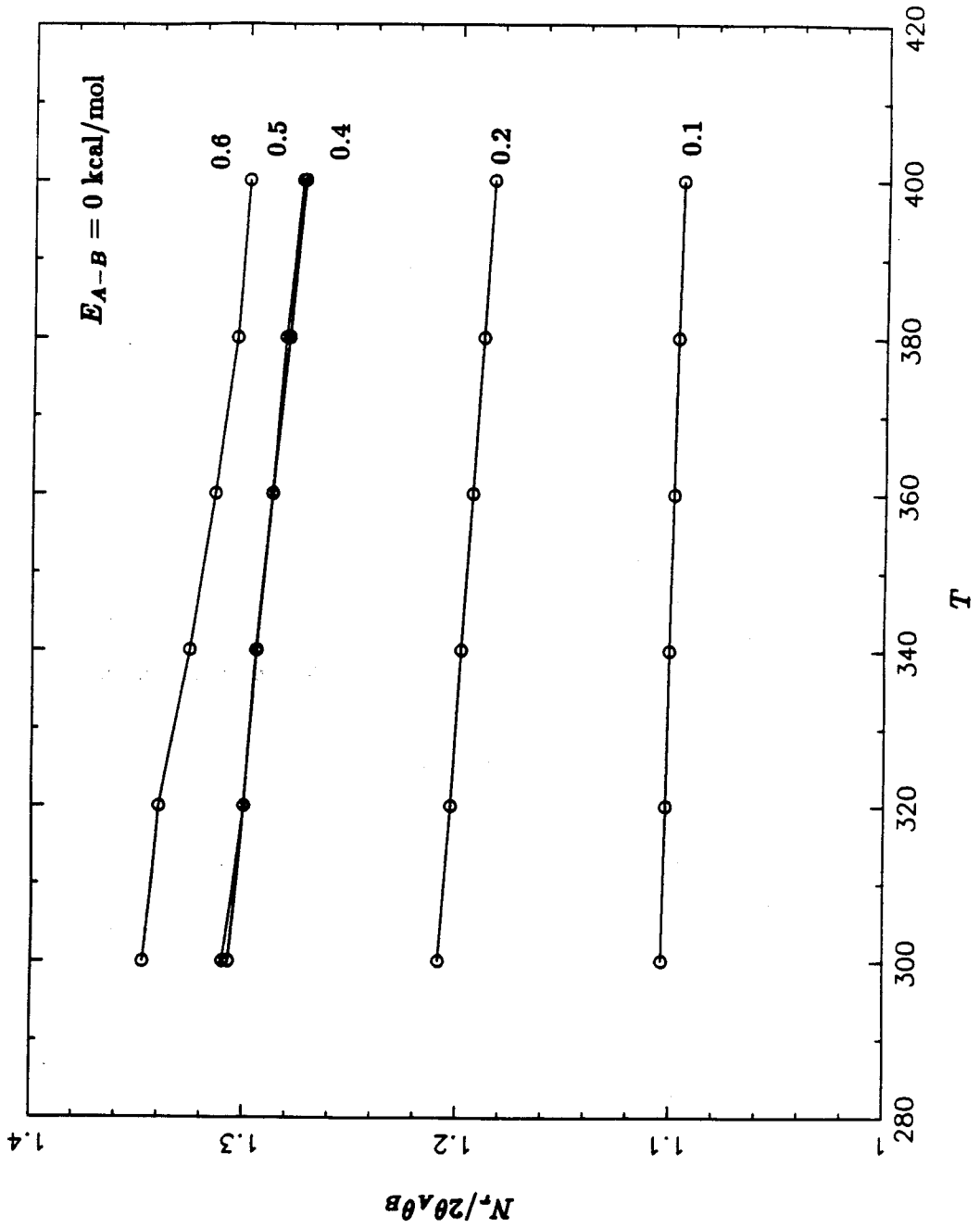
$E_{A-B} = 0$ kcal/mol
0.6
0.5
0.4
0.2
0.1
$N_r/2\theta_A\theta_B$
1.4
1.3
1.2
1.1
1
280
300
320
340
360
380
400
420
T

Figure 3(a)

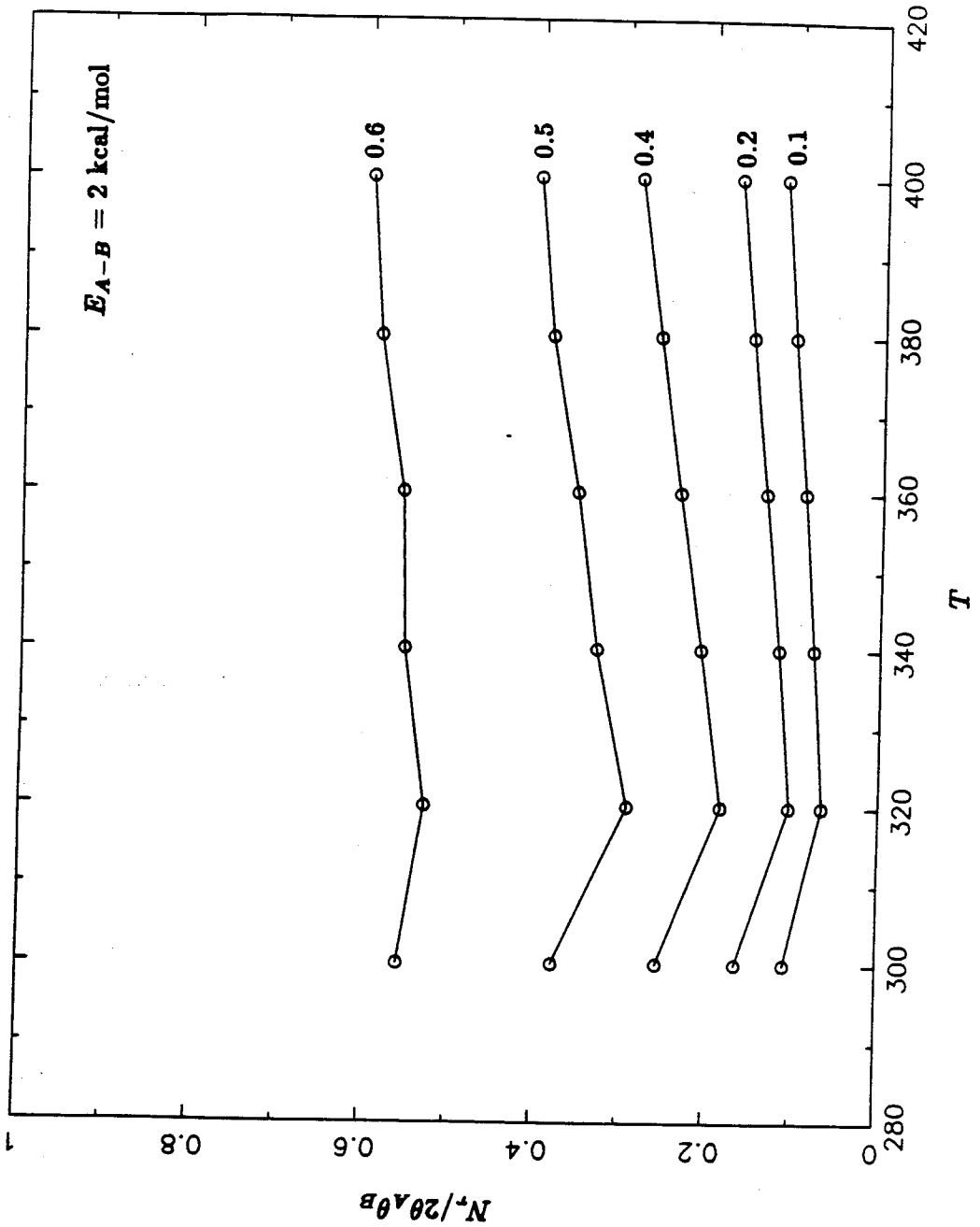
$E_{A-B} = 2$ kcal/mol
0.6
0.5
0.4
0.2
0.1
$N_r/2\theta_A\theta_B$
T
0
0.2
0.4
0.6
0.8
1
280
300
320
340
360
380
400
420

Figure 3(b)

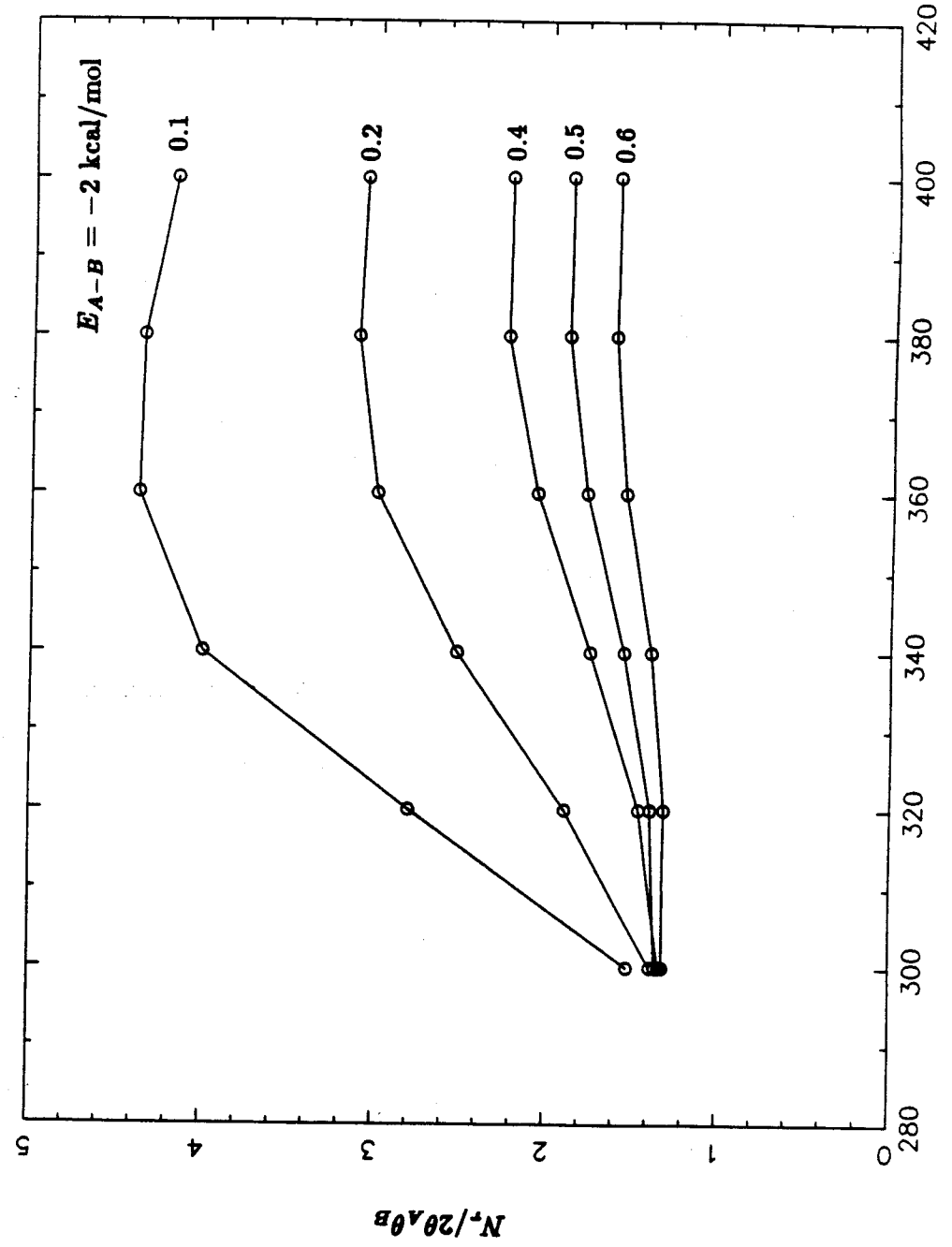
$E_{A-B} = -2$ kcal/mol
0.1
0.2
0.4
0.5
0.6
$N_r/2\theta_A\theta_B$
T
0
1
2
3
4
5
280
300
320
340
360
380
400
420

Figure 3(c)

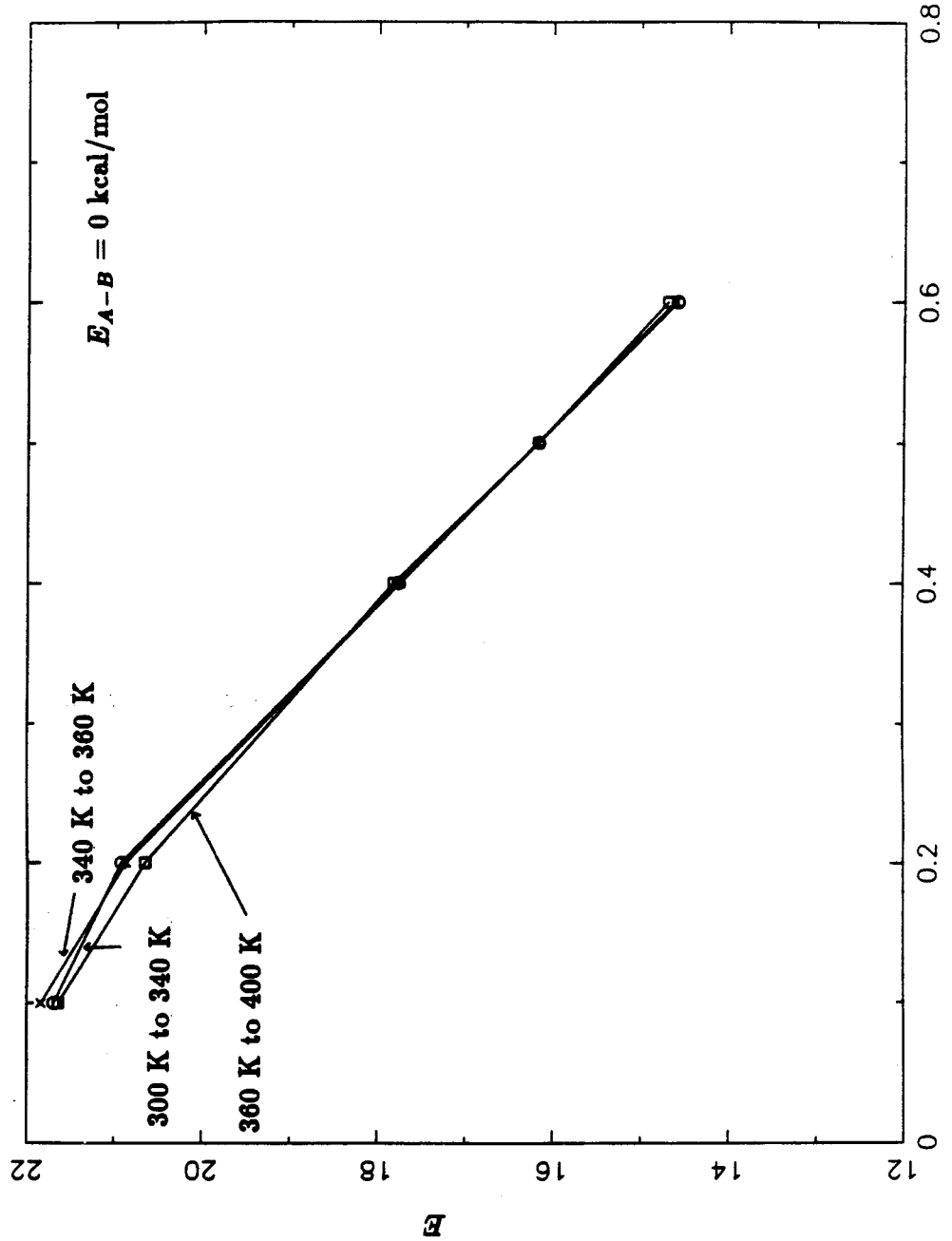
$E_{A-B} = 0$ kcal/mol
340 K to 360 K
300 K to 340 K
360 K to 400 K
E
θ_A
22
20
18
16
14
12
0
0.2
0.4
0.6
0.8

Figure 4(a)

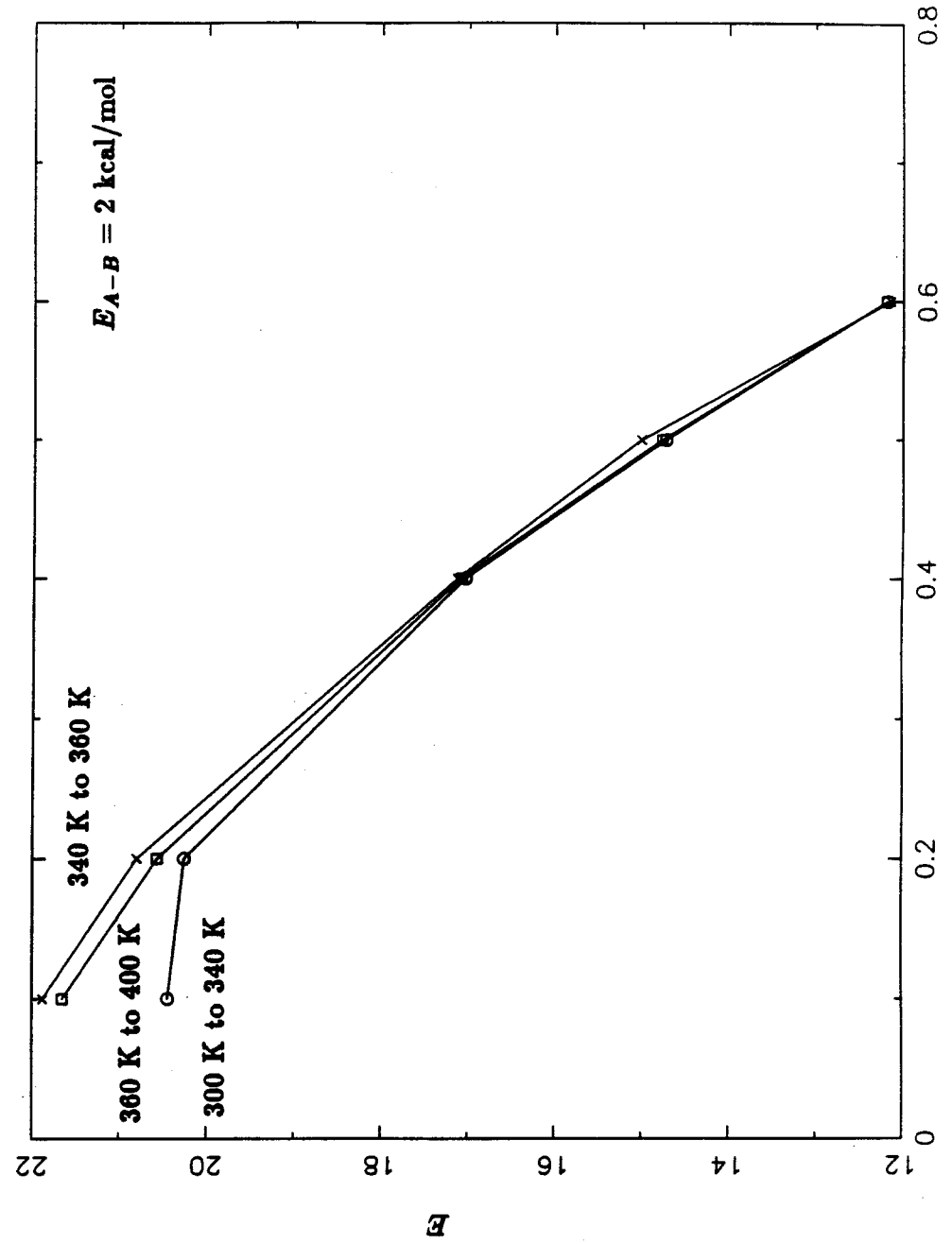
E_{A-B} = 2 kcal/mol
340 K to 360 K
360 K to 400 K
300 K to 340 K
E
θ_A
22
20
18
16
14
12
0
0.2
0.4
0.6
0.8

Figure 4(b)

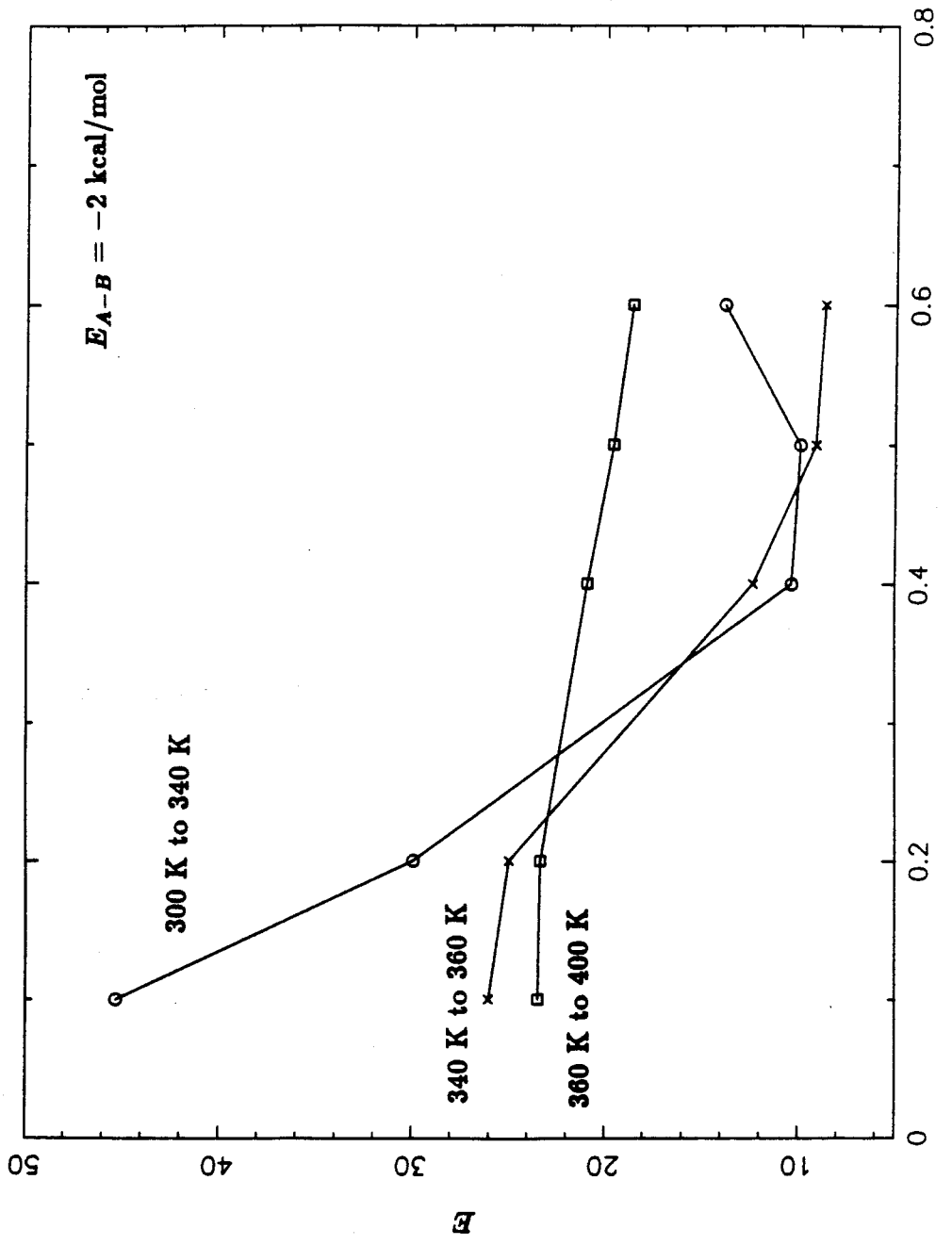
$E_{A-B} = -2$ kcal/mol
300 K to 340 K
340 K to 360 K
360 K to 400 K
E
θ_A
0
0.2
0.4
0.6
0.8
10
20
30
40
50

Figure 4(c)

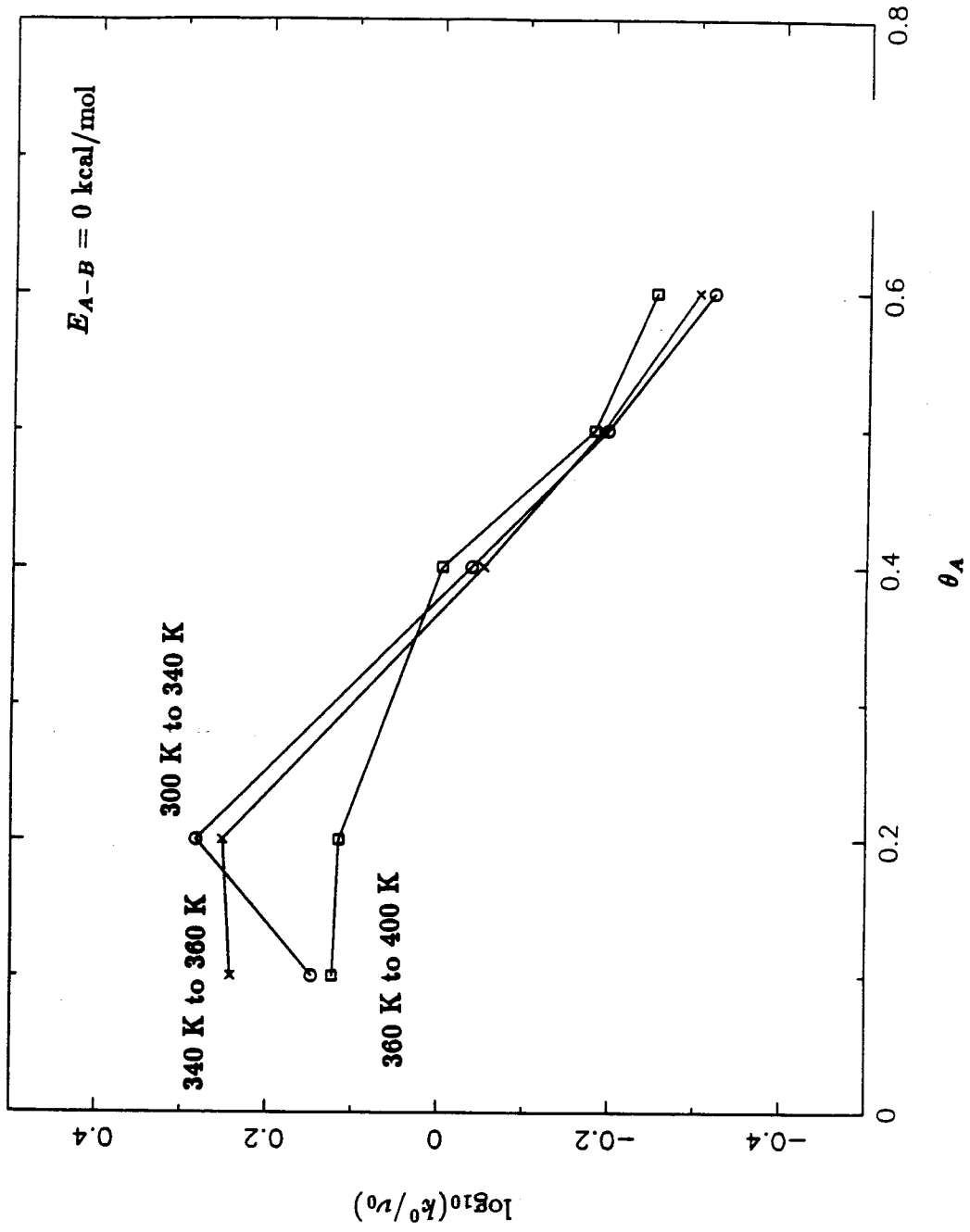
$E_{A-B} = 0$ kcal/mol
300 K to 340 K
340 K to 360 K
360 K to 400 K
$\log_{10}(k^0/\nu_0)$
θ_A
0.4
0.2
0
−0.2
−0.4
0
0.2
0.4
0.6
0.8

Figure 5(a)

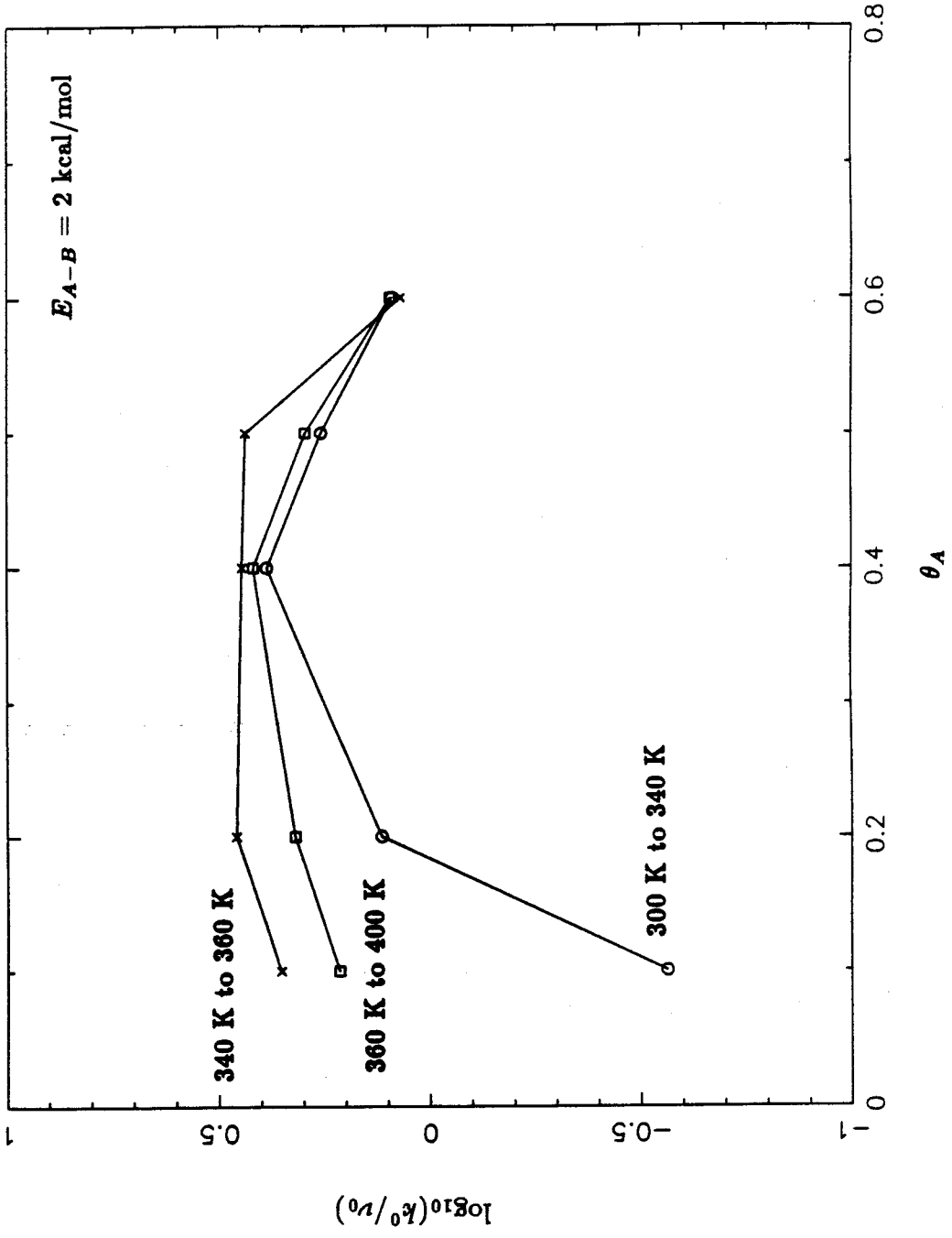
$E_{A-B} = 2$ kcal/mol
340 K to 360 K
360 K to 400 K
300 K to 340 K
$\log_{10}(k^0/\nu_0)$
θ_A
1
0.5
0
−0.5
−1
0
0.2
0.4
0.6
0.8

Figure 5(b)

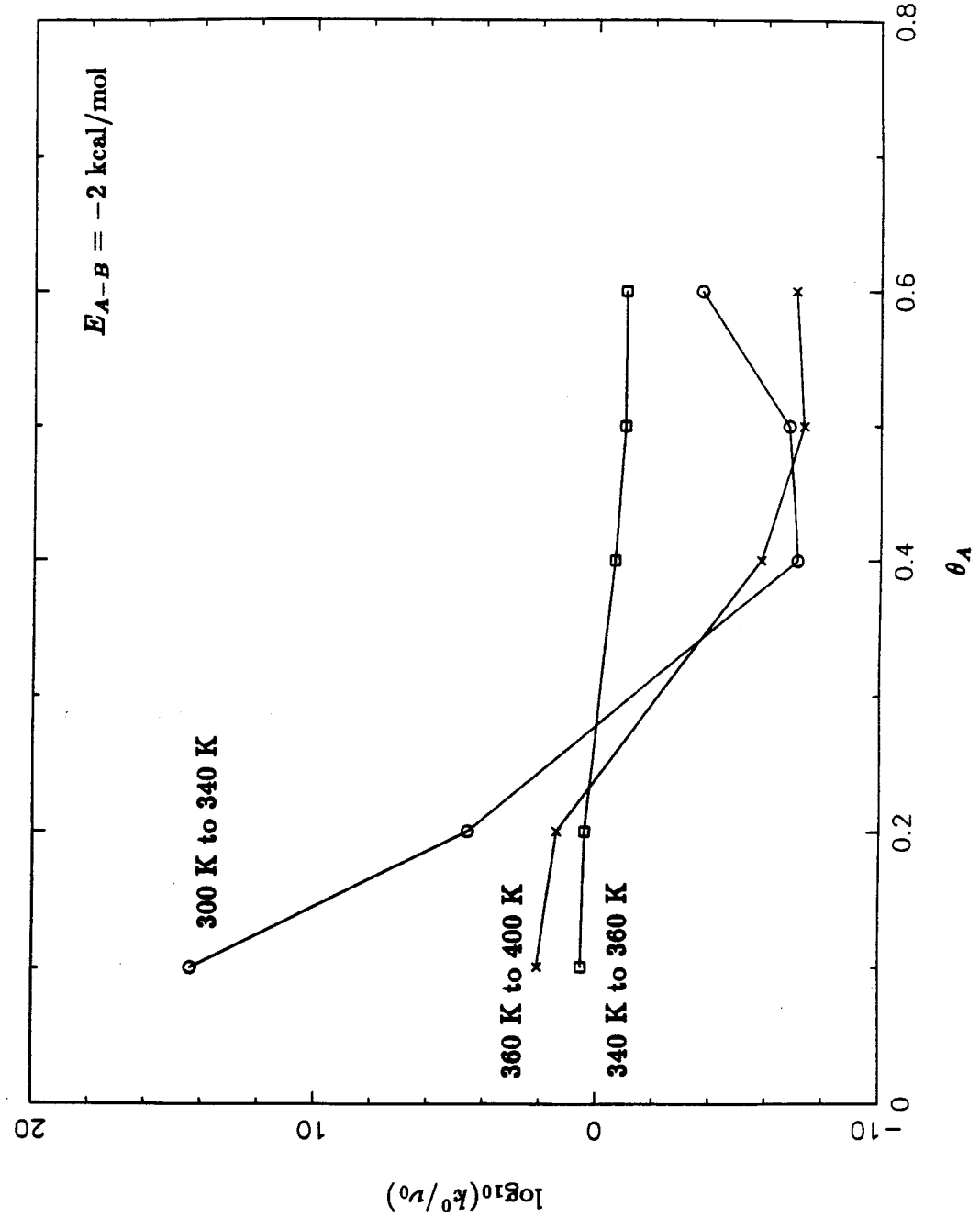
$E_{A-B} = -2$ kcal/mol
300 K to 340 K
360 K to 400 K
340 K to 360 K
$\log_{10}(k^0/\nu_0)$
θ_A
20
10
0
−10
0
0.2
0.4
0.6
0.8

Figure 5(c)

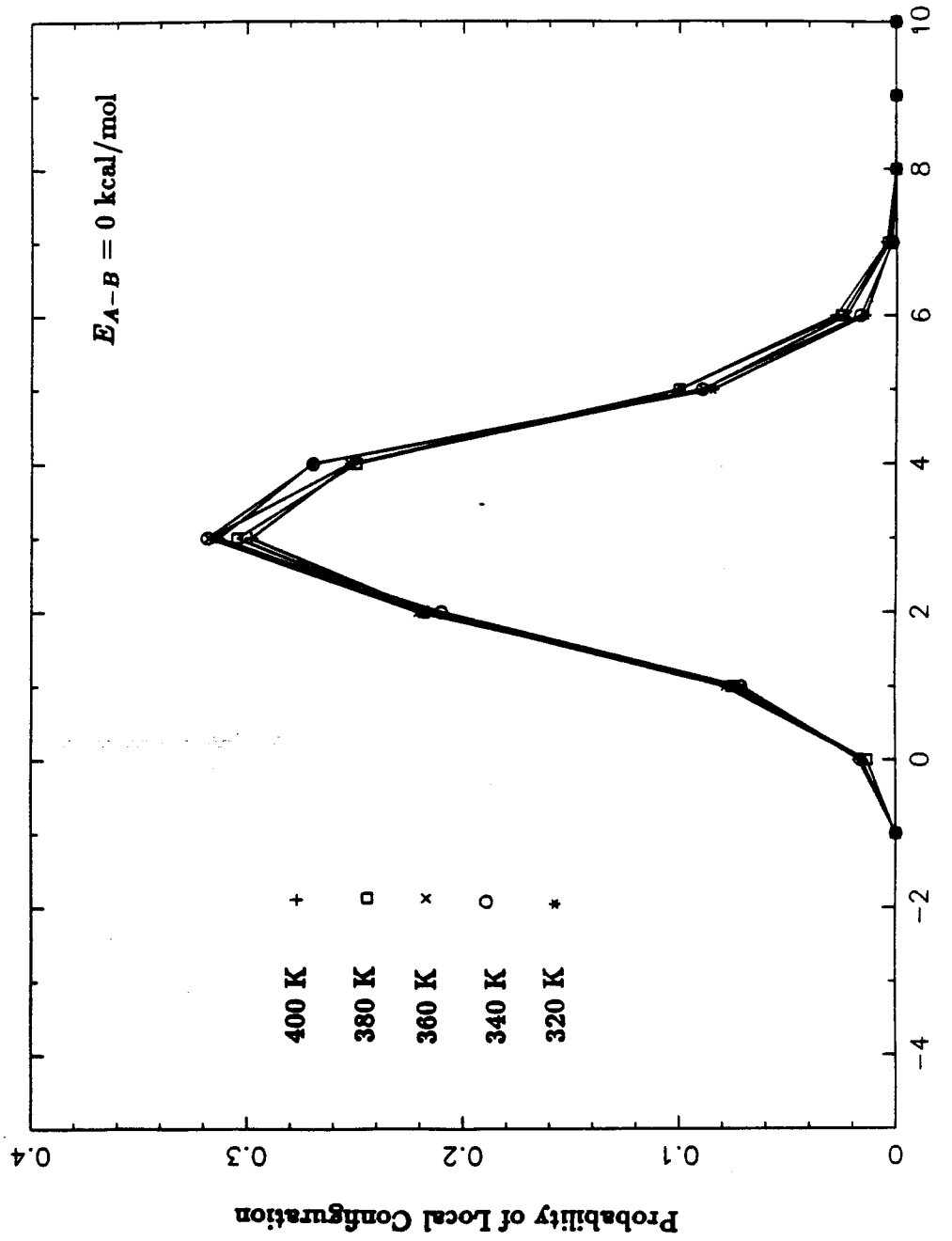
$E_{A-B} = 0$ kcal/mol
400 K
380 K
360 K
340 K
320 K
Probability of Local Configuration
Lateral Interaction Energy
0
0.1
0.2
0.3
0.4
−4
−2
0
2
4
6
8
10

Figure 6(a)

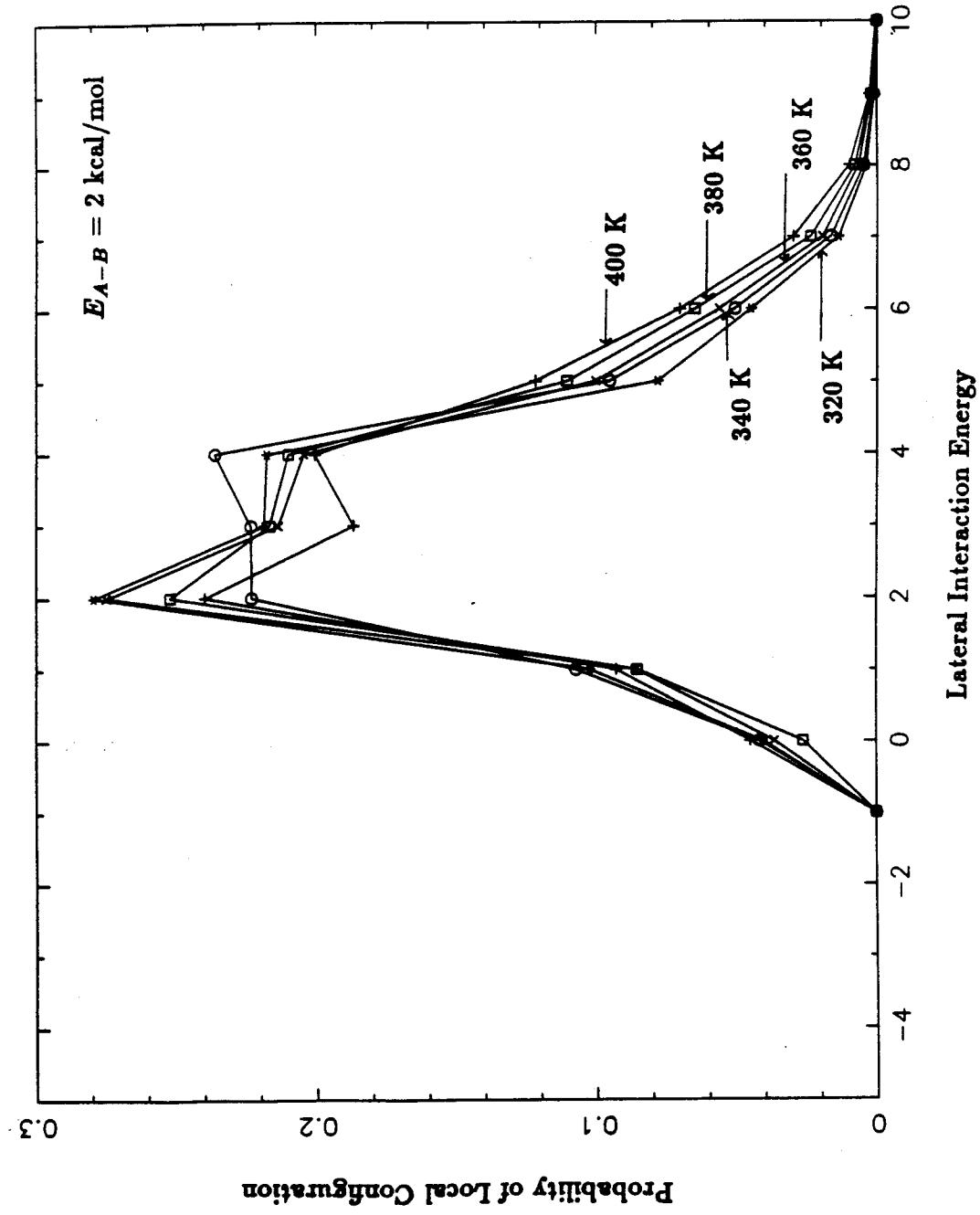
E_{A-B} = 2 kcal/mol
400 K
380 K
360 K
340 K
320 K
Probability of Local Configuration
Lateral Interaction Energy
0
0.1
0.2
0.3
−4
−2
0
2
4
6
8
10

Figure 6(b)

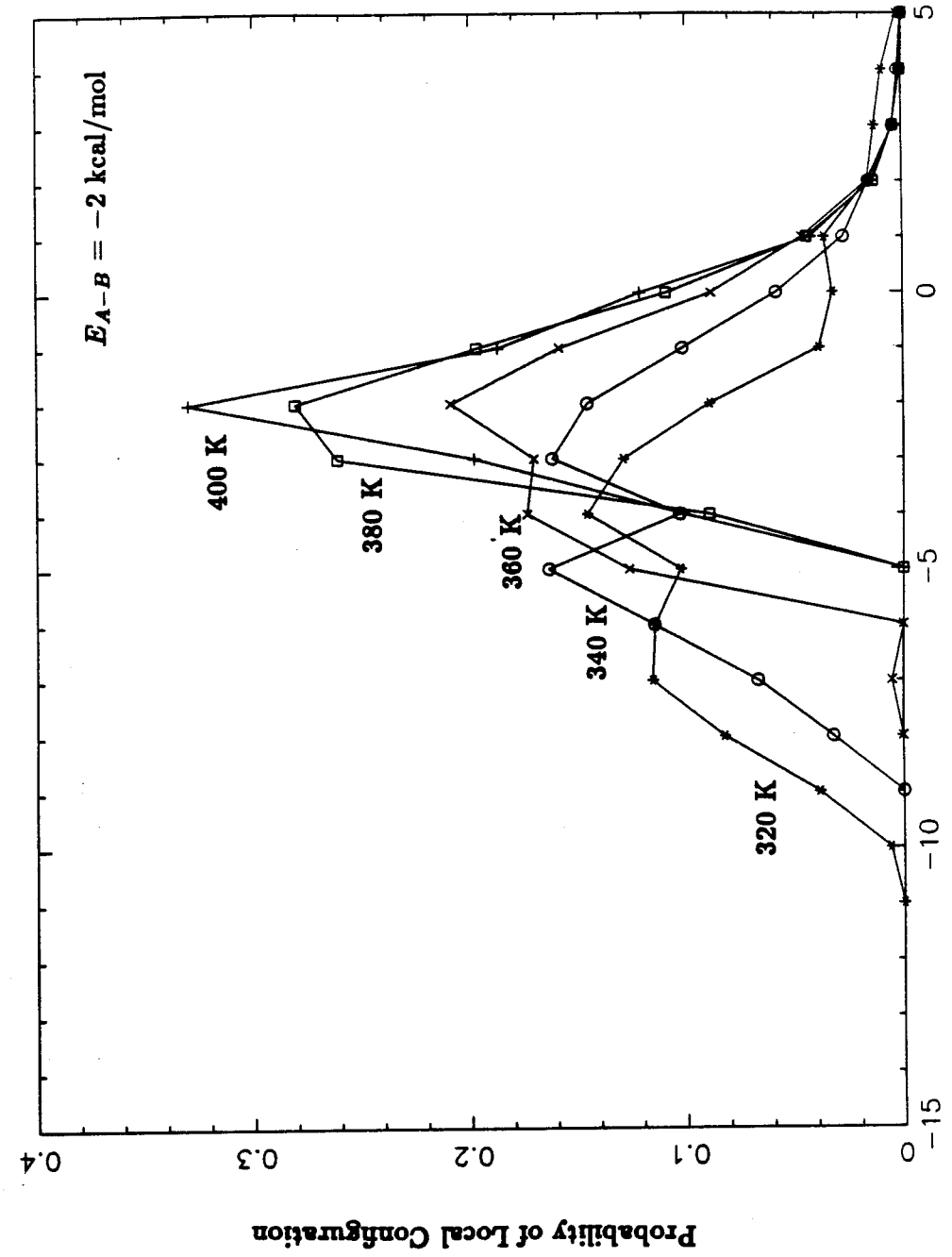
$E_{A-B} = -2$ kcal/mol
400 K
380 K
360 K
340 K
320 K
Probability of Local Configuration
Lateral Interaction Energy
0.4
0.3
0.2
0.1
0
5
0
−5
−10
−15

Figure 6(c)

Figure 7

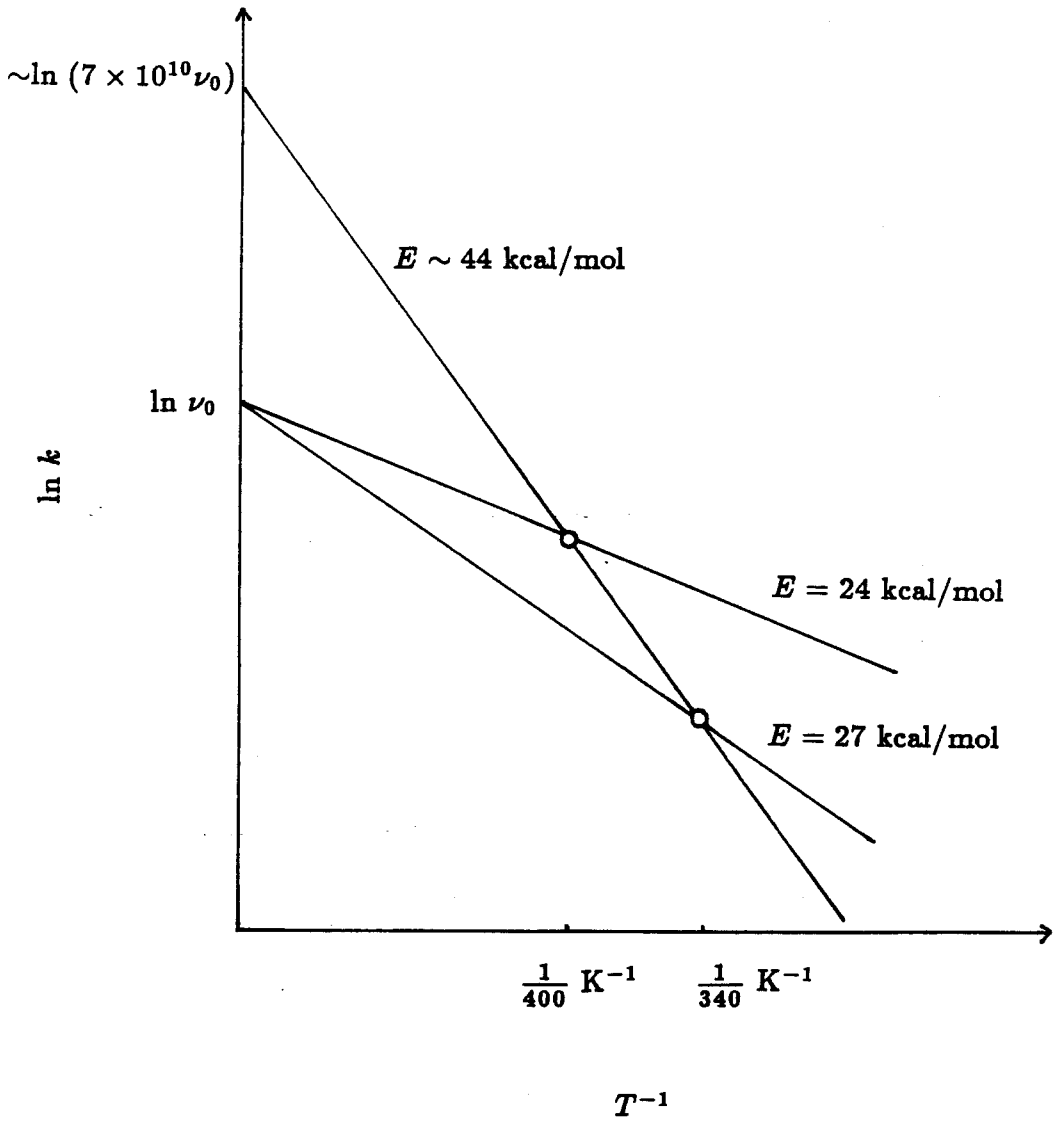
$\sim\ln (7 \times 10^{10}\nu_0)$
$E \sim 44$ kcal/mol
$\ln \nu_0$
$\ln k$
$E = 24$ kcal/mol
$E = 27$ kcal/mol
$\frac{1}{400}$ K^{-1}
$\frac{1}{340}$ K^{-1}
T^{-1}

Figure 8

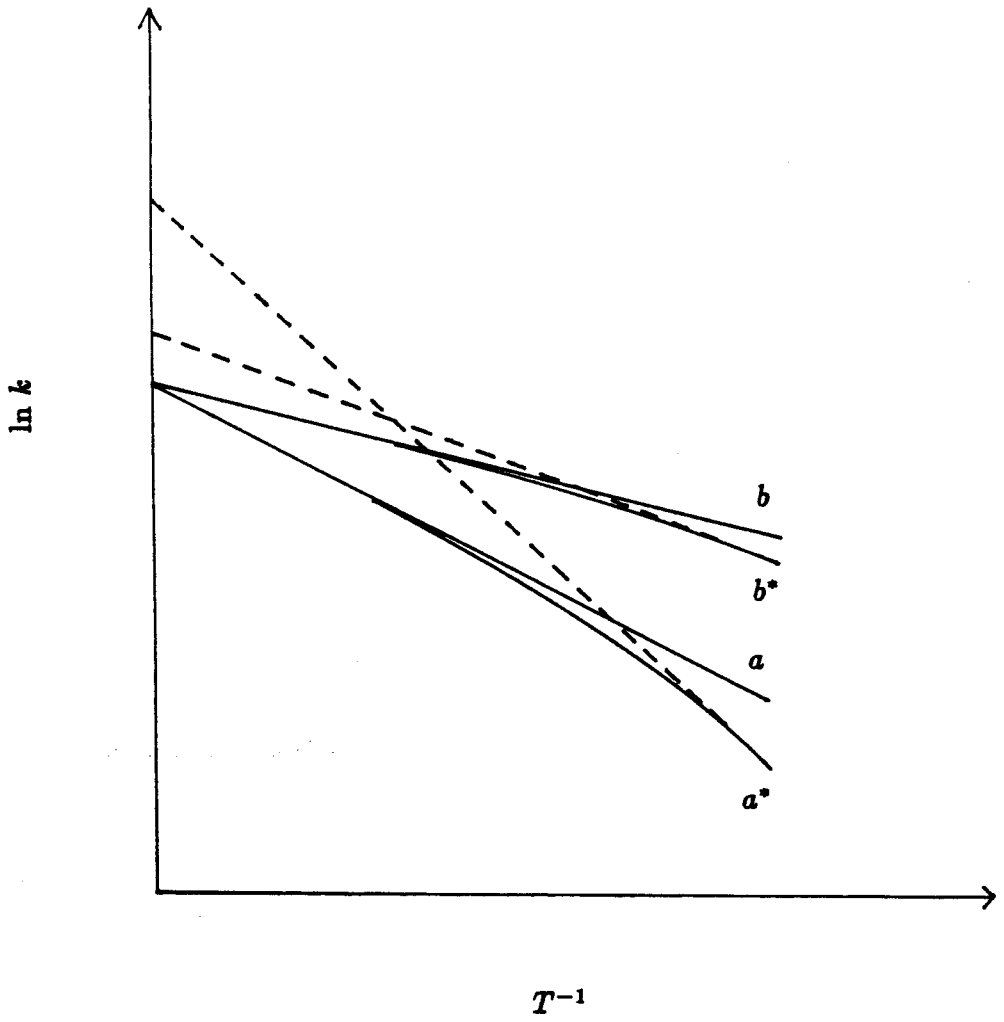

Chapter 7.

Reactant Segregation in a Langmuir-Hinshelwood Surface Reaction.

This chapter has been submitted as a paper by H.C. Kang, M.W. Deem and W.H. Weinberg, to *The Journal of Chemical Physics.*

ABSTRACT

We have performed Monte-Carlo simulations of a Langmuir-Hinshelwood reaction between two species A and B adsorbed on a square lattice. Adsorption of each species occurs when a gas-phase molecule, either A or B, impinges upon a vacant lattice site. The probability that a molecule impinges upon and adsorbs successfully into a vacant lattice site per unit time is $p_a/2$ for both species. Desorption is not allowed and the surface reaction is allowed to occur only between nearest-neighbor AB pairs. For each nearest-neighbor AB pair, the probability of reaction per unit time is p_r. Particles of both species are allowed to migrate by hopping to vacant nearest-neighbor sites, where the probability of a hop per unit time is p_m. In all these simulations we have set p_m to be unity, and varied p_r from 0.01 to unity. We have also set $p_a = p_r/5$ for all the simulations in order to maintain moderately low fractional surface coverages. 'Islanding' of each type of particle occurs even for the lowest value of p_r. For the range of values of p_r used, the 'islands' grow to a finite steady-state size. We also found that the 'islands' that are formed are not fractal. It is possible to define quantities describing the process of 'islanding' which are analogous to the order parameter and the temperature in thermal phase transitions. We find that the exponent for the order parameter in this model is a mean-field exponent.

1. Introduction

Recently, there has been considerable interest in Monte-Carlo simulations of surface reactions **(1-14)**. The essential difference between Monte-Carlo simulations and the more traditional statistical or kinetic **(15-21)** approaches to studying surface reactions is that in Monte-Carlo simulations the exact microscopic configurations of the reacting particles on the surface are used, whereas in the earlier approaches this information is integrated over and approximated by macroscopic averages of, for instance, the number of nearest-neighbor reactive pairs. The quasichemical approximation has also been used to calculate the rates of reaction and desorption of interacting lattice gases **(22-26)**. In such calculations an approximation is made in order to account for nearest-neighbor pair correlations. Clearly, when the adsorbate particle density is not homogeneous, i.e. when there is 'islanding,' the microscopic configurations will be important in determining the rates of reactions occurring on the surface. One of the reasons for the formation of 'islands' or ordered superlattice structures in the adsorbed layer is the existence of lateral interactions, either through the substrate or directly between the adsorbed particles. When this occurs, thermally driven order-disorder phenomena can occur also, and the configuration of the overlayer is strongly dependent upon the temperature and the fractional surface coverage of the adsorbed particles. However, even when there are no lateral interactions between the adsorbed particles, the configurations of the adsorbed particles can be quite different from the spatially random occupation of sites that might have then been expected. Such spatial inhomogeneities can result from kinetic phase transitions **(27,28)** and, in the context of surface chemical reactions, have been investigated recently by both Monte-Carlo simulations **(29-33)** and mean-field methods **(34)**.

One surface chemical system which has been investigated is the following

Langmuir-Hinshelwood reaction scheme:

$$A(g) + V \rightarrow A(a), \tag{1}$$

$$B_2(g) + 2V \rightarrow 2B(a), \tag{2}$$

and

$$A(a) + B(a) \rightarrow AB(g), \tag{3}$$

where (g) denotes gas-phase particles, and (a) denotes adsorbed particles. Vacant sites on the surface are denoted by V. In the limiting case of infinitely fast reaction with zero desorption and diffusion, this reaction system has been studied by Monte-Carlo simulations **(29)** and mean-field approximations **(34)**. The key parameter under these conditions is the rate of adsorption y_A of $A(g)$ relative to the rate of adsorption $(1 - y_A)$ of $B_2(g)$. The Monte-Carlo simulations found that reactive steady states are stable only in the range $0.389 < y_A < 0.525$ **(29)**. When y_A is less than approximately 0.389, the surface poisons with B, the poisoning being a second-order transition. On the other hand, when y_A is greater than approximately 0.525, the surface poisons with A, the poisoning in this case being a first-order transition. The mean-field calculations, at the level of site and pair-approximations, accurately reproduce the position of the first-order transition. Although the second-order transition is not described so well, higher level approximations would probably be satisfactory **(34)**. The nature of poisoning in this system has recently been studied under conditions where desorption is allowed, and these results will be reported elsewhere **(35)**.

Another Langmuir-Hinshelwood reaction system which has been investigated using Monte-Carlo simulations **(31-33)** is the following:

$$A(g) + V \rightarrow A(a), \tag{1}$$

$$B(g) + V \rightarrow B(a), \tag{4}$$

and

$$A(a) + B(a) \rightarrow AB(g). \tag{3}$$

It has been shown that a reactive state is stable only when y_A is 0.5 **(32,33)**. Even in this reactive state, with infinitely fast reaction and no desorption, the 'islands' of A and B never reach a finite steady-state size, i.e. these 'islands' grow indefinitely with time. Monte-Carlo simulations performed on a (1000x1000) lattice showed that after 6000 Monte-Carlo steps per site the 'islands' of A and B, although compact in the core, have a boundary that is not compact **(32)**. A fractal dimension of approximately 1.8 was reported, and it was suggested that the 'islands' do not have a dimension of two because of the cascade of length scales that result from clusters of all sizes connecting to form a large 'island.' This Langmuir-Hinshelwood system has also been simulated with infinitely fast reaction and non-zero desorption with Monte-Carlo techniques on lattices of size (32x32) **(31)**. It was found that for sufficiently high desorption rates the stable surface configuration is one in which the fractional coverages of A and B are equal. Presumably, the sizes of the 'islands,' if they are formed at all, are not large. However, for sufficiently low desorption rates, the stable configuration on the surface is one in which there is a preponderance of either A or B.

The 'islanding' that occurs in the Langmuir-Hinshelwood systems described above are the result of kinetic phase transitions. In order to observe such spatial inhomogeneities in the fractional surface coverage, it is necessary that there be fluctuations which allow the system to 'probe' its neighborhood in configurational space. The source of the fluctuations in these simulations is the stochastic nature of the adsorption and reaction events. In analogy to thermal phase transitions in Ising systems, reaction corresponds to a ferromagnetic interaction since it is the surface chemical reaction that removes unlike nearest-neighbor particle pairs from the lattice and favors the 'islanding' of like particles. This increases the degree of order in the system. In this paper we attempt to include a source of disorder in the

description of the system. This is accomplished by allowing the particles to diffuse on the surface. A competition occurs between reaction which leads to ordering and diffusion which leads to the decay of spatial inhomogeneities. A higher ratio of the rate of reaction to the rate of diffusion would be expected to lead to a greater degree of order. We study the influence of this competition on the surface chemical reaction rate.

2. Algorithm and Finite Size Effects

The surface is modeled by square lattices of sizes ranging from (50x50) to (300x300). Periodic boundary conditions are used, and we always begin with a completely vacant lattice. The simulations take into account adsorption, reaction and diffusion. Two types of molecules, A and B, are present in the gas phase, and each type of molecule is adsorbed onto a single lattice site with a probability of $p_a/2$ in each Monte-Carlo step. Only nearest-neighbor pairs of AB can react, and the probability of reaction is p_r in each Monte-Carlo step. Both types of particles can migrate on the surface by hopping from one lattice site to a vacant nearest-neighbor lattice site. The probability of migration is p_m in each Monte-Carlo step. The simulations are performed as follows. First, a site is picked at random. If the site is occupied, then one of its four nearest-neighbor sites is picked at random. If the nearest-neighbor site is vacant, then the particle in the site picked first hops into this nearest-neighbor site with a probability of p_m. If the nearest-neighbor site is occupied with a particle of type different from that occupying the site picked first, then reaction occurs with a probability of p_r. If the two particles are of the same type, the configuration is not altered and the procedure is repeated from the beginning. If the site picked first is vacant, then a particle of type A is adsorbed there with a probability $p_a/2$ and, similarly, a particle of type B is adsorbed there with a probability of $p_a/2$. In the results presented here, time is in units of Monte-Carlo steps/site, one Monte-Carlo step/site being LxL iterations of

the above procedure, where (LxL) is the size of the lattice used.

Desorption is not allowed in this model. Hence, any finite-sized lattice that becomes completely occupied by particles of either type A or type B will be poisoned irreversibly. This, however, need not be the case for a finite-sized *sublattice* embedded in an infinite lattice. Simulations have been performed on (LxL) lattices with periodic boundary conditions in order to study the behavior of (LxL) sublattices embedded in an infinitely large lattice. In order to ensure that the simulations are performed on sufficiently large lattices that this goal is realized, it is necessary to check for finite-size effects. In particular, we examine the effects arising from the poisoning of a finite-sized lattice. Consider the process of adsorption. Since a particle of either type A or type B is chosen with equal probability, the difference $n_A - n_B$ between the number of type A particles adsorbed n_A and the number of type B particles adsorbed n_B can be treated as a random walk. The total number of adsorption events n_T plays the role of time in this case. Since the simulations always start with completely vacant lattices and each reaction involves one A and one B particle, we obtain $N_A - N_B = n_A - n_B$, where N_A and N_B are the numbers of particles of type A and type B, respectively, on the lattice at any particular time. For an infinitely large lattice which is initially vacant, the probability of occurrence of a configuration in which $N_A - N_B = \delta N$ after n_T adsorption events is given by

$$P(\delta N, n_T) = (1/2\pi n_T)^{1/2} \exp[-(\delta N)^2/2n_T]. \tag{5}$$

However, for an (LxL) lattice, where L is finite, irreversible poisoning of the entire lattice implies that the random walk is performed in a domain with perfectly absorbing walls situated at $\delta N = \pm \mathrm{L}^2 = \pm z$. This is described by

$$P(\delta N, n_T) = z^{-1} \sum_{\nu=1}^{\infty} \exp(-\nu^2 \pi^2 n_T/8z^2) \cos(\nu \pi \delta N/2z), \tag{6}$$

where the sum is over odd integers ν.

By comparing these two expressions for $P(\delta N, n_T)$, the effects of the finite size of the lattices can be assessed. We plot these equations in Fig. 1, where in each plot the abscissa is $(N_A - N_B)/\mathrm{L}^2$ and the ordinate is the probability of occurrence of such a state. The size of the finite lattice is $\mathrm{L}^2 = z$, and the total number of adsorption events n_T is indicated for each plot. We begin to observe finite size effects, i.e. deviations between the two equations, for lattices of size smaller than approximately (100x100). The values of n_T used in calculating the curves in Fig. 1 are 4000 L^2. In all our simulations, the runs are allowed to reach 4000 Monte-Carlo steps/site; hence in the simulations the number of adsorption events is smaller than that used in obtaining the results of Fig. 1. Consequently, the effect of the finite size of the lattice is even less pronounced in the simulations that are presented in the next section.

3. Results and Discussion

A. Definitions and Lattice Size Effects

In the limit of infinitely fast diffusion and an infinitely large lattice, the steady-state fractional surface coverages are given by $\theta_A = \theta_B = \theta$ and $4p_r\theta^2 = p_a(1-2\theta)$. In the simulations that we performed, p_a was set equal to $p_r/5$. With this choice, the fractional surface coverages in the limit when p_m is infinitely larger than p_r are $\theta_A = \theta_B \simeq 0.179$. This ratio of p_r/p_a is chosen so that a moderately low coverage is obtained in the limit of infinitely fast diffusion. If a higher probability of adsorption were chosen, the possible formation of percolating 'islands' when the ratio p_r/p_m is increased would have to be considered **(32)**. In the limit of infinitely fast diffusion, the particles on the surface are 'well-mixed' and the rate of reaction for each site is $4p_r\theta_A\theta_B$ per Monte-Carlo step/site. When $p_r/p_m \to \infty$, on the other hand, the configurations of particles on the surface are not homogeneous. 'Islands' consisting of each kind of particle form and grow indefinitely, i.e. any finite

region of an infinitely large surface will ultimately become poisoned by particles of either type A or type B **(32)**. In order to quantify the behavior of this system between the limits of $p_r/p_m = 0$ and $p_r/p_m \rightarrow \infty$, we define an *order parameter* ϕ, where $\phi \equiv (N_{AA} + N_{BB} - N_{AB})/(N_{AA} + N_{BB} + N_{AB})$. The quantity N_{XY} is the number of nearest-neighbor pairs of particles of type XY. The value of ϕ is zero when the particles occupy sites selected at random and tends to unity when 'islands' of each type of particle become infinitely large. The order parameter that we have defined can be regarded as a "chemical" analogue of the magnitude of the magnetization of a ferromagnetic solid. In addition to monitoring ϕ and hence the degree of order of the lattice-gas configuration, it is also of practical interest to study the dependence of the reaction rate on the value of p_r/p_m. We define a quantity $l \equiv (N_{AA} + N_{BB})/(N_{AB} + N_{AV} + N_{BV})$, where V denotes a vacant site. This quantity is the ratio of unreactive occupied nearest-neighbor pairs to potentially reactive nearest-neighbor pairs. If the 'islands' that are formed have a dimension of two, then l is the ratio of the total area occupied by the 'islands' to the total length of the boundaries of the 'islands.' Hence l would be proportional to the length scale of the 'islands' in the configuration. As mentioned above, when the rate of migration of the particles is infinitely larger than the rate of reaction (and adsorption), the surface configuration is 'well-mixed.' When this is the case, $N_{AA} = 2\mathrm{L}^2\theta_A^2$, $N_{BB} = 2\mathrm{L}^2\theta_B^2$ and $N_{AB} = 4\mathrm{L}^2\theta_A\theta_B$; and, as discussed earlier, $\theta_A = \theta_B \simeq 0.179$ when $p_r/p_a = 5$. Thus, in the limit of $p_r/p_m = 0$, the order parameter ϕ is zero and the quantity l is approximately 0.1225. Hence, for $p_r/p_a = 5$ the value of l would range between 0.1225 and infinity, the latter limit being reached when $p_r/p_m \rightarrow \infty$ and the 'islands' grow indefinitely large.

We performed simulations in which p_m was set equal to unity and p_r/p_m was varied from 0.01 to unity. Unless otherwise stated, the simulations were performed on lattices of size (200x200). For the case in which $p_r/p_m = 1$, we performed simulations on lattices of size (50x50), (100x100), (200x200) and (300x300). The

values of l as a function of time in Monte-Carlo steps/site for each of these lattice sizes are plotted in Fig. 2. Each of the curves in Fig. 2 is the average of the results from ten simulation runs. On a lattice which is sufficiently large that the 'islands' are not affected by its finiteness and by the consequent irreversible poisoning that a finite lattice can undergo, the value of l would be smaller than on a lattice in which this latter phenomenon affects the simulations. Therefore, when the lattice size used in the simulations is too small, we can expect the observed value of l to be too high, i.e. a smaller lattice is more likely to poison completely than a larger lattice. As may be seen in Fig. 2 finite-size effects begin to be apparent for lattices of size (100x100). The finite-size effect for the (50x50) lattice is very clearly observed. This observation of finite-size effects for lattices of sizes (50x50) and (100x100) is consistent with the simple analysis discussed in the previous section. Typical configurations from these simulations are shown in Figs. 3(a-d). Each empty square denotes a particle of type A and each filled square denotes a particle of type B. Blank regions are vacant sites. For the simulation runs from which these configurations were obtained, the average fractional surface coverages of A and B are shown in the corresponding figure. These average coverages were obtained by averaging the coverages at every tenth Monte-Carlo step/site between 2000 Monte-Carlo steps/site and 4000 Monte-Carlo steps/site for each simulation run. It can be seen in Figs. 3(c) and 3(d) that the length scale of the inhomogeneity in the fractional surface coverage is certainly larger than 50 lattice units. This is an indication that lattices of size (50x50) are not sufficiently large. The average surface coverages of A and B are seen to be quite different from each other. Indeed the particular run from which the configuration in Fig. 3(a) is obtained is slowly being poisoned by particles of type B. These observations apply to a lesser extent to the lattices of size (100x100). The results presented in Fig. 2 and a visual inspection of Fig. 3 indicate that lattices of size (200x200) are sufficiently large that finite-size effects are avoided in simulations for which $p_r/p_m = 1$. In the simulations that we

performed, p_r/p_m was varied between 0.01 and unity. Since the length scale of the spatial inhomogeneities of the fractional surface coverage increases with increasing values of p_r/p_m, (200x200) lattices, which do not show significant finite size effects in simulations for which $p_r/p_m = 1$, are sufficiently large for the simulations at the other, smaller values of p_r/p_m.

B. 'Islanding' and Reactivity

Typical configurations for five different values of p_r/p_m are shown in Figs. 4(a-e). As in Figs. 3(a-d) an empty square denotes a particle of type A and a filled square denotes a particle of type B. Blank vacant regions are vacant sites. The values of p_r and p_m are shown for each of these configurations. We also show the average coverage for the particular simulation runs from which the configurations were obtained. These averages, as in Figs. 3(a-d), were obtained by averaging the coverages at every tenth Monte-Carlo step/site between 2000 Monte-Carlo steps/site and 4000 Monte-Carlo steps/site. The configurations shown in Figs. 4(a-e) were obtained at a time of 4000 Monte-Carlo steps/site after starting the runs. The initial configuration for all these simulations is a completely vacant lattice. These configurations provide a qualitative picture of the increase in length scale of the inhomogeneities in the fractional surface coverage at constant $p_m = 1$ when p_r is increased from 0.01 in Fig. 4(e) to unity in Fig. 4(a). The distribution of particles on the lattice in Fig. 4(e) is uniform, at least upon mere visual inspection, whereas the distribution in Fig. 4(a) is clearly not uniform. If we had set p_r/p_a to be larger than 1/5, the 'islands' would have been more apparent visually. However, we did not do this in order to avoid possible percolation of the 'islands.' Even if this did not occur, 'island' sizes larger than those obtained in the results presented here would require larger lattice sizes in order to avoid finite-size effects. Hence, consideration of such effects would be neccesary if simulations with larger values p_r/p_a are attempted. The time dependence of the quantity l for each of these simulations

is shown in Fig. 5, where each plot is labeled with its corresponding value of p_r/p_m. The value of l for $p_r/p_m = 0$ is $l_0 \simeq 0.1225$. Each curve in Fig. 5 is the average of l for ten simulation runs on (200x200) lattices. As would be expected, increasing p_r/p_m increases the length scale of the 'islands.' When $p_r = 1$ and $p_m = 0$, only reaction and adsorption can occur. As a result, the 'islands' increase in size indefinitely. In the limit of infinitely fast diffusion, there can be no spatial inhomogeneity in the surface coverage, and, hence, no 'islands' can be formed. Our simulations investigate the change in this behavior when p_r/p_m is increased slightly from zero. In particular, it is not clear whether the transition from no 'islanding' to 'islanding' occurs at $p_r/p_m = 0$ or at some finite value of p_r/p_m. Although it cannot be seen from an inspection of the configuration in Fig. 4(a), it is clear from Fig. 5 that even at $p_r/p_m = 0.01$ the configuration is not totally random since the value of l is larger than l_0. This indicates that it is more probable, albeit only slightly, to find nearest-neighbor particles of the same type in the configuration in Fig. 4(a) than in a configuration in which the particles are distributed randomly on the surface. Thus, the transition from a random distribution to 'islanding' probably occurs at $p_r/p_m = 0$. Even when the probability of a particle hopping from one site to a nearest-neighbor vacant site is one hundred times larger than the probability of reaction of a nearest-neighbor pair, the configuration on a catalyst surface may not be completely random, and some correction has to be made to macroscopic kinetic equations which assumes that the reaction rate is proportional to $\theta_A\theta_B$. *Note that this is so even when there are no lateral interactions.*

When $p_r/p_m \to \infty$, the 'islands' grow indefinitely large, and the reactivity of the catalytic surface diminishes to zero with increasing time. In this case, any finite sized surface will become completely poisoned by either A or B. It is interesting to ascertain whether the transition from a random distribution to 'islanding' can result in steady-state 'islands' of finite size when the parameter p_r/p_m is not infinitely large, i.e. when the adsorbed molecules can diffuse. Although the quantity l is not

the size of the 'islands,' it is a measure of their length scale. As may be seen in Fig. 5, l apparently reaches a steady value after approximately 2000 Monte-Carlo steps/site. It should be noted that as the 'islands' become larger, the rate of growth would be expected to slow down. Therefore, in the case in which $p_r/p_m = 1$, which produces the largest 'islands' in our simulations, l might still be increasing slowly at 4000 Monte-Carlo steps/site. However, for this case the rate of adsorption of particles at each site is approximately 0.1 per Monte-Carlo step/site. Note that this is not equal to p_a because not all the sites on the lattice are vacant. Hence, there is on average one complete turnover of particles on the entire lattice every ten Monte-Carlo steps/site. Actually, only the boundaries of the 'islands' are reactive, so that the turnover rate for each of these sites is even higher. Since this is the rate which governs the motion of the boundaries of the 'islands' and, hence, their growth, the value of l, which does not change appreciably between 2000 Monte-Carlo steps/site and 4000 Monte-Carlo steps/site, is probably rather close to its steady-state value. Therefore, we can conclude that for finite values of p_r/p_m, the sizes of the 'islands' that are formed are finite. It should be noted that finite-size effects would set in if these simulations were allowed to run for an indefinitely long time. In that case the entire lattice would at some point in time become poisoned with either A or B. This, however, would be an artifact of the finite size of the lattice, and care has to be taken, as demonstrated earlier, to ensure that the simulations are not performed for such long times that this affects the results.

In these simulations, the reaction rate was also monitored by counting the number of AB pairs that actually reacted and were removed from the surface. In order to quantify the deviation of this measured reaction rate N_r from the reaction rate N_0 that would be observed if the configuration on the surface were 'well-mixed,' we plot the dependence of N_r/N_0 on p_r/p_m in Fig. 6. Even for the smallest value of p_r/p_m, which is 0.01, there is a deviation from the 'well-mixed' limit. Frequently, rate coefficients for second-order surface reactions are calculated assuming that the

reaction rate is proportional to $\theta_A\theta_B$. However, even when there are no lateral interactions, it is necessary in systems such as the one simulated here to check and correct for deviations that result from nearest-neighbor pair correlations arising from the chemical reaction itself. A decrease in the reaction rate as a result of 'islanding' is not the sole effect of an increase in p_r. As the 'islands' form and the reaction rate decreases, there is an increase in the fractional surface coverage of both A and B. This increase in θ_A and θ_B results because as p_r is increased the adsorption probability p_a increases **(36)** while the reactivity per pair of adsorbed A and B particles decreases. The increase in surface coverage is the same for the two types of particles, and the average value of $\langle\theta\rangle = (\theta_A + \theta_B)/2$ is plotted as a function of p_r/p_m in Fig. 7. These values of $\langle\theta\rangle$ are the average of ten runs for each value of the parameter p_r. If one wishes to calculate the catalytic reactivity of the surface, it is necessary to normalize for the increase in reaction rate due to this increase in the fractional surface coverages of A and B when p_r/p_m is increased. This is achieved by dividing N_r by N_0.

When p_r/p_m is increased, the reaction rate tends to decrease because of the formation of 'islands.' In order to clarify further the effect of 'islanding' on the catalytic reactivity of the surface, we plot in Fig. 8 the dependence of N_r/N_0 upon the steady-state value of l^{-1} obtained from Fig. 5. We have defined $l \equiv (N_{AA} + N_{BB})/(N_{AB} + N_{AV} + N_{BV})$ and, as discussed earlier, if the 'islands' have a dimension of two, then l is proportional to the length scale of the 'islands.' Since the reaction can occur only at the boundary of an 'island,' the reaction rate must be proportional to the product of two factors: the number of 'islands' per unit area of the surface and the average length of the boundary of each 'island.' When the 'islands' that are formed have a dimension of two, the first factor is inversely proportional to the square of the length scale of the 'islands,' and the second factor is directly proportional to the length scale of the 'islands.' When this is the case, the reaction rate would be inversely proportional to the length scale of the 'islands.'

It is clear from the results presented in Fig. 8 that N_r/N_0 is proportional to l^{-1}. Therefore, we conclude that the 'islands' formed have a dimension of two. The scaling relation $N_r/N_0 \sim l^{-1}$ is observed in all cases except for the datum point obtained from simulations in which we set $p_r = 0.01$. The configuration seen in Fig. 4(a) is a typical configuration for this case. We have noted that even for this value of p_r/p_m, the distribution of particles on the surface is not random since the steady-state value of l/l_0 is slightly greater than unity. However, the 'islands' formed in this case probably contain too few particles for l to be proportional to their length scale, i.e. the continuum limit is not yet reached. The conclusion that the 'islands' that are formed in our simulations have a dimension of two is rather different from the results of recent Monte-Carlo simulations which yielded a fractal dimension of approximately 1.8 for 'islands' that are formed in the limit in which reaction is infinitely fast and diffusion is not allowed **(32)**. However, the cores of the 'islands' that were formed there are in fact compact **(32)**. In comparing our results with the results obtained with infinitely fast reaction and no diffusion, two facts should be considered. First, it should be noted that in our simulations steady states with 'islands' of finite sizes are obtained, whereas, in the latter case, the 'islands' grow indefinitely with time. Second, the fractional surface coverages in our simulations reach a steady-state value. This value becomes progressively larger as p_r/p_m increases, and for $p_r/p_m = 1.0$ it is given by $\theta_A = \theta_B \simeq 0.239$. The dependence of the fractional surface coverage upon p_r/p_m is shown in Fig. 7. The fractional coverage in the case where reaction is infinitely fast increases continuously with time. As a consequence of the finite steady-state size of the 'islands,' it is not unreasonable that the effective surface tension produced by the reaction of unlike nearest-neighbor pairs drives the shape of the 'islands' to a structure with a dimension of two. On the other hand, when the fractional coverage is sufficiently high, percolation of the 'islands' can occur. This will cause a cascade of length scales that result from the coalescence of clusters of all sizes. The consequence of

this is the formation of fractal 'islands.' This was suggested previously to explain the fractal dimension of approximately 1.8 that was found **(32)**. If we extrapolate our results to large l using the scaling relation $N_r/N_0 \sim l^{-1}$ (cf., Fig. 8), we find that the reaction rate goes to zero at some finite value of l. This clearly cannot be physically meaningful, since the reaction rate would not be zero unless the limit of infinitely large l were reached. Therefore, at some value of l larger than the values that we obtained in our simulations, the scaling $N_r/N_0 \sim l^{-1}$ must break down. Indeed, the actual reaction rate would be higher than that which is predicted by this scaling. This can be explained by the occurrence of percolation, as was suggested for the case in which p_r/p_m is infinitely large **(32)**.

C. Order Parameter

The order parameter at steady state as a function of p_r/p_m is plotted as circles in Fig. 9. Since 'islanding' occurs whenever p_r/p_m is nonzero, we see that the order parameter goes to zero at $p_r/p_m = 0$. We also plot in Fig. 9 the curve $\phi = k(p_r/p_m)^{1/2}$, where k is a constant equal to 0.607. Therefore, for values of p_r/p_m up to unity, the results of the simulations are consistent with the scaling $\phi \sim (p_r/p_m)^{1/2}$. Although the formation of 'islands' in this system is due to kinetic phase transitions and not due to thermal phase transitions, it is informative to compare the quantity ϕ of this Langmuir-Hinshelwood reaction system to the order parameter in thermal phase transitions, for example, in magnetic materials or in binary alloys. In the case of a ferromagnetic solid the order parameter is the magnetization. Since increasing the reaction rate increases the size of the 'islands' and, hence, the degree of order in the system, we can compare increasing the parameter p_r/p_m of the Langmuir-Hinshelwood system to decreasing the temperature in a system which can undergo a thermal phase transition. We have also noted that 'islanding' occurs as soon as p_r/p_m is raised above zero. Hence, if we make the correspondence $(T_c - T) \leftrightarrow p_r/p_m$, where T_c is the critical temperature of the thermal

system, we obtain $\phi \sim (p_r/p_m)^\beta$, where β is the exponent for the order parameter in a system undergoing a thermal phase transition. The mean-field value of $1/2$ is obtained for the exponent β. Our simulation results, therefore, suggest that the 'islanding' behavior can be described by a mean-field theory. This is, perhaps, not too surprising. A mean-field calculation, at the level of only pair-approximations, has been shown to agree rather well with Monte-Carlo simulations of the Langmuir-Hinshelwood system in ref. 29. This is true in particular insofar as predictions of the position of the first-order poisoning transition are concerned. The formation of 'islands' as p_r/p_m is increased from zero would not be dependent upon long-range collective effects if it is well described by a mean-field theory. The assertion that this 'islanding' behavior is of a mean-field nature is based on the validity of the correspondence $(T_c - T) \leftrightarrow p_r/p_m$ and $m \leftrightarrow \phi$. It remains to be seen whether a mean-field calculation can describe the properties of the system when p_r/p_m is close to zero.

4. Conclusions

We have investigated, using Monte-Carlo simulations, the reactivity of a surface catalyzed Langmuir-Hinshelwood reaction that is described by the following model:

$$A(g) + V \rightarrow A(a),$$

$$B(g) + V \rightarrow B(a),$$

and

$$A(a) + B(a) \rightarrow AB(g).$$

Since the adsorption steps are irreversible, it is important to consider possible finite-size effects in the simulations. We find that lattices of size (200x200) are sufficiently large for simulations in which up to 4000 Monte-Carlo steps/site are

allowed. For simulations of longer duration, larger lattices would have to be used; however, for this investigation (200x200) lattices are adequate. Although we have performed simulations only on square lattices, we do not expect the results we have presented here to be affected qualitatively by a change in the lattice symmetry. It is possible, however, that if 'island' percolation indeed occurs at a high fractional surface coverage, the coverages and the corresponding values of p_r and p_m at which it occurs would be dependent on the lattice symmetry. The parameters in our model are p_r, p_m and p_a, the probability of successful reaction of a nearest-neighbor AB pair, the probability of successful hopping of an A or B particle to a nearest-neighbor vacant site, and the probability of successful adsorption of a particle into a vacant site, respectively. In all of our simulations, p_a is set equal to $p_r/5$, and p_m is set equal to unity. The range of values of p_r used in the simulations is from 0.01 to unity. We observed that 'islanding' occurs even for the lowest value, 0.01, of p_r. Hence, 'islanding' probably occurs whenever p_r/p_m is nonzero. This means that the surface coverage of reactants in many bimolecular surface reactions may not be spatially homogeneous, even in the absence of lateral interactions. Therefore, in order to extract accurate rate coefficients from experimental measurements, it is necessary to correct for this deviation from a random distribution of adsorbed molecules. We also find that the 'islands' are finite in size for values of p_r/p_m less than unity and $p_a = p_r/5$. Above this value of p_r, the fractional surface coverages may be sufficiently high for percolation to occur.

A quantitative measure of the 'island' size is $l \equiv (N_{AA} + N_{BB})/(N_{AB} + N_{AV} + N_{BV})$. The simulations indicate that N_r/N_0 scales as l^{-1}, where N_r is the observed reaction rate and N_0 is the reaction rate that would be observed if the adsorbed particles were randomly distributed on the surface. We have argued that the 'islands' are compact, i.e. they do not have a dimension lower than two. This scaling fails when p_r and, consequently, l become too large, and this failure can possibly be due to the occurrence of percolation since the surface coverage increases

with p_r **(32)**. For values of p_r/p_m close to zero, we find that the order parameter, which is defined as $\phi \equiv (N_{AA} + N_{BB} - N_{AB})/(N_{AA} + N_{BB} + N_{AB})$, scales as $(p_r/p_m)^{1/2}$. Arguing that p_r/p_m corresponds to $T_c - T$ in magnetic systems, we propose that this indicates the mean-field nature of the 'islanding' phenomenon in this system.

Acknowledgment : This work was supported by the Office of Basic Energy Sciences of the Department of Energy under grant number DE-FG03-89ER14048.

References

1. M. Silverberg and A. Ben-Shaul, J. Chem. Phys. **83**, 6501 (1985).
2. M. Silverberg and A. Ben-Shaul, J. Chem. Phys. **87**, 3178 (1987).
3. M. Silverberg and A. Ben-Shaul, Chem. Phys. Lett. **134**, 491 (1987).
4. M. Silverberg and A. Ben-Shaul, J. Stat. Phys. **52**, 1179 (1988).
5. M. Silverberg and A. Ben-Shaul, Surf. Sci. **214**, 17 (1989).
6. E.S. Hood, B.H. Toby and W.H. Weinberg, Phys. Rev. Lett. **55**, 2437 (1985).
7. P. Araya, W. Porod, R. Sant and E.E. Wolf, Surf. Sci. **208**, L80 (1989).
8. M. Dumont and P. Dufour, Comp. Phys. Comm. **41**, 1 (1986).
9. M. Dumont, M. Poriaux and R. Dagonnier, Surf. Sci. **169**, L307 (1986).
10. J.L. Sales and G. Zgrablich, Phys. Rev. B **35**, 9520 (1987).
11. J.L. Sales and G. Zgrablich, Surf. Sci. **187**, 1 (1987).
12. D. Gupta and C.S. Hirtzel, Chem. Phys. Lett. **149**, 527 (1988).
13. D. Gupta and C.S. Hirtzel, Surf. Sci. **210**, 322 (1989).
14. O.M. Becker and A. Ben-Shaul, Phys. Rev. Lett. **61**, 2859 (1988).
15. W.H. Weinberg, in **Kinetics of Interface Reactions**, Eds., H.J. Kreuzer and M. Grunze, Springer-Verlag, Heidelberg, 1987, p. 94.
16. P.W. Tamm and L.D. Schmidt, J. Chem. Phys. **52**, 1150 (1970).
17. P.W. Tamm and L.D. Schmidt, J. Chem. Phys. **55**, 4253 (1971).
18. L.R. Clavenna and L.D. Schmidt, Surf. Sci. **22**, 365 (1970).
19. C. Kohrt and R. Gomer, J. Chem. Phys. **52**, 3283 (1970).
20. D.A. King and M.G. Wells, Surf. Sci. **23**, 120 (1971).
21. D.A. King and M.G. Wells, Proc. Roy. Soc. (Lond.) **A339**, 245 (1974).
22. V.P. Zhdanov, Surf. Sci. **111**, 63 (1981).

23. V.P. Zhdanov, Surf. Sci. **123**, 106 (1982).

24. V.P. Zhdanov, Surf. Sci. **133**, 469 (1983).

25. V.P. Zhdanov, Surf. Sci. **137**, 515 (1984).

26. S. Sundaresan and K.R. Kaza, Surf. Sci. **160**, 103 (1985).

27. G. Nicolis and I. Prigogine, **Self-Organization in Nonequilibrium Systems**, Wiley Interscience, New York, 1977.

28. H. Haken, **Synergetics**, Springer-Verlag, New York, 1983.

29. R.M. Ziff, E. Gulari and Y. Barshad, Phys. Rev. Lett. **56**, 2553 (1986).

30. K.A. Fichthorn, R.M. Ziff and E. Gulari, in **Catalysis**, Ed., J.W. Ward , Elsevier Science Publishers, B.V., Amsterdam, 1987.

31. K.A. Fichthorn, E.Gulari and R.M. Ziff, to be published.

32. R.M. Ziff and K.A. Fichthorn, Phys. Rev. B **34**, 2038 (1986).

33. E. Wicke, P. Kumman, W. Keil and J. Scheifler, Ber. Bunseges. Phys. Chem. 4, 315 (1980).

34. R. Dickman, Phys. Rev. A, **34**, 4246 (1986).

35. H.C. Kang, R. W. Verhoef and W.H. Weinberg, to be published.

36. Note that we have set $p_a = p_r/5$ for all the simulations here.

Figure Captions

Figure 1(a-d). The abscissa is the difference δN between the number of particles of type A and the number of particles of type B. We have divided this difference by the number of lattice sites (LxL). The ordinate is the probability $P(\delta N, n_T)$ of finding a configuration with the difference in the number of particles δN after n_T adsorption events. Assuming a lattice of size (LxL) embedded in an infinitely large lattice, $P(\delta N, n_T)$ is given by the circles [Eq. 5]. The line indicates the $P(\delta N, n_T)$ distribution if the lattice were a finite one of size (LxL) [Eq. 6]. The size of the lattice and the number of adsorption events are indicated in each figure.

Figure 2. The dependence of the quantity l on time is shown where the abscissa is time in units of Monte-Carlo steps/site and the ordinate is l. The parameters used here are $p_r = 1$ and $p_m = 1$. Each curve is labeled with the size of the lattice used in the simulations.

Figure 3(a-d). These are typical configurations obtained from simulations in which $p_r = 1$ and $p_m = 1$. The configurations were obtained after a time of 4000 Monte-Carlo steps/site. The size of the lattice is shown on each figure. An empty square denotes a particle of type A, and a filled square denotes a particle of type B.

Figure 4(a-e). These are typical configurations obtained from simulations in which $p_m = 1$ and p_r ranges from 0.01 to 0.8. The lattice size is (200x200) for all these configurations. The configurations were obtained after a time of 4000 Monte-Carlo steps/site. An empty square denotes a particle of type A, and a filled square denotes a particle of type B.

Figure 5. The dependence of l upon time for all the simulations are shown here. The abscissa is time in units of Monte-Carlo steps/site and the ordinate is l. The parameter $p_m = 1$ for all these curves, and p_r ranges from 0.01 to unity. Each curve

is labeled with its value of p_r. Note that the value of l in the case of infinitely fast diffusion l_0 is indicated in the figure by an arrow. Each curve is obtained from an average of ten simulations on (200x200) lattices.

Figure 6. The dependence of the quantity N_r/N_0 upon the value of p_r/p_m is shown here. The abscissa is p_r/p_m and the ordinate is N_r/N_0, where N_r is the reaction rate and N_0 is the reaction rate which would be observed if the particles were randomly distributed on the surface.

Figure 7. The dependence of the average fractional surface coverage $\langle\theta\rangle = (\theta_A + \theta_B)/2$ upon p_r/p_m is shown here. The value of $\langle\theta\rangle$ for each value of p_r/p_m is obtained from an average of ten simulation runs. The averages of θ_A and θ_B are equal and, if plotted here, would fall on the same curve.

Figure 8. The relationship between the reaction rate and the quantity l is shown here. The abscissa is l^{-1} in units of ${l_0}^{-1}$, where l_0 is the value of l when the fractional surface coverages are $\theta_A = \theta_B \simeq 0.1791$, and the particles are randomly distributed. The ordinate is N_r/N_0, i.e., the reaction rate normalized by the reaction rate that would be observed if the particles were randomly distributed.

Figure 9. The dependence of the order parameter ϕ upon the value of p_r/p_m is indicated by the circles. The line is the curve $\phi = 0.607(p_r/p_m)^{1/2}$ and shows for values of p_r/p_m between zero and unity that the simulation results are consistent with the scaling $\phi \sim (p_r/p_m)^{1/2}$. When p_r/p_m is increased further, causing an increase in the surface coverage, this scaling is expected to break down beyond some value of p_r/p_m.

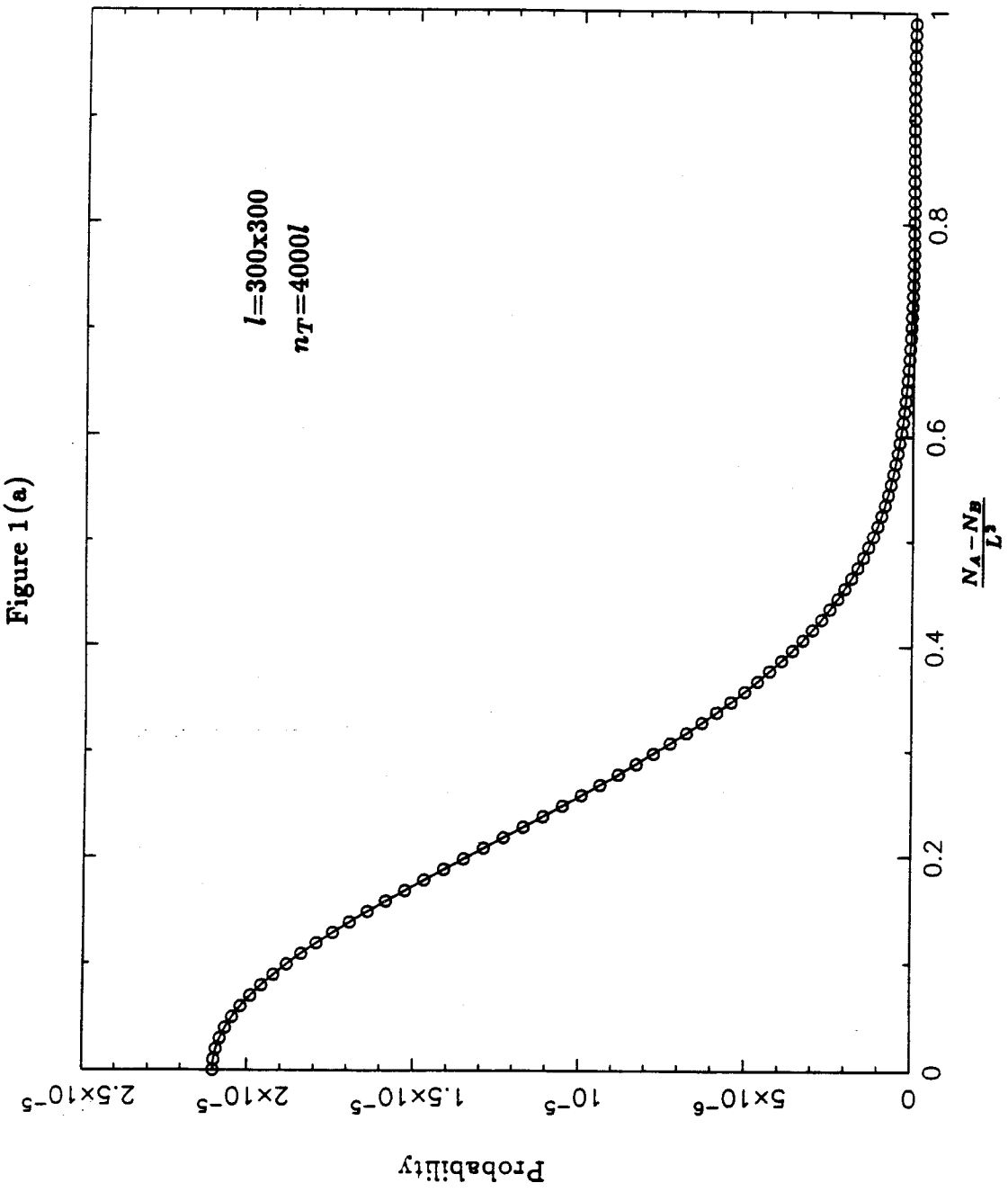
l=300x300
n_T=4000l
Probability
0
5×10⁻⁶
10⁻⁵
1.5×10⁻⁵
2×10⁻⁵
2.5×10⁻⁵
0
0.2
0.4
0.6
0.8
1
(N_A−N_B)/L²

Figure 1 (a)

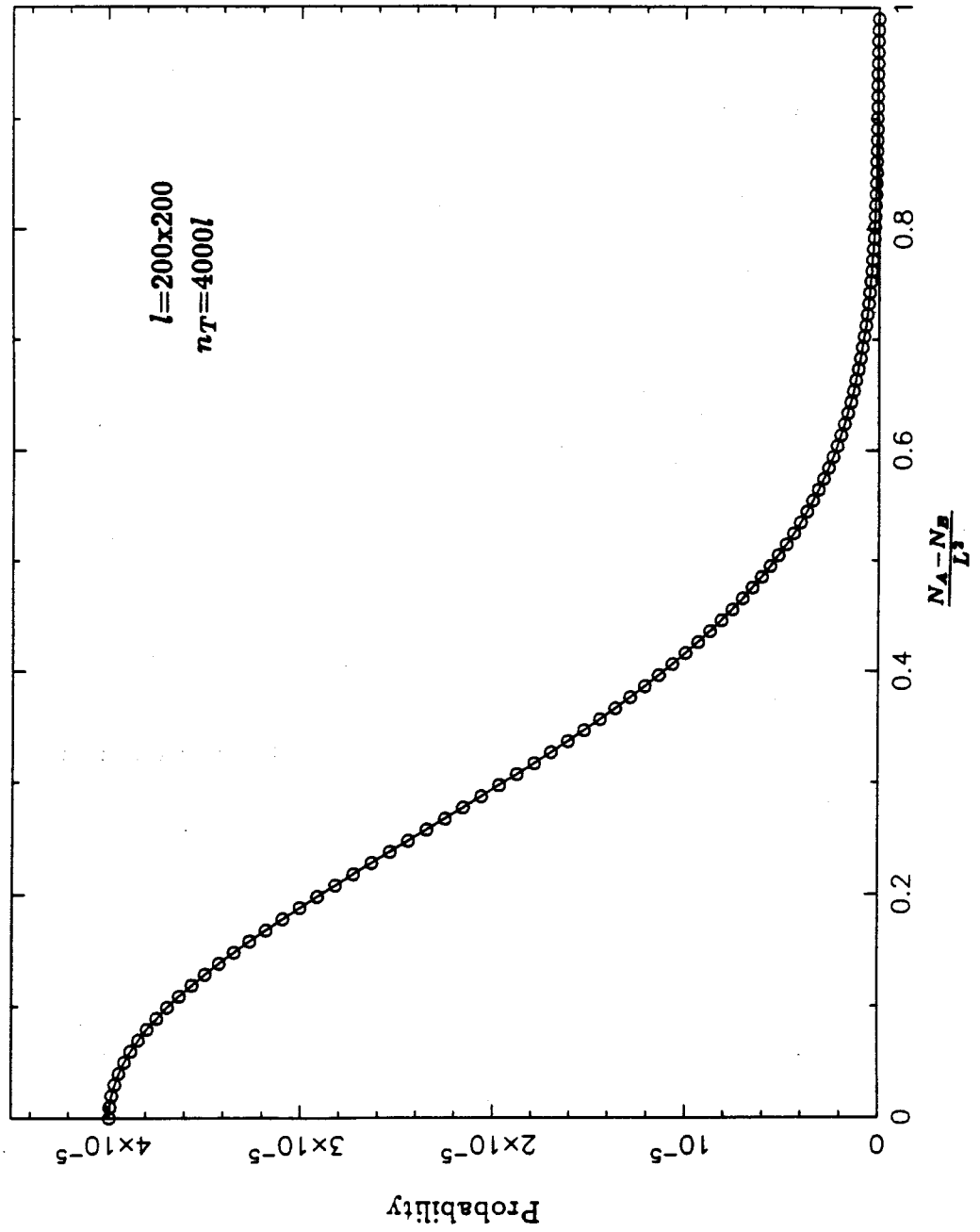
l=200x200
n_T=4000l
Probability
0
10^{-5}
2×10^{-5}
3×10^{-5}
4×10^{-5}
0
0.2
0.4
0.6
0.8
1
$\frac{N_A-N_B}{L^2}$

Figure 1(b)

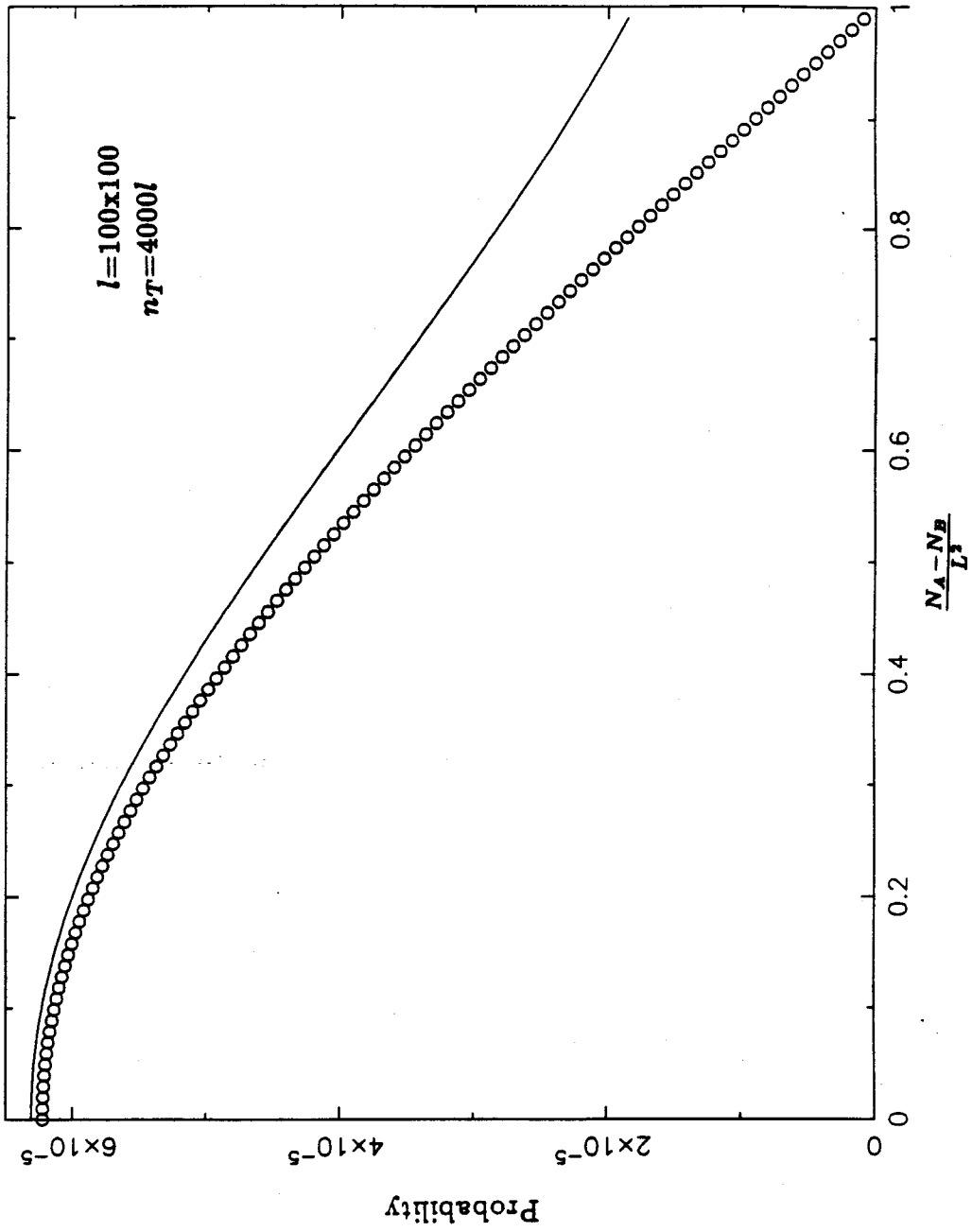
l=100x100
n_T=4000l
Probability
6×10⁻⁵
4×10⁻⁵
2×10⁻⁵
0
0
0.2
0.4
0.6
0.8
1
$\frac{N_A-N_B}{L^2}$

Figure 1(c)

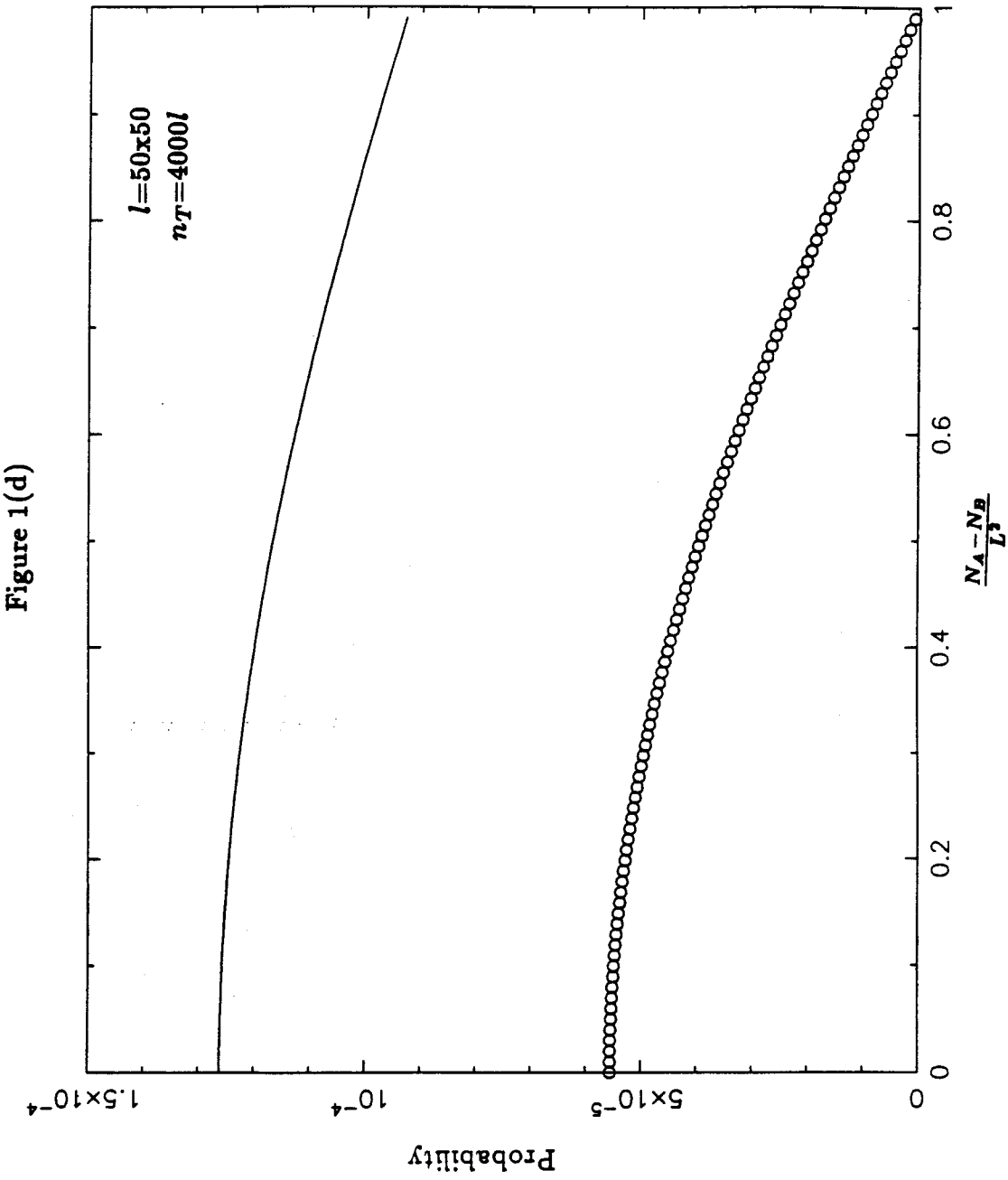
l=50x50
n_T=4000l
Probability
1.5×10^{-4}
10^{-4}
5×10^{-5}
0
0
0.2
0.4
0.6
0.8
1
$\frac{N_A-N_B}{L^3}$

Figure 1(d)

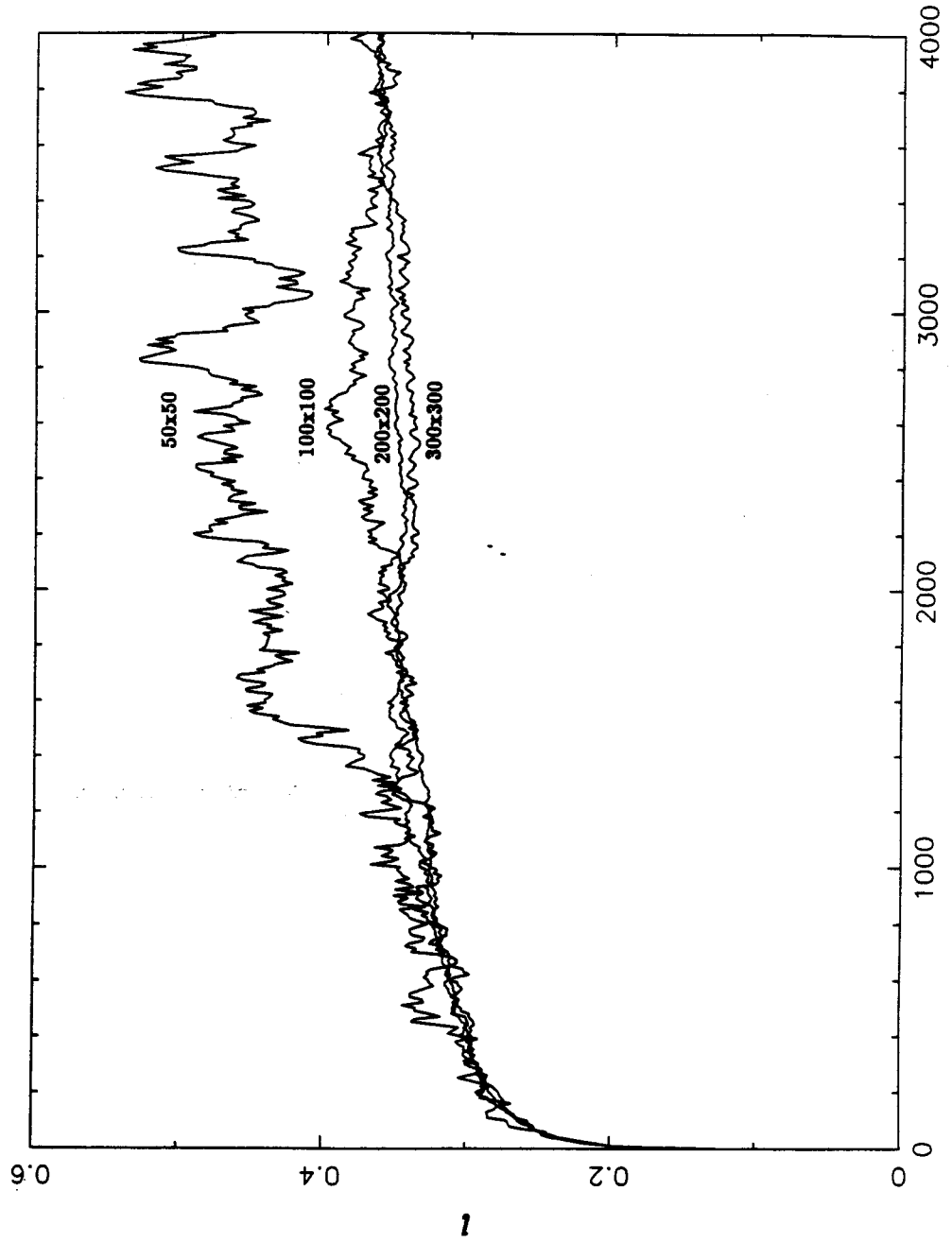
50x50
100x100
200x200
300x300
0
0.2
0.4
0.6
1000
2000
3000
4000
I
Monte-Carlo steps/site

Figure 2

Figure 3(a)

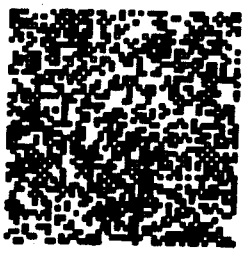

(50x50)

$\langle \theta_A \rangle = 0.16912$

$\langle \theta_B \rangle = 0.33756$

Figure 3(b)

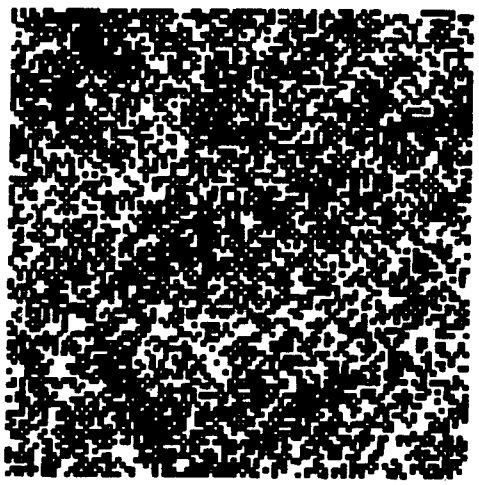

(100x100)

$\langle \theta_A \rangle = 0.22863$

$\langle \theta_B \rangle = 0.25814$

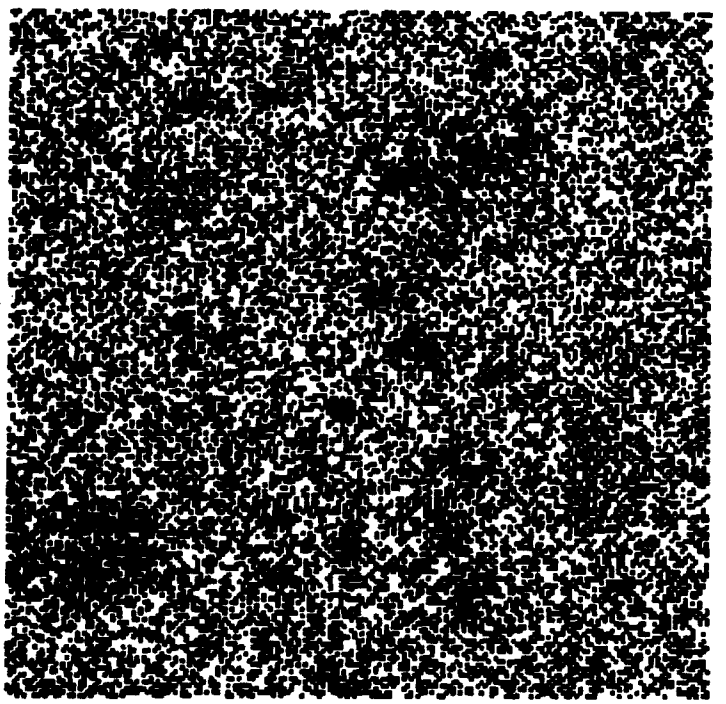

(200x200)

$\langle \theta_A \rangle = 0.24355$

$\langle \theta_B \rangle = 0.24026$

Figure 3(c)

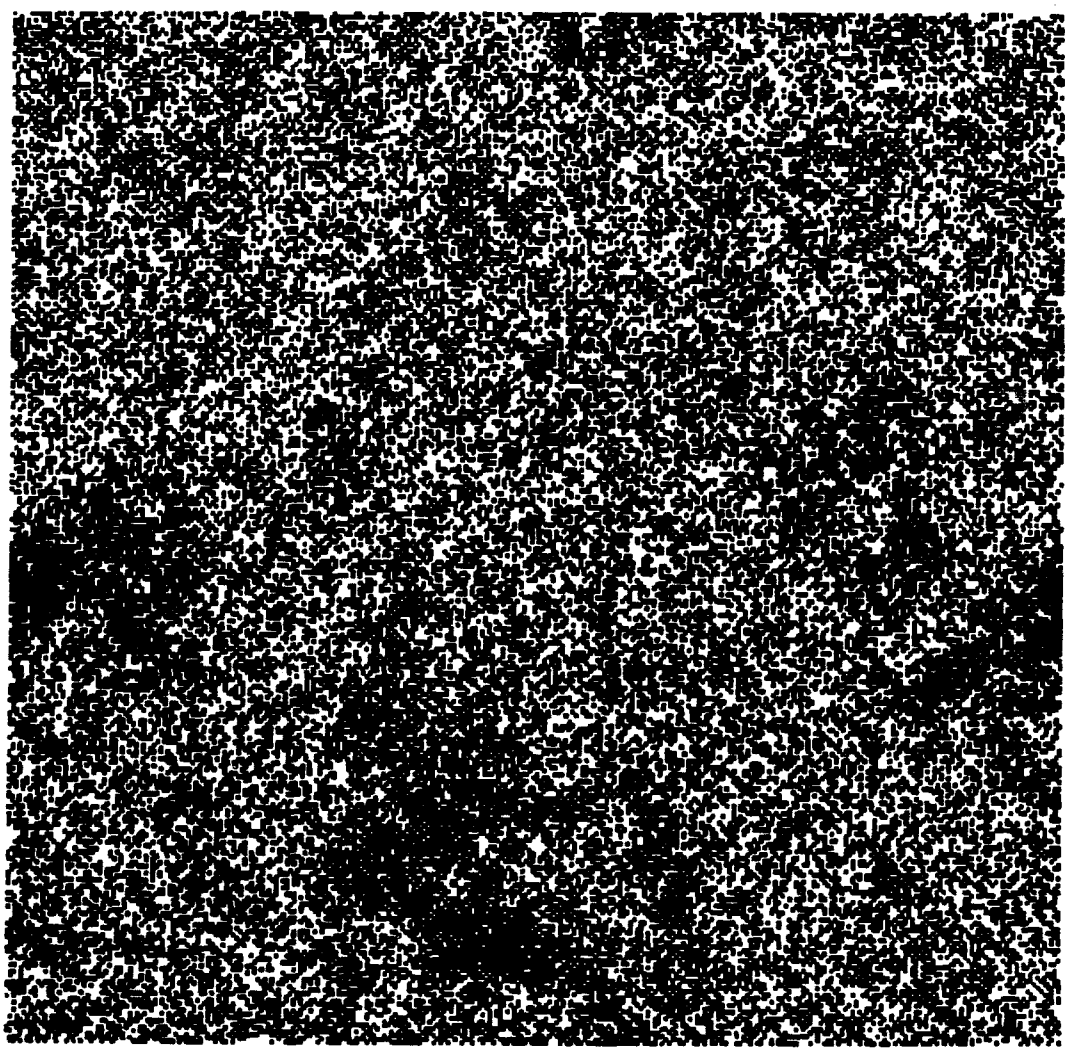

Figure 3(d)

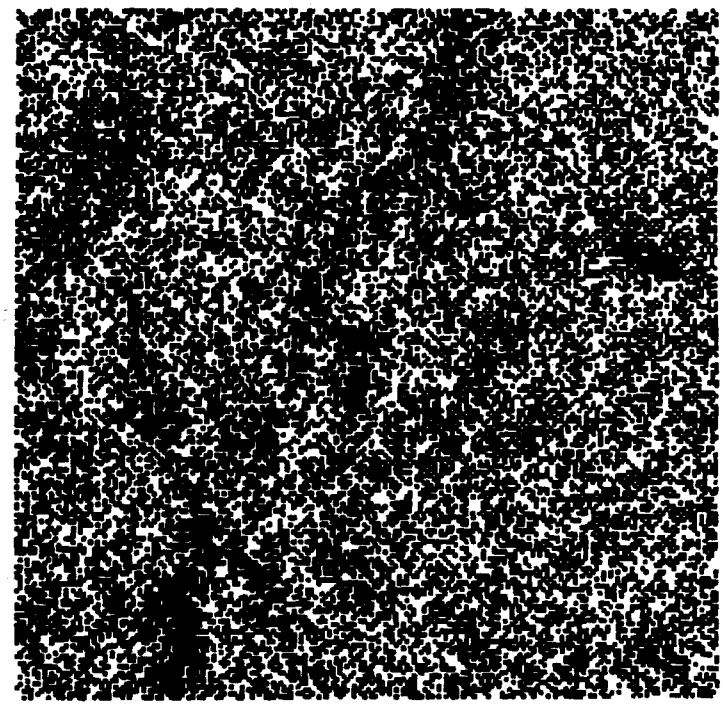

$p_m = 1,\ p_r = 0.8$

$\langle \theta_A \rangle = 0.23584$

$\langle \theta_B \rangle = 0.25404$

Figure 4(a)

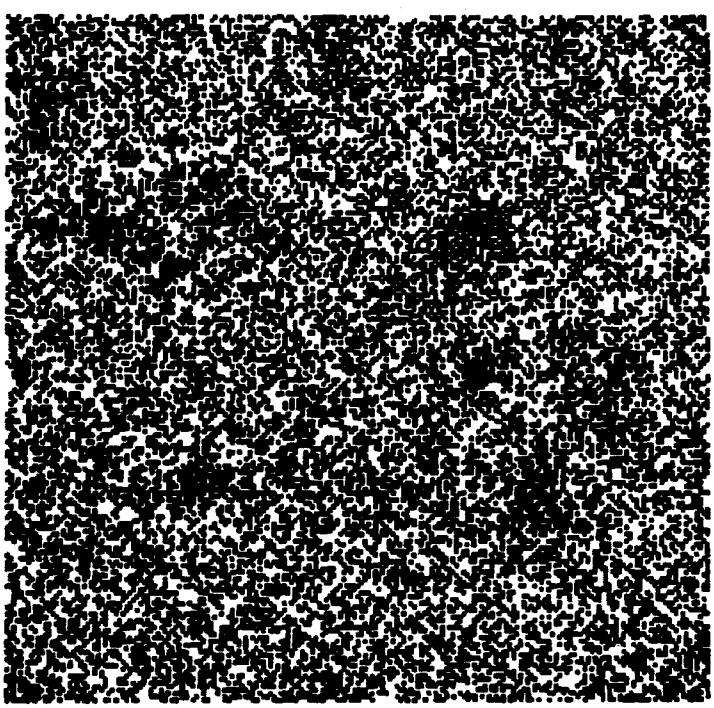

$p_m = 1, p_r = 0.6$

$\langle \theta_A \rangle = 0.22086$

$\langle \theta_B \rangle = 0.23124$

Figure 4(b)

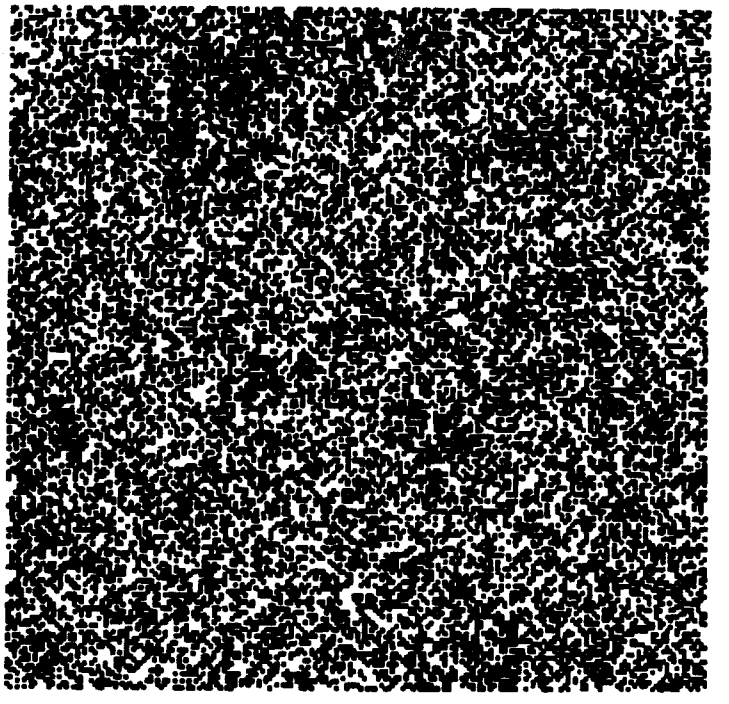

$p_m = 1,\ p_r = 0.4$

$\langle \theta_A \rangle = 0.23174$

$\langle \theta_B \rangle = 0.20215$

Figure 4(c)

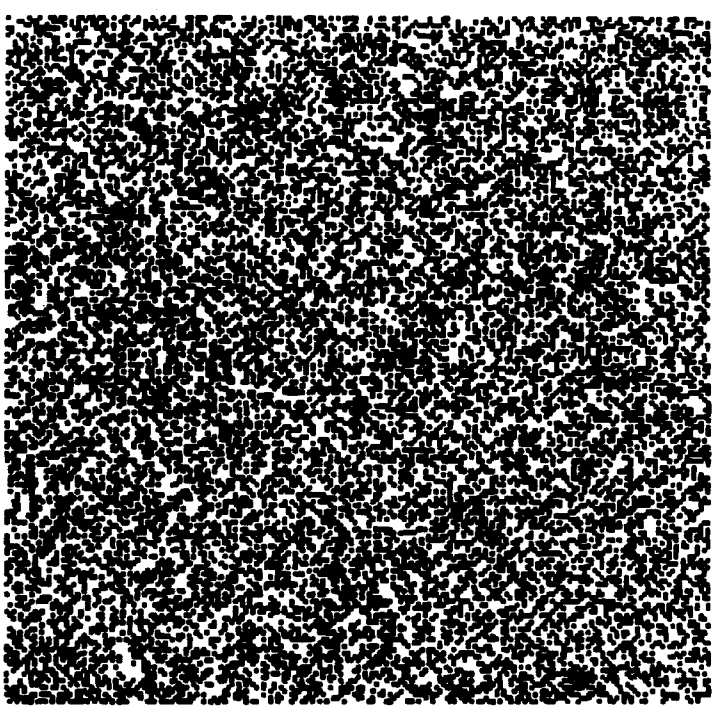

$p_m = 1,\ p_r = 0.1$

$\langle \theta_A \rangle = 0.19876$

$\langle \theta_B \rangle = 0.18683$

Figure 4(d)

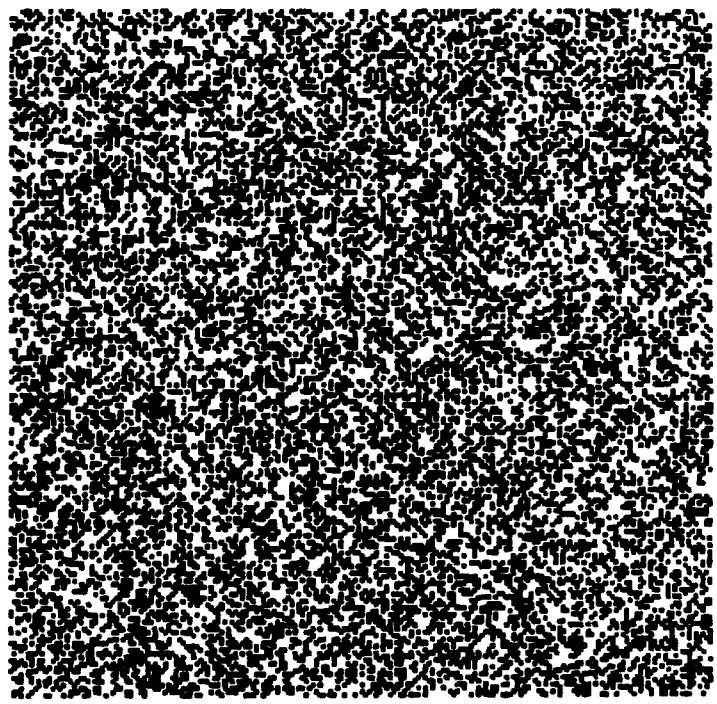

$p_m = 1,\ p_r = 0.01$

$\langle \theta_A \rangle = 0.18475$

$\langle \theta_B \rangle = 0.17734$

Figure 4(e)

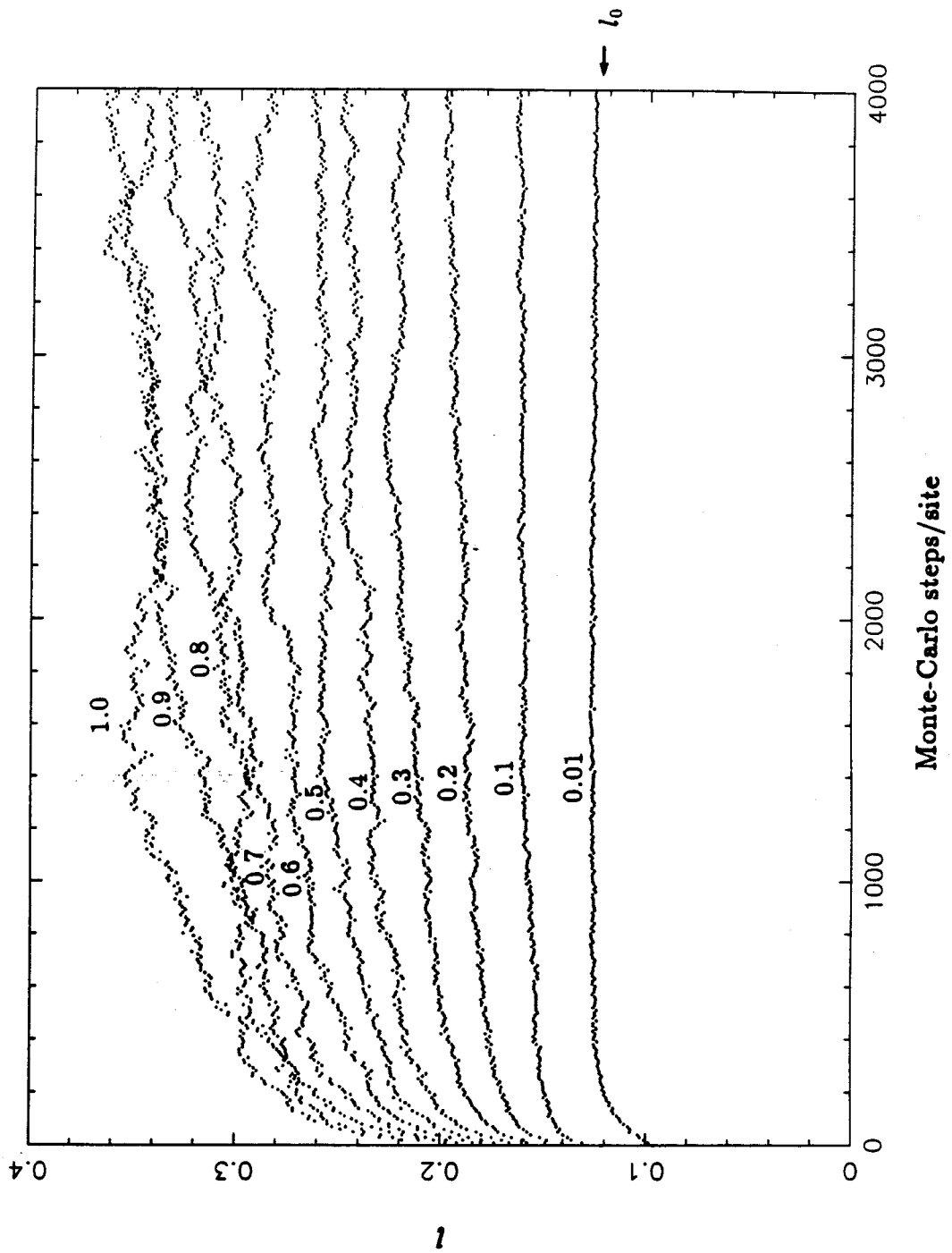
l_0
1.0
0.9
0.8
0.7
0.6
0.5
0.4
0.3
0.2
0.1
0.01
0
0.1
0.2
0.3
0.4
l
0
1000
2000
3000
4000
Monte-Carlo steps/site

Figure 5

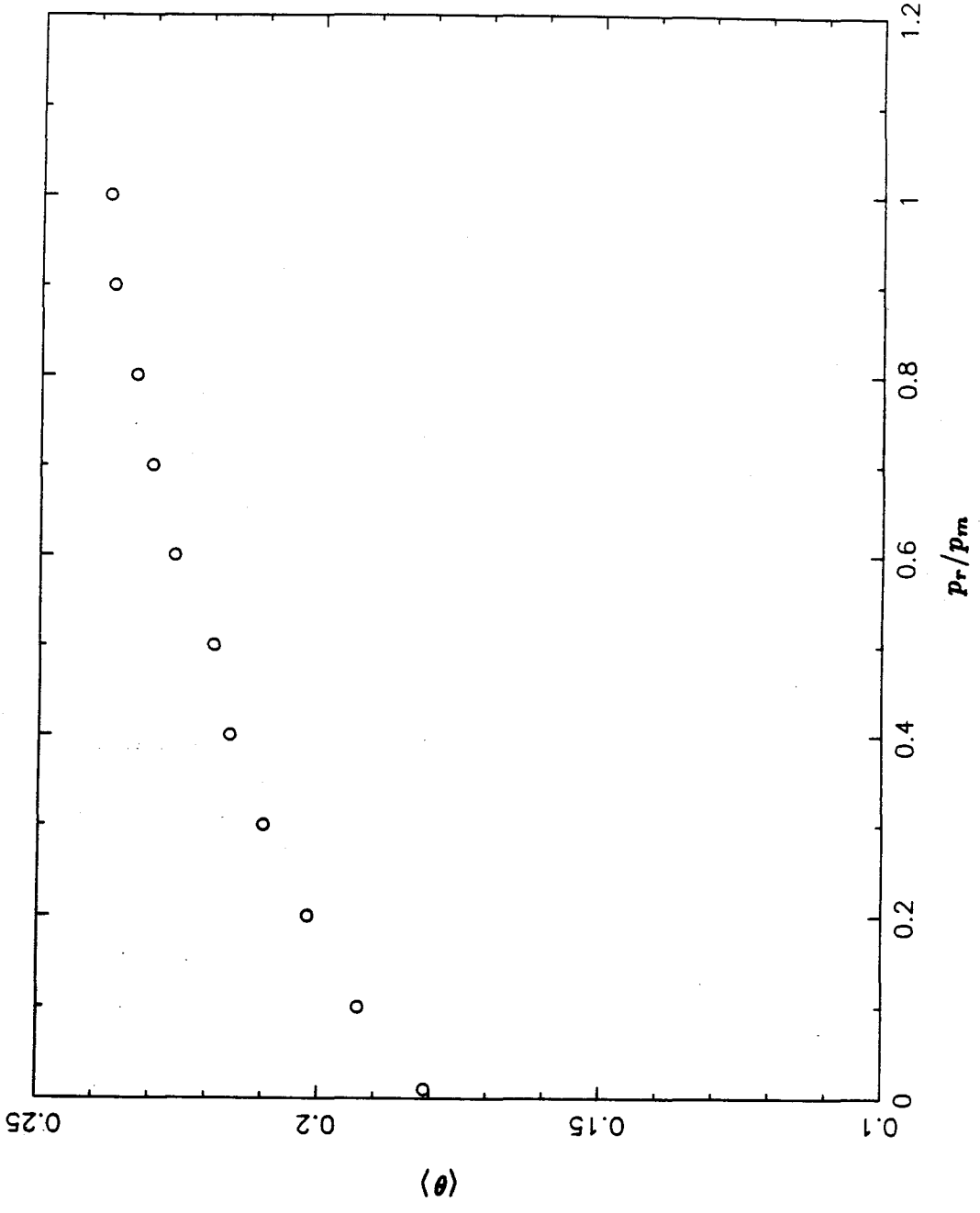

Figure 7

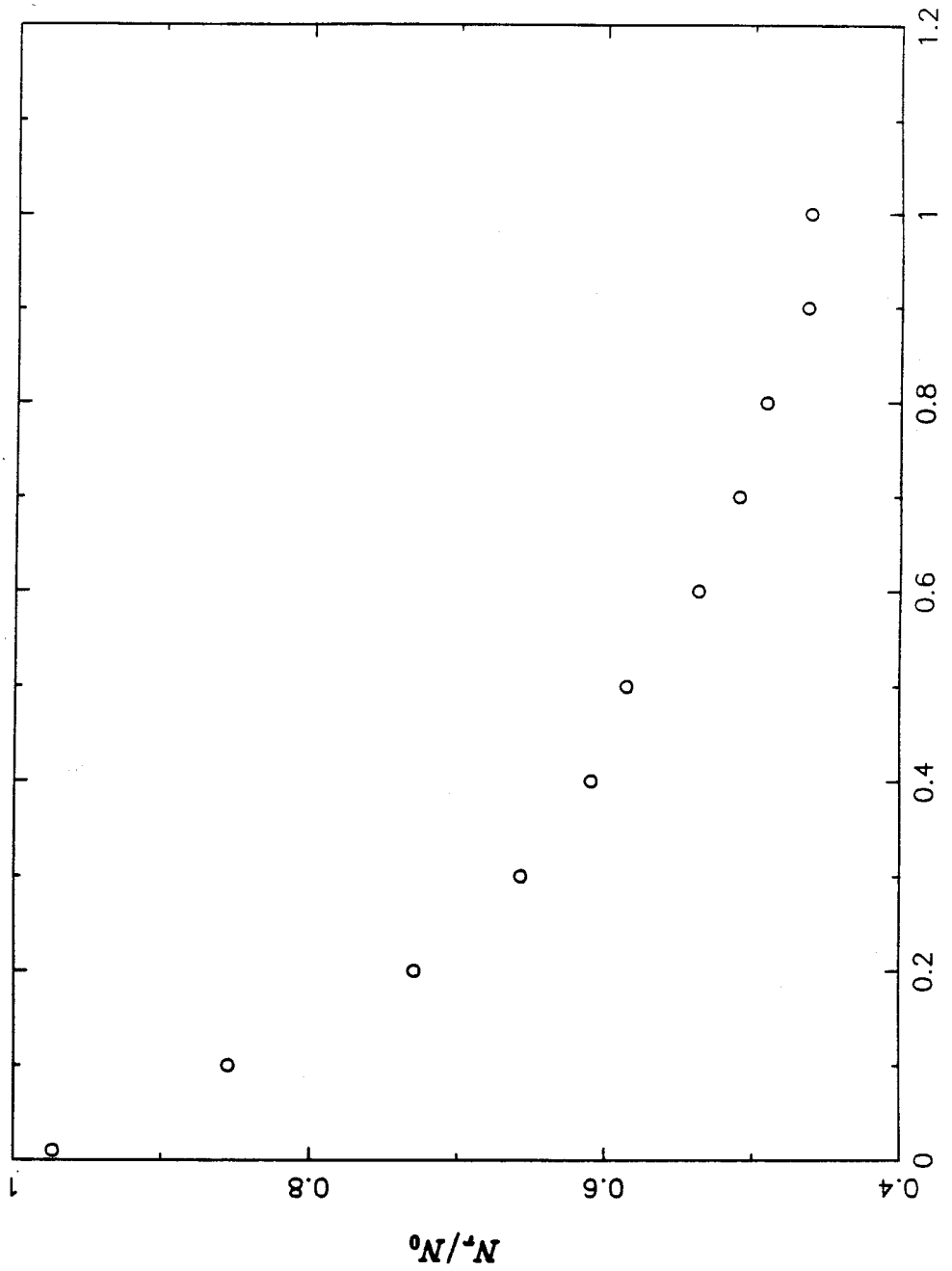

Figure 6

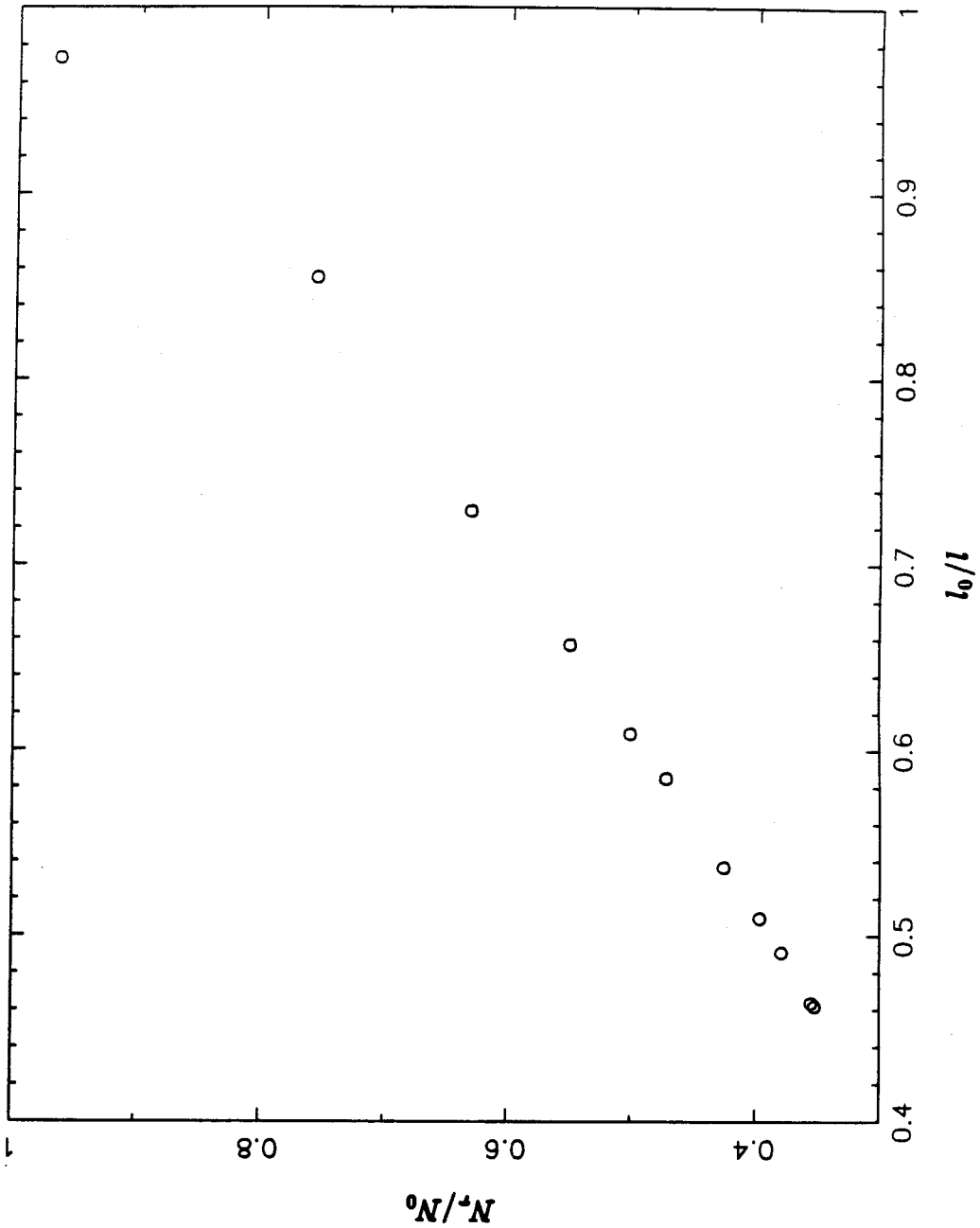

Figure 8

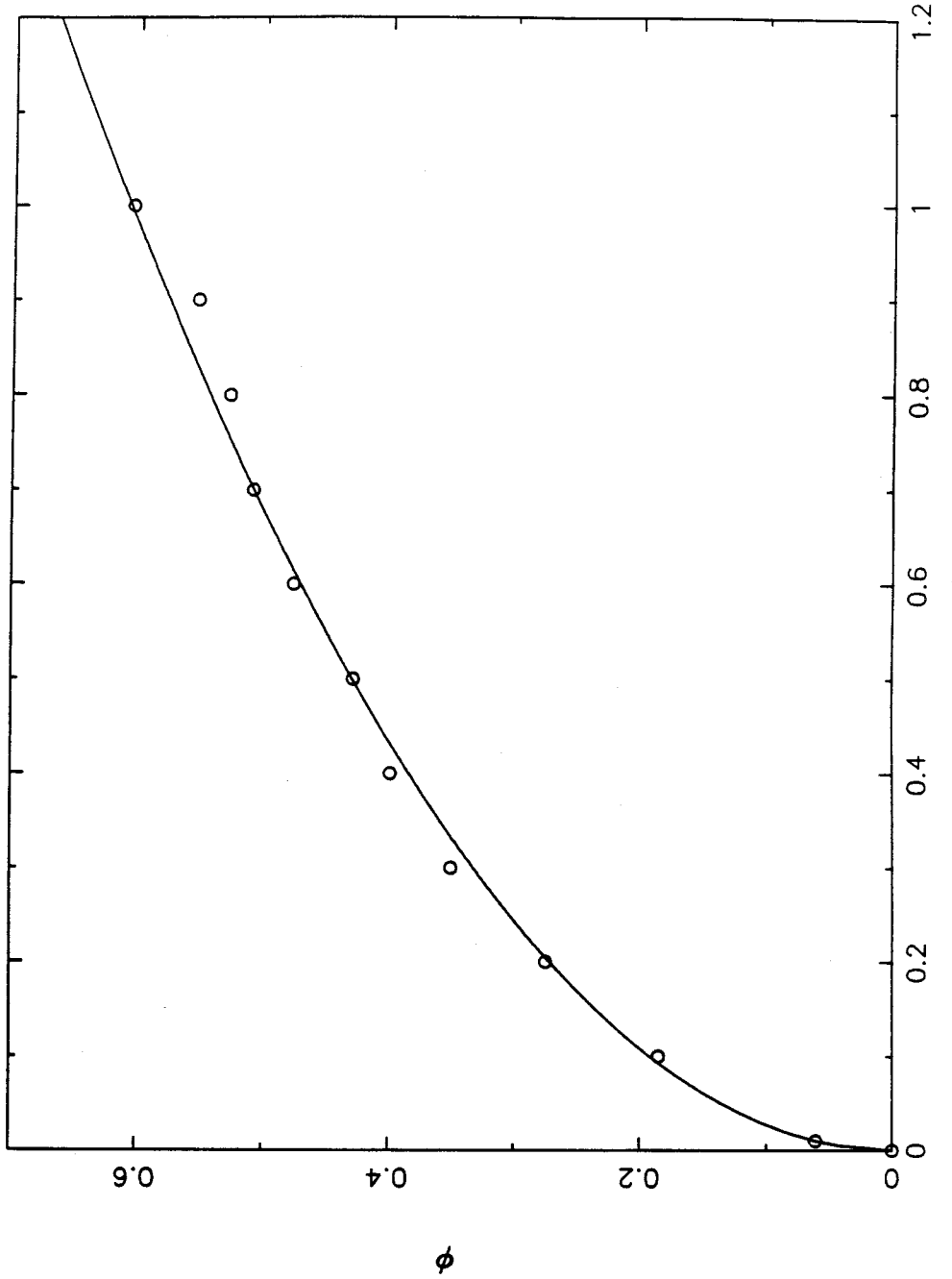

Figure 9

CONCLUSIONS

We can divide our work into four sections. The first section reports our examination of the use of Monte-Carlo methods for simulating time-evolving systems. This is contained in Chapter 1. The second section, contained in Chapters 2 to 4, is the study of the kinetics of domain growth. The third section discusses the results of simulations performed with the purpose of studying the influence of lattice gas configurations on the kinetics of reaction and adsorption. This is the content of Chapters 5 and 6. The fourth section, contained in Chapter 7, is the study of adsorbate 'islanding' which can occur in Langmuir-Hinshelwood reactions. Our conclusions for each section are as follows:

Section 1

The proper choice of the transition probabilities in Monte-Carlo simulations is rather important if dynamic properties such as the diffusion coefficient are to be accurately calculated. As shown in Chapter 1, the use of Kawasaki dynamics implies that the rate of the thermally excited microscopic processes, such as particle hops from site to site, is increased. However, the rates of the same process occurring in different local configurations are increased by different amounts. In particular, in the case of diffusion, we have shown that for different choices of the transition probabilities there is a different temperature dependence of the calculated diffusion coefficient. This is true even though it is required that the different choices of transition probabilities all satisfy detailed balance and lead to the same equilibrium configurations. Thus, in using Monte-Carlo methods to simulate dynamic (as opposed to static) phenomena, it is necessary to use the proper transition probabilities if quantitatively accurate answers are needed.

Section 2

We find that the exponent for growth of (2x1) domains on a square lattice is 1/2, regardless of the mobility of the precursor. However, in the early stages of domain growth, the effective growth exponent is smaller than 1/2. It is important to realize this when experimental measurements of domain growth are performed. This is because the coherence width of the electron beams usually achievable in low-energy electron diffraction, the tool currently used in such studies, is on the order of only about 100 Å. Hence, the domain size which can be measured may not be sufficiently large for scaling to occur. The inevitable presence of defects, such as steps, on the surface of the crystals will also limit the size of the overlayer domains that can be grown. If we write the growth law as $l \sim At^{1/2}$, the simulations show that A obeys the scaling relation $A \sim D^{1/2}$. This result was obtained from simulations of a model in which particle migration is precursor-mediated but may not be be applicable to models in which particle migration occurs by nearest-neighbor hops. The Lifshitz Allen-Cahn theory which is applicable to curvature-driven domain growth predicts the same scaling.

The growth of ordered $(\sqrt{3}\text{x}\sqrt{3})R30°$ domains on a triangular lattice was also simulated. Two lattice gas models were used. The particles of the first interact with each other through nearest-neighbor repulsion and next nearest-neighbor attraction of the same magnitude. The particles of the second interact with each other only through nearest-neighbor repulsion. Growth kinetics at zero temperature were simulated using Kawasaki dynamics and allowing hops of various ranges. We find that, in the case in which only nearest-neighbor hops are allowed, domain growth is frozen in the lattice gas with next nearest-neighbor attractive interactions, but it is not for the lattice gas with only nearest-neighbor repulsive interactions. We also find that increasing the range of the allowed hops to include next nearest-neighbor hops prevents domain growth in the former lattice gas model from becoming frozen. Domain growth in this case, however, occurs as a result of the diffusion of ordered

$(\sqrt{3}x\sqrt{3})^*R30°$ domains and domains of vacant lattice sites. Since the nature of domain growth in this system is strongly dependent upon the hop length, at low temperatures domain growth in adsorbed systems which form ordered domains of the same symmetry will be strongly influenced by the presence of precursor states.

One of the issues in the area of domain growth is whether the degeneracy of the ground state of the lattice gas affects the growth exponent. For twofold degenerate ground state simulations and theories, such as the Lifshitz Allen-Cahn theory, all show that the growth exponent is 1/2. Although previous simulations seem to indicate an exponent of 1/3 for the growth of the fourfold degenerate (2x1) domains on a square lattice, our simulations have shown that it is 1/2. We have also investigated, at finite temperatures, growth of the threefold degenerate $(\sqrt{3}x\sqrt{3})R30°$ for which the zero temperature behavior is reported in Chapter 3. We find a growth exponent of 1/2. Therefore, we conclude that the growth exponent is probably not dependent upon the degeneracy of the ground state.

Section 3

In Chapter 5 the molecular adsorption of ethane on the Ir(110)-(1x2) surface was studied. Monte-Carlo simulations were used to analyze molecular beam reflectivity measurements of the probability of adsorption. We show that molecular adsorption can occur directly when an ethane molecule impinges upon the bare iridium surface or indirectly when an ethane molecule impinges upon a previously adsorbed ethane molecule. The "extrinsic" precursor in this case is the mobile ethane molecule trapped in a second layer on top of the first layer of molecularly adsorbed ethane. As the fractional surface coverage of ethane increases, the 'islands' of the adsorbed ethane molecules in the first layer increases in size. Using Monte-Carlo methods it is easy to simulate the diffusion of the ethane molecules trapped on top of such 'islands' properly accounting for the change in the probability of such a trapped ethane molecule migrating to the edge of the 'island' with a change in the

'island' size. It is possible from fitting the simulations to the experimental results to obtain the energy barrier for desorption E_{des} of an ethane molecule trapped on top of a first layer of ethane molecularly adsorbed on the Ir(110)-(1x2) surface. It is also possible to obtain the energy barrier for diffusion E_{diff} of the trapped ethane molecule. We find that E_{des} is approximately 4.5 kcal/mol and that E_{diff} is approximately 3.7 kcal/mol.

In Chapter 6 we simulate the Langmuir-Hinshelwood reaction between two laterally interacting species. We investigate the utility of using the Arrhenius parametrization in analyzing the reaction rate coefficient. The importance of the configuration of the reacting adlayer of particles is clearly demonstrated. In particular, we show that a strong temperature dependence of the adlayer configuration can lead to a compensation effect between the effective energy barrier and the effective preexponential factor obtained from an Arrhenius parametrization of the reaction rate coefficient. Therefore, we conclude that the compensation effects frequently observed experimentally may be due, in part, to the temperature dependence of the adlayer configuration. This will explain the anomalously high reaction or desorption preexponentials that have been observed experimentally in many cases.

Section 4

In this final section we investigate the adsorbed molecule 'islanding' that results not from lateral interactions but from the process of reaction itself. A Langmuir-Hinshelwood reaction between particles of species A and B is simulated. Desorption is not allowed, and the adsorption rates for A and B are equal. 'Islanding' occurs because reaction takes place between nearest-neighbor AB pairs, and therefore reduces the probability of configurations in which the particles of the two species are 'mixed.' The probability of forming 'islands' of particles of only one species is increased. In order to quantify the process of 'islanding,' we defined an order parameter ϕ and a quantity l, the latter of which we show to be proportional

to the 'island' sizes for non-fractal 'islands.' We find that 'islanding' is controlled by the ratio of the probability of migration p_m to the probability of reaction p_r and that it occurs for all non-zero values of p_r/p_m. We show that the 'islands' formed in our simulations have a dimension of two so that the reactivity of the catalyst surface is inversely proportional to l. We also find that the order parameter, which is a chemical analogue of the magnetization in a ferromagnetic material, scales as $(p_r/p_m)^{1/2}$. If we make the correspondence between $T_c - T$ and p_r/p_m and between the magnetization m of a ferromagnet and the order parameter ϕ of our system, this scaling relation implies that 'islanding' in the Langmuir-Hinshelwood reaction model that was simulated can be described by a mean-field model. It is, therefore, not due to a collective behavior of all the particles in the system as in the critical behavior of magnets or fluids. At higher fractional coverages than is reached in our simulations (approximately 0.24), percolation is expected to occur, and this would change the nature of our conclusions.